THE UNIVERSITY OF MICHIGAN

INDUSTRY PROGRAM OF THE COLLEGE OF ENGINEERING

A PHOTOGRAPHIC STUDY OF BOILING IN AN ACCELERATING SYSTEM

William A. Beckman

A dissertation submitted in partial fulfillment
of the requirements for the degree of
Doctor of Philosophy in the
University of Michigan
Department of Mechanical Engineering
1963

January, 1964

IP-653

Doctoral Committee:

Associate Professor Herman Merte, Jr., Chairman
Associate Professor Vedat S. Arpaci
Associate Professor Richard E. Balzhiser
Professor John A. Clark
Professor Arthur G. Hansen
Professor Robert C. Juvinall

ACKNOWLEDGMENTS

The writer would like to express his gratitude to Professor Herman Merte Jr., Chairman of the Doctoral Committee, for his advice and guidance throughout the course of this investigation.

The writer also expresses his appreciation to the other members of the Doctoral Committee, Professors V. S. Arpaci, R. E. Balzhiser, J. A. Clark, A. G. Hansen, and R. C. Juvinall for their many helpful suggestions.

The financial assistance of the National Science Foundation and the Bendix Corporation Fellowship Program are gratefully acknowledged.

The cooperation of the Industry Program of the College of Engineering in the preparation of the manuscript is highly appreciated.

TABLE OF CONTENTS

TABLE OF CONTENTS CONT'D

APPENDICES

LIST OF TABLES

LIST OF FIGURES

LIST OF FIGURES (CONT'D)

LIST OF FIGURES (CONT'D)

NOMENCLATURE

Other nomenclature is defined as necessary

a	Acceleration
a/g	Dimensionless acceleration
A	Area
C	Constants
C_p	Specific heat
D	Diameter
E	Voltage
f	Frequency
Fr	Froude number
g	Local gravitational acceleration
g_c	Mass-force conversion constant
Gr	Grashof Number
h	Convective heat transfer coefficient
I	Current
k	Thermal conductivity
ℓ	Length
Nu	Nusselt Number
Pr	Prandtl Number
q'''	Volumetric heat generation
q/A	Heat flux
R	Radius

T	Temperature
W	Uncertainty
α	Thermal diffusivity
β	Contact angle
δ	Thickness
θ	Angle or temperature difference
μ	Absolute viscosity
ν	Kinematic viscosity
ρ	Density
σ	Surface tension
τ	Time
ω	Angular velocity

Subscripts

b	Bubble or bulk
c	Center
f	Fin
ℓ	Liquid
sat	Saturation
sur	Surface
v	Vapor

CHAPTER I

INTRODUCTION

A. Purpose

For most practical heat transfer systems the influence of a variable force field is not significant, since most applications are only concerned with the earth's gravitational system. However, with the advent of space technology, the role of a variable force field, which may be produced by vehicle acceleration or by other gravitational systems, must be understood.

In recent years considerable effort has been expended in an attempt to describe the phenomena of boiling heat transfer. Owing to the complexity of the boiling process, many different physical models have been postulated and used in correlating heat transfer data. However, none of these correlations have been adequate in completely describing the boiling process. The major variable in all these correlations is the action of the bubbles in promoting the heat transfer. An understanding of the effect of a variable force field upon the action of the bubbles may lead to a better understanding of the boiling process and increases its effective application.

The purpose of this investigation was to study, by high speed photographic techniques, the effect of acceleration in the range 1 to 100 times the standard gravitational acceleration upon individual bubbles in boiling water, for a heat flux range of 15,000 to 75,000 BTU/hr-ft^2. From these high speed films the following bubble information has been obtained:

growths rates, departure size, maximum size, and frequency of departure. In conjunction with this bubble data, the heat flux, surface temperature, bulk liquid temperature and test surface saturation temperature were measured and are presented.

B. Literature Survey

The high rates of heat transfer in boiling systems have been ascribed by different researchers (5,16,21) to one or a combination of essentially three different phenomena. The first presumes the rapid growth of a vapor bubble on the surface imparts kinetic energy, and thereby high velocities, to the otherwise stagnant layer covering the heat transfer surface. The second presumes a latent heat transport from the heat transfer surface to the liquid, both by the latent heat required for the formation of bubbles and by mass transfer through the bubble. The third presumes the bubbles act as pumps to first push superheated liquid into the colder bulk liquid and then permits colder bulk liquid to replace the voids left by the collapsing or departing bubbles. The element common to all three modes of heat transfer is their dependence upon bubbles.

The first analysis of bubbles was performed by Rayleigh (45), who formulated the hydrodynamic aspects of bubble growth in an infinite, incompressible and inviscid fluid. His work was later modified by Plesset (3) in a study of cavitation bubbles by the addition of a surface tension term, resulting in the following expression:

$$R\ddot{R} + \frac{3}{2}\dot{R}^2 = \frac{\Delta P}{\rho_\ell} - \frac{1}{R}\frac{2\sigma}{\rho_\ell} \tag{1}$$

Fritz$^{(4)}$ formulated a relation for maximum bubble volume at departure by considering static equilibrium of surface forces and body forces. This equation is of the form:

$$V^{1/3} = .0119\,\beta\sqrt{\frac{2\sigma}{(a/g)(g/g_c)(\rho_\ell - \rho_v)}} \qquad (2)$$

where β is the outer contact angle in degrees. This equation has been validated by Jacob$^{(5)}$ for low heat flux saturated boiling at one standard gravity. Usiskin and Siegel$^{(6)}$, in a study of saturated boiling of water from a flat surface under reduced gravity conditions, found bubble departure diameters increased with a negative 1/3 to 1/4 exponent on gravity as compared with Fritz's theoretical exponent of -1/2. However, no measurements were made of the associated contact angles, which were assumed constant and thus independent of gravity. In a more recent investigation of boiling water by Siegel and Kenshock$^{(59)}$ under reduced gravity conditions, the bubble contact angle was found to be essentially independent of gravity. Slember$^{(48)}$, studied the saturated boiling of water from a .1 inch diameter wire and found the average bubble departure diameter to be proportioned to a/g raised to -.462 power for accelerations between 1 and 20 a/g at a nominal heat flux at 69,000 BTU/hr-ft^2.

The role of bubble dynamics as one of the contributing factors for bubble departure has been noted by Ellion$^{(52)}$, who observed bubbles being injected a considerable distance into the bulk liquid from both the upper and lower surfaces of a heating strip during subcooled boiling, and by Rohsenhow and Clark$^{(54)}$ in a study of forced convection boiling.

Griffith(53), photographed bubbles departing from a vertical heating surface, and postulated the following: as a bubble grows through the superheated layer near the surface and into the colder bulk liquid its growth rate decreases, and the rapidly moving liquid in front of the bubble must be decelerated. This deceleration creates a low pressure area in front of the bubble which tends to draw the bubble off the surface.

A photographic study of saturated boiling water in the absence of gravity by Siegel and Usiskin(56) seems to discount the influence of inertia forces in the mechanism of bubble removal. No evidence was observed of vapor bubbles being ejected away from the heat tranfer surface.

The equation of Fritz was emperically modified for saturated boiling by Staniszewski(7) to include a dynamic effect, resulting in:

$$R_d = R_o(1+\alpha \dot{R}_d) = .00355\,\beta \sqrt{\frac{2\sigma}{(a/g)(g/g_c)(\rho_l-\rho_v)}}\,(1+.435\dot{R}_d) \quad (3)$$

where $\dot{R}_d$ is the growth rate at departure, R_o is the bubble radius when $\dot{R}_d$ is zero and α is an experimentally determined constant.

Han and Griffith(8) have modified the Fritz equation on semi-theoretical grounds. These authors developed a departure criteria based upon the velocity and acceleration of the solid-liquid-vapor interface and have derived an expression for the departure radius in terms of this moving triple interface which is referred to as a "dynamic contact angle".

Zuber(55) developed a departure criterion based upon an analogy between gas bubbles being formed at an orifice and vapor bubbles being formed at a cavity in nucleate boiling. By relating the orifice diameter to a thermal boundary layer thickness, the following equation was obtained:

$$D_d = \left[\frac{6\sigma}{(a/g)(g/g_c)(\rho_l - \rho_v)} \, \frac{K(T_{sur} - T_{sat})}{q/A} \right]^{1/3} \tag{4}$$

The product of the frequency of bubble departure (f) and the departing diameter (D) has been shown by Jakob(5) to vary between 75mm/second and 150mm/second for water and carbon tetra-chloride for saturated boiling at atmospheric pressure. A number of investigators (e.g. (21) and (58)) have postulated, from Jakob's data, that the product fD is a constant. Staniszewski(7) reports an average fD product for water and methyl alcohol as independent of heat flux for low values of heat flux and increasing with heat flux at high heat fluxes.

The growth of vapor bubbles may be divided into three regions: initial, intermediate, asymptotic. The initial stage is characterized by a very slow growth from a nuclei where the effects of surface tension and vapor pressure control the process. The intermediate stage is a period of growth where liquid inertia is the controlling factor. In the asymptotic stages of growth, the effects of surface tension and liquid inertia became small and the growth is controlled by the heat and mass transfer process between the surrounding liquid and the vapor bubble.

One of the first theoretical expressions for bubble growth in the asymptotic stage was formulated by Fritz and Ende(51) in 1936. By assuming a temperature profile in the region of the bubble boundary equal to that for an infinite slab in unsteady conduction, the following expression was derived:

$$R = \frac{2k(T_{sur} - T_{sat})}{h_{fg}\rho_v\sqrt{\pi\alpha}}\tau^{1/2} \tag{5}$$

The asymptotic growth of bubbles, using the modified Rayleigh equation coupled with various heat transfer assumptions, has been studied by Plesset and Zwick(9), Forster and Zuber(10), and Bankoff and Mikesell(12)

Plesset and Zwick assumed that a linear temperature profile exists in a thin layer surrounding a spherical bubble and derived an expression similar to (5) except for a multiplying constant of $\sqrt{3}$. Forester and Zuber's theoretical expression is also of the same form as Equation (5), except for a multiplying constant of $\pi/2$. Bankoff and Mikesell assumed an exponentional temperature distribution in a thin thermal boundary layer and found bubble growth rates to be generally slower than that predicted by the square root of time as Equation (5). All used the same physical model of a spherical bubble in a uniformly superheated, infinite liquid, in thermodynamic equilibrium and with no gravity effects on the bubble or surrounding liquid. Griffith(11), modified these assumptions by assuming a hemispherical bubble in a region of linear temperature gradient. Each of these bubble growth equations have been compared by their respective authors, with the data of Dergrabedian (13,14,15), who measured the growth rates of bubbles in an infinite fluid, and all are found to be in fair agreement.

Direct effects of acceleration on bubble growth rates have not been considered in any theoretical growth expression but it might be expected that bubble growth rates will be influenced if the thermal boundary layer or if, for a given heat flux, $(T_{sur}-T_{sat})$ in Equation (5) is affected by acceleration.

An estimation of the relative importance of bouyant forces and inertia forces for a hemispherical bubble has been given by Forster and Adelberg(20) in terms of a bubble Froude number, which is the ratio of the inertia forces to bouyancy forces. Their results may be expressed as follows:

$$Fr = \frac{F_i}{F_b} = \frac{3R^2\dot{R}^2 + R^3\ddot{R}}{R^3(a/g)\,g} \qquad (6)$$

If the Froude number is on the order of unity, the inertia forces and bouyant forces will be approximately equal. For Froude numbers greater than unity the inertia forces would be expected to predominate, and for small values of the Froude number bouyancy forces will predominate. Consequently, it might be expected that an increase in the force field will significantly affect the boiling process for small values of the bubble Froude number, and will have little or no effect on the boiling process for large values of the bubble Froude number.

Clark and Merte(60) further evaluated Equation (6) by using the bubble growth equation of Forster and Zuber (Equation (5) with a multiplying constant of $\pi/2$) and calculated the Froude number for various liquids. They concluded from the large value of Froude number ($Fr = 13{,}900$) obtained for water with $R = .005$, $a/g = 1$, and $T_{sur}-T_{sat} = 16\,°F$, that the inertia forces certainly predominate under these conditions. If the bubble radius were on the order of the departure size ($R \cong .06$ inches for saturated boiling of water at atmospheric pressure) the Froude number at departure will be about 8 , which still indicates that inertia forces predominate. Using the departure radius in calculating the Froude number may be in serious error since the bubbles no longer approximate hemispheres, but if the Froude number were to remain constant for departing bubbles in a variable force field, the departure size would be preportional to $(a/g)^{-1/3}$.

Forster and Zuber(16) and Forster and Grief(17) used the growth equations of Forster and co-workers(10,18,19) to correlate boiling heat transfer data by equations of the form:

$$Nu = C\,(Re)^{m}\,(Pr)^{n} \tag{7}$$

where the values of C , m and n are determined experimentally. The Reynolds number used in this correlation was a so-called bubble Reynolds number of the form $\frac{R\dot{R}}{\nu}$, where R and $\dot{R}$ are determined from theoretical bubble growth rate equations and do not explicitly involve gravity effects. However, Forster and Adelberg(20) noted that this correlation is not necessarily independent of gravity, since the effects, if any, would be manifested in a new value of the experimentally determined constant C . Rohsenow(21) also used the general form of Equation (4) but utilized the following definition of a bubble Reynolds number in his correlation:

$$Re = \frac{G_b D_b}{\mu_\ell} \tag{8}$$

where G_b is the mass velocity of the bubbles at departure, D_b is the bubble diameter at departure and μ is the liquid viscosity. Since the departure diameter was calculated from Equation (2) by Fritz, a gravity effect is explicit in this correlation and predicts the heat flux for a given temperature difference as proportional to $(a/g)^{1/2}$. The correlations of Kutateladze(22) and Michenko(23) also used the results of Fritz and thus predict a gravity effect. The results of Labountzo(24), Levy(25), Mumm(26), and Chang(27) do not involve a gravity term.

Harrach(46), correlated boiling heat transfer data in a form generally used for natural convection:

$$Nu = C(Gr \cdot Pr)^n \tag{9}$$

Where the characteristic length in the Grashof and Nusselt numbers is an experimentally determined average maximum bubble radius.

It is evident, from the lack of consistent predictions concerning the effects of a variable body force in boiling heat transfer correlations, that experimental observations are necessary. In addition to the investigations already mentioned on the effects of a variable force field, a number of additional investigations have been performed in recent years.

Merte and Clark(1,2) have presented data on the effects of acceleration upon natural convection and pool boiling of nearly saturated water in the range of 1 to 21g's. Natural convection data was correlated by the standard Nusselt-Grashof-Prandtl numbers. For saturated boiling at low values of heat flux the temperature difference $T_{sur} - T_{sat}$, decreased with increasing acceleration and at high fluxes, increased with increasing acceleration. Since for increasing acceleration, Equation (2) by Fritz predicts a decrease in the departing bubble size with a possible corresponding decrease in liquid agitation, the authors postulate that the non-boiling convection at low heat flux increases sufficiently to lower the wall temperature and decrease the number of active nucleation sites. For subcooled boiling up to rates of 25,000 BTU/hr-ft^2, a maximum was observed in the value of $T_{sur} - T_{sat}$ as the subcooling was reduced to zero. This influence of subcooling had not previously been reported in the literature.

The data of Costello and Tuthill(33), in the range of acceleration $20 \quad a/g \leq 40$ and heat flux $10^5 \leq q/A \leq 2x10^5$ BTU/hr-ft^2, confirmed the general trends observed by Merte and Clark.

Graham and Hendricks,(50) have presented heat transfer data for $1 \leq a/g \leq 9$ and a limited amount of high speed photographic data for a/g equal to 1 and 7. When the boiling was characterized by vapor columns or bubble conglomerates, acceleration did not appreciably effect the overall heat transfer results. However, acceleration was reported to effect conditions for isolated bubbles near the threshold of nucleate boiling. Under these conditions, an increase in acceleration was reported to decrease the number of active sites, bubble growth rate, frequency of bubble formation and the maximum bubble size.

The theories for nucleate boiling do not predict the critical heat flux and therefore do not predict the effect of a variable body force upon the critical heat flux. However, a number of investigators(22,28,29) have predicted the critical heat flux to be proportional to $(a/g)^{1/4}$

Costello and Adams(30) reported burnout heat flux in an accelerating system as proportional to $a/g^{.25}$ for $10 < a/g < 45$ and proportional to $(a/g)^{.15}$ for $1 < a/g < 10$. Ivey(31), however, reports burnout data for water as proportional to $(a/g)^{.273}$ for $1 < a/g < 157$. Usiskin and Siegel(6), in experiments on burnout with water in a reduced gravity field from a ribbon insulated on one side, found that the maximum heat flux decreased with decreasing gravity, and that an exponent of 1/4 on a/g could be considered only as a limiting value.

CHAPTER II

EXPERIMENTAL APPARATUS

A. Introduction

In order to produce large accelerations for extended periods of time, a centifuge capable of accelerating a test package of 100 pounds mass to a maximum of 1000 times standard gravitational acceleration, was designed and built in the Heat Transfer and Thermocynamics Laboratory of the Mechanical Engineering Department.

The test package installed in the centrifuge was designed to photographically study the boiling of distilled and degassed water from a flat surface oriented perpendicular to the vectorial sum of the standard gravitational acceleration and the centrifugal acceleration. In order to provide flexibility, the system was designed with capabilities beyond those anticipated in this investigation. The initial design concept consisted of seven necessary capabilities the completed centrifuge should posses. These design requirements were:

1. Acceleration of a 100 pound test package to 1000g's.
2. Provisions for taking high speed photographs of the boiling process.
3. Provisions for 23 separate low resistance instrumentation channels.
4. Three separate and externally controlled high current AC connections to the rotating assembly.
5. Two separate fluid connections to the rotating assembly.

6. One constant low resistance, high current DC circuit to the rotating assembly.

7. Safety of personnel in case of mechanical failure.

The following sections describe the main features of both the centrifuge and the test package, with particular emphasis on the use of each component in this investigation. An overall view of the experimental apparatus is shown in Figure 1, and a cut-away drawing is shown in Figure 2.

B. Test Section

The design of the test section centered around the requirement of obtaining a high speed photographic record of the boiling process under high gravity conditions. In order to obtain clear pictures of bubbles and to simulate pool boiling, a flat narrow test section, directly heated by passing DC current through the strip was selected. Three observations made during a series of preliminary tests determined the final configuration of the test section. First, when a uniform cross section test strip was used, nucleating sites located along the edge of the strip emitted bubbles that obstructed the view of the bubbles being formed on the top of the strip. Second, the probability of photographing the complete life of an individual bubble would be very small if the test strip were too wide, since it is possible that more than one active nucleating site would be located along the optical axis, thus obscuring the field of view. Finally, density gradients in the water at distances far removed from the area of interest could distort the photographs.

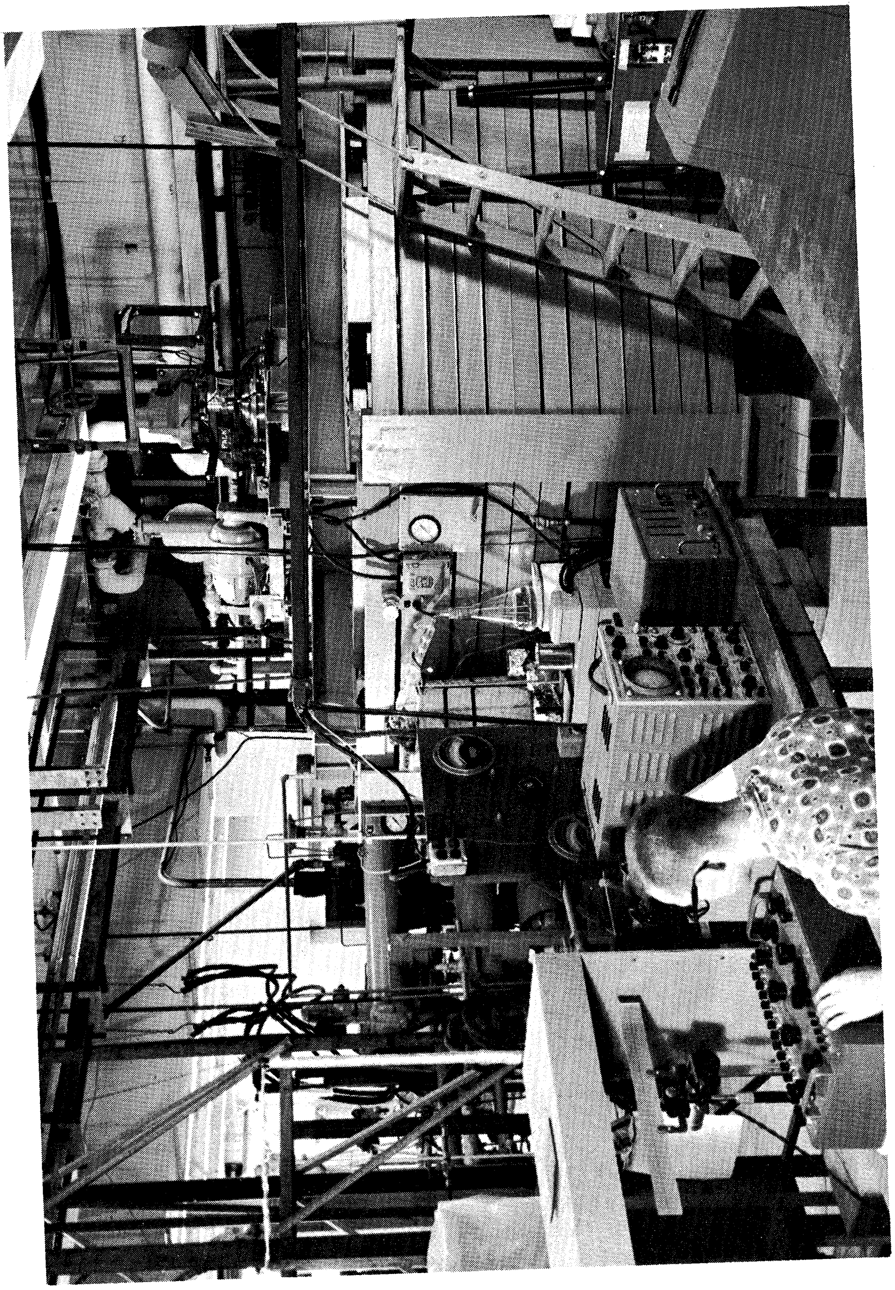

Figure 1. Overall View of Test Apparatus.

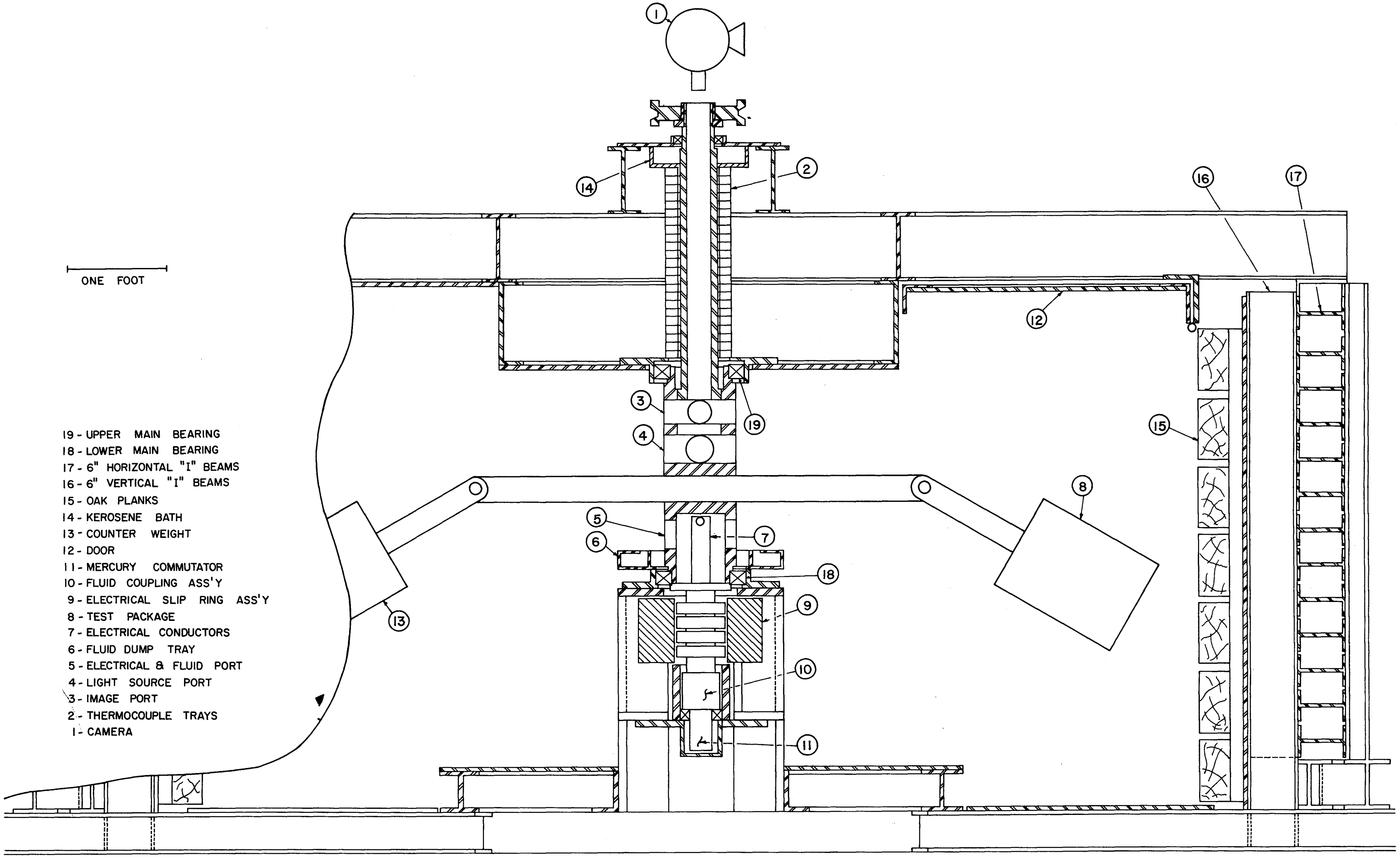

Figure 2. Section View of Centrifuge.

A scale drawing of the cross section of the assembly is shown in Figure 3 and two views of the test section assembly are shown in Figure 4. The test strip was constructed of two pieces of Chromel A resistance ribbon, silver soldered together. The upper section, which was the heat transfer surface and in contact with the water, was 0.250 inches wide by .002 inches thick by 5 3/4 inches long. Soldered to the bottom side and along the centerline of this thin section was a strip .09375 inches wide by .008 inches thick by 5 3/4 inches long. The silver soldering of the two pieces of Chromel A was accomplished by coating the narrow strip with a mixture of flux and powdered silver solder, and placing the two strips together in a pre-heated furnace. During the heating, small amounts of the solder flowed from between the two strips onto the underside of the strip. All traces of the silver solder were removed from the exposed portions by pickling the strip in a dilute nitric acid solution. An oxide layer, however, could not be removed by pickling without destroying the silver solder bond. It was therefore necessary to mechanically polish the test surface before it was used. No attempt was made to measure the surface roughness. However, the same test surface was used for the entire program, eliminating the surface conditions as a test variable. After the silver soldering operation, the ribbon assembly was bonded with epoxy to a 3/8 inch wide insulating support constructed from a fiberglass impregnated phenolic. The thermal coefficient of expansion of this phenolic was close to that of Chromel A, which permitted adhesion between the ribbon and the

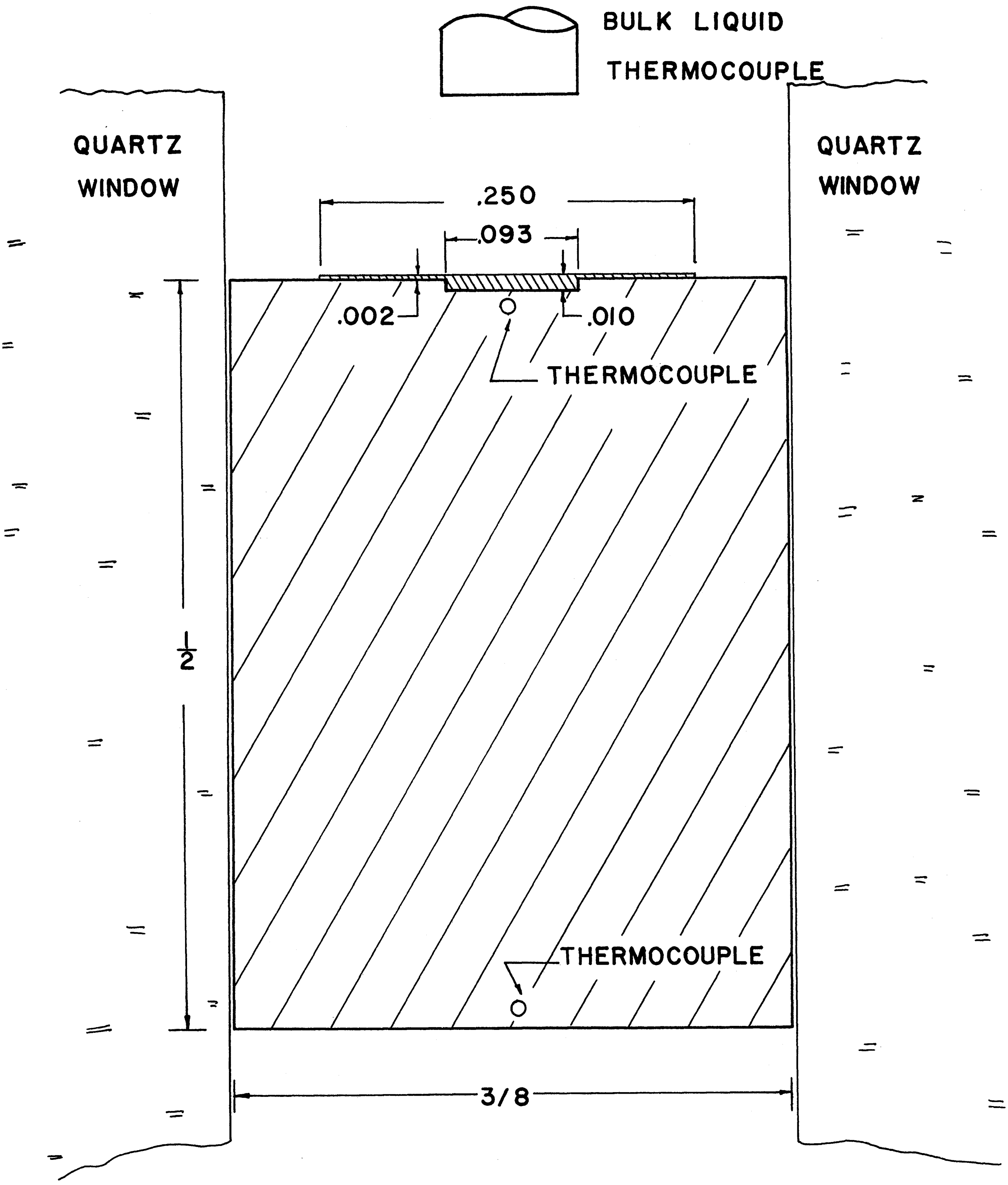

Figure 3. Scale Drawing of Test Section Assembly.

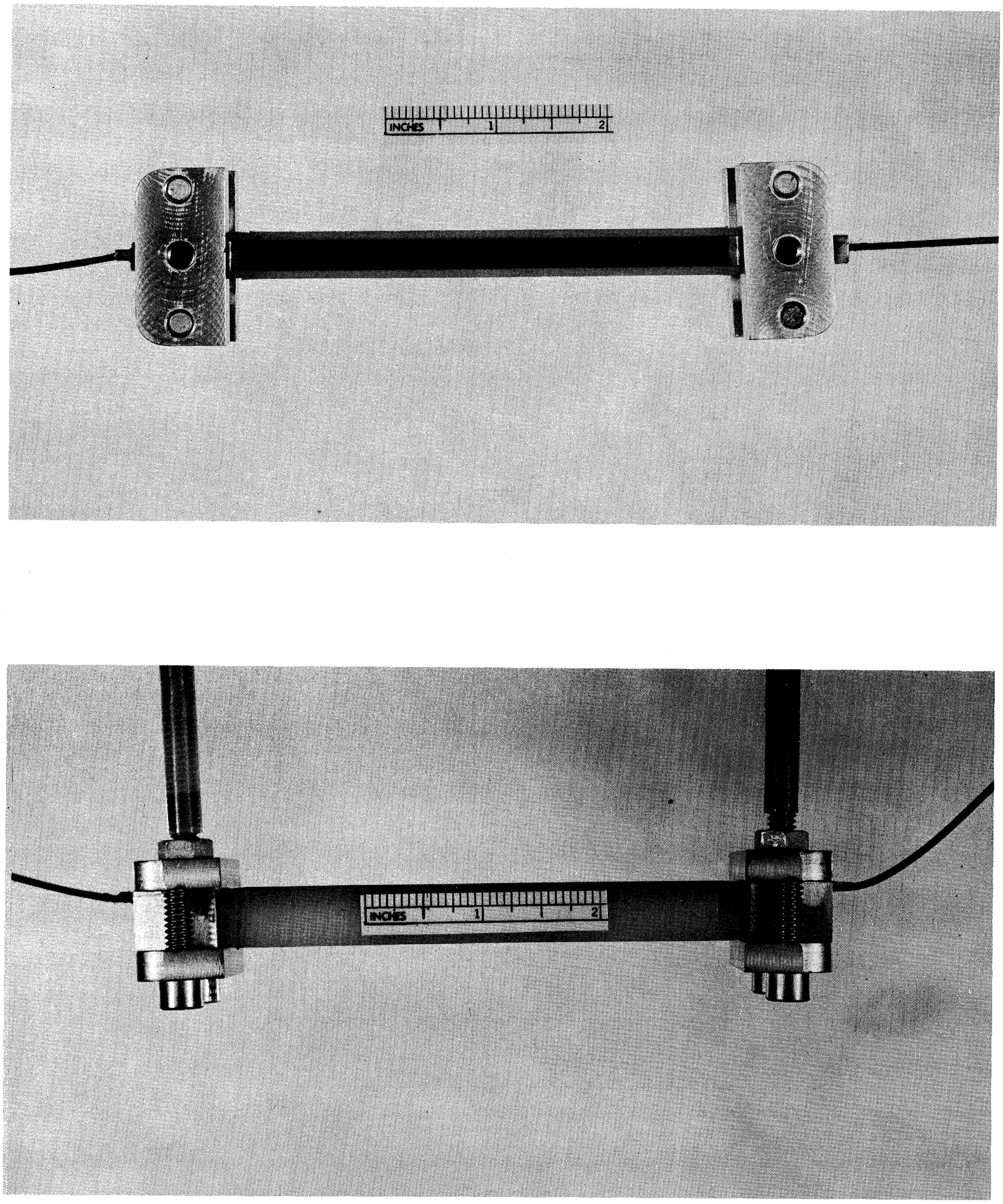

Figure 4. Side and Top View of Test Section.

support even with a 200°F change in the temperature level. With direct electrical heating of the test strip, the total heat generation in the center portion is greater than that along the sides, and with the lower side being insulated, boiling takes place only from the center portion of the top strip.

In order to minimize optical distortions caused by density gradients in the water at distances far removed from the test section, and to minimize the absorption of the light by the water, circular windows (viewing tubes) were placed against the insulating support. Stainless steel skirts (flow guides) were attached flush to the front of the viewing tubes and placed against the insulating support so that the area above the test strip assumed the shape of a regular prism with a width of 3/8 inches, a height of 1 1/2 inches and a length of 4 inches. A complete description of the construction of the sight tubes and flow guides is given later in this chapter.

Since the temperature difference between the heat transfer surface and the saturation temperature at the surface is the driving force which controls the boiling process, a thermocouple junction was placed under the test strip, from which the surface temperature was calculated. The thermocouple wires leading to the junction were placed parallel to and under the test surface to eliminate conduction losses along the wires. A complete discussion of the method used in calculating the surface temperature and the errors involved is presented in Chapter V.

C. Optical System

A high speed framing camera (Dynafax Model 326) manufactured by the Beckman and Whitley Company was used to photograph the boiling process. The framing rate of this camera is continuously variable from 200 to 26,000 frames per second, with the choice of three shuttering speeds at the top framing rate of 1, 2.5 or 5 microseconds. This camera uses both a rotating film drum and a rotating octagonal mirror to take a maximum of 224 pictures on a 33 7/8 inch long 35 mm film strip with a uniform framing rate. The framing rate was determined within ± .02% by means of a built-in magnetic pickup which provides an input signal to an electronic counter.

The pictures are the size of a standard 16 mm frame and are positioned side by side on the 35 mm film. The film can be either the standard 35 mm perforated or unperforated, or special triple perforated 35 mm. With the triple perforated film, the film may be slit into 3 pieces (two 16 mm wide strips and one piece of scrap 3 mm wide) and projected in a standard 16 mm projector.

Two different types of shutters are used with the Dynafax. One is internal to the camera, utilizing the rotating mirror and diamond shaped stops which control the shuttering of the individual frames. The other shutter is a standard type and controls the total writing time by opening, remaining open for one revolution of the film drum, and then closing. If the open time is too short, fewer than the maximum of 224 frames will be taken. If the open time is too long, some frames will be double exposed. Due to the normal variations in the open time of this shutter, only 180 to 200 frames were generally available.

The short length of film permitted development and examination of the film within 15 minutes after exposure. A disadvantage to this short film length is that only a short period of time was recorded (20 ms at 10,000 frames/second). In order to obtain representative samples, it was necessary to take a number of films at each test condition.

Loading and unloading of the camera was performed in daylight by means of a light tight cassette which is loaded and unloaded in a darkroom.

Since this camera cannot withstand acceleration forces other than normal gravity, provisions were made for transmitting the picture from the test package to a point on the axis of rotation just above the top of the centrifuge. This system enabled the camera to be supported from the ceiling of the laboratory in a fixed position that is isolated from any vibrations. Figure 5 is a photograph of the camera in its operational position.

Figure 6 is a schematic drawing of the optical system used to transmit a picture from the test strip to the camera. Since the minimum distance between the camera and the test strip was 110 inches, it was necessary to use a highly efficient back lighting system to illuminate the test area. The light source used was a 100 watt zirconium arc lamp placed on the axis of rotation within the main shaft to minimize centrifugal acceleration imposed on the lamp. This lamp has a small .030 inch diameter source enabling an approximately parallel light beam to be generated with a 6 inch focal length condensing lens located at the focal distance from

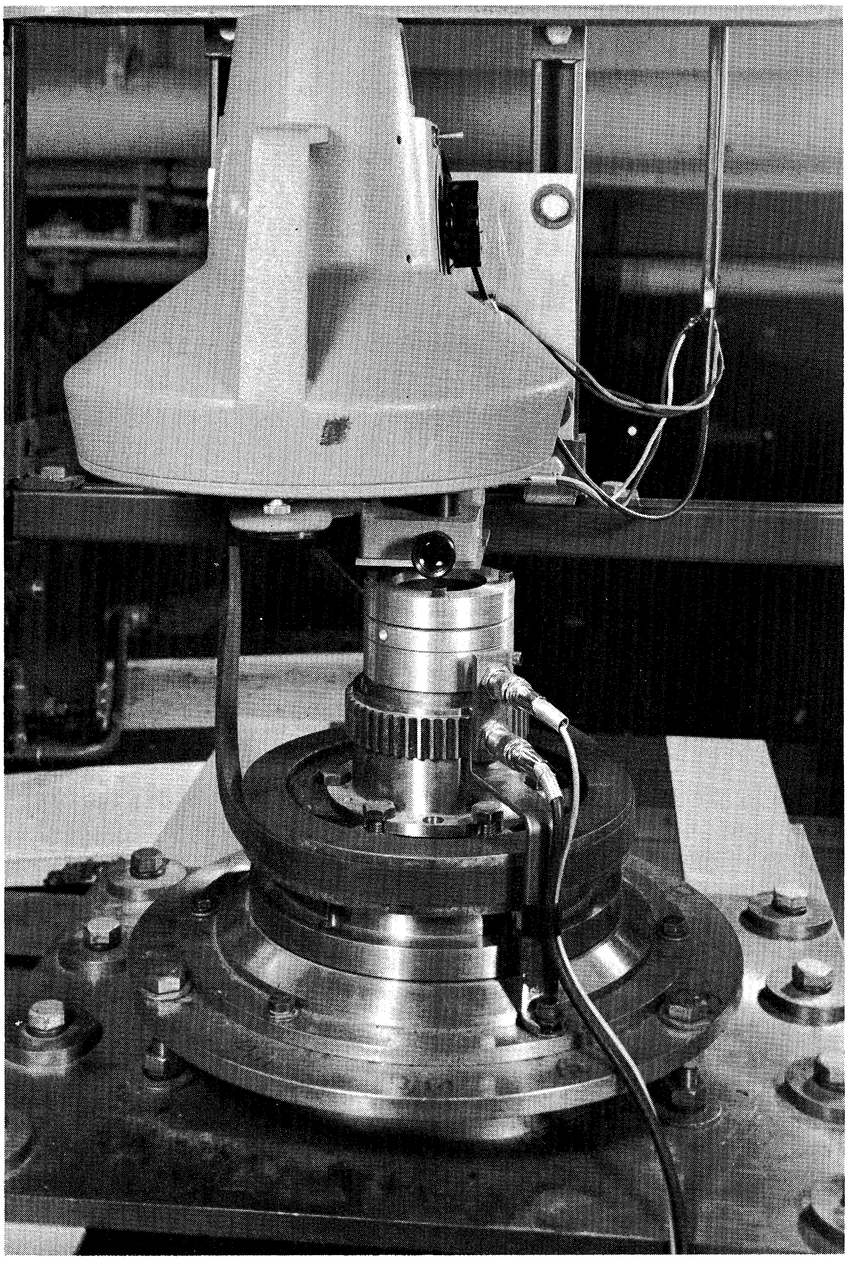

Figure 5. Camera in Position Above Centrifuge.

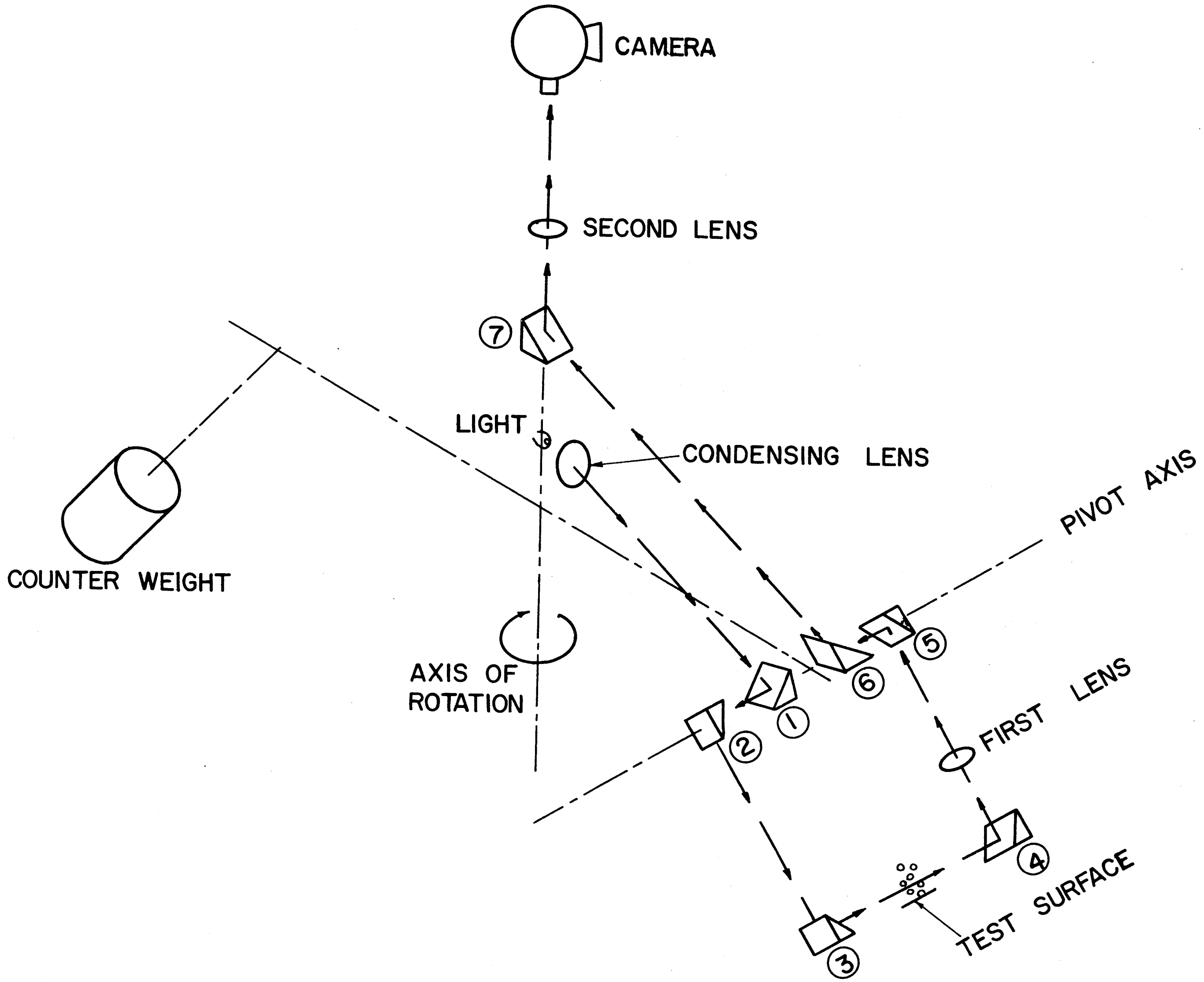

Figure 6. Optical System.

the source. By changing the position of the condensing lens relative to the light source, a diverging light beam could be generated which would reduce the light intensity at the camera. This was the method used for controlling the exposure of the film. The starting voltage for this lamp is 2000 volts and the operating voltage is 50 volts. The electrical connections to the lamp from the external power supply were made through four of the instrument channels. With this lighting system, a medium speed, fine grain film (Kodak Plus X) was sufficiently exposed at all camera speeds used (5,000 to 20,000 frames per second).

The light beam was transmitted by a mirror system to the test area. The beam then passed through two objective lenses mounted on the rotating assembly as it was transmitted to the camera by another mirror system. The two objective lenses were a matched pair with 18.25 inch focal lengths and 2.50 inch diameters. The first lens was placed so that its focal point was near the test area. The second lens had its focal point placed at the front focal plane of the camera. With the two lenses in these positions, a picture of unity magnification was transmitted a distance of 110 inches with little light loss and high resolution. By adjustments of the location of the two lenses, the magnification could be varied between .8 and 1.2. Due to an optional mismatch between the requirements of this external optical system and the internal optical system of the camera, a certain amount of vignetting of the photographs was unavoidable. In Appendix A are examples of the photographs which illustrate the quality obtained.

A total of seven front surface mirrors (numbered one through seven on Figure 6) were required to transmit the light beam to the test area and then to the camera. Two of the mirrors (1 and 6) were mounted on the test package pivot axis but fixed to the cross arm. Two more mirrors (2 and 5) were mounted on the pivot axis but were fixed to the test package and thereby permitted to rotate about the pivot axis with the test package. These four mirrors enabled the light beam to be transmitted to the test package and remain in the same position relative to the test package for all angular positions of the test package with respect to the cross arm. One mirror was mounted on the end of each viewing tube (3 and 4) which transmitted the light beam across the test strip. The last mirror (7) was located on the axis of rotation of the main shaft to transmit the beam up through the second lens and to the camera.

D. Test Package

The function of the complete test package assembly is twofold: first, to provide controllable test conditions and second, to provide mechanical support for the associated components. Figure 7 is a detail drawing of the test package assembly and Figure 8 is a view of the assembly as it is supported from the cross arm.

The basic test vessel (inner container) was constructed of 6 inch diameter 304 stainless steel pipe, the upper portion of schedule number 10 and the lower portion of schedule number 40. Two stainless steel tubes with internal threads were welded into

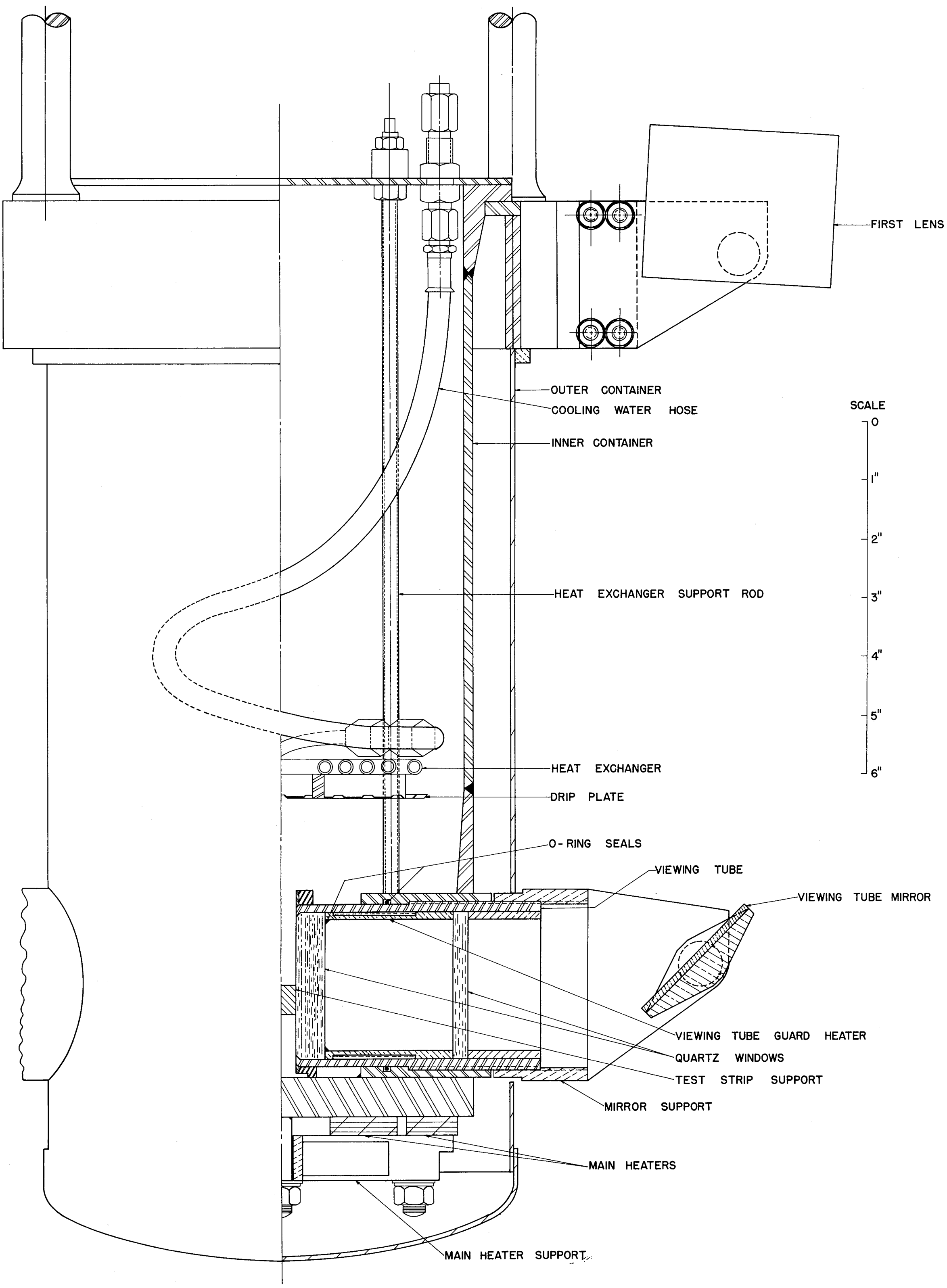

Figure 7. Detail Drawing of Test Package.

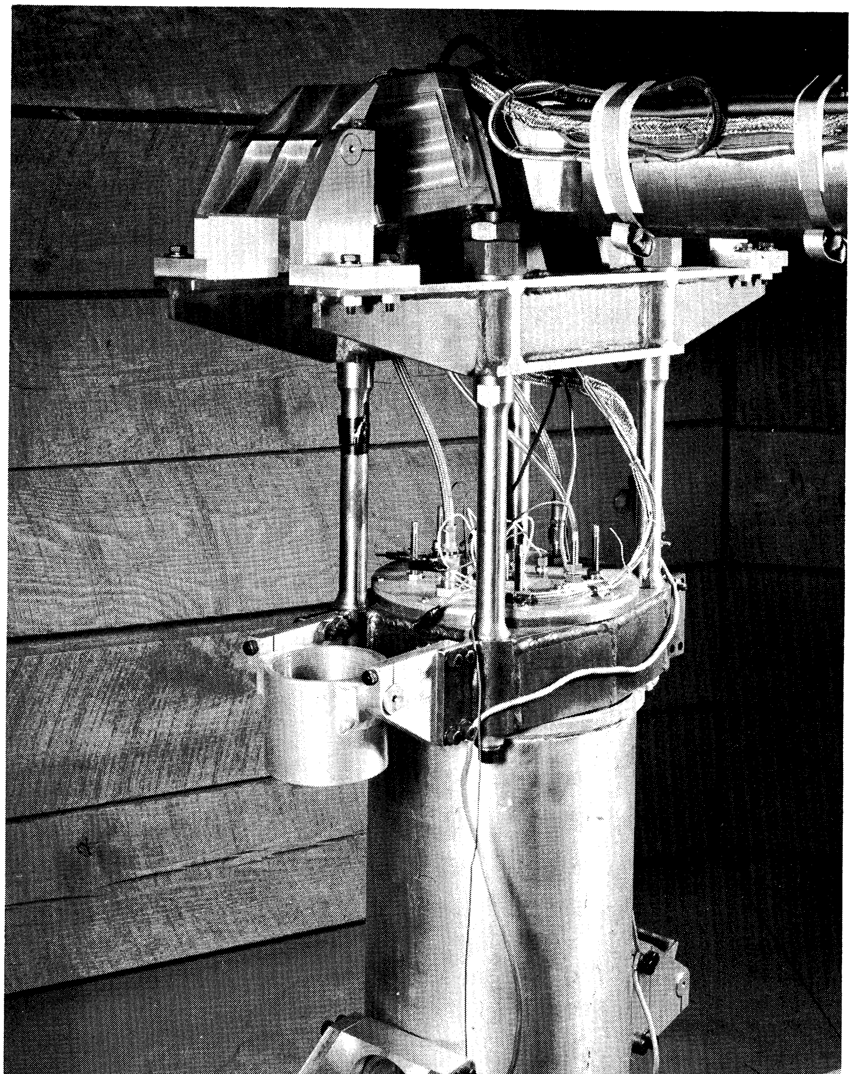

Figure 8. Test Package.

the schedule number 40 portion to support the viewing tubes and lower mirrors. The inner container was supported in a fixed position by four high alloy steel rods connected to an upper frame as seen in Figure 8. The upper frame served as a support for mirrors two and five (see Figures 6 and 8) and as the pivot point for the test package. Pivoting of the test package assembly is necessary in order to maintain the vectorial sum of gravitational acceleration and centrifugal acceleration approximately perpendicular to the test surface. The inner container was wrapped with fiberglass insulation to minimize heat losses. An outer container, fabricated from thin wall aluminum tubing, was fastened to the bottom of the four rods and helped insulate the inner package.

Fastened to the flat bottom of the inner container were two ring Chromalex heaters of 700 watt total capacity. These heaters were held to the bottom of the inner container by an I section cross frame. Thermal contact between the heaters and the inner container was enhanced by embedding the heaters in Thermen cement. These heaters were used before a test to de-aereate the water, and during a test to control the bulk liquid temperature.

The cover for the inner container supported an assembly consisting of the test section, heat exchanger, and thermocouples. This inner assembly is shown in Figure 9. The heat exchanger served the purpose of condensing the water vapor formed either during a test or during the de-aereation of the test water. The heat exchanger was constructed from 1/4 inch wall stainless steel tubing, wound in a helical manner, and attached to a cross arm. This cross frame was

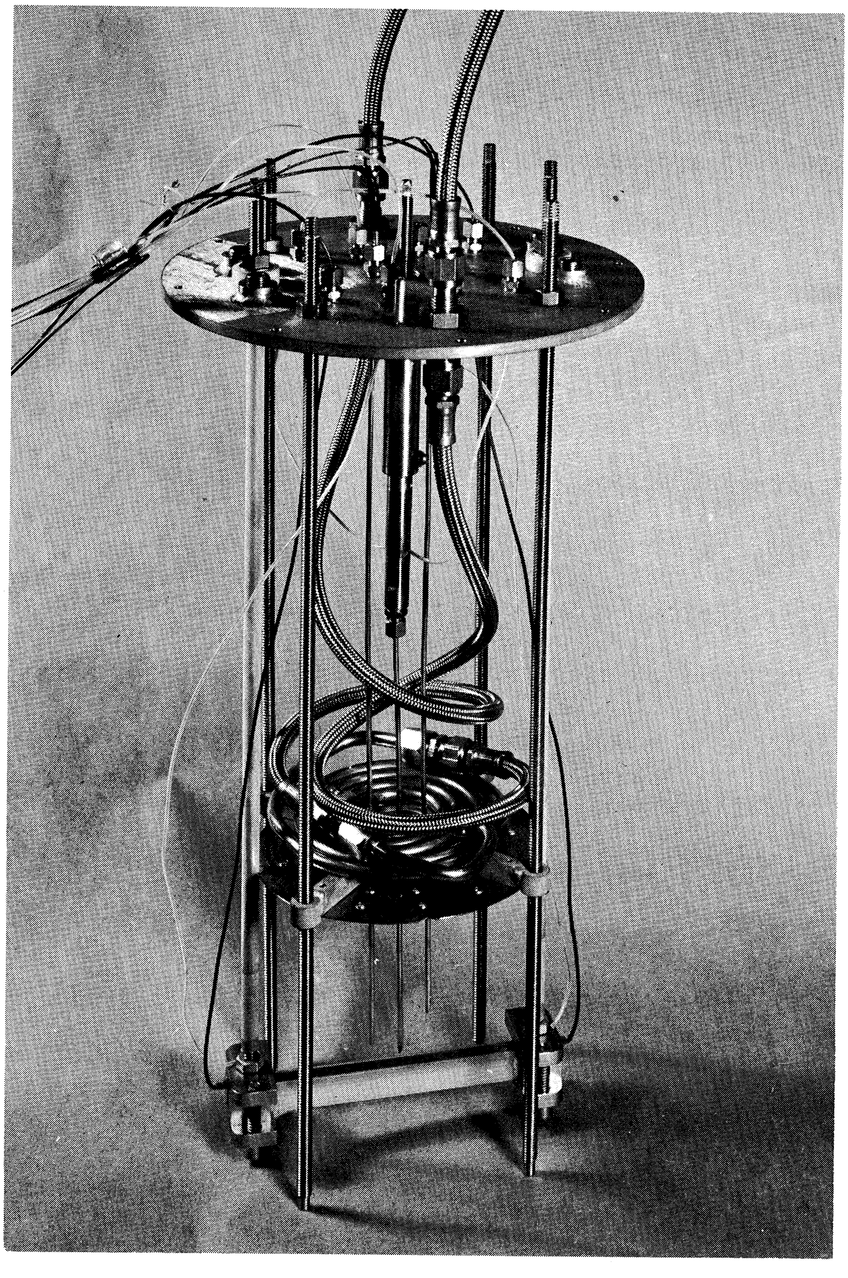

Figure 9. Inner Assembly.

supported from the cover by four 1/4 inch diameter threaded stainless steel rods, thus allowing the heat exchanger to be positioned at any desired level within the inner container. A drip plate was attached to the bottom of the cross frame and acted as a counter flow heat exchanger. This construction prevented cold water from falling directly from the heat exchanger coils into the test area. The drip plate was fabricated from 16 gauge stainless steel sheet and contained numerous 1/16 inch holes with turned up edges. Since the heat exchanger position was not fixed, the connections from the cover to the heat exchanger were by necessity flexible. These flexible connections were commercially available teflon tubing with a stainless steel braid outer jacket for strength.

Three thermocouples were mounted through the cover by means of Conax thermocouple glands. The thermocouples were positioned 1/8, 1/4, and 1 inch above the test strip to measure the bulk liquid temperature. The thermocouple sheaths were constructed from thin wall, .093 inch outer diameter stainless steel tubing. One end of each tube was pinched off, ground to shape, silver soldered closed and chrome plated. The thermocouple junctions were covered with a thin coating of epoxy for electrical insulation and then coated with Technical G copper cement for thermal contact and inserted into the sheath.

The test section was supported from the cover by two 1/4 inch stainless steel rods attached to the cover through teflon insulators. The bottom end of the rods were threaded into stainless steel blocks which clamped around the test support. Electrical contact between the blocks and the test strip was made through a small piece of lead compressed between the strip and the block at the front edge. The portion of the strip under the block was electrically insulated from the block by a piece of teflon and thus at a constant potential. The voltage taps were connected to the strip in this region.

The viewing tubes were constructed from 2 1/2 inch diameter schedule number 160 stainless steel pipe. The test package detail drawing (Figure 7) shows the construction of the viewing tubes. An exploded view of the viewing tubes is shown in Figure 10. External threads were machined on the outside of the tube for about 1/2 of the length to permit the tubes to be screwed into the test package. A water tight seal was made between the test package and the tubes by means of O-rings sealing against the unthreaded portion of the tube. The internal portion of each tube consists of two optical flat circular quartz windows, a heater, two spacers and a lock nut. The front quartz window of each tube was beveled to match a similar bevel inside the tube so that the window was flush with the front of the tube. The guard heater was fabricated from an aluminum tube with the center section of the outside diameter machined down to permit a 16 foot length of resistance wire to be wound on it. One end of the heater was beveled and used to compress an O-ring seal against the front quartz window. A rear quartz window was used to enclose a quantity of air within the tube. The guard heater was used during a test to

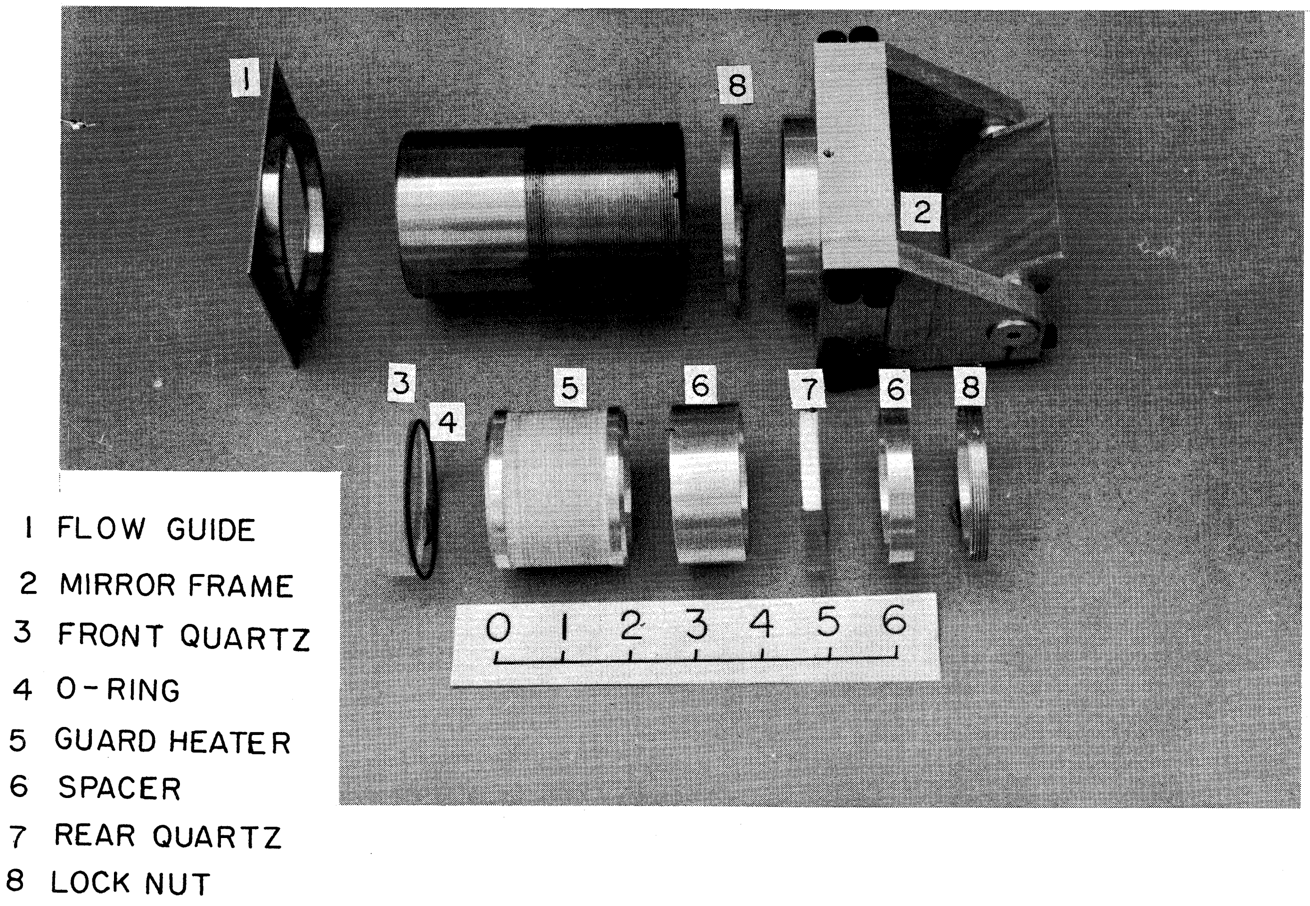

Figure 10. Exploded View of Viewing Tubes.

heat both the enclosed air within the tube and the front window to a temperature level equal to the bulk liquid above the test strip. The temperature level within the viewing tube was monitered by a thermocouple placed against the front window.

The flow guides consisted of a 3 inch by 4 inch by 16 gauge stainless steel plate with a circular hole in the center screwed to a circular ring as seen in Figure 10. The ring and the viewing tube were beveled so that when the flow guide was placed over the end of the viewing tube, the front face of the flow guide was flush with both the front sight quartz and the front edge of the tube.

E. Counterweight

The outer construction of the counterweight was made to resemble the outer configuration of the test package to minimize any unbalanced torques introduced by unequal air resistance during rotation. Figure 11 is a photograph of the counterweight as it is supported from the cross arm.

The inner portion of the counterweight was constructed from six inch schedule number 10 stainless steel pipe with an elliptical end cap welded on one end. This inner container was supported on threaded rods connected to the upper frame work in such a manner that the center of gravity of the counterweight could be adjusted to equal the center of gravity of the test package. In order to make the weights of the test package and counterweight equal, lead shot and water was added to the inner container of the counterweight.

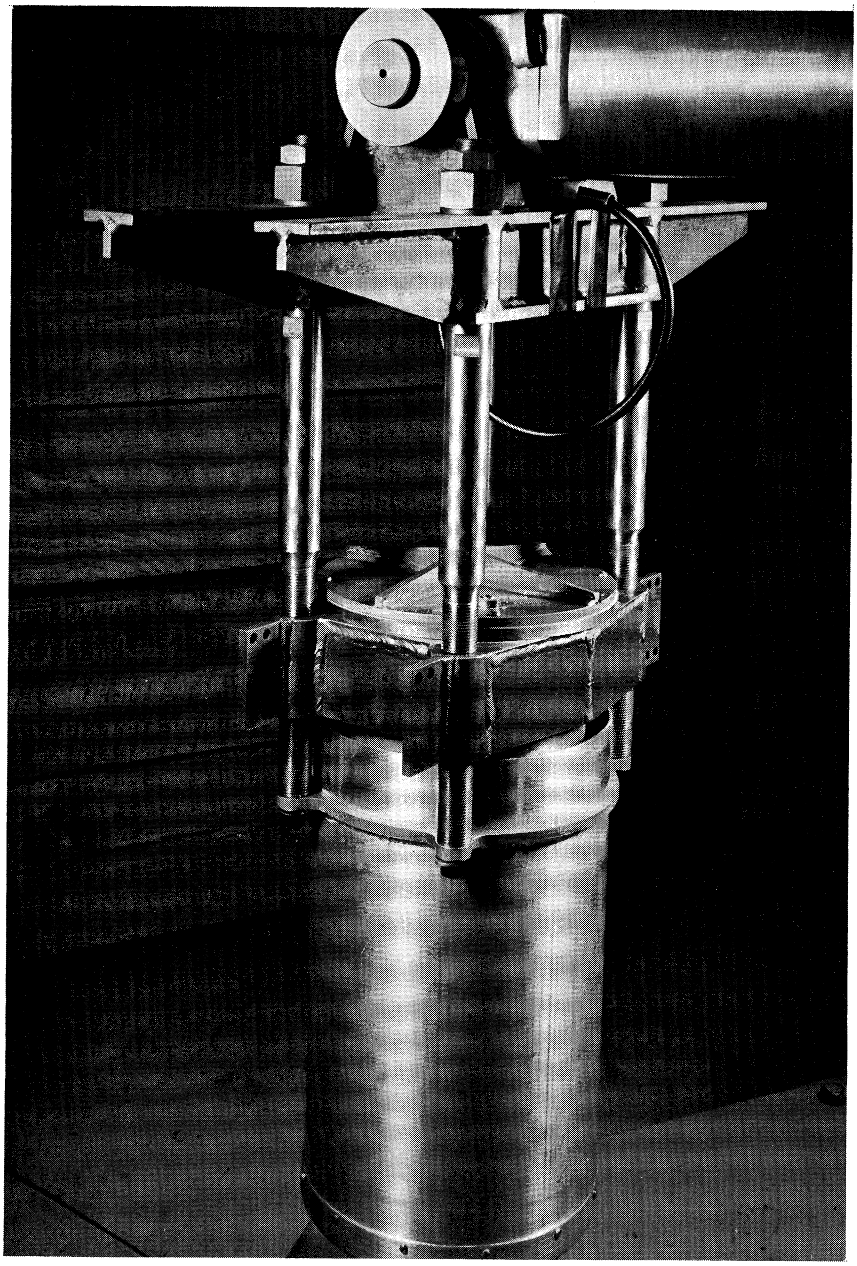

Figure 11. Counterweight.

Threaded into the cover of the counterweight is a 1/2 inch diameter by 12 inch long rod used for fine adjustment of the center of gravity. The threaded rod was connected to a small reversible AC gear motor that could be operated in either direction while the centrifuge was operating. By means of the course adjustment of the inner package and fine adjustment of the threaded rod, the unbalanced force could be reduced to below 25 pounds force.

F. Main Shaft

A detail drawing of the main shaft assembly is shown in Figure 12. This assembly is divided into three sub-assemblies; upper, center, and lower. The upper sub-assembly (the portion above the upper main bearing) contains the 23 instrument channels, second objective lens, v-belt drive sheave and kerosene bath. The center sub-assembly (between the two main bearings) consist of the center shaft, cross arm, light source, condensing lens, and one mirror. The lower sub-assembly (below the lower main bearing consists of the AC and DC electrical power connections and the rotating fluid couplings.

1. Upper Sub-Assembly

All components in the upper sub-assembly are positioned around a 4 foot long by 3 1/2 inch diameter hollow drive tube. This tube is keyed to the sheave at its top and to the center sub-assembly at its bottom. All side thrust from the sheave is taken by a ball bearing located just below the drive sheave.

In order to remove thermocouple voltages from the rotating equipment and to provide low power connections to the light source,

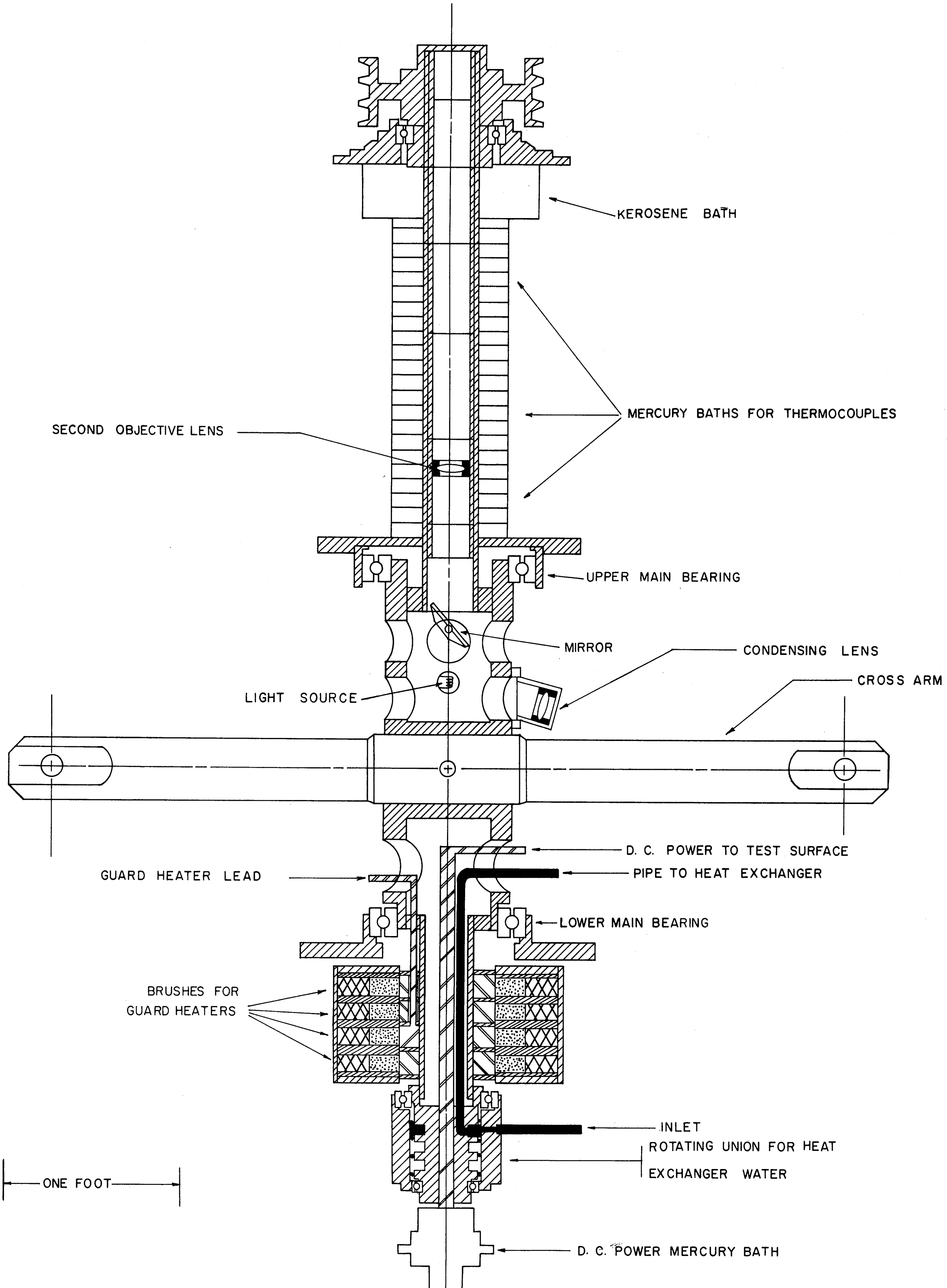

Figure 12. Detail Drawing of Main Shaft.

23 instrument channels (mercury slip rings) were provided. The construction of these slip rings is shown in Figure 13. Each individual slip ring assembly consists of a circular plexiglas trough (stator) partially filled with mercury and machined to interlock with identical troughs above and below. The stationary wire enters into the mercury through the plexiglas near the bottom of the stator. A plexiglas rotor fits between each pair of stators and carries the rotating wire. At high rotational speeds, the rotating wire creates a highly turbulent flow pattern in the mercury necessitated labyrinth seals and close tolerances to prevent mercury from escaping.

Figure 13 also shows a large kerosene bath assembly located above the top mercury slip ring. The construction of this kerosene bath is similar to the mercury slip rings but on a larger scale. A labyrinth seal system was also necessary for the kerosene bath to prevent kerosene from falling into the mercury. Section I in this Chapter describes in detail the thermocouple circuit and the use of the kerosene bath.

2. Center Sub-Assembly

The center sub-assembly consists of an 8 3/4 inch diameter by 27 inch long center shaft with numerous mounting brackets, access holes and a cross arm. Of the two main bearings, one at each end, only the lower bearing supported the weight of the rotating assembly. Figure 14 is a photograph of the center sub-assembly.

The 60 inch long by 4 1/2 inch diameter cross arm was fabricated from type 4340 steel quenched and tempered, and pinned

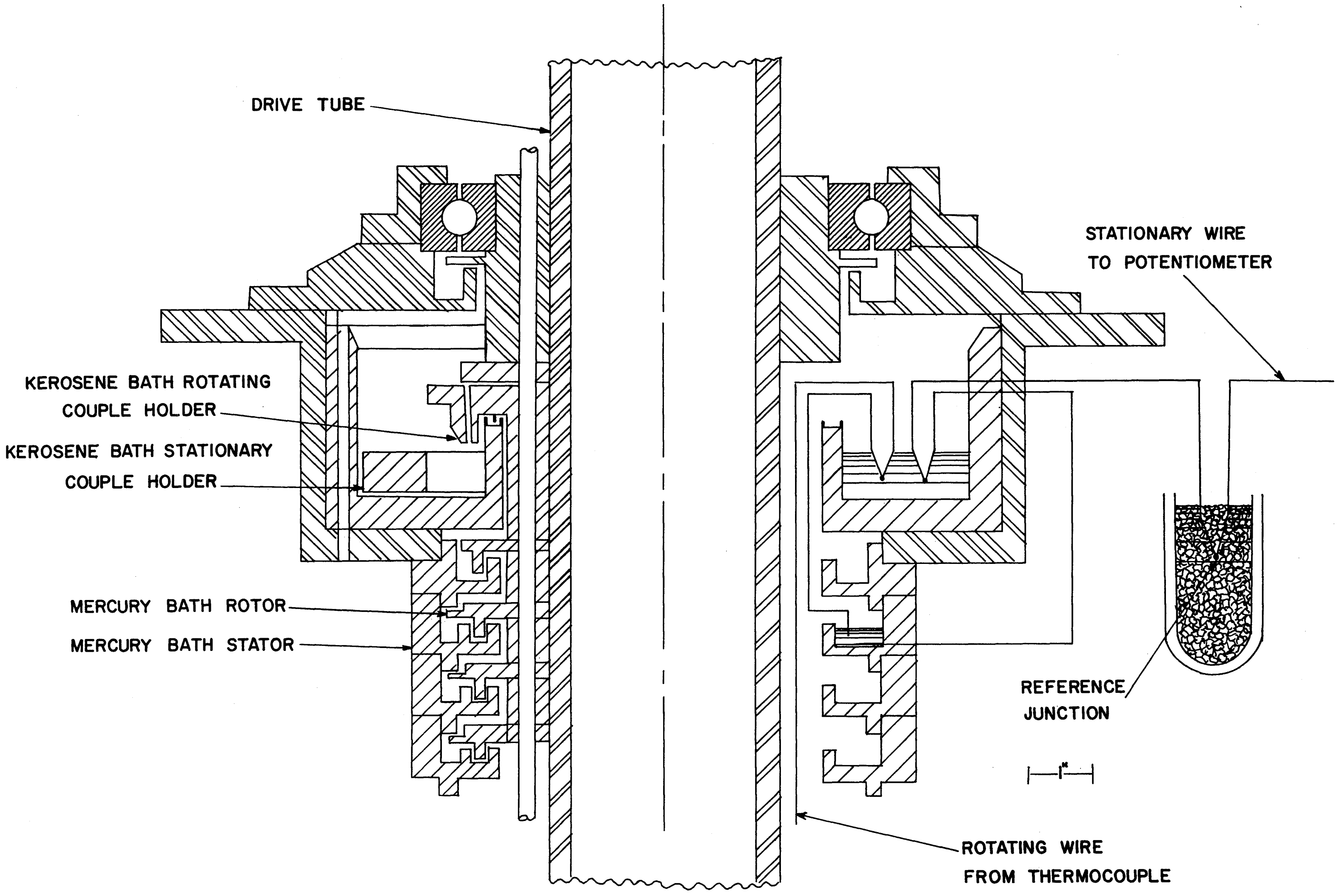

Figure 13. Detail Drawing of Mercury Slip Rings and Kerosene Bath.

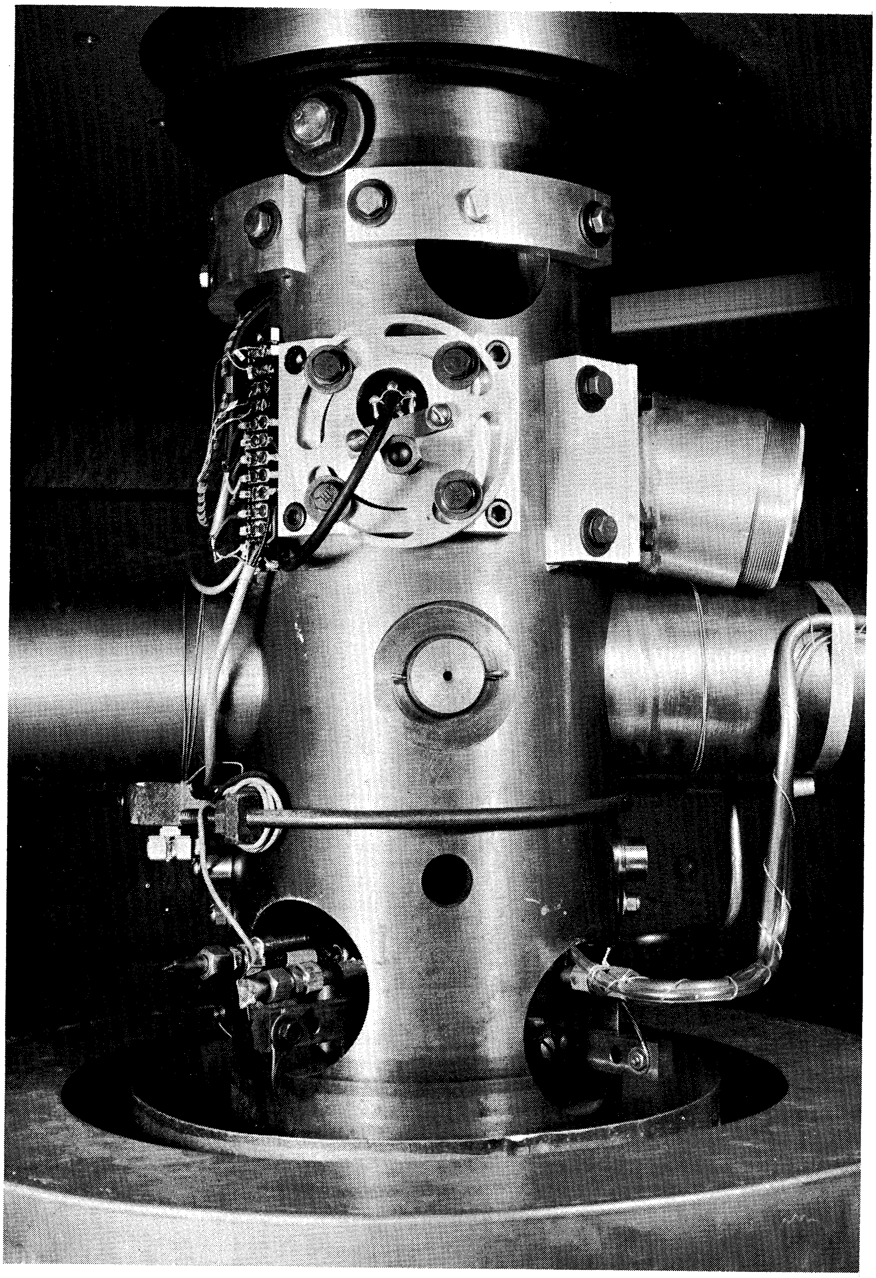

Figure 14. Center Sub-Assembly.

to the center shaft. Pinning of the cross arm was used so that in case of mechanical failure of either the test package or the counterweight the cross arm would not slide out of the center shaft.

Mounting brackets for the lamp and condensing lens were designed with sufficient adjustment capabilities to enable the light beam to be correctly aleigned with respect to the condensing lens and the first mirror. The bracket for the number seven mirror (Figure 6) provided rotational adjustment of this mirror to permit the center of the image to proceed up the hollow drive tube along the axis of the tube.

3. Lower Sub-Assembly

The lower sub-assembly, consisting of the electrical power and fluid connections, was supported below the lower main bearing by a 3/4 inch diameter copper rod, screwed into a pin mounted across the main shaft and held in correct alignment by the fluid coupling stator. The main features of the lower sub-assembly may be seen in Figure 12. Torque was transmitted to the lower sub-assembly from the center shaft by a key located above the AC slip rings. All power and fluid connections from this assembly passed through the center of the lower main bearing and out to the test package through four access holes in the center shaft.

The direct current power for the test section was supplied through a dual channel mercury slip ring assembly shown in Figure 15. This assembly is located at the lower portion of the main vertical shaft, and is supported by the 3/4 inch diameter copper rod attached

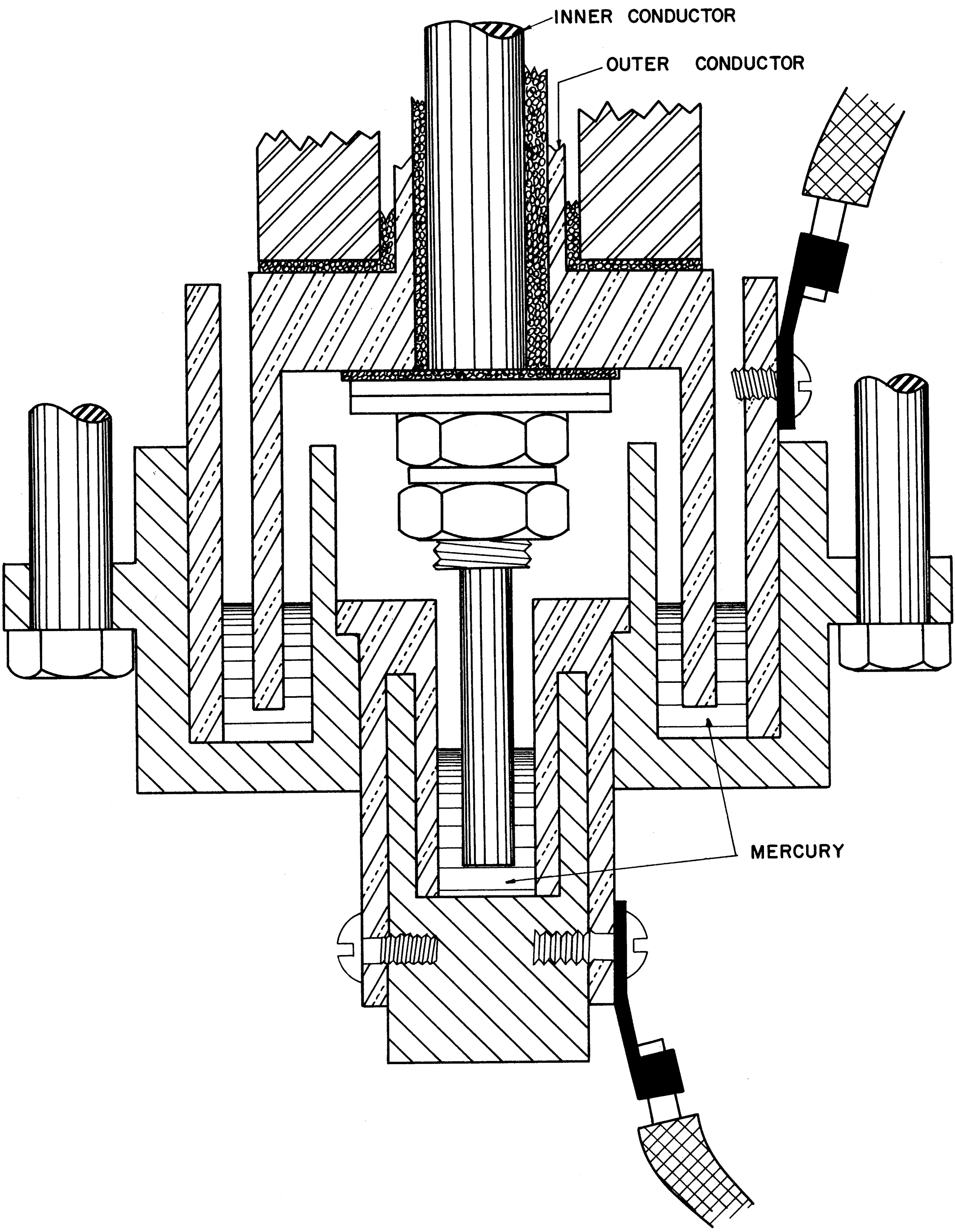

Figure 15. Detail Drawing of DC Mercury Commutator.

to but insulated from the center shaft. This rod also acted as one of the rotating conductors. The other conductor was constructed from a 1 1/4 inch diameter copper tube which was concentric with and insulated from the inner conductor. Electrical contact was made through the mercury from a stationary to a rotating copper electrode. Due to the large size of these copper electrodes, the deterioration of the copper by mercury amalgamation was not a problem.

The direct current supply was furnished by a motor generator set capable of producing a maximum current of 3000 amps at 15 volts. In order to reduce the 400 cps ripple, which amounted to approximately 6% of the average DC value, a bank of automobile batteries were placed parallel with the DC line. By adjusting the voltage output of the MG set to a value slightly in excess of the battery voltage (2, 6, 8, or 12 volts), the ripple was reduced to approximately 2% of the nominal value. The voltage was then controlled at the desired level with a large series resistor.

The current was determined by measuring the voltage drop across a .01 ohm Leeds and Northrup precision resistor in series with the test strip, using a type K-3 Leeds and Northrup potentiometer. The test strip voltage was measured by utilizing a 100:1 voltage divider connected in parallel with the test strip. This voltage divider was calibrated by reducing the impressed voltage to below 1.5 volts and measuring both the divided voltage and the actual voltage on the K-3 potentiometer.

Located just above the DC mercury commutator are three rotating fluid couplings. These couplings enabled cooling water to flow to the test package and return. Only two of the three couplings were used in the present test. The rotating seals were Buna-N O-rings which sealed and rotated against highly polished lands on the rotor. Two bearings, one at each end of the rotor were used to keep the rotor and stator concentric. The stator was held in a fixed but adjustable position so that the complete lower sub-assembly could be positioned to rotate about the axis of the two main bearings.

All heaters in the test package were furnished with 60 cycle voltage, controlled by Variacs and supplied to the rotating section by means of silver graphite brushes riding on copper rings. All three heaters were operated from a common ground, necessitating only four individual slip rings. The complete slip ring assembly is located above the fluid coupling and below the bottom main bearing and may be seen in Figure 12.

G. Balance Equipment

Balancing of the rotating assembly was accomplished by attaching strain gauges to four thin aluminum webs and restraining the horizontal movement of the main upper bearing plate with these webs, as shown in Figure 16.

The four strain gauges were connected as a four gauge bridge network, the output being displayed on an oscilloscope. Any tendency for horizontal movement of the upper bearing plate

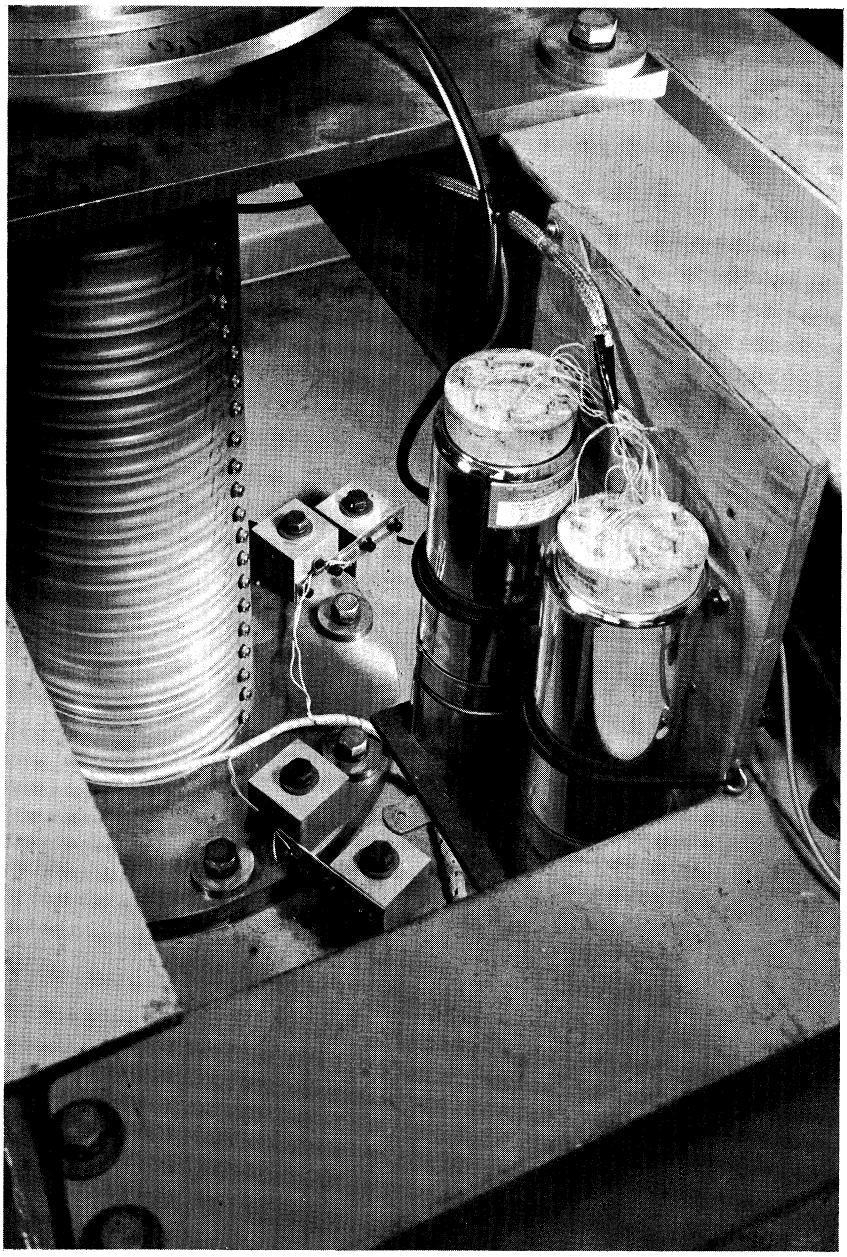

Figure 16. Balancing Webs and Mercury Slip Rings.

due to unbalanced forces in the rotating assembly was restrained by these webs and resulted in an approximately sinusoidal voltage output. The angular position of the unbalance was determined by triggering the sweep of the oscilloscope from a known angular position of the shaft assembly by a magnetic pickup.

H. Drive Unit

A 7 1/2 horsepower General Electric dynamometer was used to rotate the main shaft assembly. The output of the dynamometer was geared down by a 6.15:1 Falk gearbox and was connected to the main shaft by a v-belt drive.

I. Thermocouples

Table I lists the seven thermocouples and their locations as used in this investigation.

Chromel-constantan thermocouples were chosen because of their inherently high EMF and corrosion resistance. A disadvantage in the use of this thermocouple was the lack of an adequate standard. The Bureau of Standards table(47) lists millivolts to three significant figures and temperatures every 10°F, which is adequate for interpolating to about 1/2°F. A more detailed standard was generated by plotting the difference between two successive millivolt values versus the average temperature, drawing an arbitrary smooth curve through these points, and graphically integrating under the curve. The curve was continuously adjusted so that the integrated value (millivolts to 4 significant figures) would, in general, round off to give the value in the original table (millivolts to 3 significant figures). By this means, a new standard is now available that may be used for interpolating to .1°F. For precision temperature measurements, the thermocouples must be calibrated in the range of interest.

The calibration of the thermocouples was performed by comparison with a calibrated platinum resistance thermometer. A group of 12 thermocouples and the resistance thermometer were placed in a constant temperature block, which is part of the equipment of the Heat Transfer and Thermodynamics Laboratory. This constant temperature block can maintain values of temperature to within .01°F at any level between room temperature and 900°F.

The maximum spread of all 12 thermocouples from their average was less than ± .1°F up to 300°F. A single deviation curve using the average value of the 12 deviations was considered adequate and was used for all the temperature measurements presented.

The thermocouple circuit as used in the centrifuge is shown in Figure 17, and contains two intermediate medals; molybdenum and mercury. By the law of intermediate metals, no error will result if both junctions of an intermediate metal are at the same temperature. The junctions between the molybdenum and the primary thermocouple wires (chromel and constantan), in both the rotating and stationary portions, were made in the kerosene bath.

The choice of molybdenum as one of the intermediate thermocouple wires was made on the basis of good wetability and chemical stability with mercury.

Merte(2), used a similar thermocouple circuit except iron wire was used in place of the molybdenum. Under non-rotating conditions

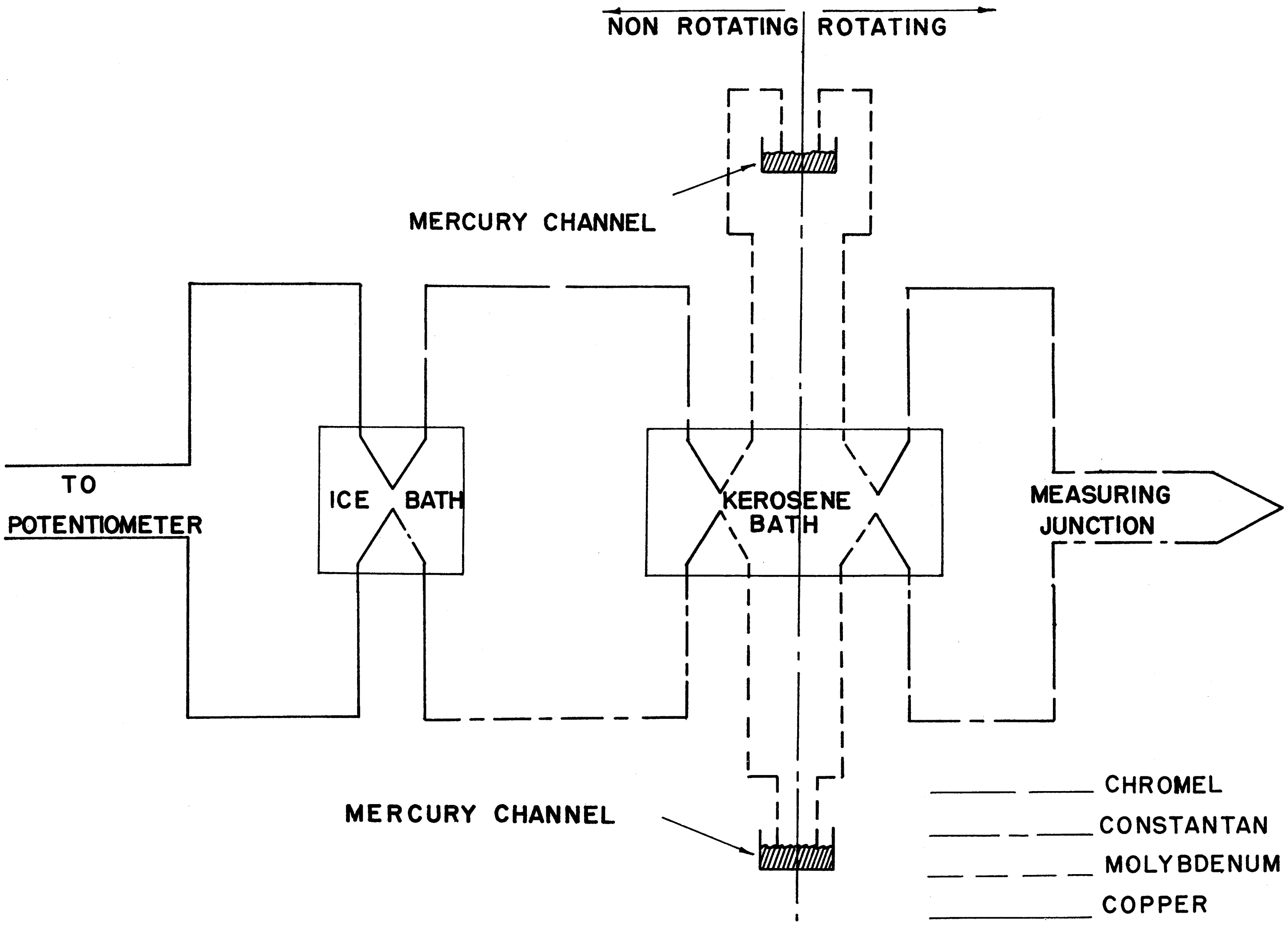

Figure 17. Thermocouple Circuit.

Merte recalibrated a previously calibrated thermocouple using the entire test circuit between the calibrated junction and the potentiometer. The measurements came within the 1 μv deviation obtained with the original calibration.

Under rotating conditions, Merte observed an induced EMF that could be related to the unequal lengths of wires between two channels of a circuit, rotating in the earth's magnetic field. By placing the channels above one another, and by taking care to have equal lengths of wire in each leg of a thermocouple rotating at a given radius, the effect of the earth's magnetic field should be eliminated. No attempt was made to determine whether or not this method actually did compensate for the earth's magnetic field because of the difficulty of maintaining a constant temperature within the test package under rotating conditions.

TABLE I

LIST OF THERMOCOUPLES AND THEIR POSITIONS

Thermocouple	Position
1	1/8 inch above test surface
2	1 inch above test surface
3	1/4 inch above test surface
4	underside of test surface
5	inside viewing tube number 1
6	inside viewing tube number 2
7	bottom of support insulator

J. Safety Barrier

An octagonal barrier approximately 6 1/2 feet high by 15 feet across was built for the protection of the personnel and to support the rotating assembly. The construction of the barrier and access door may be seen in Figures 2 and 18.

An octagonal shape was chosen to prevent the rotating equipment from imparting a direct blow to the barrier in case of a failure. The inner wall of the octagon was lined with 4 inch by 6 inch oak beams which were expected to function as energy absorbers in case of failure. The oak was fastened to a 1/2 inch thick steel plate, which in turn was bolted to vertical 6 inch I beams placed on 9 inch centers. The outer frame consisted of horizontal 6 inch I beams on 5 inch centers, bolted to vertical 12 inch I beams at each corner of the octagon and to the vertical 6 inch I beams. Inside, at the center, a rectangular pedestle was welded to eight I beam runners extending toward the center from each corner. This pedestal supported the lower main bearing, (which supported all the rotating weight) and other non-rotating equipment of the lower sub-assembly. The floor of the centrifuge consisted of 1/2 inch thick steel plates bolted to the eight runners.

The top was basically a weldment consisting of 4, 8 inch I beams arranged in a "tick-tack-toe" pattern. Each corner was bolted to one of the eight vertical corner I beams. Steel plates were bolted to the top to make the centrifuge completely enclosed except for a counter weighted access door located at one side of the top as shown in Figure 18. The center plate of the top was recessed about 12 inches below the level of the other plates and supported the upper main bearing.

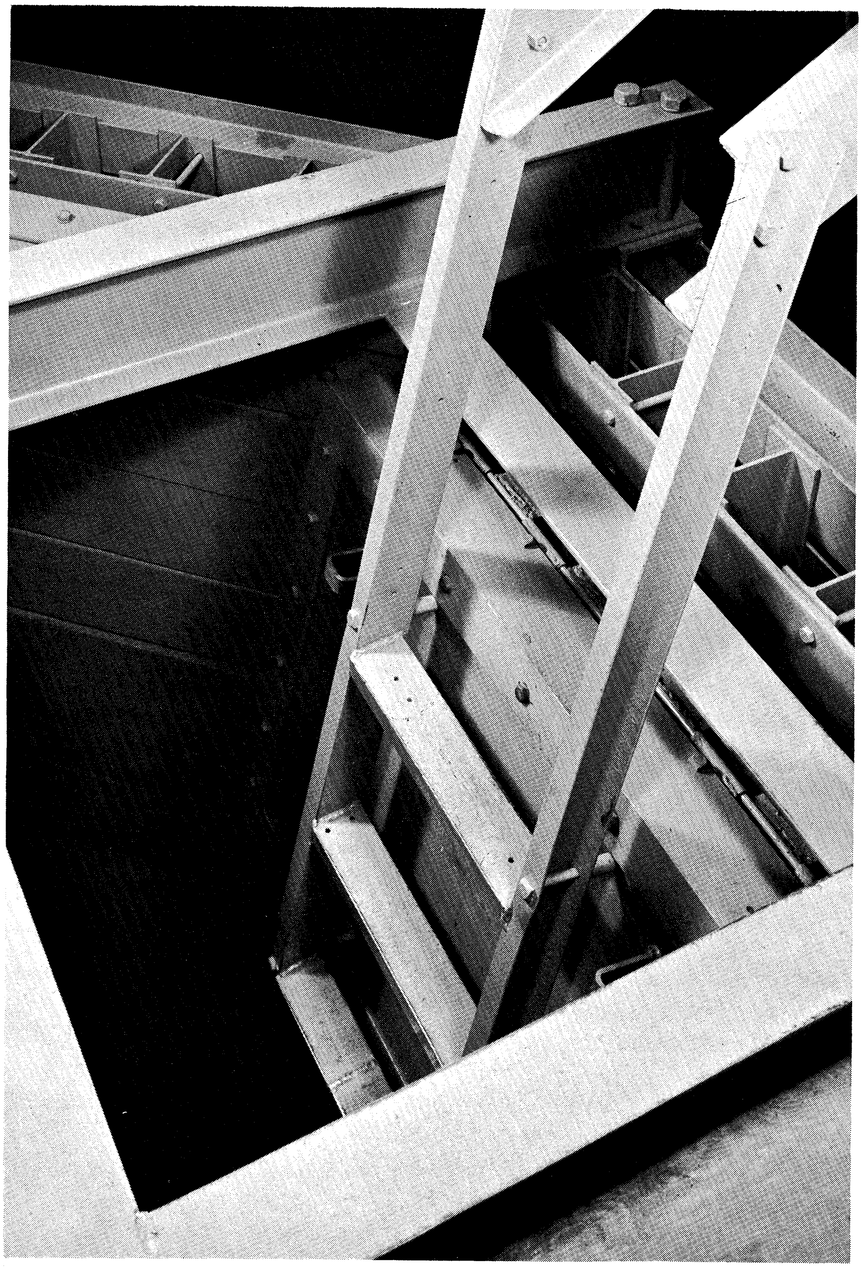

Figure 18. Barrier Construction.

CHAPTER III

TEST CONDITIONS

Distilled and de-gassed water was selected as the test fluid for this investigation because its properties are well known, and large quantities of heat transfer data are available for comparison.

Jakob(5) has shown that in an insulated container under standard gravitational conditions and with boiling taking place from the bottom surface, the liquid temperature near the free surface is somewhat higher than the saturation temperature at the free surface. The magnitude of this temperature difference was about .7°F and was independent of heat flux at least up to 14,000 BTU/hr-ft^2. For liquid levels greater than 8 inches in an insulated container, Fritz and Homann (see Jakob(5)) have shown that the bulk liquid temperature does not vary appreciable between the heater surface and the free surface except in the close proximity of the heat transfer surface. Thus, the saturation temperature profile in the liquid, which increases with the hydrostatic pressure head, twice crosses the actual temperature profile. Figure 19 shows a typical temperature profile and the saturation temperature profile for a boiling system under saturated conditions.

In saturated boiling then, the liquid near the free surface and near the heat transfer surface may be superheated, and the liquid in between may be subcooled. For small liquid levels, under standard gravitational conditions, the bulk liquid at all depths may be slightly superheated. If a boiling system with a fixed liquid depth is accelerated, the

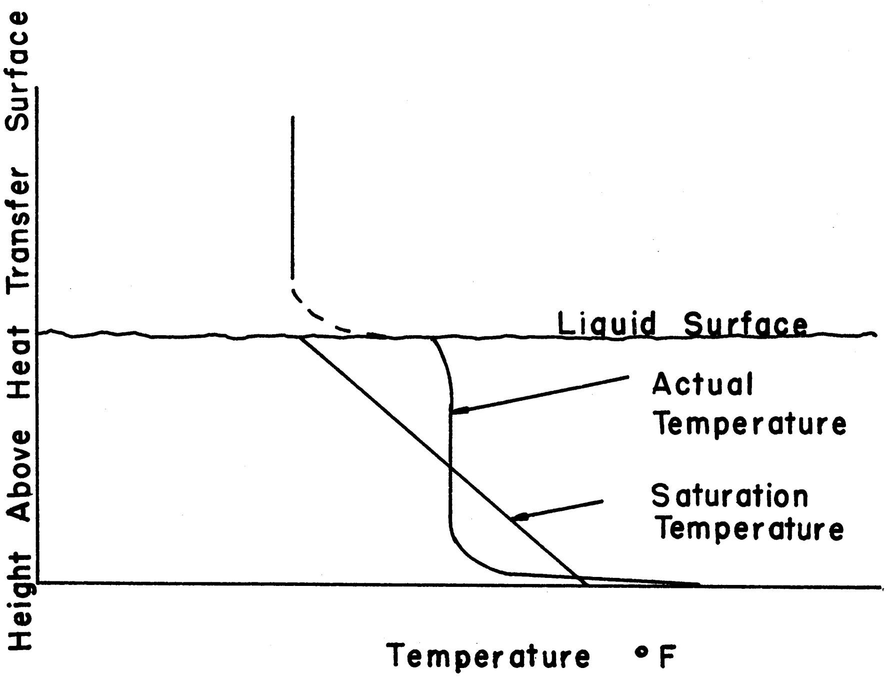

Figure 19. Temperature Profile in a Typical Boiling System.

saturation temperature profile will become steeper, and Merte(2) has shown that the maximum possible bulk liquid temperature at a location 1/4" from the heat transfer surface will increase slightly, although less than the increase in the local value of the saturation temperature. Consequently one result of accelerating a boiling system is that in the bulk liquid near the heat transfer surface (but outside thermal boundary layer), the difference between the local saturation temperature and the bulk liquid temperature increases. This natural phenomena, in which the bulk liquid immediately above the thermal boundary layer may actually be subcooled, can exist to some extent at all levels of acceleration (except $a/g = 0$) and will be referred to as "natural subcooling". The degree of natural subcooling is governed by the acceleration and the freedom from constraint of the fluid motion.

When the bulk liquid temperature is reduced below the level associated with natural subcooling, the term subcooled boiling is generally applied.

A numerical value can be assigned to the level of subcooling by means of the difference between the saturation temperature at the heat transfer surface and the liquid temperature measured at some arbitrarily specified position in the bulk liquid. Since for many boiling systems the bulk liquid temperature above the thermal boundary layer is essentially uniform, the position used for measuring the bulk liquid temperature does not materially effect the numerical value of subcooling.

The level of the natural subcooling for a particular boiling system cannot be pre-determined and is dependent upon the level of acceleration. Consequently, it is desirable to eliminate subcooling as a test variable. The method used in this investigation to eliminate subcooling as a test variable was to specify the difference between the saturation temperature at the heat transfer surface an the temperature level at a specified position in the bulk liquid, and to maintain this difference constant over the complete range of acceleration.

The location chosen for specifying the bulk liquid temperature was 1/8 of an inch above the heat transfer surface. The temperature level at this location will be referred to as the bulk liquid temperature.

The pressure and thus the saturation temperature at the heat transfer surface can be maintained constant over a range of acceleration if the liquid level is reduced as the acceleration is increased so that the hydrostatic pressure head remains constant. This method was used in this investigation. The same result could have been obtained with a constant liquid level by pressurizing the test package with an inert gas, but this is a much more complicated solution since an external control and read-out system would be required to control the pressure of the gas.

The maximum liquid height was 11 inches and the minimum liquid height was arbitrarily selected as 1 inch. A slightly non-linar relation exists between the liquid height and the pressure at the surface due to the dependence of the local acceleration and therefore the pressure gradient upon the length of the local radius arm. The hydrostatic pressure at the heat transfer surface is equal to the intergrated value of the local pressure gradient between the test surface and the free liquid surface. Consequently, with an 11:1 range of liquid level, the test surface saturation temperature can be maintained constant only over a 10:1 range of acceleration. In order to cover an acceleration range of 100:1. two different values of the test surface saturation temperature are required. The first level chosen corresponds to a liquid height of 11 inches and the hydrostatic pressure head of .38 psi which exists at 1g. For all acceleration levels between 1 and 10 g's, the difference in the saturation temperature between the free surface, which is essentially at atmospheric pressure, and the heat transfer surface is maintained constant at 1.3°F.

The second level of surface saturation temperature also corresponds to a liquid height of 11 inches but at an acceleration of 10 g's. The hydrostatic pressure head for accelerations between 10 and 100 g's is 3.8 psi and the difference between the saturation temperatures at the free surface and the heat transfer surface corresponding to this hydrostatic pressure is 10.8°F.

In all, five different accelerations were used in this test program, and were chosen on the basis of equal increments on a logarithmic scale (nominal values of 1, 3, 10, 30, and 100 g's). At accelerations of 1 and 10 g's the liquid level was 11 inches, at accelerations of 3 and 30 g's the liquid level was 3.4 inches, and at accelerations of 10 and 100 g's the liquid level was 1 inch. The 10 g test was performed at both the 1 and 11 inch liquid levels. A schematic representation of these conditions is shown in Figure 20 and a complete summary of all the test conditions is given in Table II.

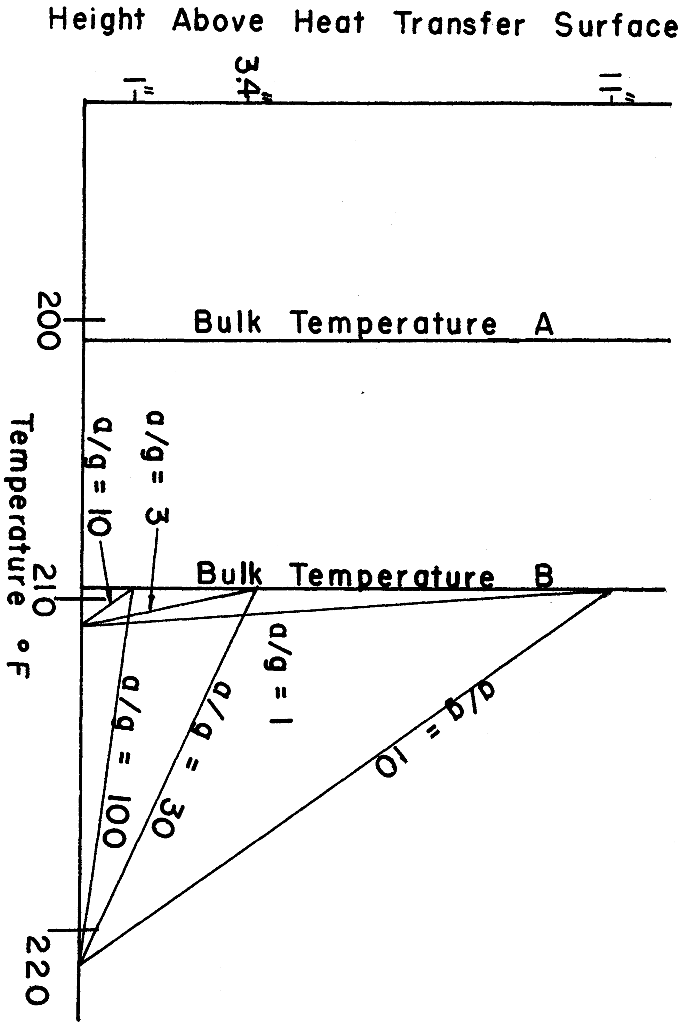

Figure 20. Schematic Representation of Test Conditions.

As stated earlier, the subcooling was to be fixed over the complete acceleration range by maintaining the difference between the bulk liquid temperature and the heat transfer surface saturation temperature a constant. Since the heat transfer surface saturation temperature is maintained constant at about 212°F for the low acceleration tests (1-10g's) and at about 222°F for the high acceleration tests (1 - 100g's), the bulk liquid temperature will also have to be maintained at different levels for the two ranges of acceleration. At the high accelerations, the bulk liquid was maintained at a temperature level equal to the saturation temperature at the free liquid surface, which results in a total subcooling of 10°F (bulk temperature B, Figure 20). No attempt was made to measure the natural subcooling at these accelerations but it is probably about 5°F. Thus the total subcooling is about 6°F greater than the natural subcooling. At the low levels of acceleration (1-10g's) the bulk liquid temperature was maintained at 202°F (bulk temperature A, Figure 20) which also results in an 10°F subcooling. These conditions are summarized by tests 1-6 in Table II.

A second series of tests (7-9 in Table II) was performed at the low acceleration. In these tests, the bulk liquid temperature was maintained equal to the saturation temperature at the free surface (bulk temperature B, Figure 20) which results in a total subcooling of about 2°F.

A third series of tests (10-12, Table II) were performed for three different accelerations ($a/g = 1, 10, 100$) and a wide range of heat flux (16,000 BTU/hr-ft^2 < q/A < 83,000 BTU/hr-ft^2). The purpose of

TABLE II

SUMMARY OF TEST CONDITIONS

Test	a/g	ΔT Sub °F	T_{sat} @ Test Surface °F	Q/A BTU/hr-ft^2 x 10^{-3}				
1	100	10	222		40	70		
2	30	10	222		40	70[1]		
3	10	10	222		40			
4	10	10	212		40			
5	3	10	212		40			
6	1	10	212		40			
7	10	2	212	16[2]	40			
8	3	2	212	16	40			
9	1	2	212	16	40[1]			
10	100	10	222	16	30[3]	48[3]	67[3]	83
11	10	10	222	16	30[3]	46[3]	65[3]	80
12	1	10	212	16	30	47[3]	68	81

[1] No isolated bubbles.

[2] No boiling.

[3] Fastex pictures taken.

these tests was to obtaind additional thermal data of the type generally presented in boiling heat transfer studies, (i.e., surface saturation temperature, surface temperature, heat flux and subcooling). These tests will be referred to as thermal tests even though some high speed photographs were taken with an 8 mm Fastex camera. At a few representative conditions (marked with the superscript 3 in Table II) a 100 foot roll of film was taken at a maximum framing rate of 13,000 frames per second with the Fastex camera. These films provide a large field of view and a long time duration so that comparisons can be made with the Dynafax films to determine if these Dynafax pictures are representative of the conditions in both the time and space domains.

CHAPTER IV

TEST PROCEDURES

After completion of the equipment installation, several trial runs were made to check out and "de-bug" the system. Two major changes were required before satisfactory system operation was obtained. Teflon O-rings were first used as seals for the fluid couplings and became completely ineffective after only 2 minutes of operation at moderate rotational speeds due to excessive wear. By replacing these teflon O-rings with a buna-N compound, the life of the seals was increased to about 20 hours at the highest rotational speeds. The second modification was the installation of the labyrinth seals to prevent spilling in both the kerosene bath and the mercury slip rings.

Before the actual testing was begun, the test vessel and all the stainless steel components in contact with the water were pickled and passivated. This was not only desirable in order to remove any contaminents from within the test vessel but was necessary because corrosion began to take place at the welds of the stainless steel vessel.

A test run was begun by first rinsing the test vessel with distilled water at least three times. The test vessel was then filled with distilled water to the desired level and an equal amount of water was placed in the counterweight for balancing purposes. The bottom guard heater was turned on and the water was deaerated by vigorous boiling for about 2 hours, with the internal heat exchanger condensing the water vapor formed.

If any readjustments in the optical system were required, these were accomplished during the de-areation process. Two magnifications were used with the Dynafax camera: for large bubbles which occurred at low accelerations and subcooling, the low magnification was used (0.8:1) for small bubbles, which occurred at high acceleration and subcooling, the high magnification was used (1.2:1).

By a slight horizontal movement of the camera the bulk liquid thermocouple, which has a known size, could be brought into the field of view. If the magnification was changed from the perceding test, a new calibration film was taken of this thermocouple which served as the reference length for determining the overall magnification during data analysis.

After the de-aeration process was complete, the centrifuge was turned on and brought up to the desired speed. The viewing tube guard heaters were turned on and the power to the test strip was turned on and adjusted to the desired heat flux level.

For the high subcooling tests, a period of up to three hours was required to adjust the power to the guard heaters and the cooling water flow rate to obtain equilibrium conditions with the desired bulk liquid temperature. The desired bulk liquid temperature for the low subcooling tests was usually reached in less than one hour.

The power to the viewing tube guard heaters was adjusted to maintain the temperature of the sight windows, monitered by thermocouple attached to the quartz inside the viewing tube, at the same level as the bulk liquid temperature. The time for the quartz temperature to reach the new equilibrium temperature after a change in the power was on the order of 2 or 3 minutes.

The primary control on the bulk liquid temperature was furnished by the bottom guard heater and secondary control was furnished by the heat exchanger. As was discussed earlier, the test area was the shape of a regular prism, 1 1/2 inches high, 3/8 inches wide and 4 inches long. The test strip support formed the bottom of the prism, the sight quartz and flow guides formed the sides, and the top and ends were open. Water, which was heated mainly by the bottom guard heater, completely surrounded this test area. Thus, decreasing the power to the bottom guard heater lowered the temperature of the surrounding water which in turn lowered the bulk liquid temperature.

After a change in the power to the bottom guard heater about 15 to 20 minutes were required to reach a new steady state condition. Actually, a true steady state condition was never attained. A complicating feature of this system was that the centrifuge speed was not constant but would slowly vary 1 or 2 rpm above and below the desired speed with a period of about 5 minutes. This variation in the acceleration often caused the bulk liquid temperatures to vary a slight amount (less than .1°F). This temperature variation is not considered significant but did complicate the determination of steady state conditions since it was not possible to tell if this temperature variation was due to a change in the speed or the change in the guard heater setting. Consequently, when the temperatures did not change more than ± .1°F over a period of about 15 minutes, and if the bulk liquid temperature was within ± 2.5°F of the desired level for the high subcooling tests or within ± .5°F for the low subcooling tests, the test conditions were considered satisfactory.

The operation of the centrifuge and the process of data taking required two people. One person continuously monitored the temperatures, speed, etc., and recorded the data at the proper time. The other person operated the camera and associated equipment and developed the films. When satisfactory test conditions were reached, the seven temperatures (see Table 1 in Chapter II), the test strip voltage and the test strip current were recorded from the measurements made on the type K-3 potentiometer. During the recording of the data the Dynafax camera was brought up to the desired speed, the light was turned on and the film exposed. The cassette was removed from the camera, the film loaded into a development tank in the darkroom and a second film was loaded into the cassett. The camera was then re-loaded and a second film was taken while a second set of test data was being recorded. This second film was also loaded into the development tank in the darkroom. Both films were then developed for 5 to 8 minutes using Kodak D-76 developer. The developed pictures were examined to see if the camera speed and exposure were suitable. The intensity of the light could not be adjusted while the centrifuge was running, but deficiencies in contrast could be partially corrected by changes in the development time for the next set of films. The camera speed was selected on the basis of obtaining about 25 to 50 total frames for a typical bubble. Higher camera speeds were not desirable since the probability of photographing the complete life cycle of suitable bubbles on the 224 available frames becomes small. The process of obtaining these first two films was generally repeated two more times so that a total of 6 films were available at each condition. Basically the same test procedure was used for the thermal tests with one exception, the films taken with the Fastex camera could not be immediately developed, but were sent to a commercial firm for processing.

CHAPTER V

DATA REDUCTION

The following sections describe the methods used in calculating the acceleration, surface saturation temperature, heat flux, surface temperature, bubble radius, and emperical bubble growth expressions. Also included for each of these parameters is an estimation of the errors involved.

A. Acceleration at the Test Surface

The total acceleration at the test surface is the vectorial sum of the standard gravitational acceleration and the centrifugal acceleration.

In order to determine the centrifugal acceleration at the test surface, the angle between the plane of rotation of the cross arm and the test package centerline must be known. This angle may be calculated from measurements of the rotational speed and knowledge of the center of gravity of the test package.

The center of gravity of the test package for each of the three different liquid levels used was determined by first weighing the complete test package assembly including the water. Then with the test package supported from the cross arm in the normal manner, a scale was fastened to the bottom of the outer container along the centerline of the test package at a known distance from the pivot pin. By swinging the test package a small angle from the vertical and holding it in this position with the scale maintained vertical, the center of gravity, as measured from the pivot pin, can be calculated:

$$WC\sin\theta = SL\sin\theta$$

or

$$C = \frac{SL}{W} \tag{10}$$

where

W = weight of test package (pounds)
C = center of gravity measured from pivot (feet)
S = scale reading (pounds)
L = distance from pivot to scale attachment point (feet)
θ = angle of test package from the vertical

During a test the liquid interface assumes the shape of a parabola of revolution which is not the same shape as when determining the center of gravity, and therefore introduces an error in the calculation of the center of gravity. However, as will be shown, the exact location of the center of gravity is not required in order to accurately determine the acceleration at the test surface.

Referring to Figure 21, which is a schematic representation of the centrifuge, the centrifugal acceleration at the test surface is:

$$a_c = \omega^2(b + \ell\sin\theta) \tag{11}$$

where the angle θ is given by the trancendental equation:

$$\theta = \tan^{-1}\omega^2\left[\frac{(b + C\sin\theta)}{g}\right] \tag{12}$$

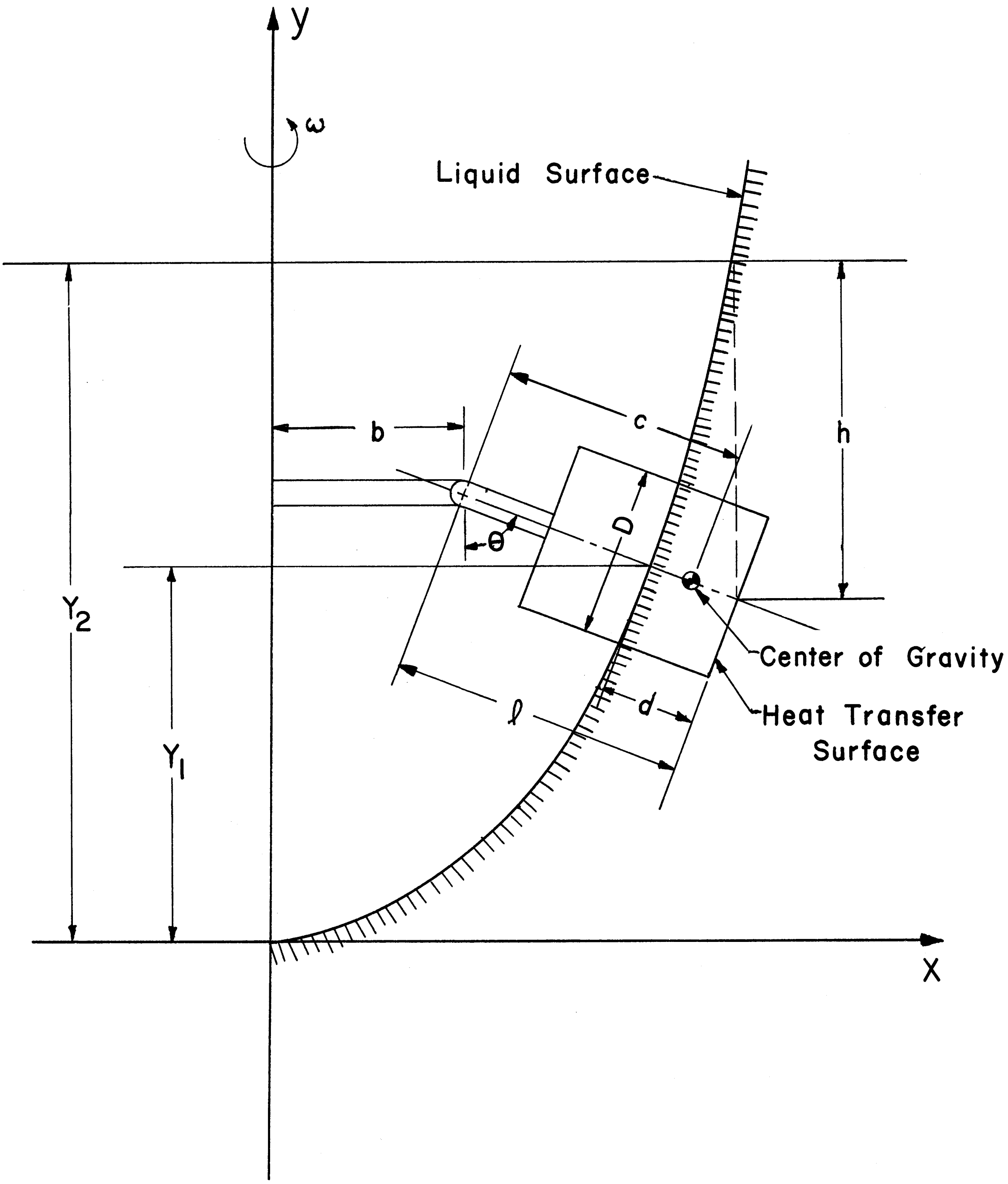

Figure 21. Schematic Representation of Centrifuge.

The total acceleration at the test surface is the vectoral sum of the centrifugal acceleration as given by Equation (11) and the standard gravitational acceleration (g) :

$$a_T = (a_c^2 + g^2)^{1/2} \tag{13}$$

and the non-dimensional acceleration a/g is:

$$a/g = \left[\frac{\omega^4}{g^2}(b + l\sin\theta)^2 + 1\right]^{1/2} \tag{14}$$

Equations (12) and (14) were used to calculate the non-dimensional acceleration.

Since the heat transfer surface is not at the center of gravity of the test package, the total acceleration vector will not be exactly normal to the heat transfer surface and will have a component parallel to the heat transfer surface (a_p) The angle (ϕ) between the total acceleration and the normal to the heat transfer surface and the acceleration a_p are given by:

$$\begin{aligned} \phi &= 90 - \theta - \sin^{-1} g/a_T \\ a_p &= a_T \sin\phi \end{aligned} \tag{15}$$

The values of ϕ and a_p were calculated for the six different liquid depths and acceleration combinations used. A maximum value of ϕ of 4.8 degrees occurred at $a/g = .3$. However, the acceleration parallel to the heat transfer surface remains nearly constant for all rotating conditions at a value of $(a_p/g) = .3$.

The uncertainty of the total acceleration may be determined by the procedure outlined by Kline and McClintock(57). If a result (R) is obtained from a number of independent variables, each of which possesses an uncertainty, then the percentage uncertainty of R is given by:

$$\frac{W_R}{R} = \left[\left(\frac{\partial R}{\partial V_1}\frac{W_1}{R}\right)^2 + \left(\frac{\partial R}{\partial V_2}\frac{W_2}{R}\right)^2 + \cdot\cdot\cdot + \left(\frac{\partial R}{\partial V_n}\frac{W_n}{R}\right)^2\right]^{1/2} \qquad (16)$$

where:

V_n = independent variable

W = uncertainty interval, subscript R refers to result, subscript n refers to independent variable

The lowest non-dimensional acceleration (excluding $a/g = 1$) used this program was $a/g = 3$, which corresponds to an angular velocity of 4.71 radians/seconds. Using this value of ω and an uncertainty in the value of the center of gravity (C) of ± 20% in Equation (16), results in a maximum uncertainty of the angle θ of less than ± 2° .

The uncertainty of ℓ is ± .125 inches and the uncertainty of b is ± .005 inches which may be neglected when compared to the uncertainty of ℓ .

The angular velocity of the main shaft was measured by counting, on a Berkly electronic counter, the pulses generated by a 48 tooth gear and magnetic pickup. This system enabled the angular velocity to be determined within ± 1.25 rev/min or ± .13 radians/second .

By performing the operations indicated by Equation (16) on Equation (11), the following expression is obtained for the percentage uncertainty of the centrifugal acceleration:

$$\frac{W_{a_c}}{a_c} = \left[\frac{4}{\omega^2} W_\omega^2 + \left(\frac{\sin\theta}{b+l\sin\theta} W_l \right)^2 + \left(\frac{l\cos\theta}{b+l\sin\theta} W_\theta \right)^2 \right]^{1/2} \tag{17}$$

Both b and l are independent of acceleration and are given by:

b = 2.25 feet

l = 2.18 ± .01 feet

At an acceleration of a/g = 3:

ω = 4.71 ± .13 radians/second

θ = 1.161 ± .035 radians

therefore the percentage uncertainty of the centrifugal acceleration at a/g = 3 is:

$$\left(\frac{W_{a_c}}{a_c}\right)_{a/g=3} = 5.6\%$$

at a/g = 100 :

ω = 26.83 ± .13 radian/second

θ = 1.558 ± .035 radian

therefore:

$$\left(\frac{W_{a_c}}{a_c}\right)_{a/g=100} = 1\%$$

The percent uncertainty of the total acceleration (a_t) is then:

$$\left(\frac{Wa_T}{a_T}\right)_{a/g=3} = \left(\frac{Wa_c}{a_c}\right)\left(\frac{a_c}{a_c+g}\right)^2 = 4.1\,\%$$

and

$$\left(\frac{Wa_T}{a_T}\right)_{a/g=100} = 1\,\%$$

B. <u>Saturation Temperature at Heater Surface</u>

The liquid saturation temperature at the heater surface is one of the established parameters of nucleate boiling and may be determined if the pressure at the test strip surface is known.

The liquid in the test package under rotating conditions assumes the shape of a parabola of revolution as shown in Figure 21. The equation for this parabola can be derived from elementary fluid mechanics and is given by:

$$Y = \frac{\omega^2 X^2}{2g} \tag{18}$$

Using the notation as given in Figure 21, the total pressure (P_T) at the test surface is:

$$P_T = \left(\frac{g}{g_c}\right) \rho_\ell h + P_v = \left(\frac{g}{g_c}\right) \rho_\ell \left(Y_2 - Y_1 + d\cos\theta\right) + P_v \tag{19}$$

where P_v is the pressure at liquid-vapor interface and Y_1 and Y_2 are equal to:

$$Y_1 = \frac{\omega^2}{2g}\left[b + l - d\sin\theta\right]^2 \tag{20}$$

$$Y_2 = \frac{\omega^2}{2g}\left[b + l\sin\theta\right]^2 \tag{21}$$

The test package was sealed container except for a vent tube running from the test package cover to the center-line of rotation. The increase in pressure due to the acceleration of the air-water vapor mixture between the centerline of rotation and the liquid free surface can be approximated by the following expression:

$$P_v = \frac{\bar{\rho}_v \omega^2}{2g_c}(b + l - d)^2 + P_a \tag{22}$$

where

P_a = atmospheric pressure

ρ_v = average density of air-water vapor mixture

The atmospheric pressure (P_a) was obtained from a calibrated barometer, accurate to within ± .005 inches of mercury.

Substituting into (19) the expressions for Y_1, Y_2, and P_v result in the following equation for the total pressure at the test surface:

$$P_T = \rho_\ell \frac{\omega^2 d}{2 g_c} \left[2b \sin\theta + (2\ell - d)\sin^2\theta + \frac{\bar{\rho}_v}{\bar{\rho}_\ell} \frac{(b+\ell-d)^2}{d} \right] + \rho_\ell d \cos\theta + P_a \qquad (23)$$

The depth of liquid (d) was measured under non-rotating conditions and is therefore not exactly equal to the liquid depth under rotating conditions due to the parabolic shape of the free liquid surface. The amount the true liquid depth differs from that measured under stationary conditions is not readily obtained, but may be estimated by considering the difference in liquid head under rotating conditions between the upper and lower boundaries of the container. Using the same notation as used in deriving Equation (23), this difference in liquid head can be shown to be:

$$\Delta h = D \left[\frac{\omega^2}{g} (b + \ell \sin\theta) \cos\theta - \sin\theta \right] \qquad (24)$$

where D is the diameter of the test vessel.

This variation in the liquid head across the test vessel is larger than the change in liquid head at the centerline between rotating and non-rotating condition. For $a/g = 3$, this variation in pressure head is .012 inches of water which corresponds to an upper limit on the change in d of .004 inches. At $a/g = 100$, Δh is equal to .24 inches of water which corresponds to a maximum change in d of .0024 inches. Thus, the variation in d, due to the parabolic shape of the free surface, may be neglected when compared to the uncertainty in the measurement of d.

The uncertainty of the saturation temperature at the heater surface as determined from the total pressure at the heater surface will now be considered. The uncertainties of both b and ℓ are small when compared to the uncertainties of the remaining terms and will be neglected. The maximum uncertainty of (P_T) will occur at the highest acceleration ($a/g = 100$) which corresponds to the smalles value of d ($d = 1$ inch). At these conditions, Equation (23) may be approximated with little error by the following:

$$P_T - P_a = \frac{\rho_\ell \omega^2 d}{g} \left[b + \ell - \frac{d}{2} + \frac{\bar{\rho}_v}{\rho_\ell} \frac{(b+\ell-d)^2}{d} \right] \tag{25}$$

Performing the required operations on this equation results in the following expression for the uncertainty of (P_T-P_a):

$$\frac{W_{P_T - P_a}}{P_T - P_a} = \left[\left(\frac{2 W_\omega}{\omega} \right)^2 + \left(\frac{1 + 2(b+\ell-d)\bar{\rho}_v/\rho_\ell \; W_\ell}{b+\ell-d/2 + \bar{\rho}_v/\rho_\ell \, \frac{(b+\ell-d)^2}{d}} \right)^2 \right.$$

$$\left. + \left(\frac{(b+\ell-d) \; W_d}{b+\ell-d/2 + \bar{\rho}_v/\rho_\ell \, \frac{(b+\ell-d)^2}{d}} \right)^2 + \left(\frac{((b+\ell-d)^2/d\rho_\ell) \; W_{\bar{\rho}_v}}{b+\ell-d/2 + \frac{\bar{\rho}_v}{\rho_\ell} \frac{(b+\ell-d)^2}{d}} \right)^2 \right]^{1/2} \tag{26}$$

Using typical values from test number 166 (see Appendix B)

P_T-P_a = 3.37 psi

ω = 26.70 ± .13 radians/second

d = .0833 ± .005 feet

ℓ = 2.185 ± .01 feet

$b = 2.25$ feet

$\bar{\rho}_V = .057 \pm .021$ lbm/ft^3

$\rho_\ell = 59.8$ lbm/ft^3

results in an uncertainty of $P_T - P_a$ of ± .04 psi. This uncertainty level in the pressure at the test strip surface corresponds to a maximum uncertainty in the saturation temperature at the surface of ± .1°F.

C. Heat Flux

The heat flux from the center portion of the test strip was calculated from knowledge of the electrical properties of Chromel A, from measured values of the total power dissipation in the test strip, and from known physical dimensions of the test strip.

Referring to Figure 22, the power dissipation in the center portion $(-a < X < +a)$ may be calculated by subtracting from the total power input, the calculated power dissipation in the two finned portions $(-(a+b) < X < (-a))$ and $(+a < X < a+b)$:

$$Q_{center} = Q_{total} - Q_{fin} \tag{27}$$

If heat conduction from the center section to the fins is neglected, and if heat conduction from the test strip to the insulating support is neglected, then Equation (27) can be divided by the top surface area of the center portion to give the surface heat flux at the center

$$\frac{Q_{center}}{2aL} = (q/A)_{center} = \frac{1}{2aL}\left(Q_{total} - Q_{fin}\right) \tag{28}$$

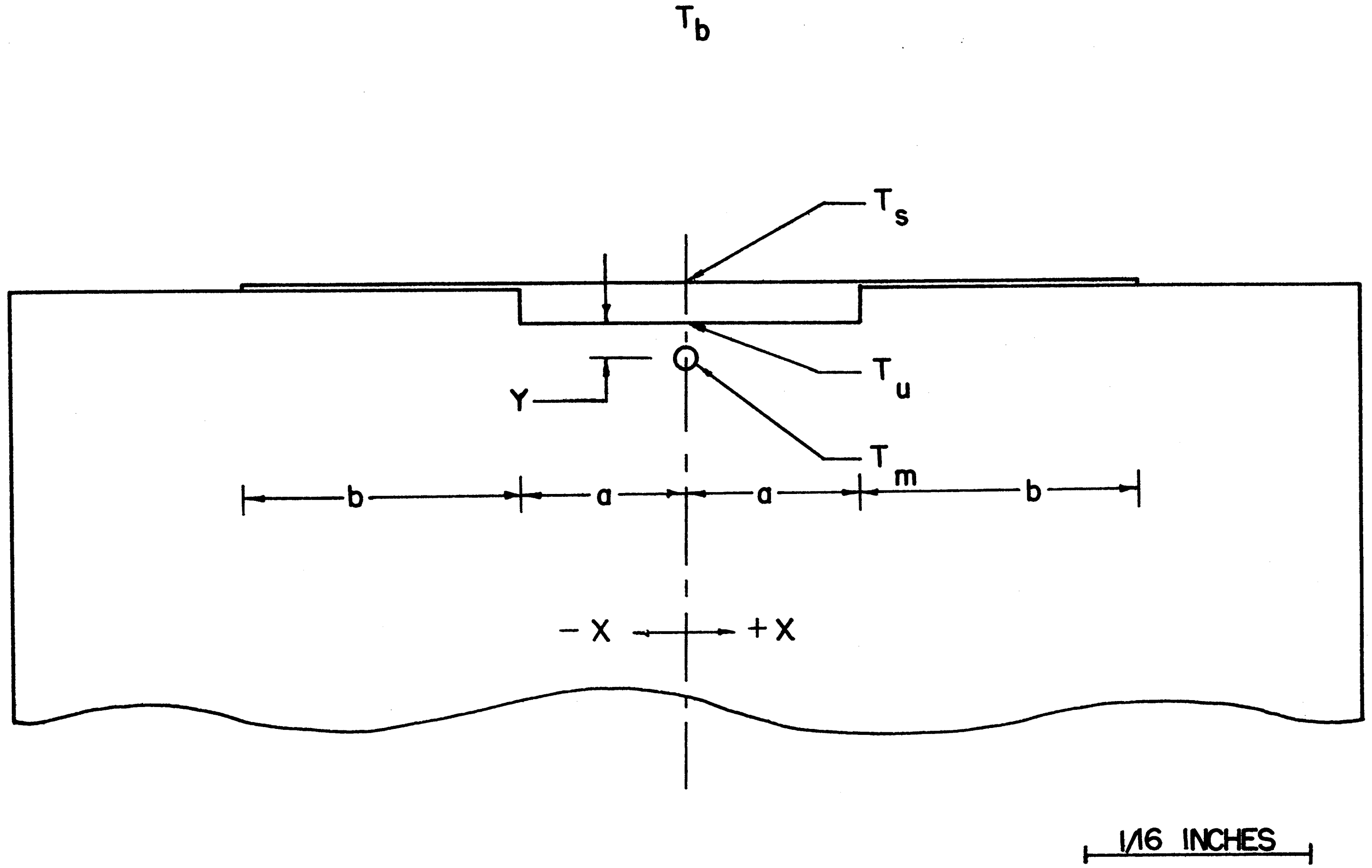

Figure 22. Scale Drawing of Test Strip.

where L is the length of strip. The total power dissipation is calculated from the measured values of voltage and current.

$$Q_{total} = 3.413\ EI \tag{29}$$

The power dissipation in the finned portion is:

$$Q_{fin} = 3.413\ E^2/R_f \tag{30}$$

where R_f is the total resistance of the fins. Substituting the equations for Q_{fin} and Q_{total} into (28), results in the following expression:

$$(q/A)_{center} = \frac{3.413}{2aL}\left(EI - E/R_f\right) \tag{31}$$

This is the equation which was used to determine the heat flux from the center portion of the strip.

The assumption of negligible heat conduction to the fins from the center portion can be evaluated by considering the fins to be one-dimensional. This one-dimensional assumption is justified since the temperature drop across the fin due to the internal heat generation is equal to

$$\Delta T = q'''\,\delta_2^2/2k \tag{32}$$

where

q''' = volumetric heat generation

δ_2 = thickness of fin

k = thermal conductivity of Chromel

and for the maximum value of q''' used in this investigation results in a value of $\Delta T = .3^\circ F$.

Referring to Figure 23 for notation, the differential equation for a one-dimensional fin with internal heat generation, one side insulated and constant properties is:

$$\frac{d^2 T_x}{dx^2} - \frac{h_2}{k\delta_2}(T_x - T_b) + \frac{q'''}{k} = 0 \tag{33}$$

where

T_b = bulk liquid temperature

q''' = volumetric heat generation

h_2 = film coefficient for fin

k = thermal conductivity

δ_2 = thickness of fin

Using the following boundary condition and definition;

$$\theta = T_x - T_b$$

$$\theta(0) = \theta_0 = T_f - T_b$$

Equation (33) may be solved and results in the following:

$$\frac{(\theta - q'''\delta_2/h_2)}{(\theta_0 - q'''\delta_2/h_2)} = e^{-\sqrt{h_2/k\delta_2}\,x} \tag{34}$$

The total heat conduction from the center region to the fin (Q_f) in terms of the unknown root temperature T_f is:

$$Q_f = L h_2 \int_0^{\infty} \left(\theta - \frac{q'''\delta_2}{h_2} \right) dx = L h_2 \left(\theta_0 - \frac{q'''\delta_2}{h_2} \right) \Big/ \sqrt{\frac{h_2}{k\delta_2}} \tag{35}$$

where L is the length of test strip.

The value of Q_f can also be calculated in terms of a uniform temperature profile for the center portion resulting from the heat conduction to the fins. A uniform temperature for the center portion will result in a temperature at the root of the fin which is higher than the actual value and consequently, Q_f as determined by Equation (35) will be higher than the actual case. If this uniform temperature profile in the center is equal to T_f , the heat loss from the center to the fins will be:

$$Q_f = h_1 a L (T_c - T_f) = h_1 a L \theta_c \tag{36}$$

By equating Equations (35) and (36) and solving for (θ_0/θ_c) gives:

$$\frac{\theta_0}{\theta_c} = \frac{a\sqrt{h_2/k\delta_2}\left(\frac{h_1}{h_2}\right) + \frac{q'''\delta_2}{h_2\theta_c}}{a\sqrt{h_2/k\delta_2}\left(\frac{h_1}{h_2}\right) + 1} \tag{37}$$

The ratio θ_0/θ_c may be considered as a test strip effeciency, which can be written in terms of the maximum heat flux (q/A) as determined by Equation (31) and the heat conducted to the fin from the center (Q_f) :

$$\frac{\theta_o}{\theta_c} = \frac{h_1 aL(T_c - T_b) - h_1 aL(T_c - T_f)}{h_1 aL(T_c - T_b)} = \frac{(q/A) - Q_f}{(q/A)} \tag{38}$$

The term $\dfrac{q''' \delta_2}{h_2 \theta_c}$ in Equation (37) is related to the total test strip resistance and the resistance of the fin in the following manner:

$$\frac{q''' \delta_2}{h_2 \theta_c} = \frac{(q''' \delta_2 bL)\left(\frac{h_1}{h_2}\right)}{(\theta_c h_1) bL} = \frac{(h_1 a / h_2 b)}{R_f/R_T - 1} \tag{39}$$

Substituting this equation into Equation (37), results in an expression for the test strip efficiency which is dependent upon the test strip dimensions, the measured and calculated electrical resistances and the film coefficients:

$$\frac{(q/A) - Q_f}{(q/A)} = \frac{a\sqrt{h_2/k\delta_2} + \dfrac{(a/b)}{R_f/R_t - 1}}{a\sqrt{h_2/k\delta_2} + (h_2/h_1)} \tag{40}$$

The total resistance (R_t) was determined by the voltage and current measurements made during the tests. The resistance of the fin (R_f) was calculated from the manufacturers values of electrical resistivity and from the physical dimension of the strip. The value of $(R_f/R_t - 1)$ was calculated to be 4.00.

Equation (40) is plotted on Figure 23 for different values of h_1 and h_2. It is noted that the lowest efficiencies occure for low

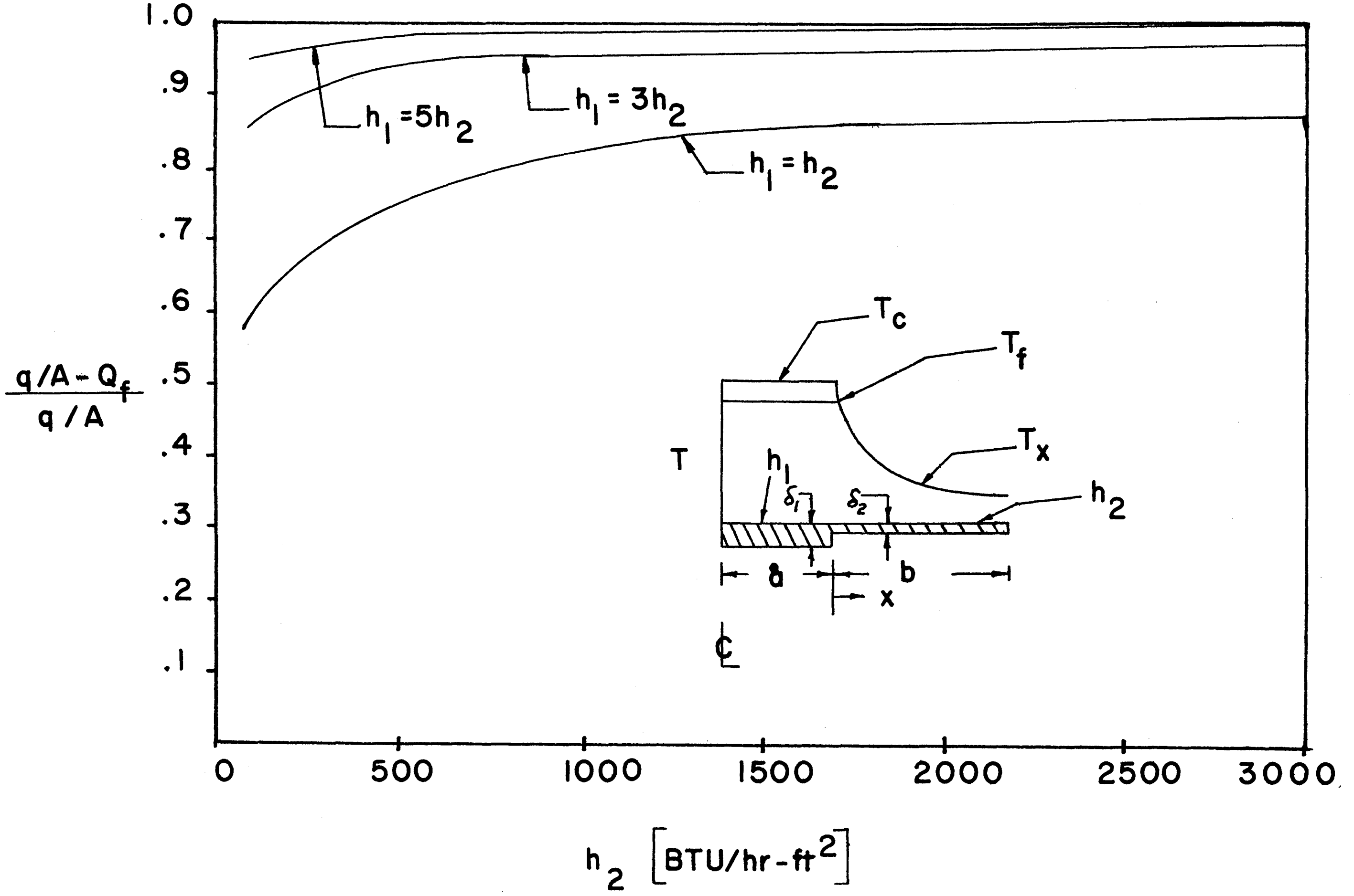

Figure 23. Test Strip Efficiency.

values of the film coefficients. From the data (Appendix B) the lowest value of h_1, as determined by $h_1 = (q/A) / (T_{sur}-T_b)$, occurs for the low heat flux tests and is equal to 1300 BTU/hr-ft^2. If $h_1 = h_2$, the test strip efficiency is 83% but the assumption of $h_1 = h_2$ may be considered unrealistic due to the boiling taking place only at the center portion of the strip. It is not possible to determine a value for h_2 since no temperature measurements were made in the region of the fins, but a more realistic assumption might be to consider $h_1/ h_2 = 3$, which then results in a test strip efficiency of 93% for $h_1 = 1300$. The maximum value of h_1 is about 2,500 BTU/hr-ft^2-°F which results in a minimum value of the test strip efficiency of 86% for $h_1 = h_2$. For $h_1/h_2 = 3$ the efficiency becomes 95%. The net result of neglecting heat conduction to the fins is that the surface heat flux at the center as determined by Equation (31) is no more than 17% too high.

The assumption of negligible conduction through the support insulator can be evaluated in terms of a classical conduction problem as shown in Figure 24. During the tests, the quartz windows were maintained at a temperature level near to the bulk liquid temperature (T_b). Since these windows were in physical contact with the sides of the support insulator, the temperature of the sides of the support insulator will be approximately equal to the bulk liquid temperature. The temperature of the water surrounding the test area was adjusted by means of the bottom guard heater to maintain the bulk liquid temperature at the desired level, which resulted in a temperature at the bottom of the support insulator of from one to five degrees below the bulk liquid temperature. As will be

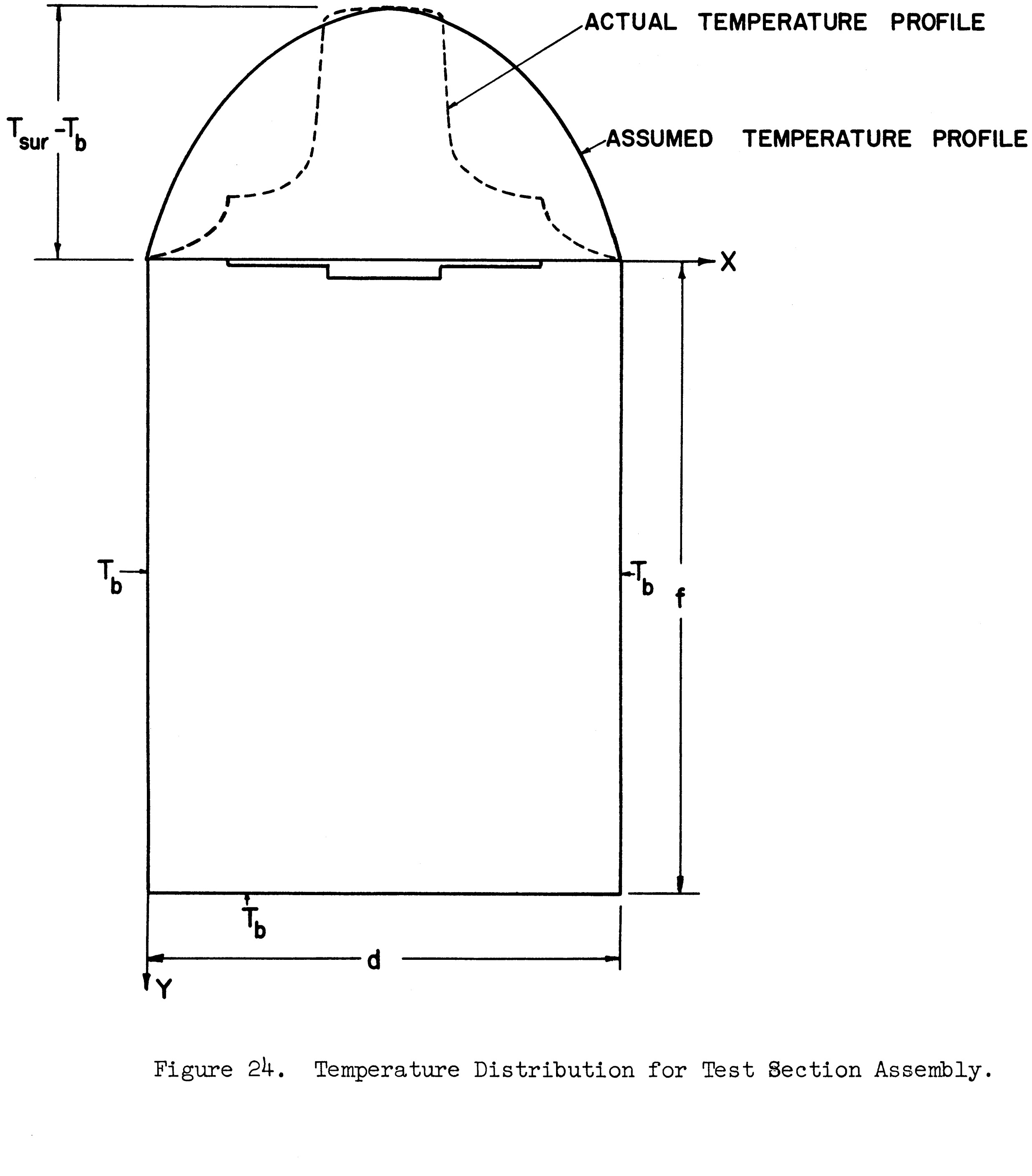

Figure 24. Temperature Distribution for Test Section Assembly.

shown, little error will result by assuming the bottom of the insulator is also at the bulk liquid temperature.

The actual temperature distribution across the heat transfer surface is unknown, but a parabolic temperature distribution with a maximum temperature equal to $(T_{sur}-T_b)$ at the center most likely will be greater than the actual profile, as indicated on Figure 24. This will result in an estimate of the heat loss through the support insulator which is greater than the actual heat loss. Referring to Figure 24 for notation, a classical conduction problem results which may be solved, and the following expression for the temperature distribution within the support insulator is obtained:

$$\frac{T_{sur}-T}{T_{sur}-T_b} = \frac{32}{\pi^3}\sum_{n=0}^{\infty}\frac{1}{(2n+1)}\sin(2n+1)\pi x/d\;\frac{\sinh(f-y)(2n+1)\pi/d}{\sinh(2n+1)\pi d/f} \tag{41}$$

The total heat loss through the support insulator may be calculated from the following:

$$(q/L) = -k\int_0^d \left.\frac{dT}{dy}\right|_{x=0} dx = \frac{64k(T_{sur}-T_b)}{\pi^3}\sum_{n=0}^{\infty}\frac{1}{(2n+1)^3\tanh(2n+1)\pi b/a} \tag{42}$$

where (q/L) is the heat transfer from $Y = 0$ into the support. Using $d = 3/8$ inches and $f = 1/2$ inches, the hyperbolic tangent in the summation is nearly unity for all values of n, which enables Equation (42) to be written as:

$$(q/L) = \frac{64k(T_{sur}-T_b)}{\pi^3}\sum_{n=0}^{\infty}\frac{1}{(2n+1)^3} \cong \frac{96k(T_{sur}-T_b)}{\pi^3} \tag{43}$$

The value of the thermal conductivity of the glass phenolic used is approximately equal to .1 BTU/hr-ft^2-°F/ft, and the maximum value of $(T_{sur}-T_b)$ is about 30°F. Using this value of k but increasing $T_{sur}-T_b$ by 5°F to compensate for the temperature at the bottom of the support insulator being too low, results in a maximum value for (q/L) of 11 BTU/ft. The minimum value of the total heat generation in the test strip is 335 BTU/ft. Thus, the maximum error in the heat flux calculation introduced by the assumption of no conduction through the support insulator is about 3%, which is negligible compared to the uncertainty introduced by the unknown values of the film coefficients.

D. Surface Temperature

The surface temperature was calculated from knowledge of the heat flux, measurements of the bulk liquid temperature and of the temperature in the test strip insulator at a point just below the test strip. A scale drawing of the insulating support and the test strip is shown in Figure 22.

The exact placement of the thermocouple within the insulating support relative to the underside of the test strip is unknown, which precludes an accurate determination of the surface temperature. However, by estimating the distance (Y) between the thermocouple and the underside of the strip and by estimating the upper and lower limits of the temperature within the insulator in the region of the thermocouple, an upper and lower bound may be placed on the computed surface temperature. Referring to Figure 22, the surface temperature (T_{sur}) may be determined from the measured temperature (T_m) if the temperature differences between the underside (T_u) and the surface (T_{sur}) and the temperature difference between the underside (T_u) and the measured (T_m) are known.

$$T_{sur} = T_m + (T_u - T_m) - (T_u - T_{sur}) \tag{44}$$

The temperature drop $(T_u - T_{sur})$ across an infinite plate with internal heat generation, one side insulated and constant properties can be shown to be:

$$T_u - T_{sur} = (q/A)\,(\delta_1)/2k \tag{45}$$

where

(q/A) = surface heat flux

δ_1 = thickness of test strip

k = thermal conductivity of Chromel

Since the centerline of the test strip is an adiabatic surface, the assumption of an infinite plate is justified in the derivation of Equation (45).

An upper and lower limit on the temperature difference $(T_u - T_m)$ can be derived in terms of the temperature difference between the underside temperature (T_u) and the measured bulk liquid temperature above the strip (T_b). The results may be expressed as follows;

$$(T_u - T_m) = F(T_u - T_b)$$

or

$$(T_u - T_m) = F\left[(T_u - T_{sur}) + (T_{sur} - T_b)\right] \tag{46}$$

where F is a multiplying factor to be determined. Substituting Equations (45) and (46) into Equation (44) and solving for T_s results in the following

$$T_{sur} = \frac{T_m - F\left(T_b - q/A\,\frac{\delta_1}{2k}\right) - q/A\,\frac{\delta_1}{2k}}{1 - F} \tag{47}$$

The value of F can be determined by assuming two temperature profiles on the top surface of the support insulator (i.e. under the test strip) which are believed to bracket the actual temperature profile, and using these two profiles to calculate limits on the temperature in the region of the thermocouple (T_m).

The first profile (designated profile A on Figure 25) is a uniform temperature distribution which is certainly the upper limit on the actual profile. The second profile (profile B) has a step change in the temperature at the joint point between the fins and the center portion. The temperature drop across the thin fin is smaller than the temperature drop across the thick center section. However, both are small and negligible error in the determination of F will result if they are both considered equal to the temperature drop across the center. Based on the assumption of an average film coefficient for the fins which is 75% of the film coefficient for the center portion, and on the assumption of no heat conduction to the fins from the center portion, the temperature difference $(T_{sur}-T_b)$ in the finned regions (θ_f) will be 1/5 of that in the center (θ_c)

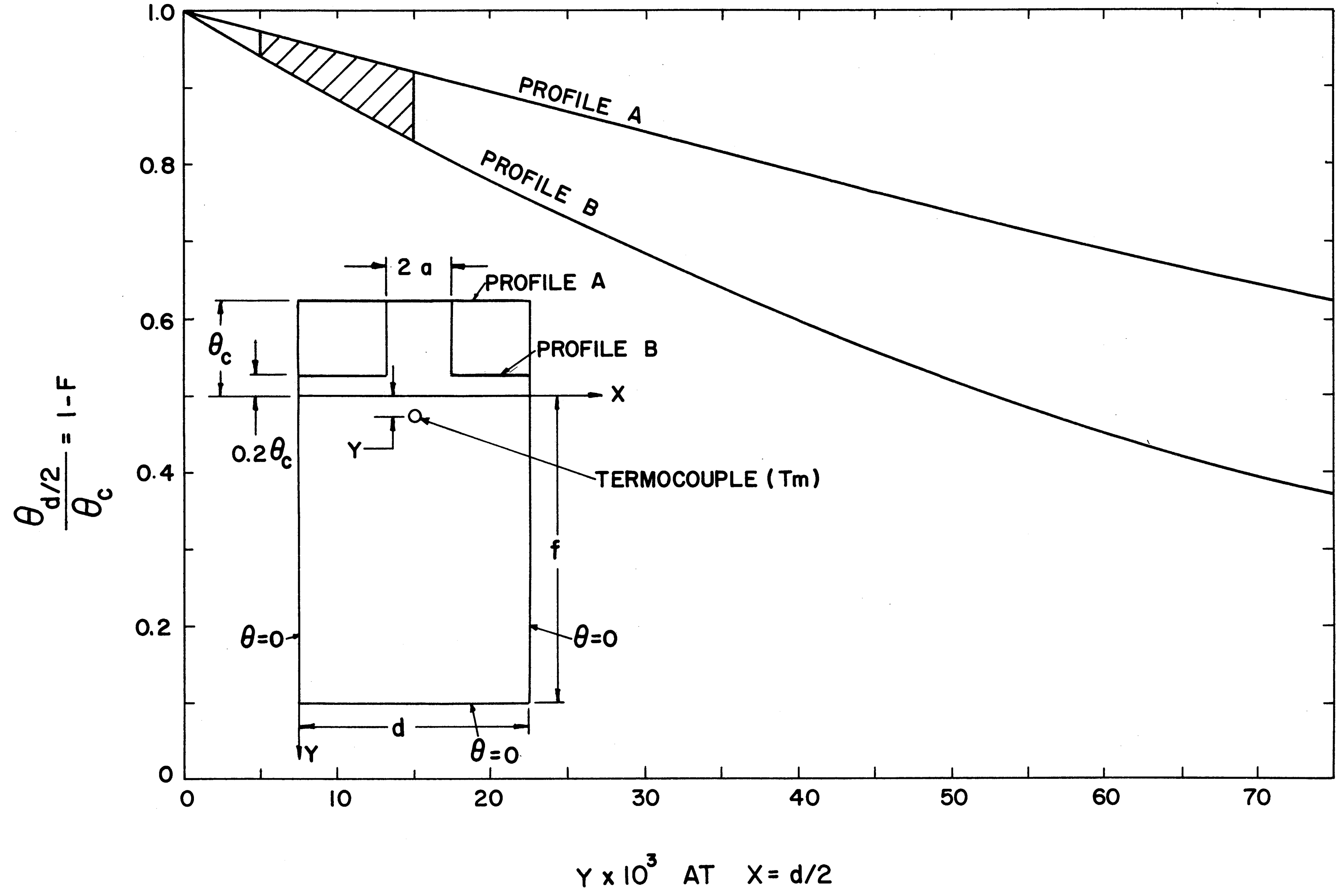

Figure 25. Temperature Profile Along Centerline of Test Support Insulator.

As was discussed Section C in this Chapter, the average film coefficient on the center portion of the ribbon will be considerably higher than the average on the fins due to the boiling taking place at the center. The assumption of only a 25% decrease in the film coefficient will consequently result in an average temperature of the fins which is lower than the actual temperature. The effect of the conduction form the center to the fins is to raise the average temperature of the fins, thus neglecting conduction will also give a lower average temperature than the actual. The value of $\theta_f/\theta_c = 1/5$ was determined from the measured total resistance of the test strip, and from the calculated resistance of the two fins, which depends on the physical dimensions and properties of the strip. By relating the temperature differences θ_f and θ_c to the surface heat flux and the film coefficients, and then in turn expressing the surface heat flux in terms of the resistances of the center section and of the fins, the following results;

$$\frac{\theta_f}{\theta_c} = \frac{(q/A)_f}{(q/A)_c}\left(\frac{h_c}{h_f}\right) = \left(\frac{h_c}{h_f}\right)\left(\frac{A_c}{A_f}\right)\left(\frac{R_c}{R_f}\right) \tag{48}$$

using the following values

$$h_f/h_c = .75 \;, \quad A_f/A_c = 5/3 \;, \quad R_f/R_c = .5/.125$$

gives $\theta_f/\theta_c = 1/5$.

The temperature distribution in the region of the thermocouple (T_m) will now be established for each of the two profiles. Referring to to Figure 25 for notation, the two temperature profiles can be described by one generalized expression:

$$\begin{aligned} \theta &= k\theta_c \quad (0 < x < d/2 - a) \\ \theta &= \theta_c \quad (d/2 - a < x < d/2 + a) \\ \theta &= k\theta_c \quad (d/2 + a < x < d) \end{aligned}$$

where

k = 1 for profile A
k = 1/5 for profile B .

Using this expression for the temperature profile on one side of a rectangle while the other three sides are held at temperature zero, the following expression can be derived for the temperature distribution within the rectangle:

$$\frac{\theta}{\theta_c} = \frac{4}{\pi} \sum_{n=0}^{\infty} \left[\frac{(1-k)(-1)^n \sin (2n+1)\pi a/d + k}{2n+1} \right] \sin (2n+1)\pi x/d \; \frac{\sinh (2n+1)\pi (f-y)/d}{\sinh (2n+1)\pi f/d} \tag{49}$$

Equation (49) was programmed for the IBM 7090 computer and solved for the centerline temperature distribution using $k = 1$ and $k = 1/5$. The results are plotted in Figure 25. Location (Y) of thermocouple T_m is estimated to be .010 ± .005 inches from the bottom of the test strip, which results in an uncertainty range for T_m as represented by the cross hatched section in Figure 25.

The maximum and minimum values of F as determined from Figure 25 are .18 and .02 respectively, which determines the uncertainty of the surface temperature T_{sur} , since the uncertainties of the other terms in Equation (47) are small compared to the uncertainty of F . The average value of F between .18 and .02 (i.e., F = .1) was used to calculated the surface temperature.

The maximum uncertainty of the surface temperature will occur at high heat fluxes where the measured temperature T_m is a maximum. Using the values from test 146 (Appendix B) the maximum uncertainty in the absolute value of T_s is about ± 3°F. This may be seen in Table III, where T_{sur} is presented as a function of F .

TABLE III

VARIATION IN T_s FOR DIFFERENT VALUES OF F

F	T_s
.02	239.0
.06	241.8
.08	241.0
.10	241.8*
.18	245.1

* This is the value presented in the data.

Some of the uncertainty in F stems from the unknown location of the thermocouple. However it is in the same location for all the tests which lowers the relative uncertainty when comparing the surface temperatures of different tests.

Suppose the temperature measured by thermocouple T_m correspons to $Y = .015$ inches, then for all tests the maximum value of F is .18 and the minimum value is .08. Since the surface temperature was calculated with $F = .10$, the uncertainty of the surface temperature will not be symmetric. This may be shown by using values from test 146 (Table III) where the uncertainty of the surface temperature for $F = .1$ becomes $+ 3.3$°F and $- .8$°F. If the average value between .08 and .18 (i.e. $F = .13$) had been used to calculate the surface temperature instead of $F = .10$, the surface temperature as presented in the data for all tests would have been about 2°F higher and the uncertainty would have been symmetric at ± 2°F. But since this is a constant amount which may be added to all the data it need not be considered when comparisons are being made between tests.

The uncertainty level is dependent upon the magnitudes of the heat flux, the bulk liquid temperature and the measured temperature, but only in a minor way. Test 146 and $Y = .015$ were selected by examination of the data as representing the maximum uncertainty level which makes all uncertainty levels less than this quantity. Consequently the relative uncertainty level of the surface temperature is ± 2°F.

E. Bubble Radius

The method generally used in the literature (e.g.[13,48,52]) to obtain bubble growth and departure data from photographs has been to determine an equivalent bubble radius by averaging the measurements of two perpendicular axes. This method has the advantage of simplicity, but may introduce unnecessary errors if axial symmetry can be assumed. Consider, for example, an oblate spheriod with major semi-axis (a) and minor semi-axis (a/k). The volume is $(4/3)\ \pi\ a^3/k$. The volume as determined by the method of average axes is $\frac{4}{3}\pi a^3 (\frac{1+k}{2k})^3$, which results in a percentage error of:

$$\%\ ERROR = \left[1 + k \left(\frac{1+k}{2k} \right)^3 \right] 100 \qquad (50)$$

Thus, if a bubble of constant volume were to change shape from a sphere to an ablate spheriod with $k = 2$, the average axes method results in an apparent volume change of 16%.

Examination of the bubble photographs demonstrated that in the plane of the photographs many bubbles maintained a condition of symmetry up to the time of departure. This symmetry was generally maintained after departure in the low subcooling tests, but with high subcooling the rapid collapse of the bubbles often resulted in highly irregular shapes.

When two bubbles grew close to one another, or when one bubble followed closely behind another bubble, the condition of symmetry was not always maintained. Except for some of the measurements made to determine departure size and frequency of departure, only symmetric bubbles have been analyzed. These symmetric bubbles are generally referred to in the literature as isolated bubbles in that they are not influenced in their growth by surrounding bubbles.

During the growth of isolated bubbles, up to a radius of about .020 inches, the effect of the walls (quartz windows) on the bubble shape and growth rate is believed to be negligible since the ratio of the wall spacing to the bubble diameter is almost 10:1. Also, these bubbles are growing in a region of uniform surface heat flux, since the width of the center portion of the test strip is .070 inches. Thus one might expect these bubbles to be axially symmetric. When a bubble grows to a radius much larger than .020 inches, the walls may tend to restrict bubble growth in the plane perpendicular to the photographic plane. Also, since the region of uniform surface heat flux is approximately .070 inches wide, the larger bubbles may not always remain in this region of uniform flux. These two effects may upset the condition of axial symmetry even though the bubble remains symmetric in the photographic plane. These effects can be evaluated only by photographing the bubbles in two perpendicular planes, which is not possible with the test surface configuration used.

Since much of the bubble life may be approximated by a condition of axial symmetry, a method is available for determining equivalent bubble radii which is considerably more accurate than the average axis method. Figure 26 shows a bubble divided into four equally spaced sections. Measurements of the bubble height (H1) and the five diameters (Y0...Y4)

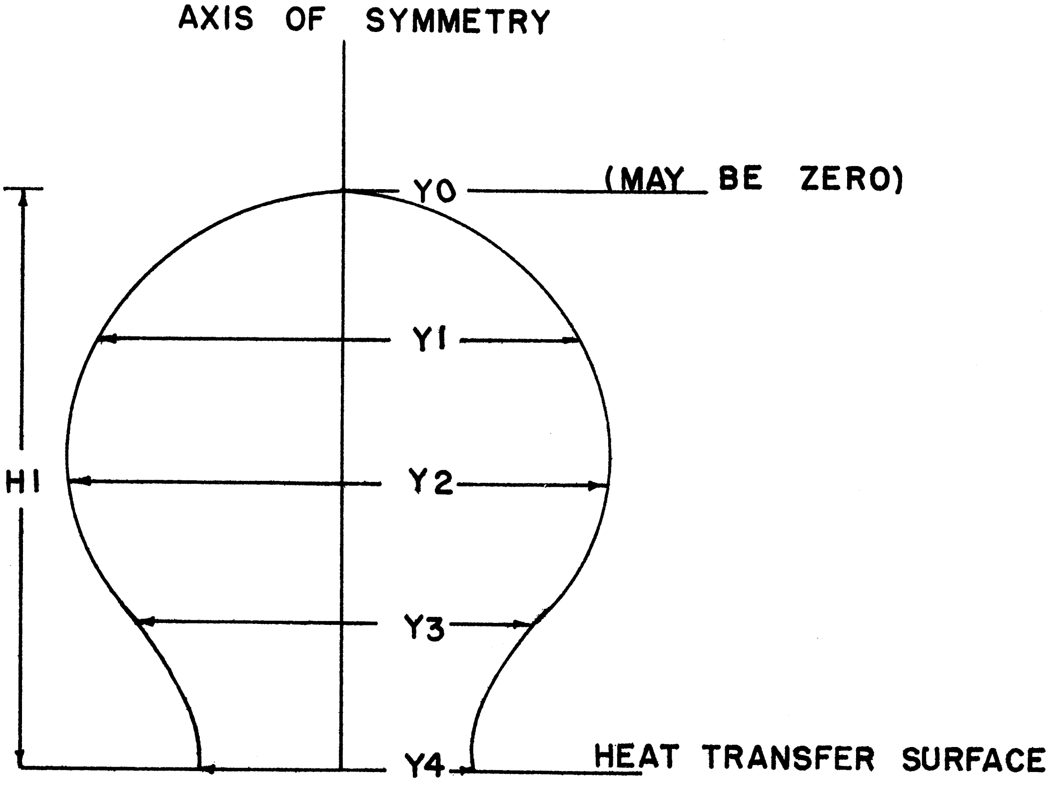

Figure 26. Illustration of Five Measurements Made on Each Bubble.

were made of each bubble picture. Using these six measurements, a fourth order polynominal was generated and integrated to determine the bubble volume. This volume was then used to determine the radius of a sphere of equal volume.

Using this method on the same oblate spheriod described earlier in this section gives an apparent volume change of 4% as compared to the average axes method of 16%.

The procedure for computing the equivalent bubble radius will now be described. From a cursory examination of each film, bubbles were selected which were to be analyzed in detail. These bubbles were of the isolated type as described earlier. The overall magnification was determined from the calibration film which was back projected onto an opalized glass screen in the same manner as the bubble pictures. From measurements of the diameter of the thermocouple sheath which was in the same plane as the bubbles, the total magnification was determined. The total magnification varied between 36 and 62.

Each bubble picture was then back projected onto the screen and the six bubble measurements, the frame number and the magnification were punched directly on IBM cards. Measurements were made for each picture of an isolated bubble, from it's first appearance on the film up to departure. Since bubble growth and departure data was the information desired, usually 1/2 to 1/4 of the remaining pictures after departure were analyzed.

The punched cards, along with a number of control cards giving the test conditions, camera speed, etc., where fed into the computer.

The computer output was in the form of a list of the bubble volume, equivalent radius, and time as determined from the frame numbers. The equivalent radius versus time data for each bubble was also plotted by the computer, and by examination of this plot for consistance any random measurement errors could easily be found and corrected. Examples of the computer plots are given in Appendix C.

F. Bubble Growth Expressions

The methods generally used to establish trends in bubble growth rates under varying conditions have been to compare graphs of bubble radii versus time (e.g.(7,52)). This method can only give equalitative results and is therefore unsuited for a quantitative examination of bubble growth rates. In the literature survey, a number of theoretical growth equations for the asymptotic growth period expresses the bubble radius as being proportional to the square root of time. These suggest an emperical equation for bubble radii of the form:

$$R = K\tau^{1/2} \tag{51}$$

or, in a more general form:

$$R = K\tau^{n} \tag{52}$$

The form of Equations (51) and (52) is such that the value of R at time zero must also be zero. However, the value of time determined from the photographs by assigning time zero to the picture just before the bubble comes into view is not the correct value for use in these equations. The bubble began it's growth at some time prior to its first appearance on the film. This is evident when the experimental values of radii are plotted against picture frame number on an expanded scale as in Figure 27. By shifting the time scale for this particular bubble approximately 1/2 of a frame, a smooth curve may be drawn through the experimental points and the new origin. If Equation (52) is to fit the data, the data points must then exhibit a straight line when plotted on log-log co-ordinates. Figure 28 shows the unshifted data points and the shifted points of the same bubble plotted on log R versus log time co-ordinates. The shifted data points assume a straight line to about 80% of the maximum bubble size whereas the unshifted points do not. The slope of this straight line is equal to n. Thus, a time co-ordinate shift must be added to Equation (52) to correct the value of the time as determined from the first frame. Equation (52) then becomes:

$$R = K(\tau - \tau_0)^n \qquad (53)$$

One method of fitting data to an emperical equation is by the method of least squares which may be expressed as:

$$L = \sum_{i=1}^{m} \left[R_i - K(\tau_i - \tau_0) \right]^2 \qquad (54)$$

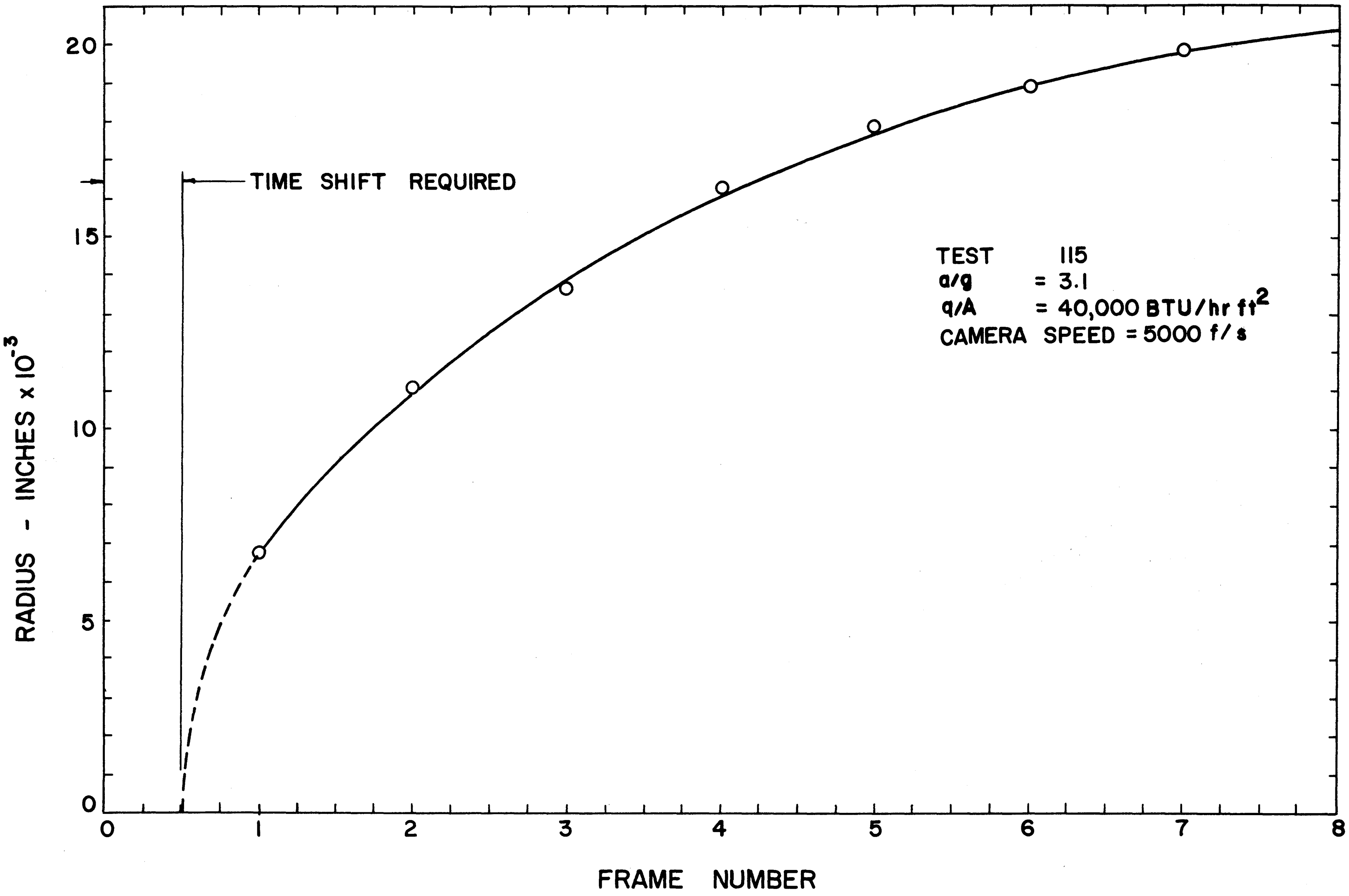

Figure 27. Typical Equivalent Bubble Radius Versus Time Data on Cartesian Co-ordinates.

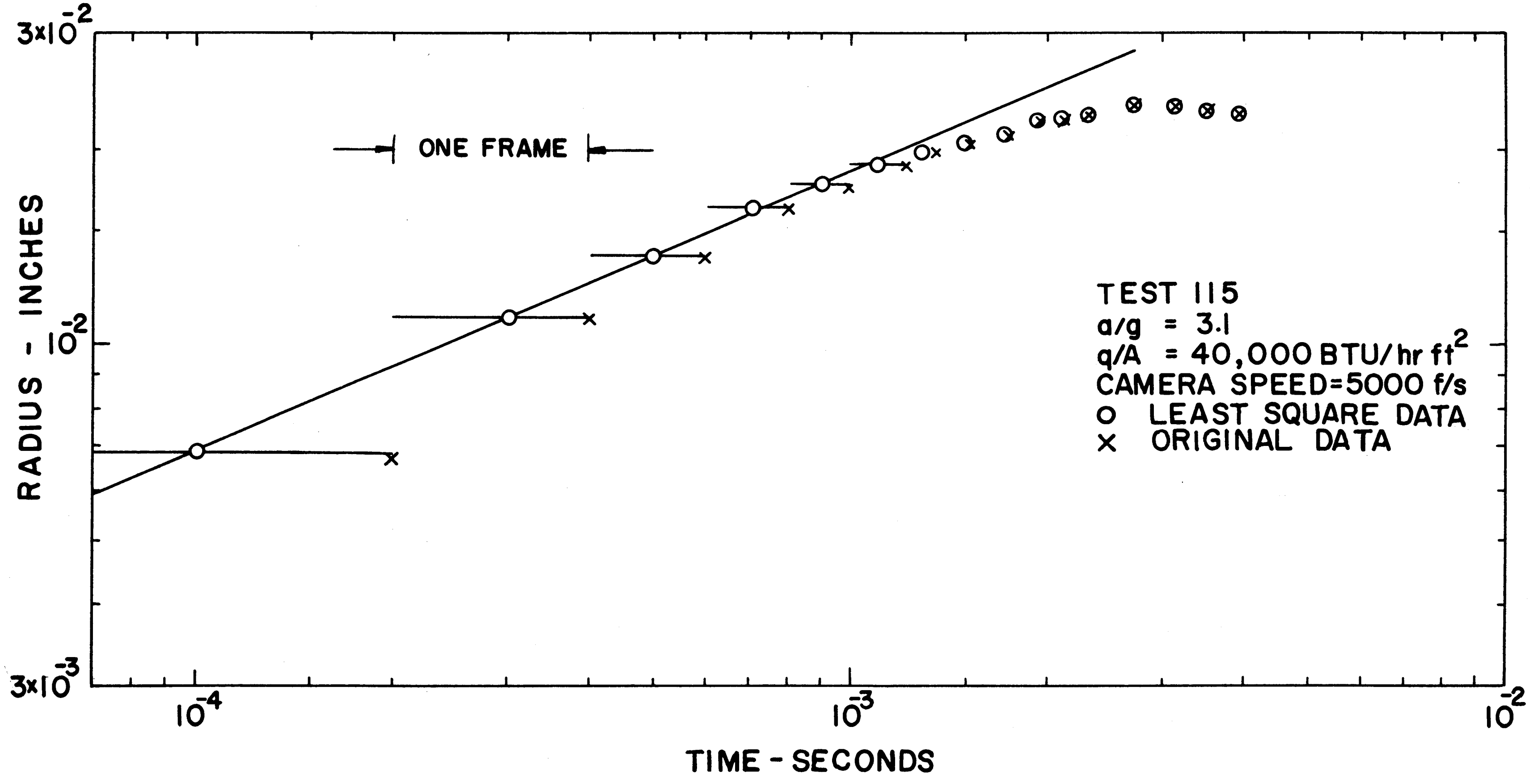

Figure 28. Typical Equivalent Bubble Radius Versus Time Data on Logarithmic Co-ordinates.

the sum (L) is differentiated with respect to K, n, and τ_0 and the resulting three equations set equal to zero. These three equations determine the least square values on K, n, and τ_0 in terms of the data points $(R_i \ldots R_m)$ and $(\tau_i \ldots \tau_m)$. However, the resulting equations are sufficiently complicated so that it is impractical to solve for the three parameters except by extensive numerical methods.

An alternative method exists whereby values for n, K, and τ_0 may be determined with a minimum of numerical analysis. If the emperical Equation (53) is expressed in terms of logarithms and all derivatives are taken with respect to logarithms, this new form facilitates the numerical analysis to such an extent that only minor numerical procedures are required. The logarithmic least square form of Equation (53) becomes:

$$L = \sum_{i=1}^{m} \left[\ln R_i - \ln K - n \ln(\tau_i - \tau_0) \right] \qquad (55)$$

By differentiating the sum with respect to $\ln K$ and $\ln n$ only, the resulting two equations may be solved for K and n in terms of τ_0 and the R_i's and τ_i's. Then if values of L are determined for a number of values of τ_0, the minimum value of L will correspond to the least square value of τ_0. This procedure was carried out on the IBM 7090 computer where τ_0 was allowed to assume values of time between 1 1/2 frames before the first picture up to the first picture, in increments of time equal to 1/10 of a frame. The reason for permitting τ_0 to cover a range of time greater than one frame is that a bubble could exist in frame zero but have a radius of less than 0.003 inches, which is estimated as the minimum discernible bubble size on the surface.

This minimum resolution of bubbles on the surface is due to distortion caused by the density gradient in the water near the heater surface. The minimum discernible bubble radius away from the surface is setimated to be 0.001 inches.

It should be noted that the values of n, K, and τ_o as determined by the logarithmic least square fit are not the same as for the normal least square fit. The reason for this difference is that the difference between the logarithms of two numbers increases when the magnitudes of numbers decrease, if the difference between the two numbers remains the same. The net effect is that the logarithmic results fit the data better in the region of small time and radius whereas the normal least square result will fit the data equally well in all regions.

The value of m, which is the number of data points used in the logarithmic least square fit for the determination of τ_o was selected as five. This choice of m was somewhat arbitrary but does not effect the results significantly. Since the bubbles do exhibit an exponential growth, as will be discussed in Chapter VI, any value of m up to the point where the growth can no longer be characterized by the same exponent will result in the same value of τ_o (within $\pm$ 1/10 of a frame).

After determining the value of τ_o for a particular bubble with m equal to five, the logarithmic least square procedure was continued, using the same value of τ_o, by successively increasing m and determining new values of n and K nutil all data points were included up to the maximum bubble size or to bubble departure. The values of n and

K presented in the data were chosen by examinating computer plots of log R revsus log $(\tau-\tau_o)$ and selecting n and K corresponding to the maximum radius which falls on the straight line drawn through the preceding data points. Consequently, the values of n and K presented are valid for a particular bubble up to 70% to 90% of it's maximum size.

The value of n will be shown in Chapter VI to be virtually independent of acceleration. If the bubble radius-time data is expressed by an equation of the form;

$$R = J(\tau - \tau_o)^{1/2} \tag{56}$$

where τ_o is the value of time shift as determined from Equation (53), then J/2 is proportional to the bubble growth rate at any value of time, and any two bubble growth rates may be compared by comparing their individual values of J.

The value of J was determined by a normal least square procedure over the same interval as was used to calculate the values of K and n. A normal least square method was used because it gives a slightly better fit than the logarithmic procedure, and for Equation (56) is no more complicated than the logarithmic procedure.

The use of J as a quantity which represents the growth rate amounts to a criteria for specifying for each bubble a time to be used in Equation (53), from which a growth rate can be calculated and compared with other growth rates calculated in the same manner. The value of J of a particular bubble can be determined from the values of K and n and from the time (τ_1) where Equations (53) and (56) have the same value of R . i.e.:

$$R = K\tau_1^n = J\tau_1^{1/2}$$

or

$$J = K\tau_1^{n-1/2} \tag{57}$$

Because of the nature of the least square procedure, τ_1 will always exist within the range of the data points used in calculating K, J and n .

The bubble growth rates at any time τ as determined by Equations (53) and (56) are:

$$\dot{R} = nK\tau^{n-1} \tag{58}$$

and

$$\dot{R} = \frac{1}{2}J\tau^{-1/2} = \frac{1}{2}\left(K\tau_1^{n-1/2}\right)\tau^{-1/2} \tag{59}$$

Equation (58) represents the actual growth rate at any time τ within the early growth period, but the growth rate as determined by Equation (59) is equal to this growth rate at only one specific time τ_2 . Thus by equating these two growth rates, the time τ_2 may be determined:

$$\tau_2 = \frac{\tau_1}{(2n)^{\frac{2}{2n-1}}} = \left(\frac{J}{2nK}\right)^{\frac{2}{2n-1}} \qquad (60$$

In other words, only at time τ_2 does Equation (56) represent the actual growth rate and using J as characteristic of the growth rate is equivalent to using τ_2 in Equation (53) for comparing growth rates.

CHAPTER VI

RESULTS

A. General

The experimental results are categorized under the general headings: Bubble Departure Size, Outer Contact Angle, Maximum Bubble Size, Time to Maximum Bubble Size and Time to Bubble Departure Size, Bubble Frequency and Departure Relations, Bubble Growth Expressions, and Heat Transfer Data. The data is presented on a series of graphs showing the relationship between acceleration and each parameter investigated. For each parameter, the arithmetic average is shown for each test condition and the spread of the data is represented by a vertical line extending to the maximum and minimum values. A number has been placed above this vertical line which corresponds to the total number of observations used to determine the arithmetic average and thus serves as an indication of the statistical weight associated with each data point. In order to represent more clearly several test conditions at each acceleration, the data points may be displaced slightly from the actual acceleration.

Examples of the bubble radius versus time data obtained from the photographs from which some of the information was derived are shown in Figure 29. Each of the bubbles was selected from a different level of acceleration used in the test program, and all were obtained at a heat flux of 40,000 Btu/hr-ft^2 and 10°F subcooling.

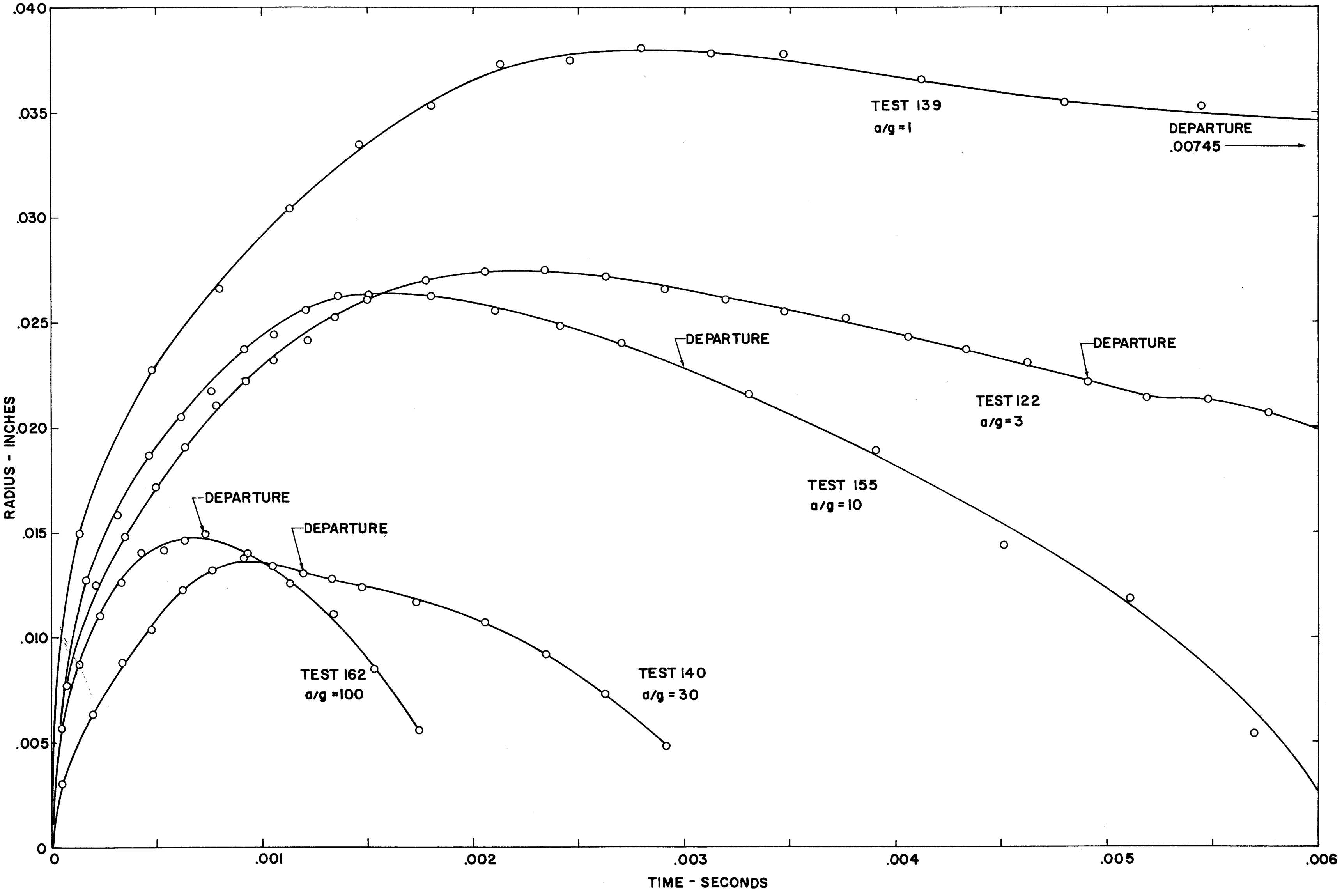

Figure 29. Typical Bubble Radius and Time Data for Five Accelerations.

These bubbles were chosen to represent only the trends observed for the time interval between initiation and departure, as this time is influenced by increasing acceleration and should not be considered as necessarily representative of other trends.

All the experimental values obtained in this investigation are divided into three groups and are tabulated in Appendix B for reference. Table V lists the heat transfer data for all the tests (i.e., heat flux, surface temperature, bulk liquid temperature, surface saturation temperature and acceleration). The tests numbered from 107 to 174 are the photographic study and the tests numbered 201 through 217 are the heat transfer study. Table VI lists for each bubble the corresponding test number, the values of volume, equivalent radius and time, and when they are available, the outer contact angle at departure and the emperical growth constants. The value of the time shift (τ_o) as determined by Equation (53) is presented in Table VI as the time corresponding to zero values of both radius and volume. The departure size of each bubble is denoted by the letter (D). Table VII is a listing, for each test, of the departure sizes and frequency of departure (to be defined in this chapter) for both isolated and certain non-isolated bubbles.

Two different types of bubbles were observed in this investigation. One type, which will be referred to as isolated, grows and departs without being distorted by or coalescing with bubbles emmited from neighboring sites or from the preceding or succeding bubble from the same site; the remaining bubbles were not isolated but were distorted by, or coalesced with, neighboring bubbles or coalesced with the preceding bubble from the same site. Included in this latter category are bubbles which originated from visible vapor remains left on the surface by the previous bubble. The isolated bubble will be given special attention in the following sections since these are the type which serve as mathematical models in the development of many boiling heat transfer correlations.

B. Bubble Departure Size

The bubble departure size is defined as the size corresponding to the instant when the bubble breaks contact with the heat transfer surface.

The arithmatic average of the bubble departure size of isolated bubbles is plotted on Figure 30 versus acceleration. For the low subcooling tests ($2^{\circ}F$), two different heat fluxes are presented. For the lowest heat flux ($q/A = 16{,}000$ BTU/hr-ft^2) no boiling was observed on the photographs at an acceleration of $a/g = 10$. When the heat flux was increased to 40,000 BTU/hr-ft^2 at $a/g = 1$, no isolated bubbles were observed on the photographs. Consequently, only two data points are available for each heat flux with low subcooling. At $a/g = 3$, the average bubble size is approximately the same for both $q/A = 16{,}000$ BTU/hr-ft^2 and $q/A = 40{,}000$ BTU/hr-ft^2, but considerably lower than at $a/g = 1$. As the acceleration is increased to $a/g = 10$ for $q/A = 40{,}000$ BTU/hr-ft^2 the average departure does not change significantly from the size at $a/g = 3$.

The departure sizes of isolated bubbles for the tests with high sub-cooling are also represented on Figure 30 and are about 50%

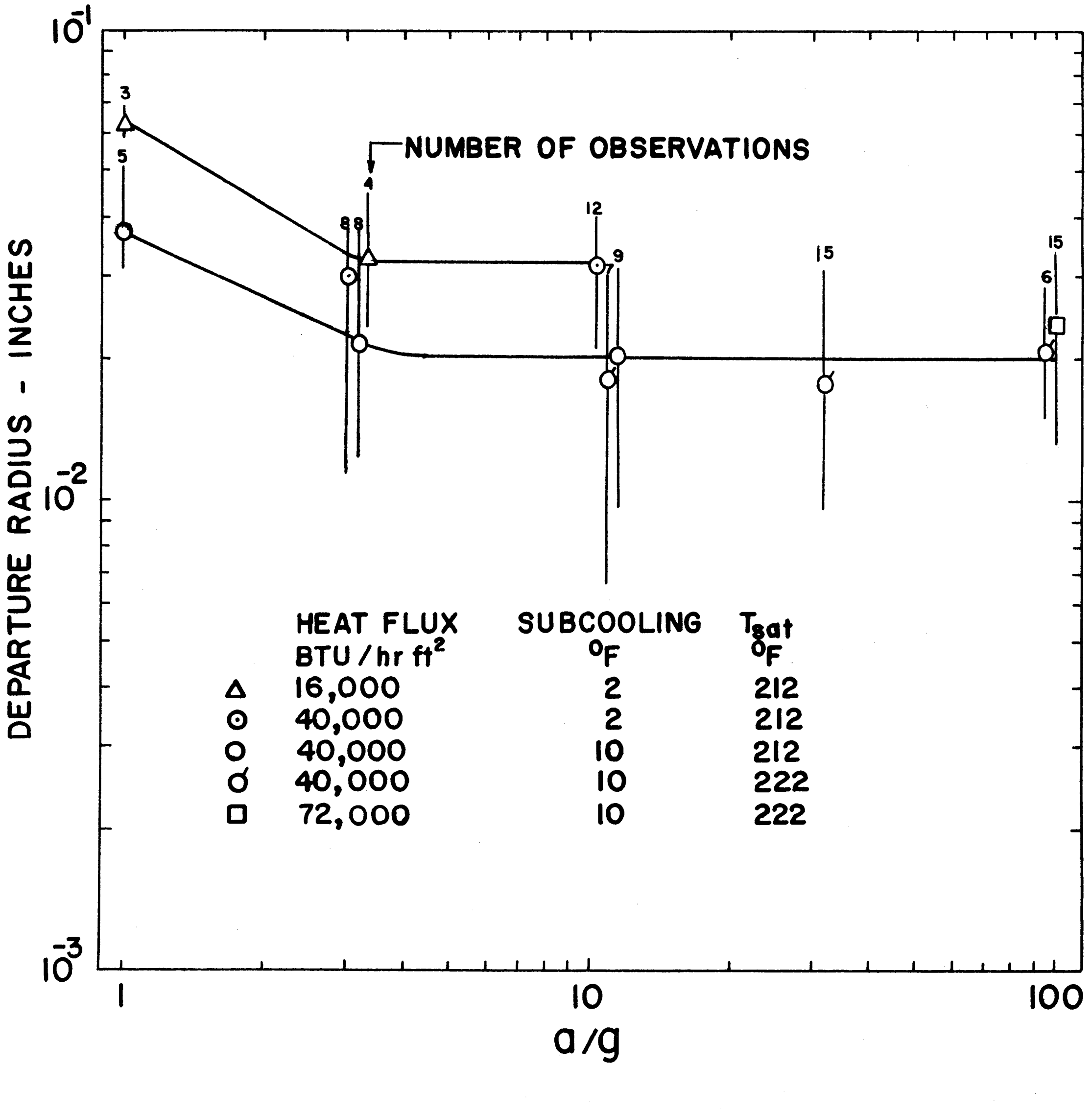

Figure 30. Departure Size of Isolated Bubbles.

smaller than the bubbles with low subcooling. With 10°F subcooling, no boiling was present at q/A = 16,000 BTU/hr-ft^2 and a/g = 1. At a heat flux of 40,000 BTU/hr-ft^2 isolated bubbles were observed at all levels of acceleration and show a decreasing trend of departure size from a/g = 1 to a/g = 10, and then remains essentially constant to a/g = 100. At a heat flux of 70,000 BTU/hr-ft^2 and an acceleration of a/g = 30, the boiling was violent and no isolated bubbles were observed, but when the acceleration was increased to a/g = 100, isolated bubbles did exist. At a/g = 100, the average departure radius at q/A = 72,000 BTU/hr-ft^2 is approximately equal to the average departure radius at a heat flux of 40,000 BTU/hr-ft^2.

In an attempt to evaluate some of the effects of bubbles interfering with one another, the average departure radii for a large number of both isolated and certain types of non-isolated bubbles are plotted on Figure 31. The non-isolated bubbles selected were distorted by, but did not coalesce with neighboring bubbles and bubbles which originated from the remains of preceding bubbles. The average departure radius of these bubbles is slightly lower than the average of the isolated bubbles alone, but exhibit the same trends as the isolated bubbles by decreasing between a/g = 1 and a/g = 3 and remaining constant between a/g = 3 and a/g = 100.

Figure 32 illustrates the random nature of the boiling process by showing the distribution of isolated bubble departure sizes for two of the conditions plotted on Figure 30. The first condition is a/g = 3 and q/A = 40,000 BTU/hr-ft^2 with 2°F subcooling, the second

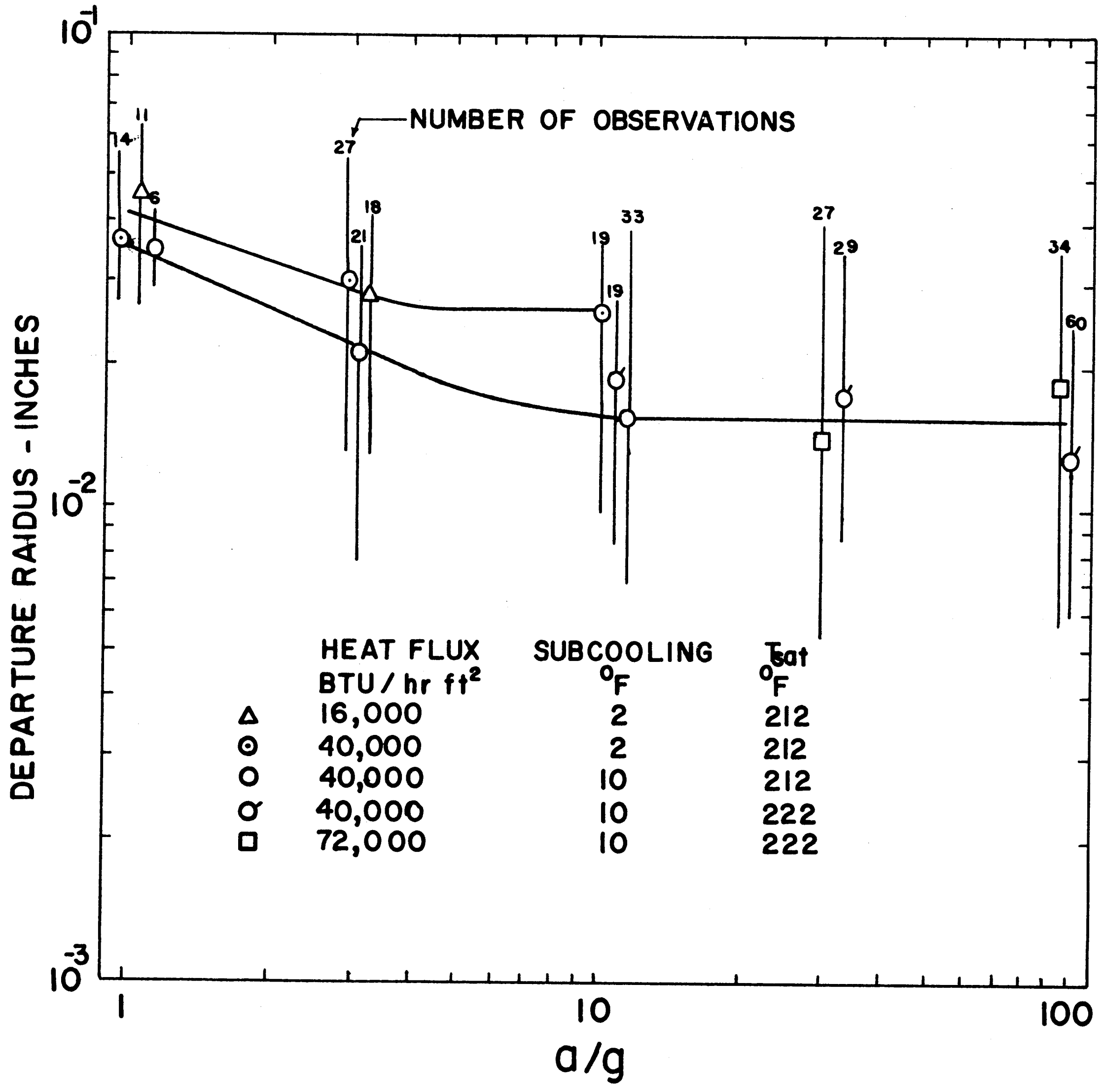

Figure 31. Departure Size of Isolated and Certain Non-isolated Bubbles.

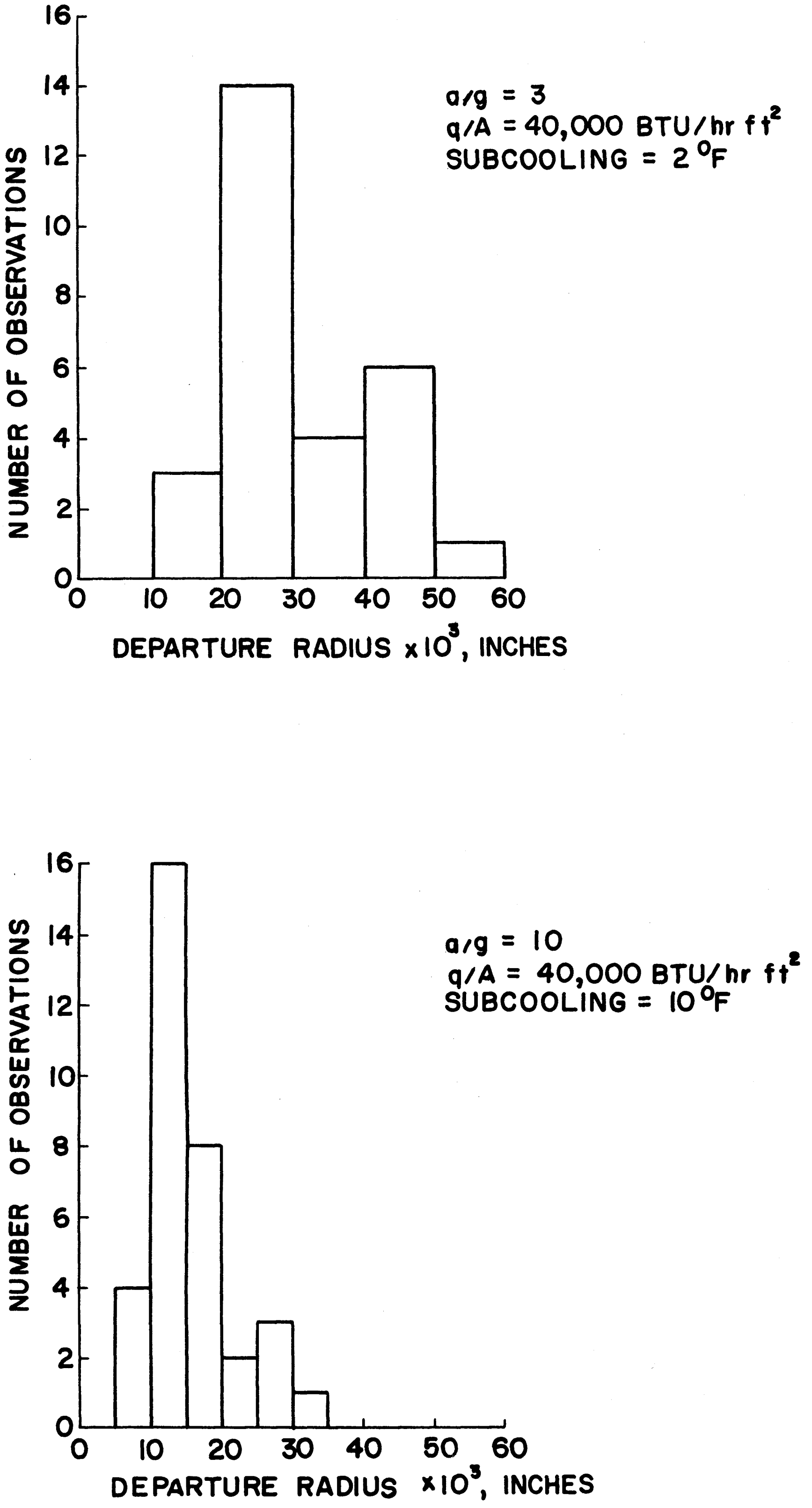

Figure 32. Statistical Distribution of Departure Radius.

is $a/g = 10$ and $q/A = 40{,}000$ BTU/hr-ft^2 with 10°F subcooling. These are typical of the distributions for all the conditions.

C. Maximum Bubble Size

The maximum bubble size for the isolated bubbles are plotted on Figure 33. Only the maximum size for the tests with high subcooling are presented. With low subcooling, the bubbles do not attain a maximum while attached to the surface, but continue to grow until they leave the field of view. The maximum size is seen to decrease from $a/g = 1$ to $a/g = 3$, and then remain essentially constant to $a/g = 100$. The maximum bubble size at $a/g = 100$ appears independent of heat flux for $q/A = 40{,}000$ BTU/hr-ft^2 and $q/A = 70{,}000$ BTU/hr-ft^2.

A comparison between the maximum size and the departure size of all isolated bubbles obtained with low subcooling is made on Figure 34, by plotting the average percentage decrease in size at departure from the maximum size. The maximum size of each bubble at accelerations between 1 and 10 is seven to thirty percent greater than its departure size. At $a/g = 100$ a significant change is noted in this percentage decrease in size. Every isolated bubble observed for both $q/A = 40{,}000$ BTU/hr-ft^2 and 72,000 BTU/hr-ft^2 at $a/g = 100$ departed before collapsing more than nine percent in size. At $a/g = 10$ and $a/g = 30$, the spread of the data is considerably greater than $a/g = 100$ but shows a definite decreasing trend with increasing acceleration.

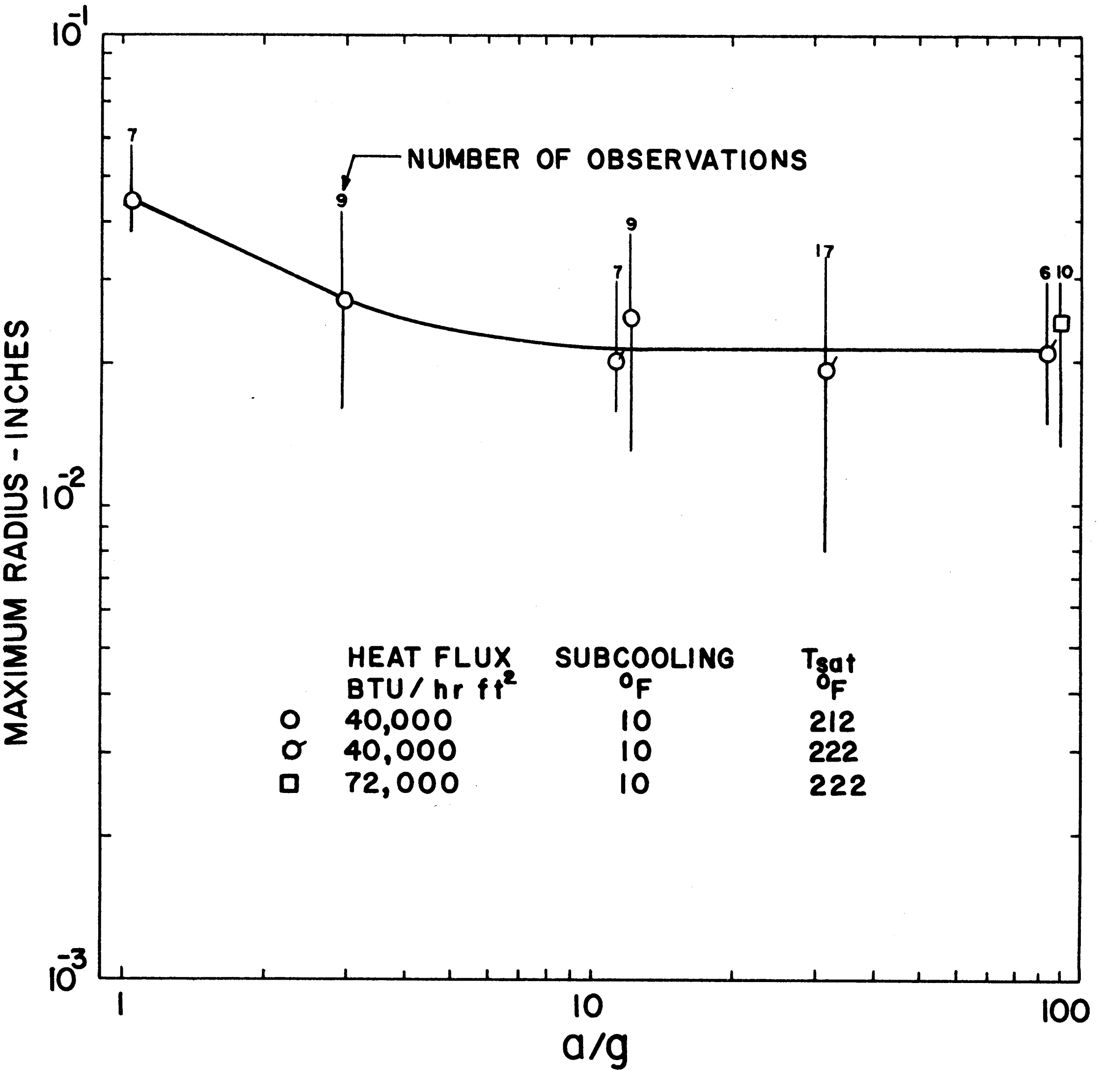

Figure 33. Maximum Size of Isolated Bubbles.

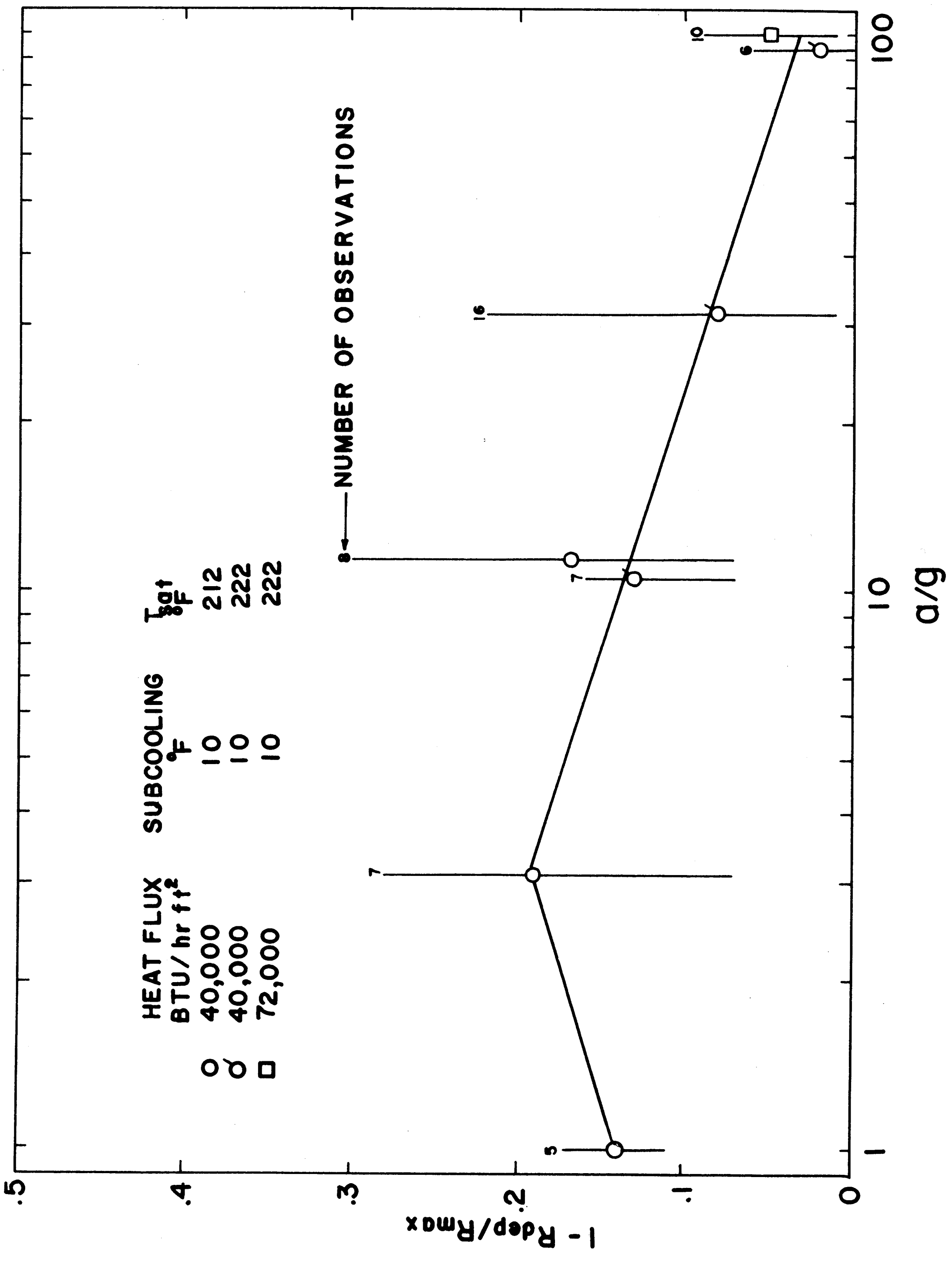

Figure 34. Percentage Decrease in Size from Maximum to Departure.

D. Outer Contact Angle

The outer contact angle (BETA in Appendix B, Table VI) at departure is defined as the angle between the heat transfer surface and liquid-vapor interface at the heat transfer surface just prior to departure. This outer contact angle is used in several predictions of bubble departure size (e.g., Equations (2) and (3)). Figure 35 is a plot of this angle versus acceleration, and even though a wide range of measure contact angles exists at each test condition, a distinct decrease with increasing acceleration is exhibited. No consistent influence of either subcooling or heat flux could be observed.

E. Time to Maximum Bubble Size and Time to Departure Size

As discussed in Chapter V, time zero for bubble growth was obtained for each bubble by fitting an emperical equation (Equation (53)) to the first five data points. This time zero will be used in the following discussion as the reference point from which all time intervals will be measured.

The average time interval required for isolated bubbles to grow to their maximum size is plotted on Figure 36. Again only the tests with high subcooling are presented, since a maximum size could not be determined for tests with low subcooling. A linear relationship exists between the logarithm of a/g and the logarithm of the time interval to maximum size such that this time interval can be represented within ± 20% by the following equation:

$$\tau_m = .32 \times 10^{-3} \, (a/g)^{-.27} \tag{61}$$

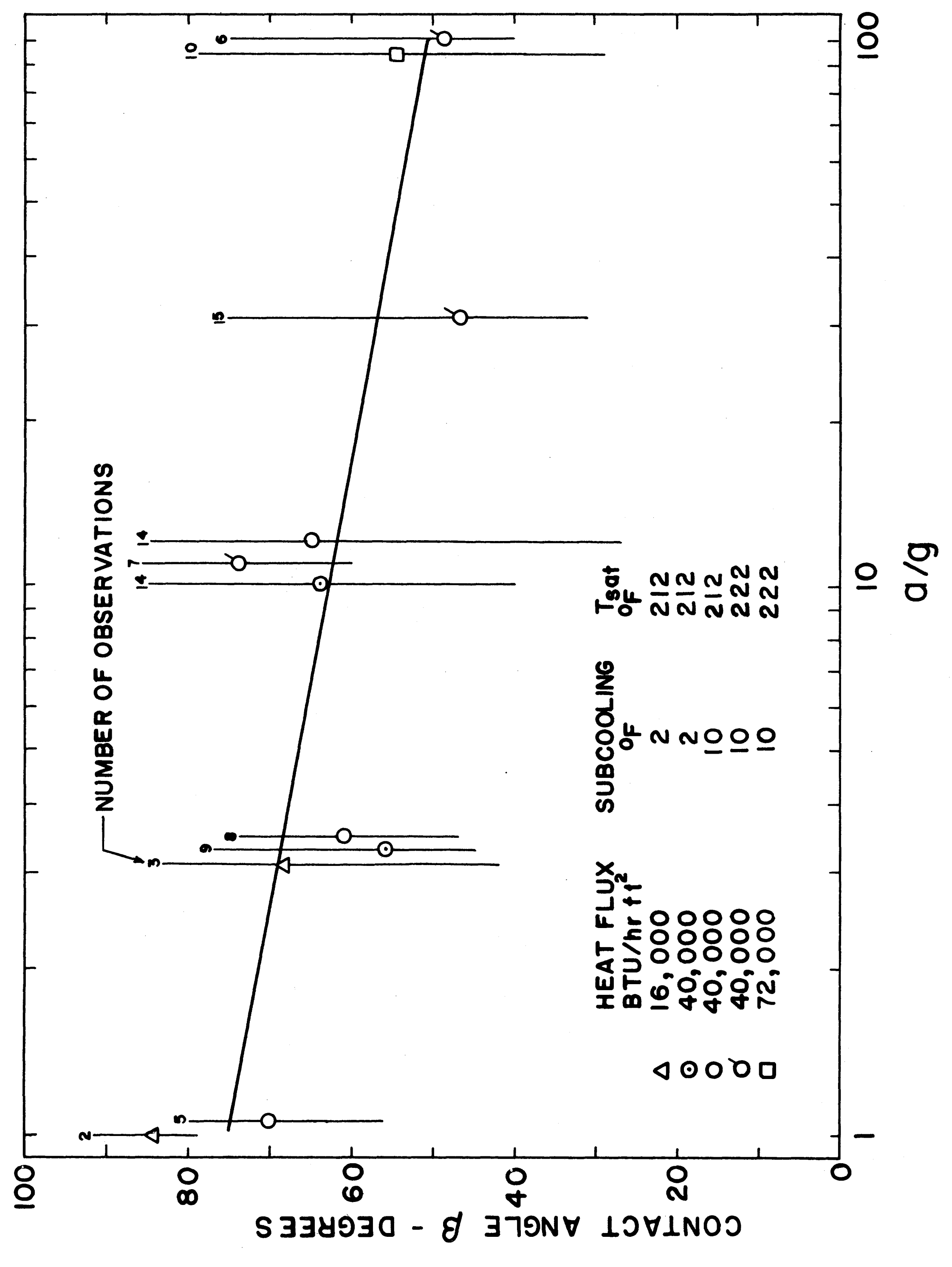

Figure 35. Outer Contact Angle at Departure for Isolated Bubbles.

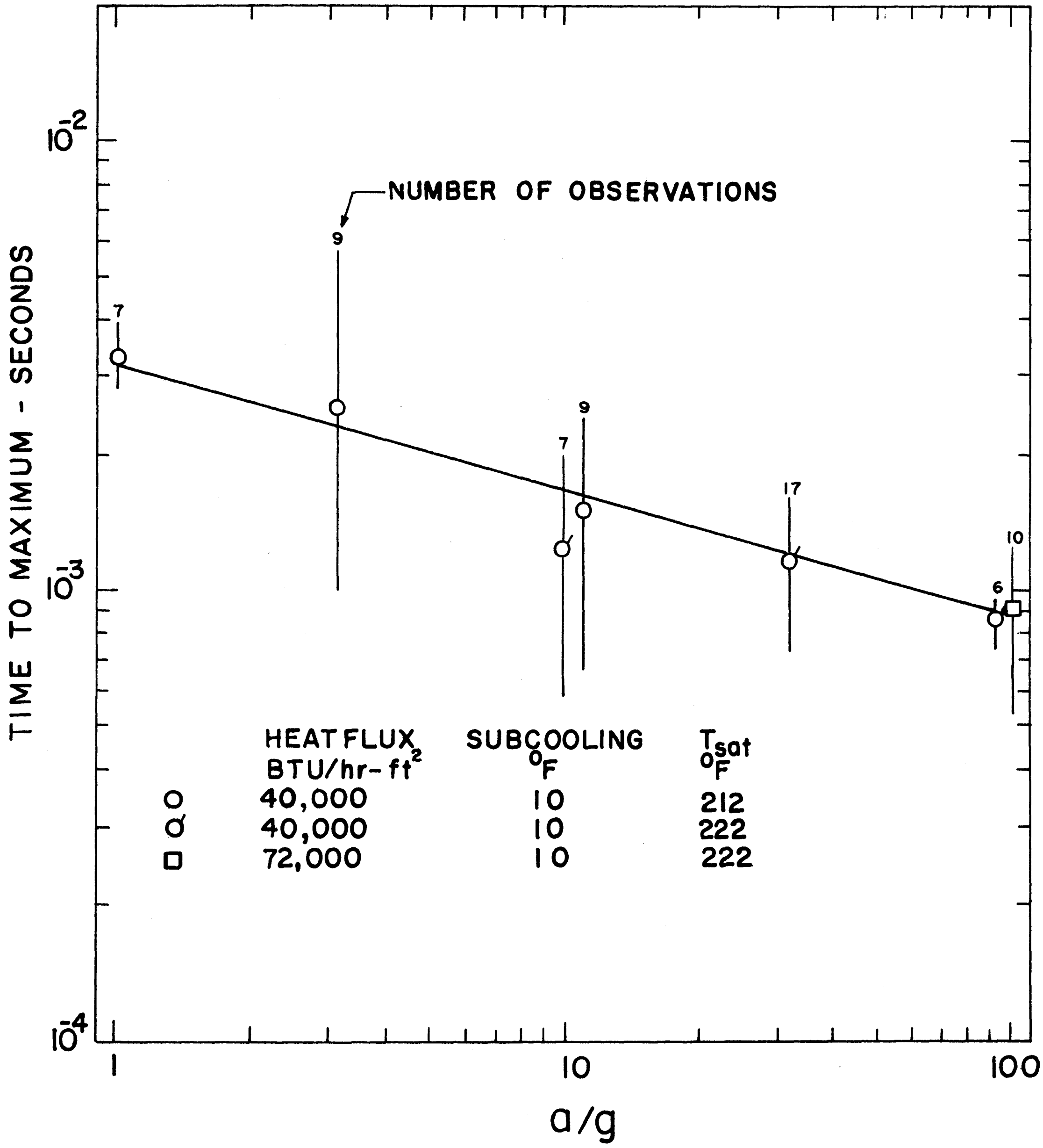

Figure 36. Time to Maximum Size for Isolated Bubbles.

Due to the random nature of the boiling process this equation will not predict the time to maximum size of an individual bubble better than ± 300%.

The average time interval between bubble initiation and departure for all the isolated bubbles analyzed (both low and high subcooling) is plotted on Figure 37. At a/g = 100, the average departure time appears to be independent of heat flux for q/A = 40,000 BTU/hr-ft^2 and q/A = 70,000 BTU/hr-ft^2. For low subcooling and a/g = 3, the average departure time for a heat flux of 16,000 BTU/hr-ft^2 is almost twice the average for q/A = 40,000 BTU/hr-ft^2 even though the average departure sizes for these two heat fluxes are approximately the same.

The average time interval from initiation to departure for the high subcooling tests can be represented within ± 10% by the following expression:

$$\tau_d = .0094\,(a/g)^{-1/2} \tag{62}$$

F. Bubble Frequency and Departure Diameter Relations

Many nucleate boiling correlations (e.g., Refs. (2), (16) and (58)) use the result first proposed by Jakob and Linke in 1935 (see Jakob$^{(5)}$), that the bubble frequency times the departure diameter is a constant.

The frequency of bubble departure is defined here as the reciprocal of the period between the departure of one bubble and the departure of the next bubble from the same site. A portion of a typical

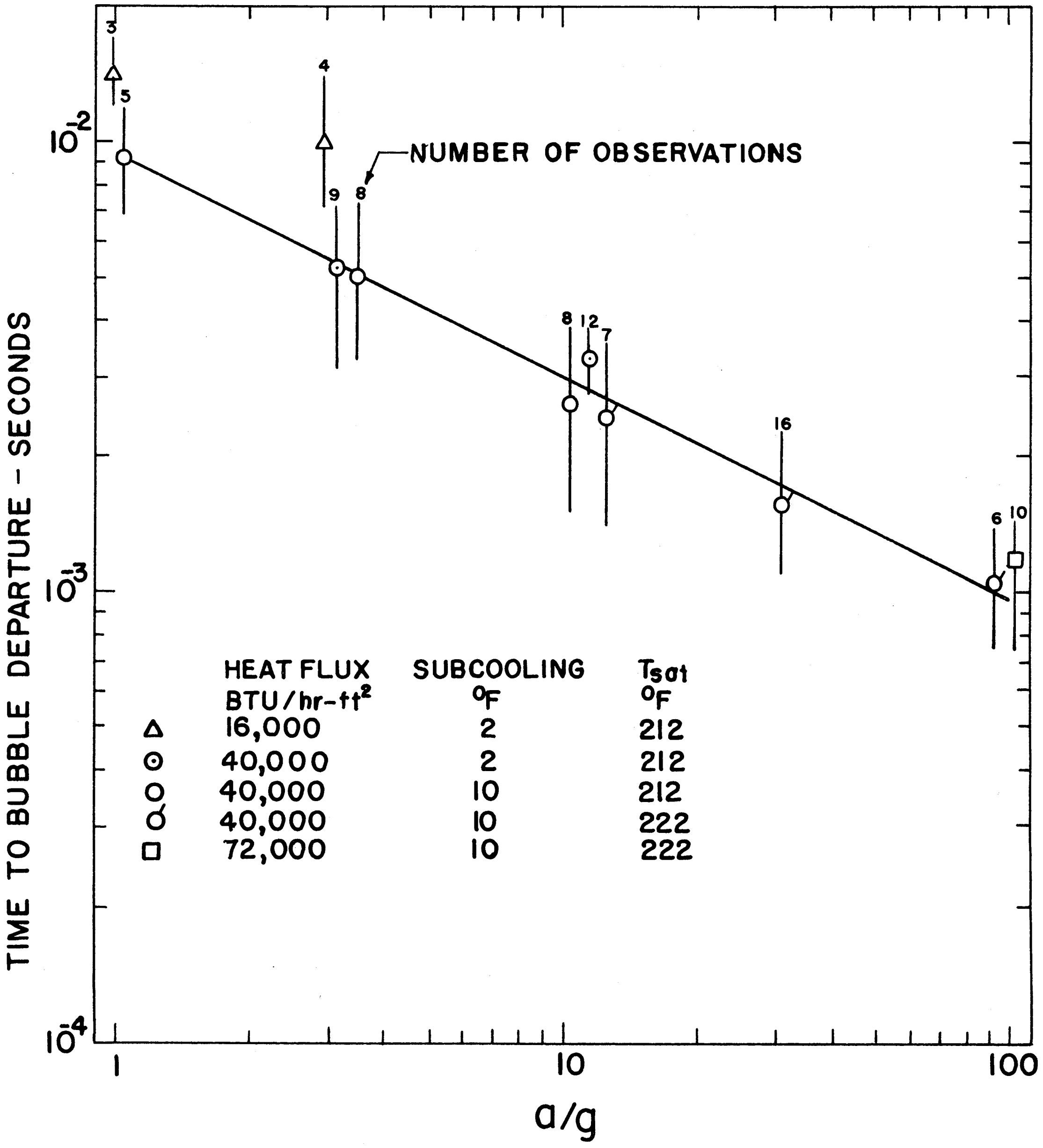

Figure 37. Time to Departure Size for Isolated Bubbles.

sequence from which frequency of departure and departure size was obtained is shown on Figure 49 in Appendix A. As described earlier, two types of departing bubbles were observed. One type left behind a small visible vapor residue after departure which immediately began to grow. Consequently, the waiting time between the departure of one bubble and the beginning of the next was zero. The other type appeared to depart with no residue remaining on the surface. After a departure of this type, a waiting period existed before the next bubble began to grow from this site. From a single site, both types of departing bubbles were observed on one film with no apparent regularity.

On Figure 38 the frequency of the departure is plotted for the same bubbles whose average departure diameters are plotted on Figure 31. The average frequency increases about one order of magnitude between a/g = 1 and a/g = 100. At a/g = 1, the average frequency of departure for low subcooling increases from 42 bubbles/second at a heat flux of 16,000 BTU/hr-ft^2 to 120 bubbles/second at a heat flux of 40,000 BTU/hr-ft^2. For these same two heat fluxes at a/g = 3, the average frequency is higher than at a/g = 1. At both a/g = 3 and a/g = 10, the frequency of departure appears to be independent of subcooling.

The product of the frequency of bubble departure and the departure radius is plotted on Figure 39 as a function of acceleration. At a/g = 1, the average FR_d product shows a marked increase with increasing heat flux. At a/g = 3, however, this dependence on heat

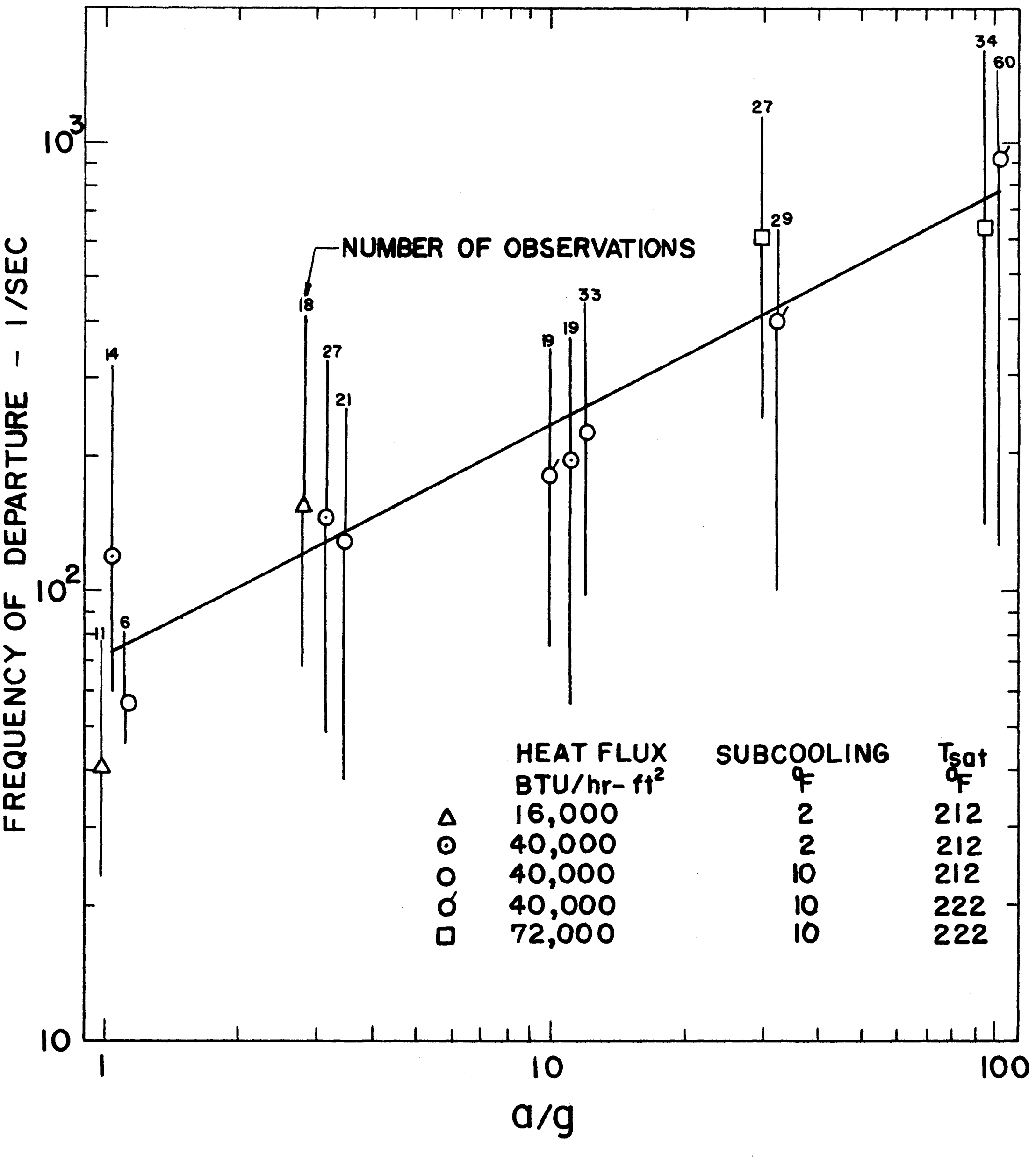

Figure 38. Frequency of Bubble Departure.

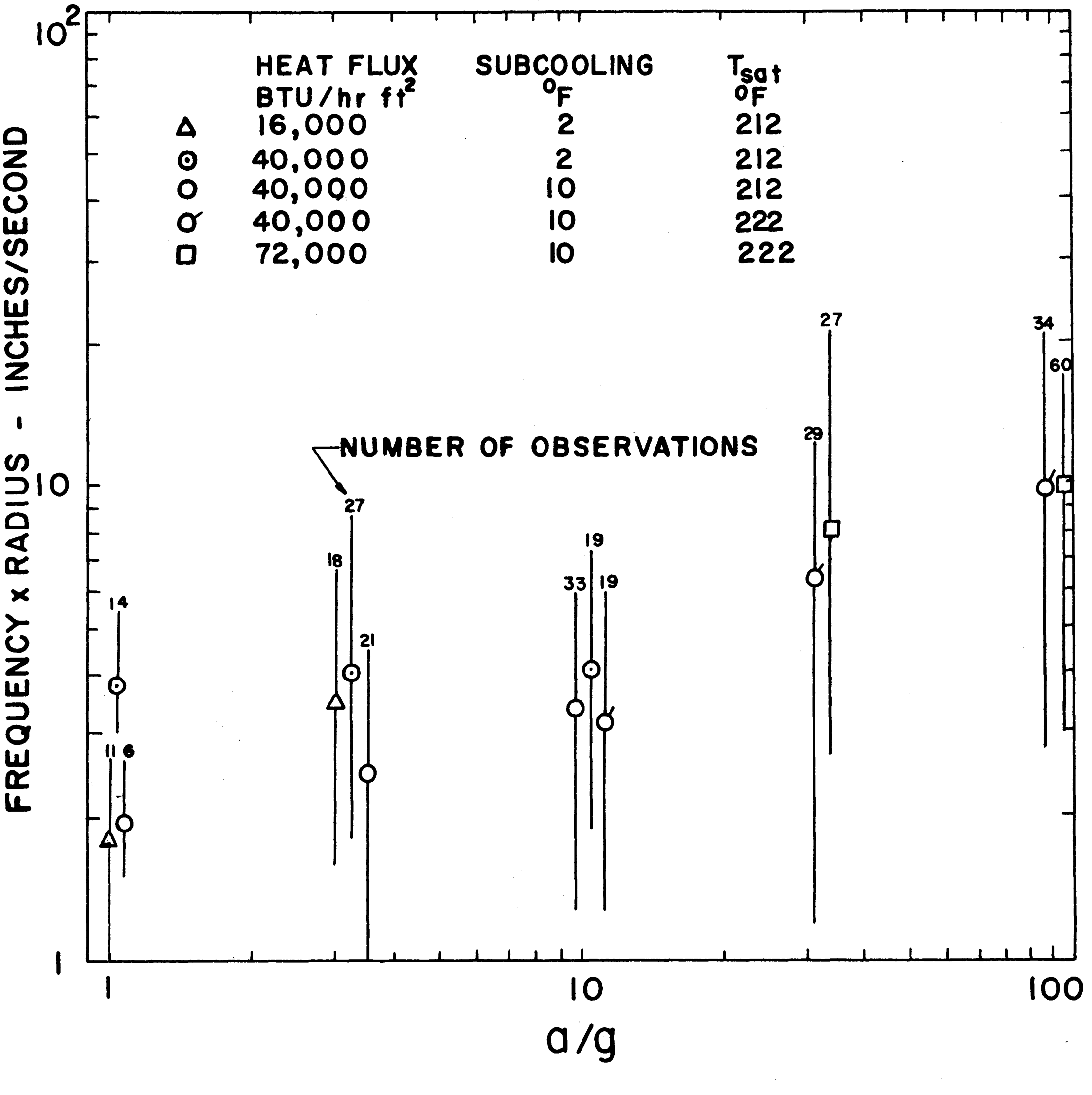

Figure 39. Product of Frequency of Bubble Departure and Departure Radius.

flux is no longer exhibited. The FR_d products for the tests with low subcooling at q/A = 40,000 BTU/hr-ft^2 are virtually independent of acceleration up to a/g = 10. However, the FR_d product for the high subcooling tests at this same heat flux and range of acceleration shows a definite increase with increasing acceleration. As the acceleration is increased to a/g = 30 and a/g = 100, the FR_d product continues to increase.

G. Bubble Growth Expressions

As discussed in Chapter V, the experimental radius-time data for each isolated bubble was fit to two different equations by a least square procedure. These equations are repeated here for convenience:

$$R = K(\tau - \tau_0)^n \tag{53}$$

$$R = J(\tau - \tau_0)^{1/2} \tag{56}$$

Figure 40 is an example showing the results of fitting, over a limited range, a particular set of data to each of the equations. It illustrates the excellent representation of the data points by Equation (53), but as expected, when the exponent n is significantly different from 1/2, Equation (56) does not describe the actual growth process well.

The average values and the range of variation of the exponent n in Equation (53) for each test condition are plotted versus acceleration on Figure 41. For a heat flux of 16,000 BTU/hr-ft^2 and low subcooling (2°F), the average value of n increases from .44 at a/g = 1 to .52 at a/g = 3 . For q/A = 40,000 BTU/hr-ft^2 and high subcooling

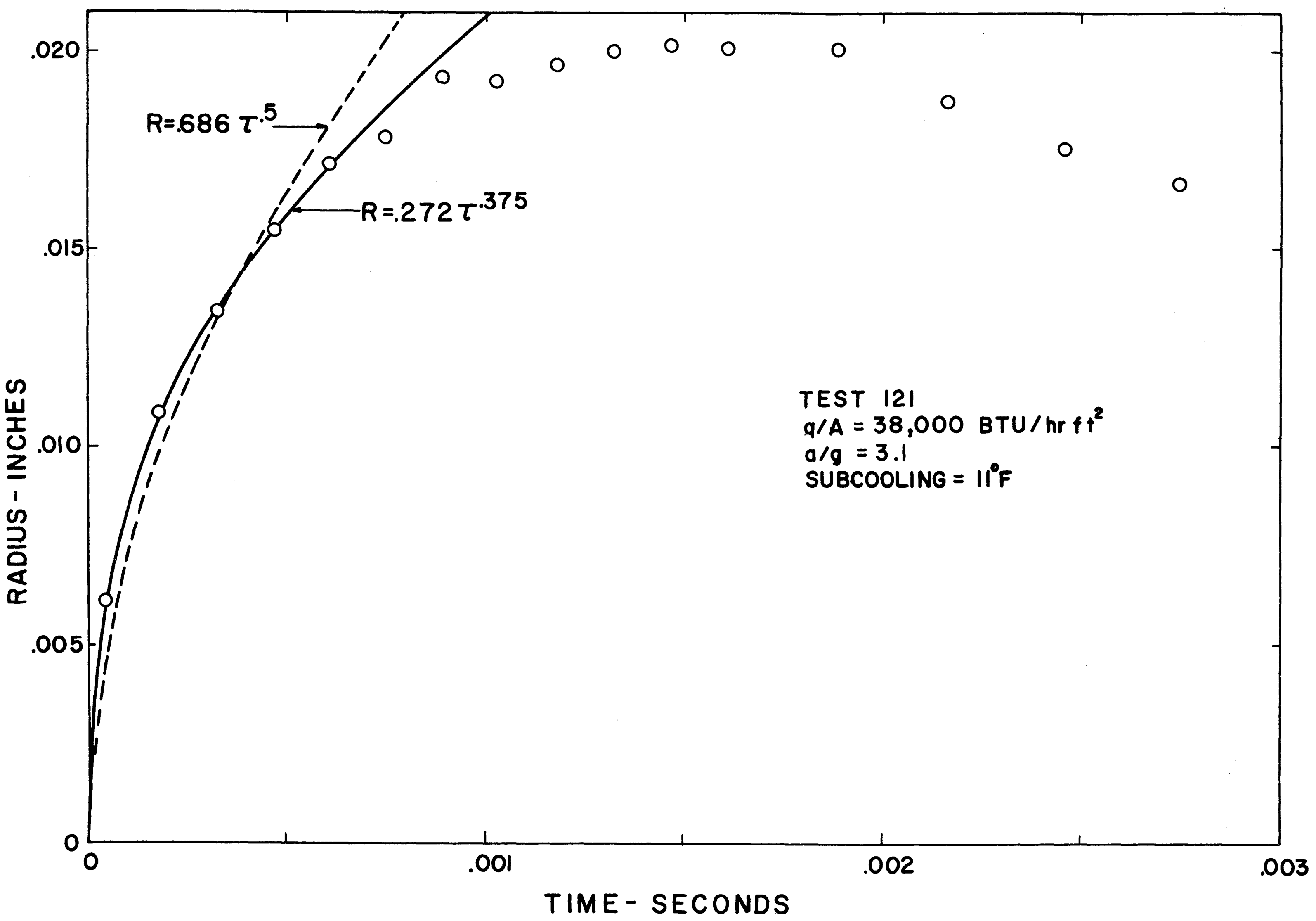

Figure 40. Example of Fit for Emperical Growth Expressions.

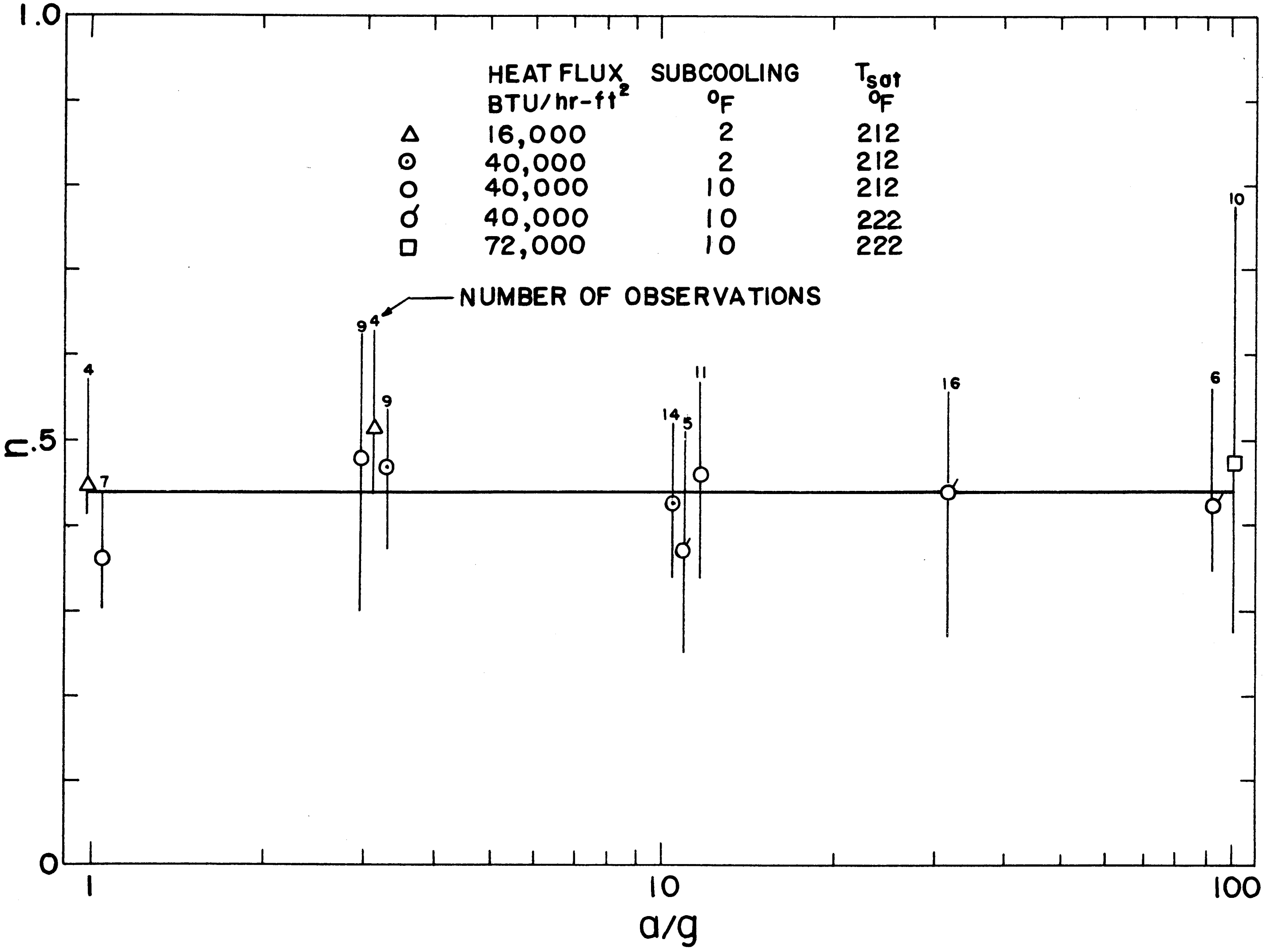

Figure 41. Bubble Growth Exponent-n.

(10°F), the value of n increases from .36 at a/g = 1 to .48 at a/g = 3 and decreases again to .37 at a/g = 10. At both a/g = 3 and a/g = 100, where two different heat fluxes are presented, the value of n is virtually independent of heat flux. Since no consistent trends are exhibited by n with acceleration or subcooling, a constant value of n can be used to represent the data. A value of n equal to .44 will represent all the data within ± 15%.

The value of J as determined by fitting the data to Equation (56) is plotted on Figure 42 as a function of acceleration. As was the case with the exponent n in Equation (53), no consistent trends are exhibited by J for heat flux, acceleration or subcooling. A constant value of J equal to .84 will represent all the data within ± 15% except the value of J at a/g = 3, q/A = 16,000 BTU/hr-ft^2 and low subcooling.

As discussed in Chapter V, the value of J is a measure of the initial bubble growth rate. Since J is not a function of acceleration, the initial bubble growth rate is also independent of acceleration. However, as will be discussed in Chapter VII, the bubble growth rate in the later stages of growth is a function of acceleration.

H. Heat Transfer Data

The temperature difference $T_{sur} - T_{sat}$ was computed on the basis discussed in Chapter V. At a fixed heat flux, acceleration and subcooling this temperature difference was reproducible only within limits of 25% or about 4°F. On Figure 43, the heat flux and

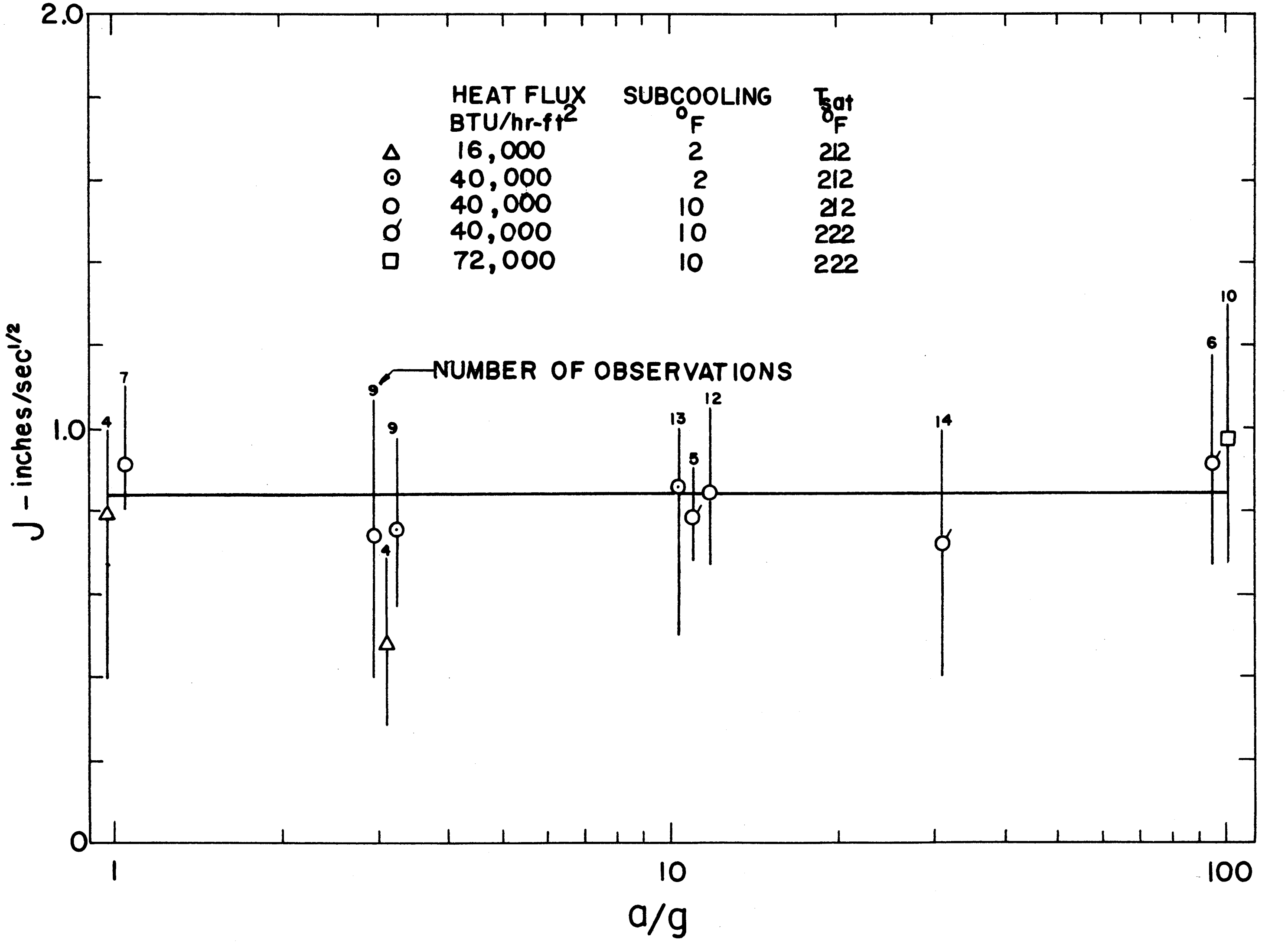

Figure 42. Bubble Growth Constant-J.

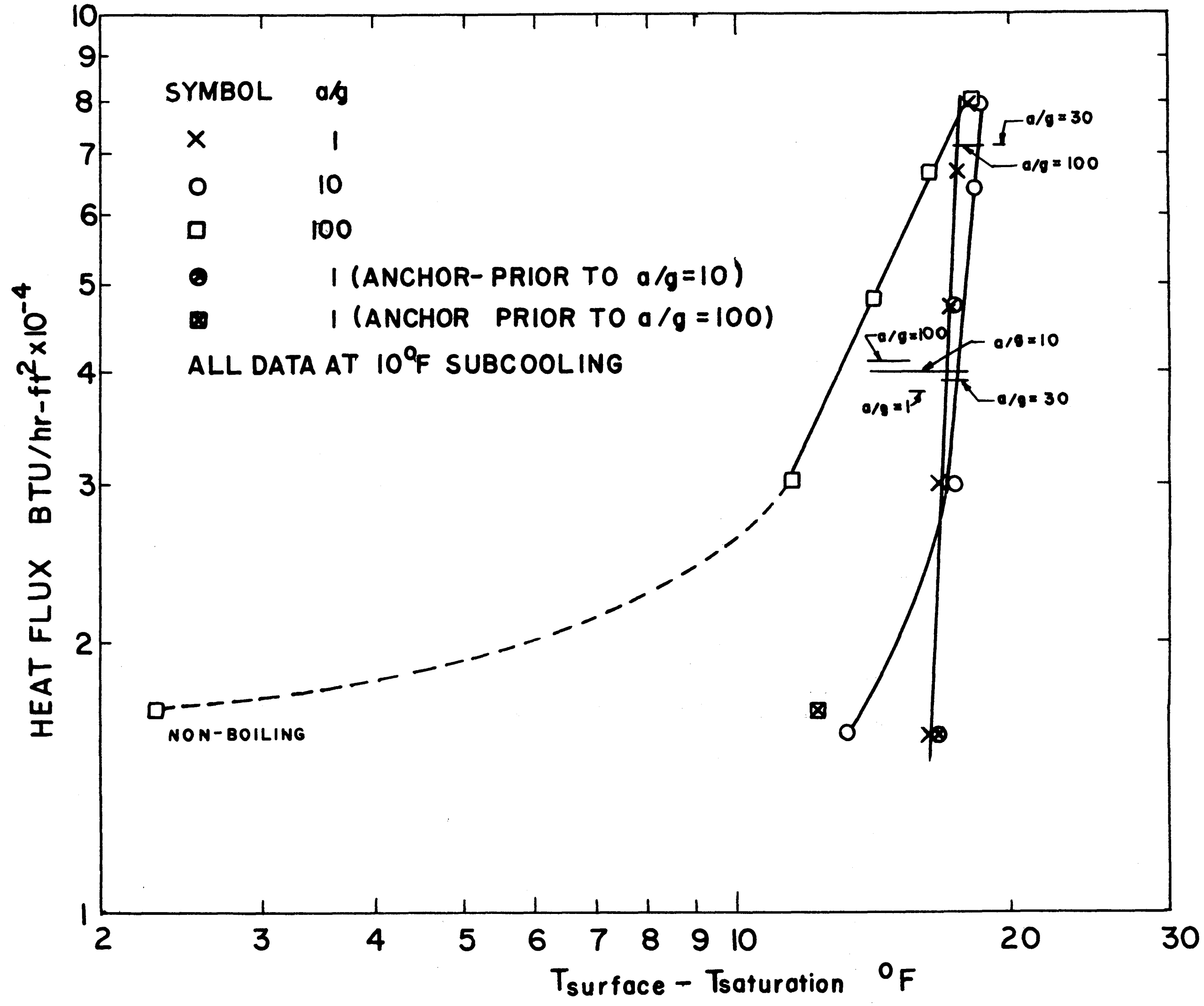

Figure 43. Heat Transfer Data.

$T_{sur} - T_{sat}$ data from the heat transfer tests (tests 201-217 in Appendix B) are plotted along with the range of the data obtained from the high subcooling photographic tests (tests 107-174 in Appendix B). The data at each of the three accelerations (a/g = 1, 10 and 100) for the heat transfer tests was obtained by increasing the heat flux and acceleration from an "anchor point". This anchor point corresponds to a heat flux of 16,000 BTU/hr-ft^2 at standard gravitational acceleration and was used to check the reproducibility of the data under standard gravitational conditions. The data for the tests conducted at a/g = 1 and a/g = 10 appear to be consistent in that a smooth curve can approximately represent the data points, and the anchor points for these two accelerations are within .6°F of each other. The results for the test with a/g = 100 can be represented by a smooth curve, but the anchor-point is about 4°F lower than the other two points.

The heat transfer data obtained simultaneously with the photographic data is limited to two heat fluxes for 10°F subcooling. At q/A = 40,000 BTU/hr-ft^2 heat transfer data was obtained for 5 different accelerations (a/g = 1, 3, 10, 30, 100) and at q/A = 72,000 BTU/hr-ft^2 for 2 different accelerations (a/g = 30, 100). The variation of the temperature difference $T_{sur} - T_{sat}$ for the photographic tests is represented by the horizontal line on Figure 43. For a/g = 1, the temperature difference is about 1°F lower than the corresponding heat transfer test at q/A = 40,000 BTU/hr-ft^2. The 4°F range of $T_{sur} - T_{sat}$ for the photographic tests at a/g = 10 and

$q/A = 40{,}000$ BTU/hr-ft^2 includes the heat transfer test data. The range of $T_{sur} - T_{sat}$ for the photographic tests at $a/g = 100$ is from 1/2°F to 2 1/2°F higher than the heat transfer data at both $q/A = 40{,}000$ BTU/hr-ft^2 and $q/A = 72{,}000$ BTU/hr-ft^2.

As discussed in Chapter V, the relative uncertainty of the temperature difference $T_{sur} - T_{sat}$ is about $\pm$ 2°F, but this maximum deviation should occur only when comparing tests performed at widely different conditions (e.g., comparing tests at $a/g = 1$ and $q/A = 16{,}000$ BTU/hr-ft^2 to tests at $a/g = 100$ and $q/A = 72{,}000$ BTU/hr-ft^2). Consequently, the nonreproducibility observed for tests at the same conditions cannot be attributed to the uncertainty of the measurements. The probable cause for most of the nonreproducibility of the data is the presence of contaminents in the water from the glass impregnated phenolic which was used as the test strip support. This particular electrical insulating material, with its low coefficient of thermal expansion, was the only material out of several tried which could be successfully used. In all the other attempts using more chemically stable materials (nylon, teflon and bakelite), the test strip would not remain cemented to the support for more than a few minutes of boiling.

The measured resistivity of the distilled water at the beginning of each test was 1.3×10^6 Ω cm or better. The degree of contamination at the end of all the tests was approximately the same, as the measured resistivity of the water was always 250,000 Ω cm to 300,000 Ω cm. This value appears to correspond to an equilibrium condition for contamination, since no lower values were recorded even though the measurements were separated by long periods of time. The rate of contamination was certainly different for different liquid levels since different amounts of water were required. This variation in the contamination rate probably influenced the temperature measurements, but no consistent trends in the surface temperature with time could be found in the data.

In order to determine if the measured variations in the surface temperature significantly influenced any of the data obtained from the photographs, each of the parameters presented in this chapter was plotted against $T_{sur} - T_{sat}$ for at least one representative condition. No trends could be established for any of the parameters as a function of the variations in $T_{sur} - T_{sat}$ at a given heat flux and acceleration. Therefore, the conclusion is made that the data obtained from the photographs is representative of the conditions regardless of the contamination.

CHAPTER VII

DISCUSSION AND CONCLUSIONS

A. Number of Active Sites

One of the more significant effects observed on the influence of an increasing acceleration is the decrease in the number of active nucleating sites. However, the limited field of view associated with the optical system prohibited measurements of the population density of nucleating sites. Even if such measurements were possible, the results would be for a linear population density since the bubbles are formed in essentially a single file straight line along the heat transfer surface. The decrease in the number of sites with increasing acceleration actually increased the number of bubbles which could be analyzed as isolated bubbles. At $a/g = 1$, and $q/A = 40{,}000$ BTU/hr-ft^2 the number of nucleating sites was so high that very few isolated bubbles existed, but as the acceleration was increased, the number of sites decreased with a resulting increase in the number of isolated bubbles.

Part of the explanation for this decrease in the number of active nucleation sites may lie in a decrease in the temperature difference $T_{sur}-T_{sat}$ at low heat flux. Gaertner(61) has shown that the population density of nucleating sites is related to the surface temperature. For $a/g = 1$ and $a/g = 10$, the temperature difference as shown on Figure 43 is independent of heat flux within the uncertainty level of the temperature measurements. The same observations can be made for accelerations $a/g = 30$ and $a/g = 100$. However, Merte(2) and Slember(48) have found a definite decrease in $T_{sur}-T_{sat}$ with increasing acceleration for low values of heat flux. Hsu and Graham(38) have proposed a physical model which can account for a decrease in active nucleation sites with increasing acceleration at a fixed temperature difference. By assuming the thermal boundary layer thickness decreases with increasing acceleration, these authors have shown that a given active site at $a/g = 1$ can become inactive at increased accelerations. Since no measurements of the thermal boundary layer thickness were made in this investigation, it is not possible to give evidence to prove or disprove this model.

The data presented by Graham and Hendricks(50), in a study of boiling water up to $a/g = 9$ with a test strip geometry similar to that used in this investigation, does not necessarily substantiate the model proposed by Hsu and Graham.(38) At a heat flux of 11,900 BTU/hr-ft^2, the number of active nucleation sites was reported to be 13, 7, and 4 for accelerations of 1, 3, and 9 respectively. This decrease in active sites was also associated with a decrease in $T_{sat}-T_{sur}$, consequently, the effect of the thermal boundary layer thickness on site inactivation as proposed by Hsu and Graham, cannot be seperated from the effect of the decrease in $T_{sur}-T_{sat}$

B. Observation on Convection Currents

At all acceleration, and especially for the tests where few nucleating sites existed, convection currents were observed in the form of shadows or lines extending outwards from the surface. In some cases where a sufficient nummber of pictures were available, it was possible to trace back in time and observe that some convection patterns resulted from the flow induced by a departing bubble. The last 20 pictures on Figure 47 in Appendix A show very clearly the convection currents associated with a departing bubble. Other convection currents seemed to stem from the turbulent free convection as shown on Figure 51. The convection patterns shown for this particular film are not in the same plane as the bubble since they are not disturbed by the growing bubble, however, other pictures have shown bubbles destroying certain currents and initiating new currents in its wake. Similar photographs at $a/g = 1$ have been made by Hsu and Graham(38), Ellion(52), Gaertner(61) and others. Hsu and Graham reported that the induced flow patterns associated with departing bubbles disturbed the thermal boundary layer approximately one bubble diameter from the nucleation site. However, no general observation as to the extent of the area of influence of each bubble could be drawn from the photographs made in this investigation.

A particularly interesting bubble sequence is shown in Figures 50 and 51 in Appendix A. The growth rate of the second bubble is greatly increase by the low pressure area behind the first bubble. As the second bubble grows, it assumes an elongated shape resulting from the fluid flow pattern induced by the first bubble and imparts sufficient inertia to the surrounding liquid that it almost passes through the first bubble. This sequence was also photographed with the Fastex camera at $a/g = 100$ and $a/g = 30$ and appeared to account for about 10% of the total bubles at $a/g = 100$ and only a few percent at $a/g = 30$.

C. Departure Size

The equations available in the literature for bubble departure size (Equations (2), (3), and (4)) have been developed for isolated bubbles in saturated boiling and are repeated here for convenience:

$$R_d = .0148\,\beta\sqrt{\frac{2\sigma}{(a/g)(g/g_c)(\rho_\ell-\rho_v)}} \tag{2}$$

$$R_d = .00355\,\beta\sqrt{\frac{2\sigma}{(a/g)(g/g_c)(\rho_\ell-\rho_v)}}\quad(1+.435\dot{R}_d) \tag{3}$$

$$R_d = .72\left[\frac{2\sigma}{(a/g)(g/g_c)(\rho_\ell-\rho_v)}\quad\frac{k\,(T_{sur}-T_{sat})}{q/A}\right]^{1/3} \tag{4}$$

The low subcooling tests (2°F) in this investigation are believed to be sufficiently close to saturation conditions that the validity of these equations may be checked by comparison with the data presented on Figure 30.

Each of these equations are functions of acceleration by virtue of the term a/g. The slope of the line shown on Figure 30 for the tests with low subcooling between $a/g = 1$ and $a/g = 3$ is $-.58$, in good agreement with Equations (2) and (3) which predict a slope of $-1/2$ if the outer contact angle and growth rate at departure are independent of acceleration within this range. The slope may be actually steeper than shown since no data was taken between $a/g = 1$ and $a/g = 3$. If these equations are valid, the independence of the departure size on acceleration between $a/g = 3$ and $a/g = 10$ can be compensated only by changes in either the outer contact angle or $\dot{R}_d$, since the surface tension and density difference are functions of acceleration only to the extent that these properties are functions of temperature. Since the measured temperatures do not vary significantly for these tests, these properties can be assumed constant.

Consider first Equation (2) by Fritz. Using the average outer contact angles shown on Figure 35, this equation predicts a departure size for both $a/g = 1$ and $a/g = 3$ which is about 30% too high and a value at $a/g = 10$ which is about 30% too low. In order for this equation to predict the trends exhibited by the data, the contact angle would have to remain constant at a value of 62° between $a/g = 1$ and $a/g = 3$ and then increase to 93° at $a/g = 10$. This type of relationship between the contact angle and acceleration is not shown on Figure 35, where in fact the contact angle appears to decrease slightly with acceleration.

Equation (3), by Staniszewski, is not only a function of the outer contact angle but is also a function of the growth rate at departure. If the outer contact angle is assumed independent of acceleration, the growth rate at departure will have to remain constant between $a/g = 1$ and $a/g = 3$ and then increase for $a/g = 10$ if this equation is to follow the observed trends. Measured values of the R_d were not obtained in this investigation but examination of the plots of radius versus time from the computer showed positive values for R_d for $a/g = 1$ and $a/g = 3$ but at $a/g = 10$, R_d was zero or slightly negative which is directly opposite to that required.

Equation (4) by Zuber predicts the departure size as proportional to the cube root of the ratio of the temperature difference

T_{sur}-T_{sat} to the acceleration at a given heat flux. Due to the uncertainty of the surface temperature measurements, it is not possible to make a direct comparison of this equation with the experimental data. For this reason a few general comments on the nature of this equation will be made. Gaertner (61) has shown that the average departure size of isolated bubbles for standard gravitational conditions is independent of heat flux at least up to q/A = 70,000 BTU/hr-ft^2. Applying this information to Equation (4), requires that the heat flux must be directly proportional to the temperature difference. However, this is not the behavior exhibited by most boiling systems in the region of isolated bubbles. The relationship between heat flux and temperature difference usually takes the form:

$$q/A = C\,(T_{sur} - T_{sat})^n \tag{65}$$

where n has been found experimentally to vary between 1.5 and 5.5. Consequently, Equation (4) does not seem to be realistic even at a/g = 1.

Han and Griffith(8) have proposed a departure criteria in terms of the thermal boundary thickness which considers dynamic forces as well as hydrostatic and surface tension forces. Since the thermal boundary thickness was not measured in this investigation, it is not possible to evaluate this criteria.

For both low and high subcooling the effects of acceleration on departure size appears to be the same, as was shown in Figure 30. The two conditions exhibit almost identical trends of decreasing departure size between a/g = 1 and a/g = 3 and constant departure size between

$a/g = 3$ and $a/g = 100$ even though the average departure sizes are significantly different. The difference in departure size for these two conditions is probably a function of the different inertia effects associated with different amounts of subcooling. For low subcooling (2°F) it was observed that the bubbles had a very slow growth rate or sometimes a very slow collapse rate at departure, whereas with high subcooling (10°F) the bubbles exhibit a rapid collapse rate after reaching their maximum size. It appears that the effect of subcooling can be studied at $a/g = 1$ and extrapolated to higher accelerations if the mechanism of bubble departure is understood for all accelerations and high subcooling. Consequently, the remaining discussion will be concerned with the departure of bubbles with 10°F subcooling and accelerations between $a/g = 1$ and $a/g = 100$.

Before attempting to formulate a criteria for the process of vapor removal, the time history of bubbles at different acceleations will be described. First consider the general characteristics of growing and departing bubbles as exhibited by all bubbles observed in this study. Photographs of typical bubbles are given in Appendix A. In the first appearance of a bubble on the surface, the bubble is hemispherical in shape and remains essentially hemispherical while it grows to a relatively large size. The first evidence of the bubble deviating from this hemispherical shape is generally the turning under of the edge. As the bubble continues to grow, the area of contact (base circle) remains essentially constant for a while and then begins to decrease. When the base circle reduces to zero, the bubble departs.

The basic differences observed between bubles at low accelerations and at high accelerations is the time required for the bubbles to pass through different stages of their life cycle. As was pointed out in Section G of Chapter VI, the early growth rates of all the bubbles observed are essentially the same and independent of acceleration. However, consider Figure 36, which is a plot of the time required for bubbles to grow to their maximum size as a function of acceleration. Since this time decreases by a factor of three between $a/g = 3$ and $a/g = 100$, while the maximum bubble size remains constant as shown on Figure 33, the later growth rates for bubbles at different accelerations cannot be the same. Figure 44 represents the radius versus time of two typical bubbles with equal values of k and n (from Equation (53)) but at different accelerations. The early growth rates for these two bubbles are equal, but the bubble at the low acceleration deviates from the emperical growth equation at an earlier time and at a slower rate than the bubble at the high acceleration.

A possible explanation for the higher bubble growth rates, in the latter stages of growth, at high accelerations than at low accelerations can be made in terms of a change in the thermal boundary thickness. Since fewer bubbles were observed as the acceleration was increased, the turbulence induced by bubbles in the thermal boundary layer will be reduced, thus increasing the average thermal boundary layer thickness. This reduction in turbulence may more than compensate for the reduction in the thermal boundary thickness due to the increased natural convection with increasing acceleration. An increased thickness of the thermal boundary layer with increasing acceleration would permit bubles to grow more rapidly in the later stage of growth.

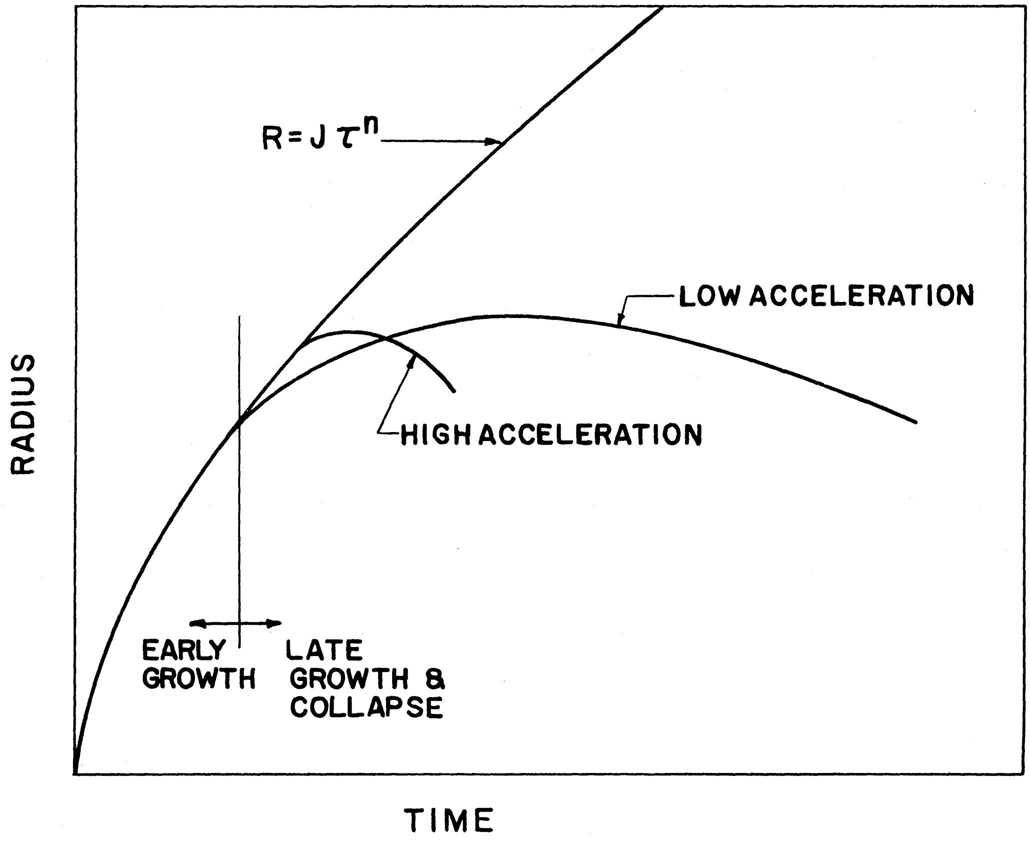

Figure 44. Comparison of Bubble Life Cycle for Low and High Accelerations.

The second major difference between bubbles at high and low acceleration is the time interval beginning when the bubble begins to deviate from a hemispherical shape and ending when the bubble departs. The bubble shown in Figure 46 for $a/g = 3$ begins to deviate from a hemispherical shape at about frame 9 but remains attached to the surface until frame 46. The time interval between frames 9 and 46 is 5 milliseconds. Figure 50 shows a bubble of slightly smaller size than on Figure 46, but at $a/g = 100$. This bubble remains hemispherical up to about frame 7 and departs at frame 15. The time interval between frames 7 and 15 is .8 milliseconds. The significance with respect to departure of the size at which the bubble begins to deviate from a hemispherical shape will be discussed later in this chapter.

The independence of bubble departure size on acceleration between $a/g = 3$ and $a/g = 100$, as shown in Figure 30, can be explained in a general manner by considering the forces acting on a bubble and their probable effects during the life cycle of a bubble. During the life of a bubble, four seperate forces are involved; surface tension forces between the liquid-vapor interface and the heat transfer surface, (triple interface), liquid inertia forces associated with the bubble growth and collapse, hydrostatic forces resulting from the pressure gradient in the liquid, and viscous forces between the solid-liquid interface and between the liquid-vapor interface. Of these forces, only the triple interface surface tension force acts to hold the bubble against the surface at all times. The inertia forces and hydrostatic forces in the early states of bubble growth will hold the bubble against the surface, and during the late stages of growth will pull the bubble from the surface. The viscous forces in the early stages of growth restrict the growth near the base of the bubble, but this only indirectly affects the departure size. Each of the four forces will be considered in more detail in the subsequent paragraphs.

Consider first the net hydrostatic forces. While the bubble remains hemispherical or nearly hemispherical in shape, as it does in the early stages of growth as may be seen in the photographs in Appendix A, the net hydrostatic force is not a bouyancy force at all but actually holds the bubble against the surface. This can be demonstrated by considering a section of a sphere placed on the bottom of a pool of liquid. If no liquid exists under the base of the spherical section, it can be shown by simple hydrostatics that the net hydrostatic force acting on the outer surface is given by the following equation

$$F_H = 2\pi \rho_l (a/g_c) R^3 \left(\frac{1}{6} - \frac{1}{3}\cos^3\beta - \frac{\cos^2}{2}\beta\right) \tag{66}$$

where β is the outer contact angle. If β is 60° then the net hydrostatic force is zero, for β less than 60°, F_H is a bouyancy force and for β greater than 60°, F_H acts to hold the section against the surface.

The presence of a liquid layer beneath each bubble as postulated by Ellion(52) and more recently discussed by Moore and Mesler(39) would result in the hydrostatic forces always acting as a bouyancy force unless the layer were so thin or the evaporation rate from this film so great that the hydrostatic pressure could not be transmitted into the layer.

The inertia imparted to the liquid by a growing bubble in the early growth stages also acts to hold the bubble against the surface. This inertia force acting to hold a growing hemispherical bubble against the surface can be calculated from Rayleigh's equation (Equation (1) without the surface tension term) by assuming the growth of the bubble is given by $R = J\tau^{1/2}$. This inertia force acting on the bubble is:

$$F_I = \pi \rho_l J^4 / 8 g_c \tag{67}$$

As stated earlier, the triple interface surface tension force always acts to keep a bubble on the surface. The existence or non-existence of a liquid layer under each bubble will determine the magnitude of the surface tnesion forces since this force is proportional to the contact length of the triple interface. For a hemispherical bubble, the maximum surface tension force can be represented by the following expression;

$$F_{ST} = 2\pi R \sigma \tag{68}$$

where σ is the triple interface surface tension.

The viscous forces between the liquid and the heat transfer surface associated with a growing hemispherical bubble tend to restrain the growth at the base of the bubble. This force is in a radial direction and parallel to the heat transfer surface, and therefore has no component which can either lift the bubble from the surface or hold the bubble against the surface.

The sum of the forces given by Equations (66), (67), and (68) results in the following expression for the force acting to hold a hemispherical bubble on the surface:

$$F_{TOTAL} = \pi \rho_l (a/g_c) R^3/3 + \frac{\pi \rho_l J^4}{8 g_c} + 2\pi R \sigma \qquad (69)$$

The term J has been shown experimentally to be essentially independent of acceleration in the early growth stages (see Figure (42)), and leaves the hydrostatic force as the only term in this equation which is a function of acceleration. Therefore the net result of increasing the acceleration on a growing hemispherical bubble is to increase the force which holds the bubble against the surface. The question remaining to be answered is: what are the conditions or forces which cause the bubble to initially assume the shape of a hemisphere and at some later time to deviate sufficiently from this shape so that the hydrostatic forces and inertia forces can lift the bubble from the surface? Some insight into this problem may be gained by considering the growth process of the bubbles.

The initial bubble growth rates at a radius of .005 inches have been found in this investigation to be as high as 100 inches/second. This high growth rate is controlled by the evaporation process at the liquid-vapor interface and is associated with a pressure inside the bubble which is exerted uniformly over the bubble surface. This uniform pressure causes the bubble to grow radially from the nucleation site with little tendency for the bubble to deform, as shown by the nearly hemispherical shape in the early growth stages. However, three forces are present which do tend to distort the bubble or restrict the growth of the bubble in certain regions. The presence of significant viscous and triple interface surface tension forces at the base of the bubble would tend to restrain the growth in this region. Since the bubble appear to grow with equal ease at the base as in other regions in the early growth stages, it is probable that the heat transfer surface is not wiped clean at the base of the bubble but that a thin liquid film does exist. When the growth rate decreases sufficiently, and if a thin liquid layer does exist under the bubble, the hydrostatic pressure will begin to be transmitted under the base. If no liquid layer exists, then the hydrostatic pressure will begin to move the triple interface back towards the bubble axis. The effect in either case is to cause the hydrostatic force to become a bouyant force which begins to lift the bubble from the surface.

For low accelerations, at approximately the same time at which the buoyancy force is beginning to lift the bubble from the surface, the growth rate begins to decrease at an even faster rate than is predicted by the inverse of the square root of time. This decrease probably results from condensation beginning at the top of the bubble while evaporation is still taking place at the base. As the growth rate decreases towards zero the moving liquid in front of the bubble must be decelerated. This deceleration creates a low pressure area near the top which begins to pull the bubble from the surface. However, the combination of the bouyancy force and the inertia force may not be sufficient to cause departure until the bubble begins to collapse. Even though the bubble size decreases during collapse, the bouyancy force tending to lift the bubble from the surface increases due to the changing shape of the bubble. During collapse while the bubble remains attached to the surface, the bubble base circle decreases at a faster rate than the maximum bubble diameter, resulting in an increasing area for the hydrostatic pressure to act againt the underside of the bubble.

As the acceleration increased, the bubble growth remains high for a longer period of time, resulting in the inertia force holding the bubble against the surface. When the growth rate decreases to zero, as it must when the bulk liquid is subcooled, the bubble is considerably larger than predicted by considering only surface tension and bouyancy forces (Equation (2)) and the bubble departs very rapidly.

D. Frequency of Departure and Departure Size Relationships

Even at standard gravitational acceleration, the product of the frequency of departure and departure radius shows a considerable variation as shown in Figure 39. The average values at the three different conditions at $a/g = 1$, as shown on Figure 39, are 1.8, 1.9, and 3.7 inches/second which is about the same range as presented by Jakob(5) but is significantly lower than the data by Staniszewski(7) who reports values between 3 inches/second and 6 inches/second for various heat fluxes. As the acceleration is increased, the bubble frequency increases, but the departure diameter remains constant between $a/g = 3$ and $a/g = 100$ and results in an increase in the FR_d product.

The waiting time between the departure of one bubble and the initiation of the next from the same site was not measured, but an approximate value of this time interval can be calculated by subtracting from the reciprocal of the frequency of departure (Figure 38) the time interval from bubble initiation to bubble departure (Equation (64)). Because of the wide variation observed for frequency of departure data, this information was not presented in equation form in Chapter VI. An equation which will predict the average frequency of departure for all accelerations within about ± 85% is;

$$f_d = 73 \, (a/g)^{1/2} \tag{70}$$

The waiting time as determined from Equations (64) and (70) is:

$$\tau_w = \frac{1}{f_d} - \tau_d = .0043 \, (a/g)^{-1/2} \tag{71}$$

Thus the average waiting time decreases with acceleration and is about 1/2 of the time interval from initiation to departure. Jakob$^{(5)}$ presents data for standard gravatational conditions showing that the waiting time is equal to the time interval from initiation to departure.

Graham and Hendricks$^{(50)}$ presented data on the ratio of the waiting time to the departure time for one site at accelerations of $a/g = 1$ and $a/g = 7$. The data indicated an increase in the ratio of waiting time to departure time with increasing acceleration. This ratio may be obtained for the data in this investigation by dividing Equation (71) by Equation (62). Since both equations are proportional to $(a/g)^{-1/2}$, this ratio is independent of acceleration and approximately equal to 1/2.

E. Bubble Growth Rates

The initial growth rate is well represented by Equation (53) but most theoretical expression for bubble growth rates utilize the form of Equation (58). An exception to this is the result of Griffith(11), which can be expressed in a manner similar to Equation (53), except that the exponent n is a function of time. In the early growth stages the exponent n is almost 1/2, decreases with time to a value of about .25, and then remains almost constant. However, it is not possible to compare the result of Griffith with the data obtaind in this investigation, since it requires a knowledge of the thermal boundry layer thickness, which was not measured.

The results of Fritz and Ende(51), Plesset and Zwick(9) and Forster and Zuber(10) can be compared with the experimental value of J as shown on Figure 43. Each of these theoretical predictions can be put in a single form differing only by a multiplying constant (C):

$$R = C \frac{2k \Delta T}{h_{fg} \rho_v \sqrt{\pi \alpha}} \tau^{1/2} \qquad (5)$$

where

C = 1 Fritz and Ende

C = $\sqrt{3}$ Plesset and Zwick

C = $\pi/2$ Forster and Zuber

The value of the temperature difference ΔT in Equation (5) should be the local value of the temperature difference $T_{sur}-T_{sat}$ in the vicinity of the bubble, but since local values cannot be measured an approximation is always made by replacing this temperature difference by the average measured temperature difference $T_{sur}-T_{sat}$. Because of the uncertainty of the values of $T_{sur}-T_{sat}$ in this investigation only a rough comparison can be made.

The physical properties in Equation (5) are evaluated at the saturation condition existing at the heat transfer surface. Since two different test surface saturation temperatures were used in the investigation ($T_{sat} = 121°F$ and $T_{sat} = 222°F$) these properties assume two different values. Table IV is a comparison of the experimental values of J and the calculated values from each of the three theories using average values of $T_{sur}-T_{sat}$ as listed in Appendix B. The predictions by Plesset and Zwick, and Forster and Zuber are both too high compared to the experimental values. The equation by Fritz and Ende predicts approximately the experimental values for the majority of the tests but predicts a value almost 100 percent too high for test number 2 and a value 40 percent too low for test number 11.

F. Conclusions

Over the range of acceleration, pressures, subcoolings, and heat fluxes employed in this investigation, the following conclusions can be drawn:

1. The averag bubble departure size decreases with increasing acceleration between $a/g = 1$ and $a/g = 3$ and remains constant between $a/g = 3$ and $a/g = 100$.

2. The early bubble growth rate is independent of acceleration. However, the average growth rates in the later growth period are greater at high accelerations than at low accelerations.
3. The average frequency of bubble departure increases with increasing acceleration.
4. The product of the frequency of bubble departure and the departure radius increases with increasing acceleration.
5. The number of active nucleating sites decreases with increasing acceleration.
6. The ratio of the waiting time between bubbles, to the time interval from bubble initiation to departure is independent of acceleration.

TABLE IV

COMPARISON OF EXPERIMENTAL AND THEORETICAL GROWTH EXPRESSIONS

Test	Subcooling	T_{sat}	$q/A \times 10^{-3}$ BTU/hr-ft^2	a/g	$T_{sur}-T_{sat}$	J	Fritz & Ende	Plesset & Zwick	Forster & Zuber
1	2 °F	212 °F	16	1	16 °F	.80	.80	1.39	1.26
2	2	212	16	3	18.5	.48	.92	1.59	1.44
3	2	212	40	1	17	.92	.85	1.47	1.34
4	2	212	40	3	16	.76	.80	1.39	1.26
5	2	212	40	10	17.5	.86	.87	1.51	1.37
6	10	212	40	10	14	.85	.70	1.21	1.10
7	10	222	40	10	15	.78	.60	1.04	.94
8	10	222	40	30	17.5	.72	.70	1.21	1.10
9	10	222	40	100	14	.92	.56	.97	.85
10	10	222	70	100	17.5	.97	.70	1.21	1.10
11	10	212	40	1	16	.92	.64	1.11	1.01
12	10	212	40	3	16	.75	.64	1.11	1.01

APPENDIX A

TYPICAL BUBBLE PHOTOGRAPHS

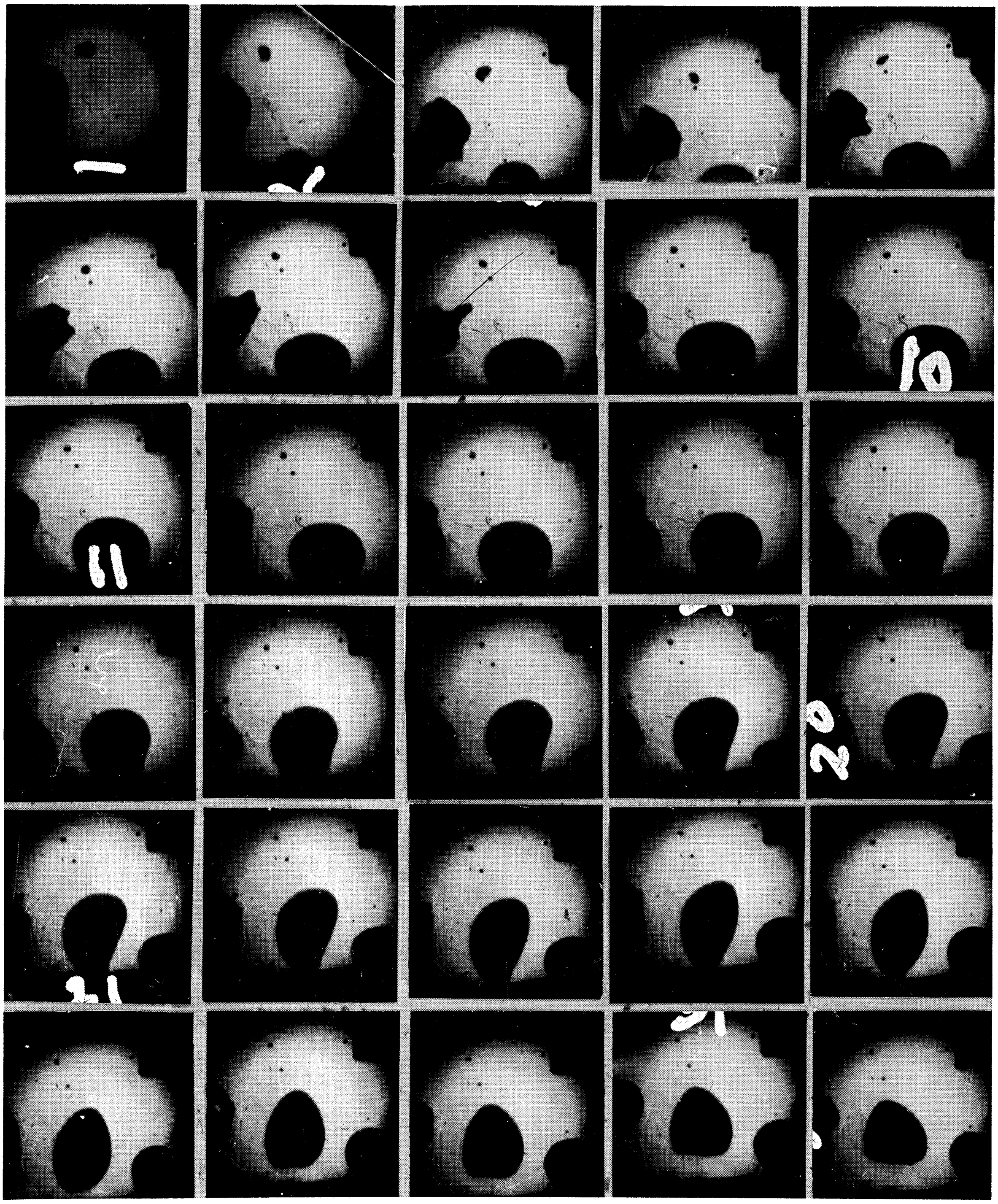

0.10" Test 138, a/g = 1, Camera Speed = 3000 f/s
q/A = 39,000 BTU/hr-ft^2, Subcooling = 8.5°F

Figure 45. Typical Bubble at a/g = 1 .

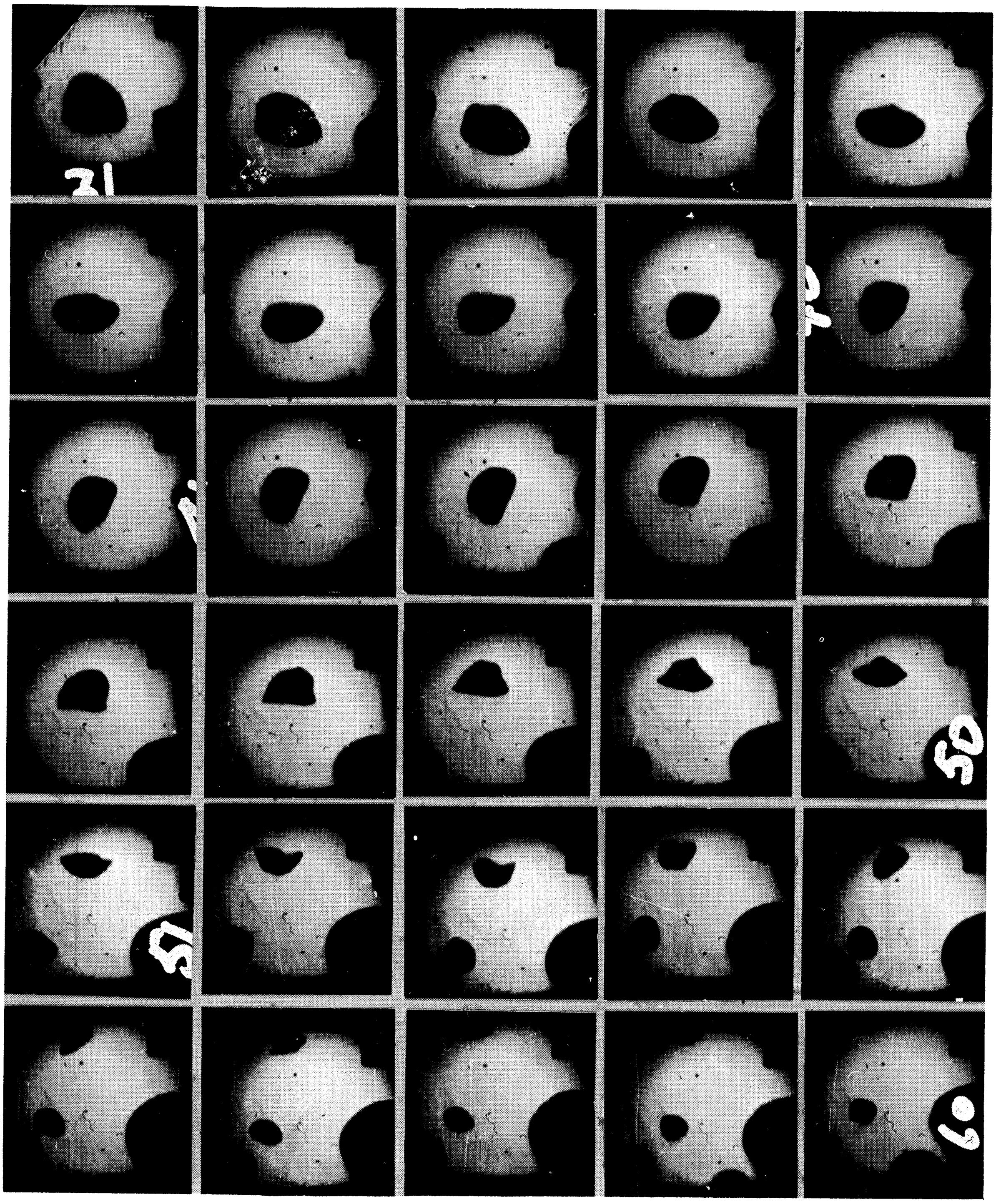

Figure 45 (Cont'd).

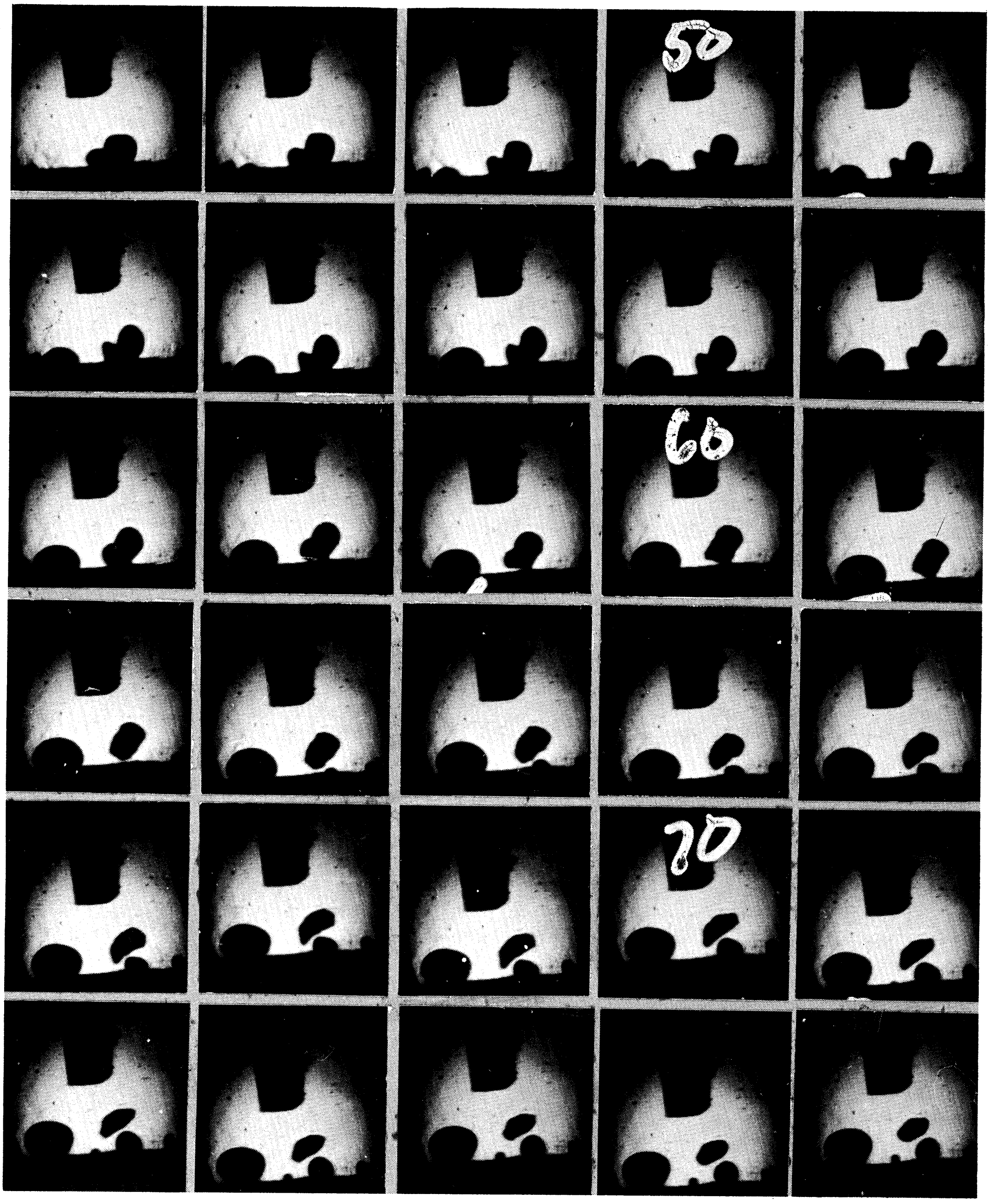

0.10" Test 122, a/g = 3, Camera Speed = 7000 f/s
q/A = 38,000 BTU/hr-ft^2, Subcooling = 11°F

Figure 46. Typical Bubble at a/g = 3 .

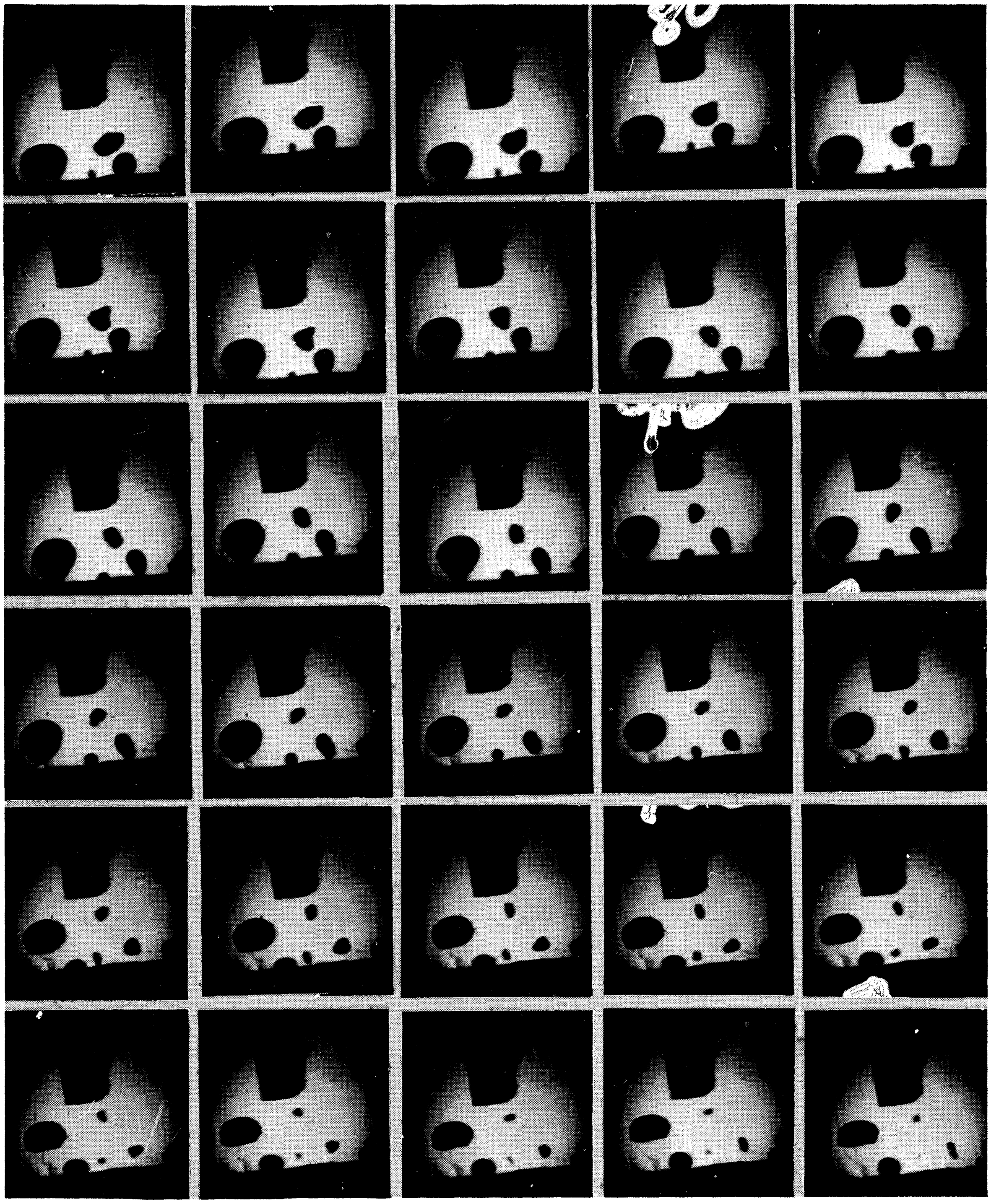

Figure 46 (Cont'd).

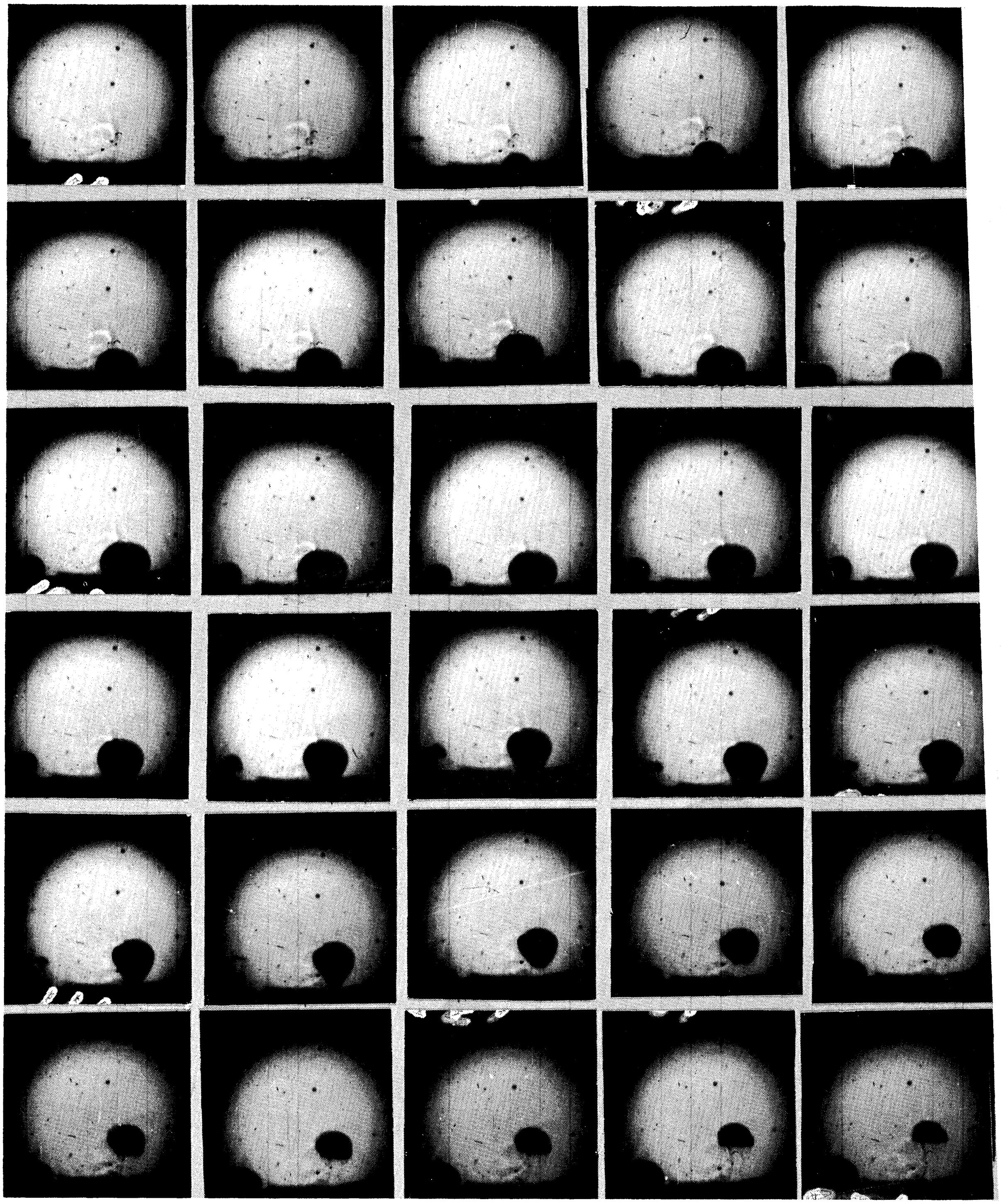

Test 155, a/g = 10, Camera Speed = 5000 f/s
q/A = 42,000 BTU/hr-ft^2, Subcooling = 13.3°F

Figure 47. Typical Bubble at a/g = 10 .

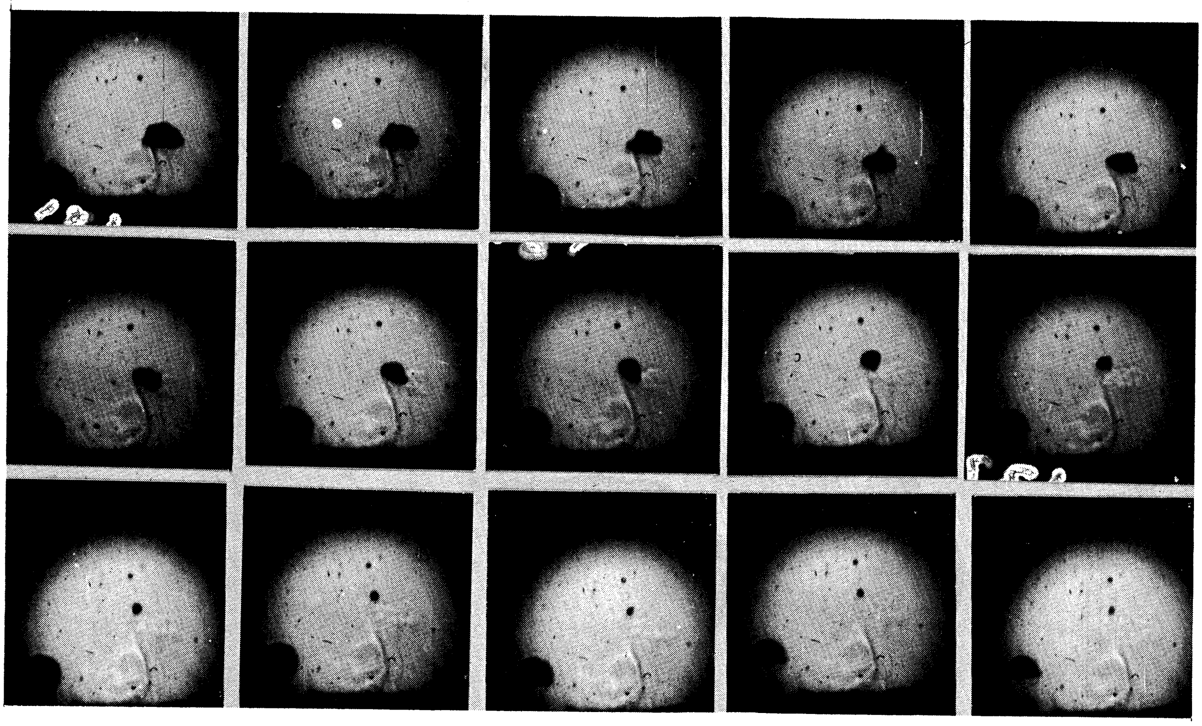

Figure 47 (Cont'd).

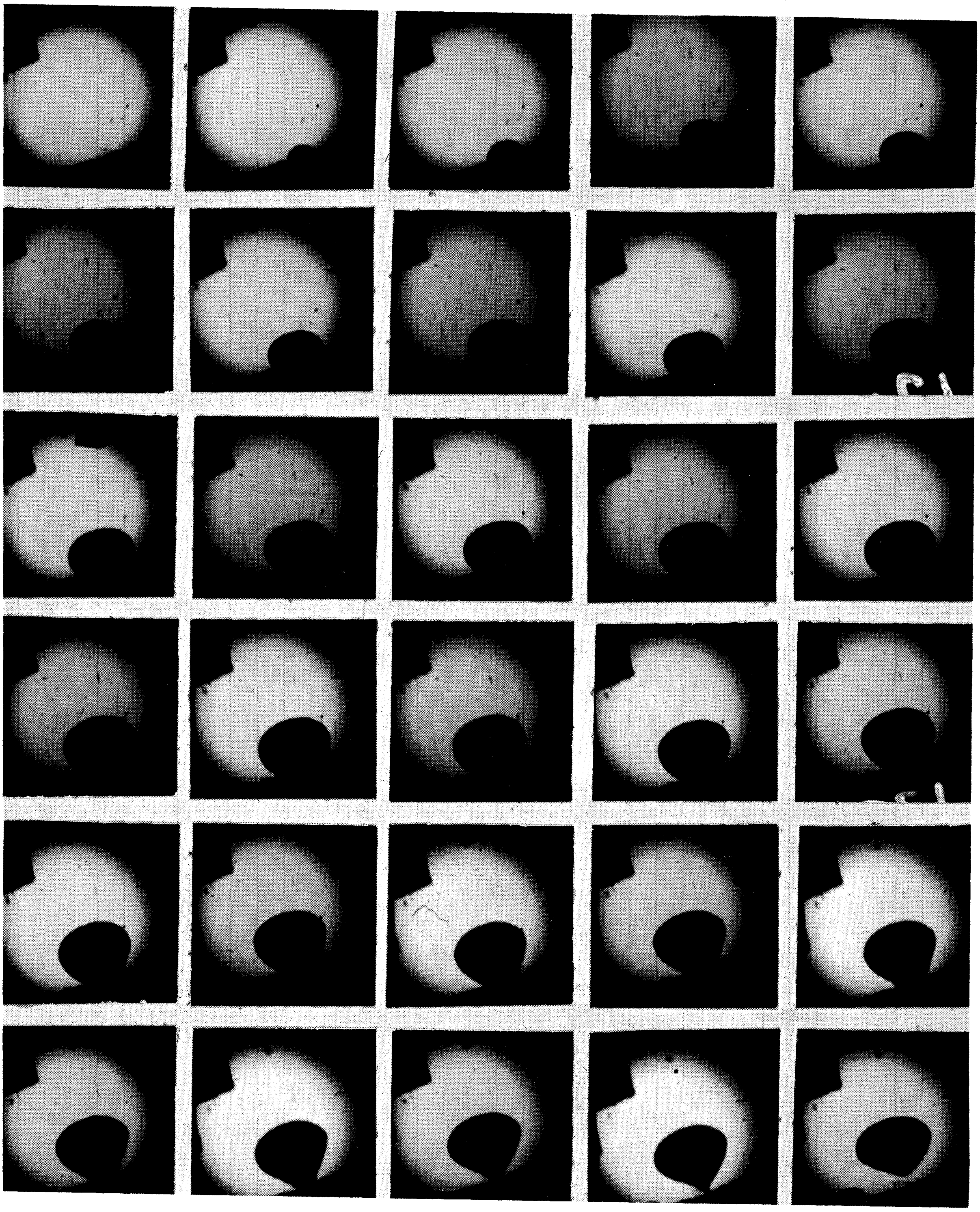

0.10"

Test 153, a/g = 10, Camera Speed = 7000 f/s
q/A = 41,000 BTU/hr-ft^2, Subcooling = 2.1°F

Figure 48. Typical Bubble at a/g = 10 .

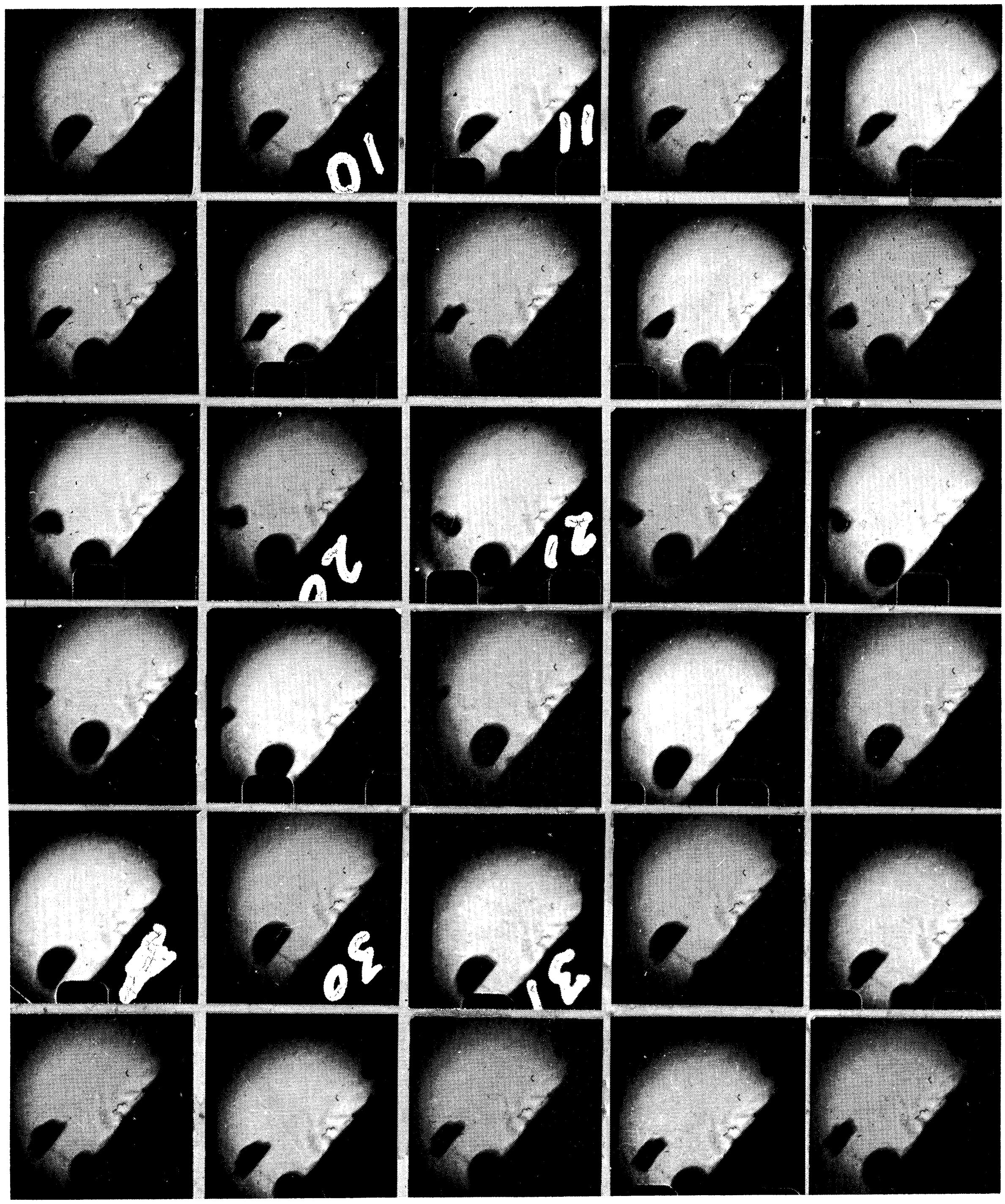

0.10" Test 143, a/g = 30, Camera Speed = 7000 f/s
q/A = 39,000 BTU/hr-ft^2, Subcooling = 11.3°F

Figure 49. Typical Bubble at a/g = 30 .

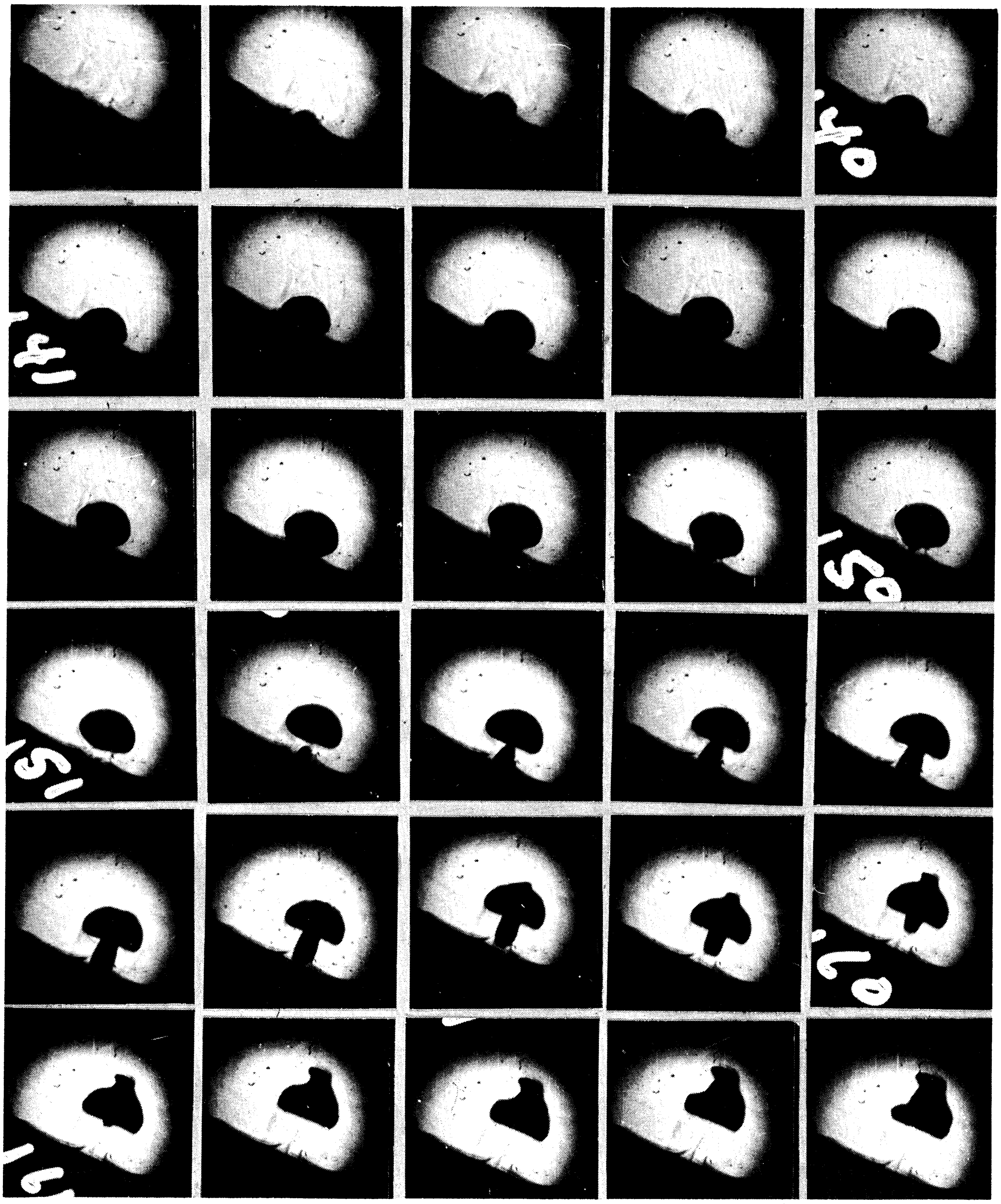

0.10" Test 164, a/g = 100, Camera Speed = 10,000 f/s
q/A = 41,000 BTU/hr-ft^2, Subcooling = 9.8°F

Figure 50. Typical Bubble at a/g = 100 .

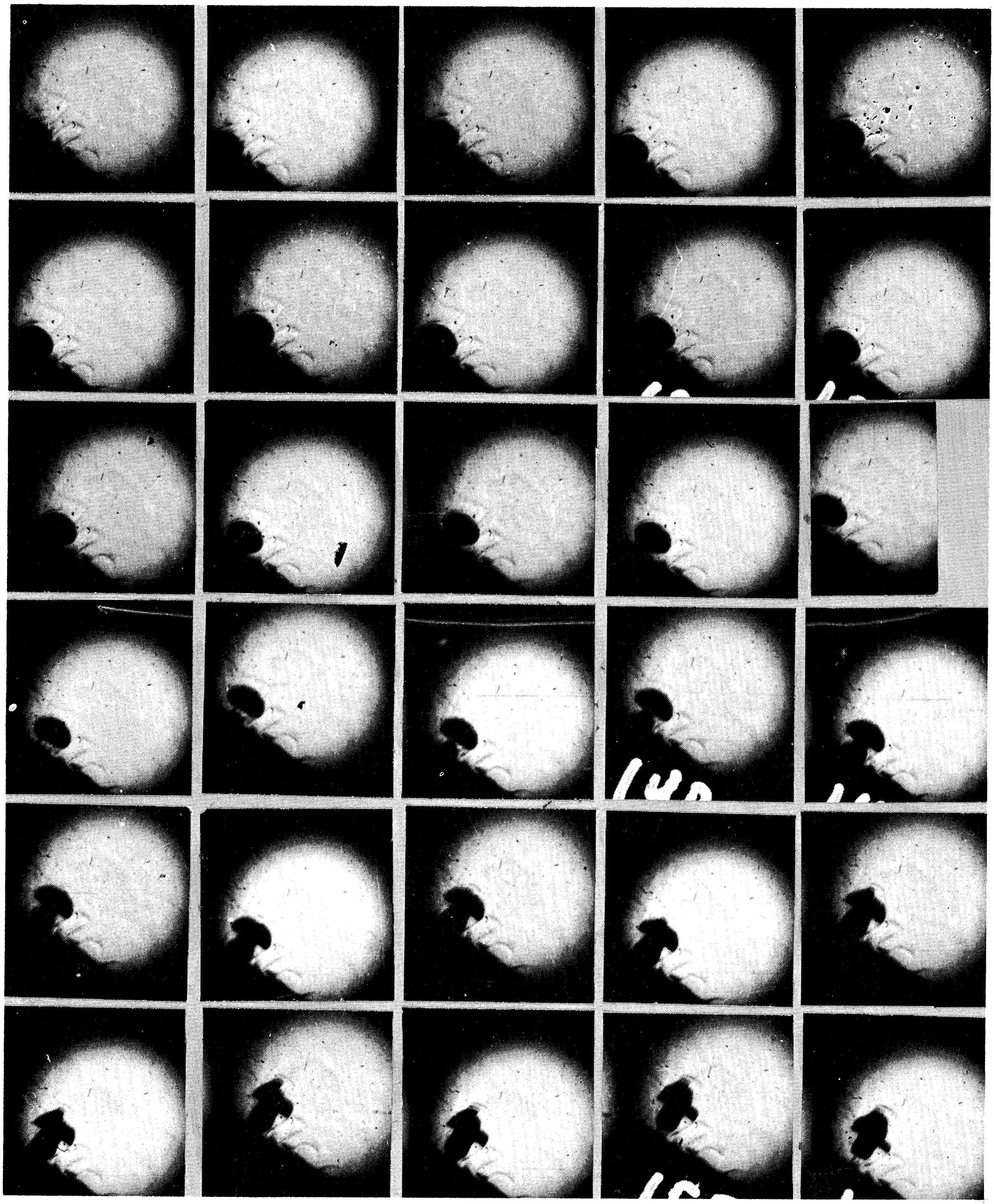

0.10" Test 166, a/g = 100, Camera Speed = 15,000 f/s
q/A = 40,000 BTU/hr-ft^2, Subcooling = 9.3°F

Figure 51. Typical Bubble at a/g = 100 .

APPENDIX B

DATA

TABLE V

HEAT TRANSFER DATA

TEST	A/G	TSAT	TSUR	TB	HEAT FLUX	TSUR-TSAT	TSAT -TB	TSUR -TB
107	1.0	210.6	227.6	209.2	16489	17.0	1.4	18.4
108	1.0	210.6	227.7	209.2	16067	17.0	1.5	18.5
109	1.0	210.6	227.0	209.4	16175	16.3	1.3	17.6
110	1.0	210.6	226.4	208.3	16492	15.8	2.4	18.1
111	3.1	210.9	229.7	209.6	15825	18.8	1.3	20.0
112	3.1	210.9	228.8	209.4	15847	17.9	1.5	19.4
113	3.1	210.9	229.6	209.2	15886	18.6	1.7	20.3
114	3.1	210.9	229.8	209.2	15639	18.9	1.7	20.6
115	3.1	211.9	230.8	210.2	39735	18.9	1.6	20.6
116	3.1	211.9	230.3	210.3	39510	18.4	1.6	20.0
117	3.1	211.9	229.8	210.4	38861	18.0	1.5	19.4
118	3.1	211.9	229.7	210.5	40103	17.9	1.4	19.2
119	3.1	211.9	227.7	200.1	39031	15.8	11.8	27.5
120	3.1	211.9	227.7	200.2	38935	15.8	11.7	27.5
121	3.1	211.9	227.7	200.9	38358	15.8	11.0	26.8
122	3.1	211.9	227.5	200.9	38295	15.6	11.0	26.5
125	1.0	212.1	229.3	210.0	36627	17.2	2.1	19.3
126	1.0	212.1	229.3	210.0	36351	17.2	2.1	19.3
127	1.0	212.1	229.4	210.2	36351	17.3	2.0	19.2
128	1.0	212.1	229.3	210.2	36151	17.2	1.9	19.1
129	10.9	222.6	236.6	211.2	38392	14.0	11.5	25.5
130	10.9	222.6	238.0	211.7	38538	15.4	10.9	26.3
131	10.9	222.6	238.6	212.0	38438	15.9	10.7	26.6
132	10.9	222.6	240.6	212.8	38322	18.0	9.9	27.8
133	10.6	222.3	238.2	212.8	38369	15.9	9.6	25.5
134	10.9	222.6	239.2	213.3	38200	16.6	9.3	25.9
135	1.0	212.1	227.6	201.3	38725	15.6	10.8	26.4
136	1.0	212.1	228.1	201.3	38754	16.0	10.8	26.8
137	1.0	212.1	228.0	204.3	38887	15.9	7.7	23.7
138	1.0	212.1	228.1	203.5	38854	16.0	8.5	24.6
139	1.0	212.1	228.1	204.2	38890	16.0	7.9	23.9
140	32.3	222.5	240.2	210.9	39488	17.7	11.6	29.3
141	32.3	222.5	239.6	210.6	39322	17.1	11.9	29.1
142	31.2	222.1	240.1	211.0	39317	18.0	11.2	29.1
143	31.2	222.1	240.4	210.8	39252	18.3	11.3	29.6
144	31.8	222.3	240.1	210.7	39091	17.8	11.6	29.4
145	32.3	222.5	240.3	210.6	39123	17.8	11.9	29.6
146	31.8	222.3	241.8	211.2	74325	19.5	11.1	30.6
147	31.2	222.1	241.6	211.4	74345	19.5	10.7	30.2
148	31.2	222.1	241.8	211.5	74373	19.6	10.7	30.3
149	10.9	212.0	229.5	210.0	41390	17.6	2.0	19.5
150	11.3	212.0	229.9	209.9	41892	17.9	2.1	20.0
151	10.6	211.9	229.7	209.9	41893	17.7	2.1	19.8
152	10.6	211.9	229.5	209.8	41725	17.6	2.1	19.7
153	10.6	211.9	229.4	209.8	41455	17.4	2.1	19.6
154	10.6	211.9	229.5	209.8	41791	17.6	2.1	19.7
155	10.9	212.2	226.4	198.9	41559	14.2	13.3	27.5
156	10.9	211.9	226.4	199.2	41491	14.5	12.7	27.1
157	10.6	211.9	226.1	198.9	41718	14.2	12.9	27.1
158	10.6	211.9	226.1	199.1	41422	14.3	12.8	27.0
159	10.9	211.9	226.0	199.1	41357	14.1	12.8	26.9
160	99.3	221.5	236.3	212.0	41407	14.8	9.5	24.2
161	99.3	221.5	235.8	211.9	41535	14.3	9.6	23.9
162	99.3	221.5	235.7	211.9	41305	14.2	9.6	23.8
163	99.3	221.5	235.5	211.8	41403	14.0	9.7	23.8
164	100.2	221.6	235.5	211.8	40610	13.9	9.8	23.8
165	100.2	221.6	235.6	211.8	40871	14.0	9.8	23.9
166	98.3	221.4	236.0	212.1	40348	14.6	9.3	23.9
167	99.3	221.5	236.6	212.4	40545	15.1	9.2	24.2
168	98.3	221.4	236.9	212.5	40349	15.5	8.9	24.4
169	94.5	221.1	239.6	211.8	73304	18.6	9.3	27.8
170	94.5	221.1	238.8	212.5	72733	17.7	8.6	26.3
171	97.3	221.4	238.9	212.2	72558	17.6	9.2	26.7
172	99.3	221.6	238.9	212.1	72469	17.3	9.5	26.8
173	97.3	221.4	239.3	212.0	72900	17.9	9.4	27.3
174	101.2	221.8	239.2	211.9	72506	17.5	9.9	27.3
201	1.0	211.2	227.4	201.1	15863	16.2	10.0	26.3
202	1.0	211.2	228.0	201.3	30052	16.8	9.9	26.7
203	1.0	211.2	228.4	201.4	47328	17.3	9.8	27.1
204	1.0	211.2	228.4	201.8	67870	17.2	9.4	26.6
205	1.0	211.2	229.2	201.1	81481	18.0	10.0	28.0
206	1.0	210.9	223.2	201.6	16799	12.3	9.3	21.6
207	101.2	221.8	224.2	210.0	16716	2.3	11.8	14.1
208	99.3	221.7	233.1	209.6	30228	11.5	12.0	23.5
209	100.2	221.7	235.8	209.2	48052	14.1	12.5	26.6
210	99.3	221.7	238.0	208.9	67406	16.3	12.8	29.1
211	100.2	221.7	239.8	208.8	83241	18.1	12.9	31.0
212	1.0	212.1	228.9	200.7	15861	16.8	11.4	28.2
213	11.3	223.0	236.2	211.4	15941	13.3	11.6	24.9
214	11.3	223.0	240.5	211.3	30170	17.5	11.7	29.2
215	10.9	222.7	239.9	211.4	46972	17.3	11.3	28.5
216	11.3	223.0	241.0	211.3	64593	18.1	11.7	29.8
217	11.3	223.0	241.6	211.0	79926	18.6	12.0	30.6

TABLE VI

ISOLATED BUBBLE DATA

```
ORUN NUMBER 107
N=.448,K=.713,J=1.00
        RADIUS(IN)   VOLUME(IN3)   TIME(SEC)
         .0000E 00    .0000E 00    .2992E-03
         .6802E-02    .1319E-05    .3320E-04
         .2157E-01    .4211E-04    .3657E-03
         .2823E-01    .9437E-04    .6981E-03
         .3302E-01    .1510E-03    .1031E-02
         .3546E-01    .1870E-03    .1363E-02
         .3954E-01    .2593E-03    .1696E-02
         .4136E-01    .2967E-03    .2028E-02
         .4374E-01    .3510E-03    .2361E-02
         .4490E-01    .3797E-03    .2693E-02
         .4718E-01    .4406E-03    .3025E-02
         .5021E-01    .5309E-03    .3358E-02
         .4954E-01    .5101E-03    .3690E-02
         .5141E-01    .5699E-03    .4355E-02
         .5183E-01    .5841E-03    .4688E-02
         .5290E-01    .6209E-03    .5020E-02
         .5285E-01    .6191E-03    .5353E-02
         .5423E-01    .6691E-03    .6017E-02
         .5561E-01    .7213E-03    .6682E-02
         .5579E-01    .7282E-03    .7347E-02
         .5662E-01    .7612E-03    .8012E-02
         .5698E-01    .7759E-03    .8677E-02
         .5732E-01    .7899E-03    .9342E-02
         .5790E-01    .8143E-03    .1001E-01
         .5768E-01    .8052E-03    .1067E-01
         .5810E-01    .8227E-03    .1134E-01
       D .6099E-01    .9515E-03    .1200E-01
         .5807E-01    .8212E-03    .1267E-01

ORUN NUMBER 108
N=.571,K=1.43,J=.894,BETA=79
        RADIUS(IN)   VOLUME(IN3)   TIME(SEC)
         .0000E 00    .0000E 00    .2992E-03
         .3286E-02    .1487E-06    .3320E-04
         .1969E-01    .3201E-04    .3657E-03
         .2599E-01    .7361E-04    .6981E-03
         .3159E-01    .1322E-03    .1031E-02
         .3487E-01    .1777E-03    .1363E-02
         .3827E-01    .2350E-03    .1696E-02
         .4058E-01    .2803E-03    .2028E-02
         .4340E-01    .3428E-03    .2361E-02
         .4522E-01    .3879E-03    .2693E-02
         .4703E-01    .4363E-03    .3025E-02
         .4922E-01    .5003E-03    .3358E-02
         .5037E-01    .5361E-03    .3690E-02
         .5086E-01    .5520E-03    .4023E-02
         .5275E-01    .6155E-03    .4688E-02
         .5417E-01    .6668E-03    .5353E-02
         .5561E-01    .7215E-03    .6017E-02
         .5688E-01    .7718E-03    .6682E-02
         .5779E-01    .8098E-03    .7347E-02
         .5892E-01    .8580E-03    .8012E-02
         .5996E-01    .9043E-03    .8677E-02
         .6026E-01    .9180E-03    .9342E-02
         .6109E-01    .9563E-03    .1001E-01
         .6173E-01    .9867E-03    .1067E-01
```

```
         .6180E-01    .9902E-03    .1134E-01
       D .6235E-01    .1017E-02    .1200E-01

         .6058E-01    .9328E-03    .1333E-01
ORUN NUMBER 109
N=.421,K=.251,J=.410
        RADIUS(IN)   VOLUME(IN3)   TIME(SEC)
         .0000E 00    .0000E 00    .2327E-03
         .5316E-02    .6297E-06    .9970E-04
         .9761E-02    .3899E-05    .4322E-03
         .1147E-01    .6320E-05    .7646E-03
         .1447E-01    .1271E-04    .1097E-02
         .1548E-01    .1554E-04    .1429E-02
         .1744E-01    .2225E-04    .1762E-02
         .1850E-01    .2656E-04    .2094E-02
         .2043E-01    .3577E-04    .2427E-02
         .2097E-01    .3867E-04    .2759E-02
         .2245E-01    .4743E-04    .3091E-02
         .2338E-01    .5357E-04    .3424E-02
         .2526E-01    .6761E-04    .3756E-02
         .2520E-01    .6713E-04    .4089E-02
         .2648E-01    .7783E-04    .4421E-02
         .2802E-01    .9223E-04    .5086E-02
         .2939E-01    .1064E-03    .5751E-02
         .3037E-01    .1175E-03    .6416E-02
         .3171E-01    .1337E-03    .7081E-02
         .3202E-01    .1377E-03    .7746E-02
         .3325E-01    .1541E-03    .8411E-02
         .3437E-01    .1702E-03    .9076E-02
         .3516E-01    .1823E-03    .9740E-02
         .3559E-01    .1890E-03    .1041E-01
         .3620E-01    .1989E-03    .1107E-01
         .3670E-01    .2073E-03    .1174E-01
         .3693E-01    .2113E-03    .1240E-01
         .3703E-01    .2129E-03    .1307E-01
         .3799E-01    .2300E-03    .1373E-01
         .3787E-01    .2278E-03    .1440E-01
         .3865E-01    .2421E-03    .1506E-01
         .3901E-01    .2490E-03    .1573E-01

ORUN NUMBER 110
N=.423,K=.599,J=.949,BETA=92
        RADIUS(IN)   VOLUME(IN3)   TIME(SEC)
         .0000E 00    .0000E 00    .9973E-04
         .1709E-01    .2092E-04    .2327E-03
         .2486E-01    .6443E-04    .5652E-03
         .3152E-01    .1313E-03    .8976E-03
         .3570E-01    .1908E-03    .1230E-02
         .3934E-01    .2553E-03    .1562E-02
         .4349E-01    .3449E-03    .1895E-02
         .4521E-01    .3876E-03    .2227E-02
         .4792E-01    .4614E-03    .2560E-02
         .5077E-01    .5489E-03    .2892E-02
         .5232E-01    .6008E-03    .3224E-02
         .5406E-01    .6626E-03    .3557E-02
         .5593E-01    .7338E-03    .3889E-02
         .5652E-01    .7572E-03    .4222E-02
         .5823E-01    .8281E-03    .4554E-02
         .5813E-01    .8240E-03    .4887E-02
```

```
         .5918E-01    .8694E-03    .5552E-02
         .6053E-01    .9304E-03    .6216E-02
         .6115E-01    .9594E-03    .6881E-02
         .6155E-01    .9781E-03    .7546E-02
         .6160E-01    .9806E-03    .8211E-02
         .6238E-01    .1018E-02    .8876E-02
         .6360E-01    .1079E-02    .9541E-02
         .6258E-01    .1028E-02    .1021E-01
         .6307E-01    .1052E-02    .1087E-01
         .6377E-01    .1088E-02    .1154E-01
         .6428E-01    .1114E-02    .1220E-01
         .6522E-01    .1164E-02    .1287E-01
         .6575E-01    .1192E-02    .1353E-01
         .6648E-01    .1233E-02    .1420E-01
         .6645E-01    .1231E-02    .1486E-01
         .6781E-01    .1308E-02    .1553E-01
         .6802E-01    .1320E-02    .1619E-01
         .6807E-01    .1323E-02    .1685E-01
       D .6800E-01    .1319E-02    .1752E-01

ORUN NUMBER 111
N=.470,K=.291,J=.350,BETA=82
        RADIUS(IN)   VOLUME(IN3)   TIME(SEC)
         .0000E 00    .0000E 00    .1819E-11
         .6954E-02    .1410E-05    .3324E-03
         .9456E-02    .3544E-05    .6649E-03
         .1082E-01    .5317E-05    .9973E-03
         .1213E-01    .7479E-05    .1330E-02
         .1380E-01    .1102E-04    .1662E-02
         .1631E-01    .1819E-04    .1995E-02
         .1710E-01    .2096E-04    .2327E-02
         .1786E-01    .2388E-04    .2660E-02
         .1922E-01    .2977E-04    .2992E-02
         .2012E-01    .3415E-04    .3324E-02
         .2063E-01    .3684E-04    .3657E-02
         .2149E-01    .4163E-04    .3989E-02
         .2196E-01    .4441E-04    .4322E-02
         .2236E-01    .4691E-04    .4654E-02
         .2325E-01    .5267E-04    .4987E-02
         .2429E-01    .6008E-04    .5652E-02
         .2472E-01    .6334E-04    .6316E-02
         .2533E-01    .6813E-04    .6981E-02
         .2577E-01    .7173E-04    .7646E-02
         .2684E-01    .8109E-04    .8311E-02
         .2722E-01    .8460E-04    .8976E-02
         .2730E-01    .8535E-04    .9641E-02
         .2773E-01    .8941E-04    .1031E-01
         .2794E-01    .9145E-04    .1097E-01
         .2848E-01    .9690E-04    .1164E-01
         .2918E-01    .1042E-03    .1230E-01
         .2945E-01    .1072E-03    .1297E-01
       D .2995E-01    .1127E-03    .1363E-01

ORUN NUMBER 112
N=.634,K=1.55,J=.646,BETA=84
        RADIUS(IN)   VOLUME(IN3)   TIME(SEC)
         .0000E 00    .0000E 00    .2992E-03
         .2196E-02    .4440E-07    .3320E-04
         .1037E-01    .4676E-05    .3657E-03
```

TABLE VI (CONT'D)

```
  .1602E-01   .1724E-04   .6981E-03
  .2095E-01   .3858E-04   .1031E-02
  .2407E-01   .5852E-04   .1363E-02
  .2711E-01   .8355E-04   .1696E-02
  .2937E-01   .1062E-03   .2028E-02
  .3199E-01   .1373E-03   .2361E-02
  .3317E-01   .1530E-03   .2693E-02
  .3517E-01   .1825E-03   .3025E-02
  .3595E-01   .1949E-03   .3358E-02
  .3719E-01   .2158E-03   .3690E-02
  .3777E-01   .2259E-03   .4023E-02
  .3892E-01   .2472E-03   .4355E-02
  .3930E-01   .2545E-03   .4688E-02
  .4024E-01   .2733E-03   .5020E-02
  .3996E-01   .2677E-03   .5353E-02
  .4110E-01   .2912E-03   .6017E-02
  .4223E-01   .3159E-03   .6682E-02
  .4275E-01   .3276E-03   .7347E-02
  .4367E-01   .3493E-03   .8012E-02
  .4362E-01   .3482E-03   .8677E-02
D .4422E-01   .3626E-03   .9342E-02

ORUN NUMBER 112
N=.440,K=.197,J=.285,BETA=42
 RADIUS(IN)  VOLUME(IN3)  TIME(SEC)
  .0000E 00   .0000E 00   .9943E-04
  .4899E-02   .4928E-06   .2330E-03
  .7308E-02   .1636E-05   .5655E-03
  .9080E-02   .3138E-05   .8979E-03
  .1043E-01   .4758E-05   .1231E-02
  .1167E-01   .6660E-05   .1563E-02
  .1247E-01   .8131E-05   .1896E-02
  .1332E-01   .9904E-05   .2228E-02
  .1386E-01   .1117E-04   .2561E-02
  .1496E-01   .1405E-04   .2893E-02
  .1582E-01   .1659E-04   .3225E-02
  .1616E-01   .1768E-04   .3558E-02
  .1681E-01   .1992E-04   .3890E-02
  .1721E-01   .2136E-04   .4223E-02
  .1934E-01   .3031E-04   .4888E-02
  .1896E-01   .2857E-04   .5220E-02
  .2004E-01   .3375E-04   .5885E-02
  .2063E-01   .3683E-04   .6550E-02
  .2132E-01   .4066E-04   .7215E-02
  .2236E-01   .4689E-04   .7880E-02
  .2251E-01   .4786E-04   .8545E-02
  .2332E-01   .5317E-04   .9210E-02
D .2378E-01   .5638E-04   .9874E-02

ORUN NUMBER 114
N=.541,K=.024,J=.648
 RADIUS(IN)  VOLUME(IN3)  TIME(SEC)
  .0000E 00   .0000E 00   .1202E-03
  .5207E-02   .5919E-06   .8010E-04
  .1034E-01   .4629E-05   .2804E-03
  .1487E-01   .1377E-04   .4808E-03
  .1651E-01   .1888E-04   .6811E-03
  .1961E-01   .3164E-04   .8818E-03
  .2087E-01   .3812E-04   .1082E-02
```

```
  .2352E-01   .5460E-04   .1282E-02
  .2416E-01   .5915E-04   .1483E-02
  .2655E-01   .7851E-04   .1683E-02
  .2673E-01   .8011E-04   .1883E-02
  .2813E-01   .9335E-04   .2084E-02
  .2802E-01   .9230E-04   .2284E-02
  .2931E-01   .1055E-03   .2484E-02
  .2956E-01   .1083E-03   .2684E-02
  .2994E-01   .1125E-03   .2885E-02
  .3013E-01   .1147E-03   .3085E-02
  .3081E-01   .1226E-03   .3285E-02
  .3087E-01   .1234E-03   .3486E-02
  .3151E-01   .1312E-03   .3686E-02
  .3156E-01   .1319E-03   .3886E-02
  .3193E-01   .1365E-03   .4087E-02
  .3164E-01   .1328E-03   .4287E-02
  .3239E-01   .1425E-03   .4487E-02
  .3235E-01   .1420E-03   .4688E-02
  .3260E-01   .1453E-03   .4888E-02
  .3263E-01   .1457E-03   .5088E-02
  .3304E-01   .1513E-03   .5289E-02
  .3278E-01   .1477E-03   .5489E-02
  .3325E-01   .1542E-03   .5689E-02
  .3308E-01   .1517E-03   .5890E-02
  .3363E-01   .1595E-03   .6090E-02
  .3364E-01   .1597E-03   .6290E-02
  .3383E-01   .1624E-03   .6491E-02
  .3389E-01   .1633E-03   .6691E-02
D .3406E-01   .1658E-03   .6891E-02
  .3427E-01   .1689E-03   .7092E-02

ORUN NUMBER 115
N=.412,K=.312,J=.573,BETA=50
 RADIUS(IN)  VOLUME(IN3)  TIME(SEC)
  .0000E 00   .0000E 00   .1002E-03
  .6853E-02   .1349E-05   .1001E-03
  .1111E-01   .5748E-05   .3004E-03
  .1365E-01   .1065E-04   .5008E-03
  .1634E-01   .1829E-04   .7011E-03
  .1786E-01   .2387E-04   .9018E-03
  .1887E-01   .2818E-04   .1102E-02
  .1986E-01   .3283E-04   .1302E-02
  .2042E-01   .3568E-04   .1503E-02
  .2125E-01   .4021E-04   .1703E-02
  .2218E-01   .4576E-04   .1903E-02
  .2228E-01   .4635E-04   .2104E-02
  .2248E-01   .4765E-04   .2304E-02
  .2366E-01   .5555E-04   .2704E-02
D .2347E-01   .5422E-04   .3105E-02
  .2344E-01   .5400E-04   .3506E-02

ORUN NUMBER 115
N=.539,K=.790,J=.595,BETA=46
 RADIUS(IN)  VOLUME(IN3)  TIME(SEC)
  .0000E 00   .0000E 00   .1603E-03
  .3384E-02   .1625E-06   .4000E-04
  .8964E-02   .3020E-05   .2403E-03
  .1277E-01   .8724E-05   .4407E-03
  .1542E-01   .1537E-04   .6410E-03
```

```
  .1696E-01   .2046E-04   .8417E-03
  .1805E-01   .2465E-04   .1042E-02
  .1951E-01   .3113E-04   .1242E-02
  .1978E-01   .3246E-04   .1443E-02
  .2097E-01   .3866E-04   .1643E-02
  .2134E-01   .4073E-04   .1843E-02
  .2237E-01   .4694E-04   .2044E-02
  .2142E-01   .4123E-04   .2244E-02
  .2268E-01   .4893E-04   .2644E-02
  .2284E-01   .4999E-04   .3045E-02
  .2259E-01   .4833E-04   .3446E-02
  .2302E-01   .5118E-04   .3846E-02
  .2347E-01   .5423E-04   .4247E-02
D .2335E-01   .5341E-04   .4647E-02

ORUN NUMBER 116
N=.427,K=.445,J=.725
 RADIUS(IN)  VOLUME(IN3)  TIME(SEC)
  .0000E 00   .0000E 00   .1002E-03
  .8638E-02   .2702E-05   .1001E-03
  .1397E-01   .1142E-04   .3004E-03
  .1733E-01   .2183E-04   .5008E-03
  .1979E-01   .3250E-04   .7011E-03
  .2276E-01   .4943E-04   .9018E-03
  .2463E-01   .6262E-04   .1102E-02
  .2657E-01   .7866E-04   .1302E-02
  .2709E-01   .8333E-04   .1503E-02
  .2917E-01   .1041E-03   .1703E-02
  .3000E-01   .1132E-03   .1903E-02
  .3068E-01   .1211E-03   .2104E-02
  .3167E-01   .1332E-03   .2504E-02
  .3272E-01   .1470E-03   .2905E-02
  .3275E-01   .1473E-03   .3305E-02
  .3201E-01   .1376E-03   .3706E-02
  .3207E-01   .1384E-03   .4107E-02
  .3135E-01   .1293E-03   .4507E-02
  .3106E-01   .1257E-03   .4908E-02

ORUN NUMBER 116
N=.372,K=.301,J=.706,BETA=71
 RADIUS(IN)  VOLUME(IN3)  TIME(SEC)
  .0000E 00   .0000E 00   .1603E-03
  .7020E-02   .1450E-05   .4000E-04
  .1331E-01   .9877E-05   .2403E-03
  .1700E-01   .2060E-04   .4407E-03
  .1948E-01   .3100E-04   .6410E-03
  .2145E-01   .4138E-04   .8417E-03
  .2314E-01   .5195E-04   .1042E-02
  .2522E-01   .6723E-04   .1242E-02
  .2674E-01   .8014E-04   .1443E-02
  .2756E-01   .8783E-04   .1643E-02
  .2904E-01   .1027E-03   .1843E-02
  .2991E-01   .1122E-03   .2044E-02
  .3056E-01   .1197E-03   .2244E-02
  .3054E-01   .1194E-03   .2444E-02
  .3073E-01   .1217E-03   .2644E-02
  .3106E-01   .1257E-03   .3045E-02
  .3045E-01   .1184E-03   .3446E-02
  .2967E-01   .1096E-03   .3846E-02
```

TABLE VI (CONT'D)

```
     .2964E-01    .1092E-03    .4247E-02
     .3043E-01    .1182E-03    .4648E-02
     .3062E-01    .1204E-03    .5048E-02
     .3099E-01    .1248E-03    .5449E-02
     .3162E-01    .1326E-03    .5850E-02
   D .3155E-01    .1317E-03    .6250E-02

ORUN NUMBER 117
N=.668,K=3.45,J=.983,BETA=45
   RADIUS(IN)  VOLUME(IN3)   TIME(SEC)
     .0000E 00    .0000E 00    .1002E-03
     .1252E-01    .8235E-05    .1001E-03
     .1765E-01    .2307E-04    .3004E-03
     .2229E-01    .4647E-04    .5008E-03
     .2566E-01    .7085E-04    .7011E-03
     .3013E-01    .1148E-03    .9018E-03
     .3105E-01    .1256E-03    .1102E-02
     .3173E-01    .1339E-03    .1302E-02
     .3271E-01    .1468E-03    .1503E-02
     .3335E-01    .1555E-03    .1703E-02
     .3421E-01    .1680E-03    .1903E-02
     .3442E-01    .1710E-03    .2104E-02
     .3543E-01    .1865E-03    .2504E-02
     .3553E-01    .1881E-03    .2905E-02
     .3515E-01    .1821E-03    .3706E-02
     .3426E-01    .1686E-03    .4107E-02
   D .3573E-01    .1913E-03    .4708E-02

ORUN NUMBER 117
N=.411,K=.468,J=.910,BETA=59
   RADIUS(IN)  VOLUME(IN3)   TIME(SEC)
     .0000E 00    .0000E 00    .1202E-03
     .9753E-02    .3890E-05    .8010E-04
     .1585E-01    .1670E-04    .2804E-03
     .2111E-01    .3944E-04    .4808E-03
     .2309E-01    .5162E-04    .6811E-03
     .2591E-01    .7293E-04    .8818E-03
     .2675E-01    .8023E-04    .1082E-02
     .2813E-01    .9340E-04    .1282E-02
     .2921E-01    .1045E-03    .1483E-02
     .3130E-01    .1286E-03    .1683E-02
     .2953E-01    .1079E-03    .1883E-02
     .3275E-01    .1473E-03    .2084E-02
     .3394E-01    .1640E-03    .2484E-02
     .3360E-01    .1592E-03    .2885E-02
     .3377E-01    .1615E-03    .3686E-02
     .3379E-01    .1618E-03    .4087E-02
     .3330E-01    .1549E-03    .4487E-02
   D .3317E-01    .1531E-03    .4888E-02

ORUN NUMBER 117
                   BETA=49
   RADIUS(IN)  VOLUME(IN3)   TIME(SEC)
     .0000E 00    .0000E 00    .1402E-03
     .1097E-01    .5531E-05    .6010E-04
     .1563E-01    .1601E-04    .2604E-03
     .1927E-01    .3002E-04    .4608E-03
     .2044E-01    .3579E-04    .6611E-03
     .2172E-01    .4297E-04    .8618E-03
```

```
     .2299E-01    .5099E-04    .1062E-02
     .2340E-01    .5376E-04    .1262E-02
     .2316E-01    .5209E-04    .1463E-02
     .2324E-01    .5265E-04    .1663E-02
     .2322E-01    .5251E-04    .1863E-02
     .2305E-01    .5136E-04    .2064E-02
     .2365E-01    .5548E-04    .2464E-02
     .2377E-01    .5635E-04    .2865E-02
   D .2451E-01    .6178E-04    .3265E-02

ORUN NUMBER 117
N=.463,K=.631,J=.817,BETA=77
   RADIUS(IN)  VOLUME(IN3)   TIME(SEC)
     .0000E 00    .0000E 00    .1603E-03
     .5715E-02    .7823E-06    .4000E-04
     .1297E-01    .9142E-05    .2403E-03
     .1851E-01    .2661E-04    .4407E-03
     .2117E-01    .3980E-04    .6410E-03
     .2321E-01    .5245E-04    .8417E-03
     .2533E-01    .6819E-04    .1042E-02
     .2832E-01    .9521E-04    .1242E-02
     .3085E-01    .1231E-03    .1643E-02
     .3194E-01    .1366E-03    .1843E-02
     .3187E-01    .1358E-03    .2044E-02
     .3262E-01    .1456E-03    .2444E-02
     .3141E-01    .1299E-03    .2845E-02
     .3050E-01    .1190E-03    .3245E-02
     .3000E-01    .1132E-03    .3646E-02
   D .3059E-01    .1200E-03    .4046E-02

ORUN NUMBER 118
N=.381,K=.315,J=.741,BETA=56
   RADIUS(IN)  VOLUME(IN3)   TIME(SEC)
     .0000E 00    .0000E 00    .1002E-03
     .9327E-02    .3402E-05    .1001E-03
     .1449E-01    .1275E-04    .3004E-03
     .1664E-01    .1932E-04    .5008E-03
     .2016E-01    .3434E-04    .7011E-03
     .2178E-01    .4332E-04    .9018E-03
     .2308E-01    .5155E-04    .1102E-02
     .2391E-01    .5730E-04    .1302E-02
     .2501E-01    .6559E-04    .1503E-02
     .2546E-01    .6921E-04    .1703E-02
     .2568E-01    .7101E-04    .1903E-02
     .2643E-01    .7742E-04    .2104E-02
     .2689E-01    .8155E-04    .2304E-02
     .2747E-01    .8689E-04    .2704E-02
     .2732E-01    .8550E-04    .3105E-02
     .2722E-01    .8460E-04    .3506E-02
     .2662E-01    .7912E-04    .3906E-02
     .2690E-01    .8164E-04    .4307E-02
     .2693E-01    .8192E-04    .4708E-02
     .2661E-01    .7899E-04    .5108E-02
     .2737E-01    .8598E-04    .5509E-02
     .2786E-01    .9073E-04    .5910E-02
     .2754E-01    .8759E-04    .6310E-02
     .2774E-01    .8952E-04    .6711E-02
   D .2821E-01    .9416E-04    .7111E-02
```

```
ORUN NUMBER 118
N=.538,K=1.10,J=.839,BETA=55
   RADIUS(IN)  VOLUME(IN3)   TIME(SEC)
     .0000E 00    .0000E 00    .1603E-03
     .4701E-02    .4355E-06    .4000E-04
     .1248E-01    .8151E-05    .2403E-03
     .1781E-01    .2368E-04    .4407E-03
     .2126E-01    .4032E-04    .6410E-03
     .2406E-01    .5844E-04    .8417E-03
     .2813E-01    .9330E-04    .1042E-02
     .2899E-01    .1022E-03    .1242E-02
     .3082E-01    .1227E-03    .1443E-02
     .3213E-01    .1392E-03    .1643E-02
     .3352E-01    .1580E-03    .1843E-02
     .3477E-01    .1763E-03    .2044E-02
     .3592E-01    .1943E-03    .2244E-02
     .3675E-01    .2082E-03    .2444E-02
     .3864E-01    .2420E-03    .3245E-02
     .3961E-01    .2607E-03    .3646E-02
     .3949E-01    .2584E-03    .4047E-02
     .4000E-01    .2684E-03    .4447E-02
     .4034E-01    .2753E-03    .4848E-02
     .3989E-01    .2663E-03    .5249E-02
     .3923E-01    .2533E-03    .5649E-02
     .3925E-01    .2535E-03    .6050E-02
     .3965E-01    .2614E-03    .6451E-02
   D .3968E-01    .2620E-03    .6851E-02
     .4024E-01    .2734E-03    .7252E-02
     .3972E-01    .2627E-03    .7653E-02
     .3993E-01    .2669E-03    .8053E-02
     .4043E-01    .2773E-03    .8454E-02
     .4017E-01    .2719E-03    .8854E-02
     .3995E-01    .2675E-03    .9255E-02
     .4091E-01    .2872E-03    .9656E-02
     .4089E-01    .2867E-03    .1006E-01

ORUN NUMBER 119
N=.541,K=.555,J=.412,BETA=54
   RADIUS(IN)  VOLUME(IN3)   TIME(SEC)
     .0000E 00    .0000E 00    .6010E-04
     .4535E-02    .3909E-06    .1402E-03
     .7069E-02    .1481E-05    .3405E-03
     .1009E-01    .4309E-05    .5409E-03
     .1178E-01    .6845E-05    .7412E-03
     .1265E-01    .8485E-05    .9419E-03
     .1350E-01    .1032E-04    .1142E-02
     .1360E-01    .1054E-04    .1342E-02
     .1350E-01    .1032E-04    .1543E-02
     .1306E-01    .9350E-05    .1743E-02
     .1263E-01    .8449E-05    .1943E-02
     .1272E-01    .8633E-05    .2144E-02
     .1187E-01    .7007E-05    .2544E-02
     .1168E-01    .6688E-05    .2945E-02
     .1119E-01    .5880E-05    .3345E-02
     .1096E-01    .5519E-05    .3746E-02
     .1152E-01    .6417E-05    .4147E-02
     .1403E-01    .1157E-04    .4547E-02
     .1521E-01    .1476E-04    .4948E-02
     .1578E-01    .1648E-04    .5349E-02
```

TABLE VI (CONT'D)

```
     .1585E-01    .1671E-04    .5749E-02
     .1509E-01    .1442E-04    .6150E-02
     .1325E-01    .9755E-05    .6551E-02
     .1246E-01    .8108E-05    .6951E-02
   D .1208E-01    .7390E-05    .7352E-02

ORUN NUMBER 119
N=.485,K=.678,J=.750,BETA=74
    RADIUS(IN)   VOLUME(IN3)   TIME(SEC)
     .0000E 00    .0000E 00    .1803E-03
     .3524E-02    .1834E-06    .2000E-04
     .1131E-01    .6058E-05    .2203E-03
     .1645E-01    .1867E-04    .4207E-03
     .1874E-01    .2761E-04    .6210E-03
     .2180E-01    .4343E-04    .8217E-03
     .2349E-01    .5433E-04    .1022E-02
     .2565E-01    .7078E-04    .1222E-02
     .2594E-01    .7318E-04    .1423E-02
     .2755E-01    .8766E-04    .1623E-02
     .2773E-01    .8939E-04    .1823E-02
     .2831E-01    .9520E-04    .2024E-02
     .2878E-01    .9993E-04    .2424E-02
     .2866E-01    .9874E-04    .2825E-02
     .2802E-01    .9225E-04    .3225E-02
     .2744E-01    .8663E-04    .3626E-02
     .2631E-01    .7640E-04    .4027E-02
   D .2457E-01    .6221E-04    .4427E-02
     .2282E-01    .4983E-04    .4828E-02
     .2149E-01    .4159E-04    .5229E-02
     .2044E-01    .3582E-04    .5629E-02
     .1938E-01    .3050E-04    .6030E-02
     .1803E-01    .2457E-04    .6431E-02
     .1572E-01    .1627E-04    .6831E-02
     .1384E-01    .1112E-04    .7232E-02
     .8958E-02    .3013E-05    .7633E-02
     .6791E-02    .1313E-05    .8033E-02
     .4356E-02    .3465E-06    .8434E-02
     .2093E-02    .3843E-07    .8834E-02

ORUN NUMBER 120
N=.625,K=1.49,J=.713,BETA=58
    RADIUS(IN)   VOLUME(IN3)   TIME(SEC)
     .0000E 00    .0000E 00    .9952E-04
     .9568E-02    .3672E-05    .9948E-04
     .1254E-01    .8263E-05    .2986E-03
     .1562E-01    .1598E-04    .4976E-03
     .1959E-01    .3155E-04    .6967E-03
     .2115E-01    .3967E-04    .8957E-03
     .2321E-01    .5243E-04    .1094E-02
     .2499E-01    .6543E-04    .1293E-02
     .2618E-01    .7524E-04    .1492E-02
     .2634E-01    .7661E-04    .1691E-02
     .2811E-01    .9314E-04    .1890E-02
     .2852E-01    .9729E-04    .2089E-02
     .2808E-01    .9286E-04    .2488E-02
     .2722E-01    .8457E-04    .2886E-02
     .2713E-01    .8370E-04    .3284E-02
     .2663E-01    .7915E-04    .3682E-02
     .2631E-01    .7639E-04    .4080E-02
```

```
     .2560E-01    .7033E-04    .4478E-02
     .2588E-01    .7267E-04    .4876E-02
     .2513E-01    .6654E-04    .5274E-02
     .2448E-01    .6153E-04    .5672E-02
   D .2302E-01    .5118E-04    .6070E-02
     .2217E-01    .4572E-04    .6468E-02
     .2056E-01    .3644E-04    .6867E-02
     .1933E-01    .3030E-04    .7265E-02
     .1759E-01    .2281E-04    .7663E-02
     .1403E-01    .1158E-04    .8459E-02
     .1225E-01    .7712E-05    .9255E-02
     .7076E-02    .1485E-05    .1005E-01

ORUN NUMBER 120
N=.476,K=.759,J=.902
    RADIUS(IN)   VOLUME(IN3)   TIME(SEC)
     .0000E 00    .0000E 00    .1194E-03
     .8420E-02    .2502E-05    .7960E-04
     .1524E-01    .1484E-04    .2787E-03
     .2035E-01    .3536E-04    .4777E-03
     .2347E-01    .5422E-04    .6768E-03
     .2602E-01    .7386E-04    .8758E-03
     .2825E-01    .9454E-04    .1075E-02
     .2924E-01    .1049E-03    .1274E-02
     .3101E-01    .1250E-03    .1473E-02
     .3158E-01    .1320E-03    .1672E-02
     .3346E-01    .1572E-03    .1871E-02
   D .3296E-01    .1502E-03    .2070E-02
     .3340E-01    .1563E-03    .2469E-02
     .3379E-01    .1618E-03    .2867E-02
     .3366E-01    .1600E-03    .3265E-02
     .3319E-01    .1533E-03    .3663E-02

ORUN NUMBER 121
N=.503,K=.832,J=.808,BETA=57
    RADIUS(IN)   VOLUME(IN3)   TIME(SEC)
     .0000E 00    .0000E 00    .9966E-04
     .5137E-02    .5684E-06    .4274E-04
     .1121E-01    .5909E-05    .1850E-03
     .1499E-01    .1413E-04    .3274E-03
     .1808E-01    .2477E-04    .4698E-03
     .2059E-01    .3660E-04    .6121E-03
     .2191E-01    .4411E-04    .7545E-03
     .2324E-01    .5262E-04    .8969E-03
     .2463E-01    .6264E-04    .1039E-02
     .2626E-01    .7598E-04    .1181E-02
     .2557E-01    .7014E-04    .1324E-02
     .2677E-01    .8047E-04    .1466E-02
     .2743E-01    .8654E-04    .1751E-02
     .2809E-01    .9296E-04    .2036E-02
     .2813E-01    .9332E-04    .2320E-02
     .2739E-01    .8613E-04    .2605E-02
     .2692E-01    .8180E-04    .3459E-02
     .2542E-01    .6885E-04    .3744E-02
     .2455E-01    .6208E-04    .4029E-02
     .2329E-01    .5295E-04    .4313E-02
   D .2276E-01    .4945E-04    .4598E-02
     .2107E-01    .3922E-04    .4883E-02
     .1972E-01    .3214E-04    .5168E-02
```

```
     .1737E-01    .2197E-04    .5737E-02
     .1558E-01    .1584E-04    .6307E-02
     .1366E-01    .1069E-04    .6876E-02
     .1087E-01    .5385E-05    .7446E-02
     .5337E-02    .6372E-06    .8015E-02
ORUN NUMBER 121
N=.375,K=.272,J=.686,BETA=71
    RADIUS(IN)   VOLUME(IN3)   TIME(SEC)
     .0000E 00    .0000E 00    .9966E-04
     .6140E-02    .9703E-06    .4274E-04
     .1091E-01    .5444E-05    .1850E-03
     .1344E-01    .1019E-04    .3274E-03
     .1550E-01    .1560E-04    .4698E-03
     .1723E-01    .2144E-04    .6121E-03
     .1776E-01    .2348E-04    .7545E-03
     .1927E-01    .3001E-04    .8969E-03
     .1918E-01    .2961E-04    .1039E-02
     .1981E-01    .3261E-04    .1181E-02
     .1995E-01    .3330E-04    .1324E-02
     .2014E-01    .3424E-04    .1466E-02
     .2045E-01    .3588E-04    .1608E-02
     .2006E-01    .3387E-04    .1893E-02
     .1872E-01    .2750E-04    .2178E-02
     .1751E-01    .2252E-04    .2463E-02
     .1666E-01    .1939E-04    .2747E-02
     .1591E-01    .1688E-04    .3032E-02
   D .1458E-01    .1301E-04    .3317E-02
     .1325E-01    .9764E-05    .3886E-02
     .1239E-01    .7980E-05    .4456E-02
     .9209E-02    .3274E-05    .5025E-02
     .6334E-02    .1065E-05    .5595E-02

ORUN NUMBER 122
N=.300,K=.157,J=.698,BETA=62
    RADIUS(IN)   VOLUME(IN3)   TIME(SEC)
     .0000E 00    .0000E 00    .1139E-03
     .6707E-02    .1265E-05    .2850E-04
     .1161E-01    .6561E-05    .1708E-03
     .1423E-01    .1207E-04    .3132E-03
     .1543E-01    .1540E-04    .4556E-03
     .1696E-01    .2046E-04    .5979E-03
     .1809E-01    .2482E-04    .7403E-03
     .1855E-01    .2676E-04    .8827E-03
     .1991E-01    .3307E-04    .1025E-02
     .1977E-01    .3240E-04    .1167E-02
     .1978E-01    .3246E-04    .1310E-02
     .1893E-01    .2846E-04    .1452E-02
     .1837E-01    .2599E-04    .1737E-02
     .1812E-01    .2496E-04    .2022E-02
     .1663E-01    .1929E-04    .2306E-02
     .1561E-01    .1595E-04    .2591E-02
   D .1477E-01    .1350E-04    .2876E-02
     .1465E-01    .1319E-04    .3445E-02
     .1445E-01    .1265E-04    .4015E-02
     .1109E-01    .5723E-05    .4584E-02
     .8406E-02    .2490E-05    .5154E-02
     .5636E-02    .7502E-06    .5723E-02

ORUN NUMBER 122
```

TABLE VI (CONT'D)

```
RUN NUMBER 122
N=.351,K=.376,J=1.07,BETA=47
      RADIUS(IN)   VOLUME(IN3)   TIME(SEC)
       .0000E 00    .0C0CE 00    .1139E-03
       .9559E-02    .3662E-05    .2850E-04
       .1830E-01    .2568E-04    .1708E-03
       .2207E-01    .4510E-04    .3132E-03
       .2473E-01    .6340E-04    .4556E-03
       .2782E-01    .9033E-04    .5979E-03
       .3012E-01    .1146E-03    .7403E-03
       .3293E-01    .1498E-03    .8827E-03
       .3355E-01    .1584E-03    .1025E-02
       .3561E-01    .1894E-03    .1167E-02
       .3603E-01    .1961E-03    .1310E-02
       .3806E-01    .2313E-03    .1452E-02
       .4115E-01    .2922E-03    .2022E-02
       .4181E-01    .3064E-03    .2591E-02
       .4166E-01    .3032E-03    .3160E-02
       .4158E-01    .3014E-03    .3730E-02
       .4016E-01    .2717E-03    .4299E-02
       .3980E-01    .2644E-03    .4869E-02
       .3885E-01    .2460E-03    .5438E-02
      D.3865E-01    .2421E-03    .6008E-02
       .3777E-01    .2259E-03    .6577E-02
       .3655E-01    .2048E-03    .7147E-02
       .3467E-01    .1747E-03    .7716E-02
       .3462E-01    .1740E-03    .8286E-02
       .3248E-01    .1437E-03    .8855E-02
       .3077E-01    .1222E-03    .9425E-02
       .2804E-01    .9243E-04    .9996E-02
       .2538E-01    .6855E-04    .1057E-01
       .2465E-01    .6282E-04    .1114E-01
       .1982E-01    .3266E-04    .1171E-01
       .1799E-01    .2443E-04    .1228E-01
       .1486E-01    .1376E-04    .1285E-01
       .9639E-02    .3754E-05    .1398E-01
       .8418E-02    .2501E-05    .1455E-01
       .7527E-02    .1788E-05    .1512E-01
       .6231E-02    .1014E-05    .1569E-01

ORUN NUMBER 122
N=.380,K=.316,J=.772,BETA=69
      RADIUS(IN)   VOLUME(IN3)   TIME(SEC)
       .0000E 00    .0000E 00    .8542E-04
       .7717E-02    .1926E-05    .5698E-04
       .1248E-01    .8143E-05    .1993E-03
       .1482E-01    .1364E-04    .3417E-03
       .1722E-01    .2142E-04    .4841E-03
       .1899E-01    .2873E-04    .6264E-03
       .2098E-01    .3872E-04    .7688E-03
       .2221E-01    .4594E-04    .9112E-03
       .2312E-01    .5180E-04    .1054E-02
       .2414E-01    .5899E-04    .1196E-02
       .2518E-01    .6694E-04    .1339E-02
       .2610E-01    .7454E-04    .1481E-02
       .2702E-01    .8270E-04    .1766E-02
       .2736E-01    .8585E-04    .2051E-02
       .2748E-01    .8700E-04    .2335E-02
       .2722E-01    .8459E-04    .2620E-02
       .2650E-01    .7808E-04    .2905E-02
```

```
       .2614E-01    .7494E-04    .3189E-02
       .2553E-01    .6977E-04    .3474E-02
       .2526E-01    .6760E-04    .3759E-02
       .2434E-01    .6048E-04    .4044E-02
       .2378E-01    .5641E-04    .4328E-02
       .2314E-01    .5197E-04    .4613E-02
     D .2206E-01    .4500E-04    .4898E-02
       .2141E-01    .4116E-04    .5183E-02
       .2129E-01    .4048E-04    .5467E-02
       .2073E-01    .3734E-04    .5752E-02
       .1989E-01    .3298E-04    .6037E-02

ORUN NUMBER 130
N=.465,K=.509,J=.669,BETA=61
      RADIUS(IN)   VOLUME(IN3)   TIME(SEC)
       .0000E 00    .0000E 00    .18C3E-03
       .3286E-02    .1487E-06    .2000E-04
       .1046E-01    .4804E-05    .2203E-03
       .1328E-01    .9823E-05    .4207E-03
       .1515E-01    .1457E-04    .6210E-03
       .1632E-01    .1821E-04    .8217E-03
       .1643E-01    .1859E-04    .1022E-02
       .1617E-01    .1772E-04    .1222E-02
       .1556E-01    .1579E-04    .1423E-02
       .1487E-01    .1380E-04    .1623E-02
     D .1396E-01    .1140E-04    .1823E-02
       .1316E-01    .9551E-05    .2024E-02
       .1261E-01    .8408E-05    .2224E-02
       .1182E-01    .6917E-05    .2424E-02
       .1096E-01    .5525E-05    .2624E-02
       .8961E-02    .3017E-05    .2825E-02
       .9108E-02    .3168E-05    .3025E-02
       .8989E-02    .3045E-05    .3225E-02
       .7047E-02    .1467E-05    .3426E-02
       .6414E-02    .1106E-05    .3626E-C2

ORUN NUMBER 130
                   BETA=61
      RADIUS(IN)   VOLUME(IN3)   TIME(SEC)
       .0000E 00    .C000E 00    .1803E-03
       .7086E-02    .1491E-05    .2000E-04
       .1019E-01    .4433E-05    .2203E-03
       .1197E-01    .7198E-05    .4207E-03
       .1293E-01    .9059E-05    .6210E-03
       .1250E-01    .8188E-05    .8217E-03
       .1205E-01    .7337E-05    .1022E-02
       .1127E-01    .6000E-05    .1222E-02
     D .1100E-01    .5576E-05    .1423E-02
       .9470E-02    .3561E-05    .1623E-02
       .9148E-02    .3210E-05    .1823E-02
       .8369E-02    .2457E-05    .2024E-02
       .7248E-02    .1597E-05    .2224E-02
       .6170E-02    .9847E-06    .2424E-02
       .4689E-02    .4323E-06    .2624E-02

ORUN NUMBER 132
N=.251,K=.142,J=.881,BETA=81
      RADIUS(IN)   VOLUME(IN3)   TIME(SEC)
       .0000E 00    .0000E 00    .1803E-03
```

```
       .9435E-02    .3521E-05    .2000E-04
       .1696E-01    .2048E-04    .2203E-03
       .2009E-01    .3402E-04    .4207E-03
       .2235E-01    .4684E-04    .6210E-03
       .2394E-01    .5755E-04    .8217E-03
       .2518E-01    .6696E-04    .1022E-02
       .2608E-01    .7439E-04    .1222E-02
       .2590E-01    .7287E-04    .1423E-02
       .2554E-01    .6991E-04    .1623E-02
       .2477E-01    .6375E-04    .1823E-02
       .2454E-01    .6195E-04    .2024E-02
       .2388E-01    .5711E-04    .2224E-02
       .2321E-01    .5244E-04    .2424E-02
       .2303E-01    .5124E-04    .2624E-02
     D .2208E-01    .4515E-04    .2825E-02
       .2095E-01    .3855E-04    .3025E-02
       .1991E-01    .3311E-04    .3225E-02
       .1938E-01    .3053E-04    .3426E-02
       .1851E-01    .2661E-04    .3626E-02
       .2138E-01    .4097E-04    .3826E-02
       .1889E-01    .2828E-04    .4027E-02
       .1770E-01    .2325E-04    .4427E-02

ORUN NUMBER 132
                   BETA=74
      RADIUS(IN)   VOLUME(IN3)   TIME(SEC)
       .0000E 00    .0000E 00    .1803E-03
       .1083E-01    .5323E-05    .2000E-04
       .1385E-01    .1114E-04    .2203E-03
       .1565E-01    .1607E-04    .4207E-03
       .1578E-01    .1649E-04    .6210E-03
       .1540E-01    .1531E-04    .8217E-03
       .1493E-01    .1395E-04    .1022E-02
       .1471E-01    .1334E-04    .1222E-02
       .1385E-01    .1115E-04    .1423E-02
      D.1368E-01    .1074E-04    .1623E-02
       .1243E-01    .8059E-05    .1823E-02
       .1184E-01    .6963E-05    .2024E-02
       .1074E-01    .5188E-05    .2224E-02
       .9992E-02    .4183E-05    .2424E-02
       .9339E-02    .3415E-05    .2624E-02
       .8356E-02    .2447E-05    .2825E-02
       .7473E-02    .1750E-05    .3025E-02
       .6329E-02    .1063E-05    .3225E-02

ORUN NUMBER 133
N=.257,K=.151,J=.857,BETA=74
      RADIUS(IN)   VOLUME(IN3)   TIME(SEC)
       .0000E 00    .0000E 00    .1402E-03
       .1244E-01    .8078E-05    .6010E-04
       .1824E-01    .2545E-04    .2604E-03
       .2036E-01    .3538E-04    .4608E-03
       .2334E-01    .5333E-04    .6611E-03
       .2444E-01    .6120E-04    .8618E-03
       .2630E-01    .7632E-04    .1062E-02
       .2716E-01    .8403E-04    .1262E-02
       .2762E-01    .8842E-04    .1463E-02
       .2758E-01    .8797E-04    .1663E-02
       .2762E-01    .8835E-04    .1863E-02
```

TABLE VI (CONT'D)

```
      .2771E-01   .8925E-04   .2064E-02
      .2721E-01   .8446E-04   .2264E-02
      .2636E-01   .7680E-04   .3065E-02
    D .2573E-01   .7149E-04   .3466E-02
      .2471E-01   .6330E-04   .3866E-02
      .2449E-01   .6158E-04   .4267E-02
      .2306E-01   .5142E-04   .4668E-02

ORUN NUMBER 134
N=.511,K=.764,J=.695,BETA=83
     RADIUS(IN)  VOLUME(IN3)  TIME(SEC)
      .0000E 00   .0000E 00   .1803E-03
      .3010E-02   .1143E-06   .2000E-04
      .1091E-01   .5447E-05   .2203E-03
      .1384E-01   .1111E-04   .4207E-03
      .1592E-01   .1693E-04   .6210E-03
      .1620E-01   .1783E-04   .8217E-03
      .1669E-01   .1949E-04   .1022E-02
      .1604E-01   .1730E-04   .1222E-02
      .1570E-01   .1624E-04   .1423E-02
      .1458E-01   .1300E-04   .1623E-02
      .1445E-01   .1265E-04   .1823E-02
    D .1405E-01   .1162E-04   .2024E-02
      .1292E-01   .9037E-05   .2224E-02
      .1296E-01   .9137E-05   .2424E-02
      .1182E-01   .6931E-05   .2624E-02
      .1132E-01   .6086E-05   .2825E-02
      .1033E-01   .4621E-05   .3225E-02
      .8328E-02   .2422E-05   .3626E-02
      .7276E-02   .1615E-05   .4027E-02

ORUN NUMBER 134
N=.387,K=.390,J=.889,BETA=85
     RADIUS(IN)  VOLUME(IN3)  TIME(SEC)
      .0000E 00   .0000E 00   .1603E-03
      .7726E-02   .1934E-05   .4000E-04
      .1550E-01   .1563E-04   .2403E-03
      .1993E-01   .3319E-04   .4407E-03
      .2309E-01   .5165E-04   .6410E-03
      .2487E-01   .6451E-04   .8417E-03
      .2703E-01   .8284E-04   .1042E-02
      .2814E-01   .9350E-04   .1242E-02
      .2894E-01   .1016E-03   .1443E-02
      .2982E-01   .1112E-03   .1643E-02
      .2974E-01   .1104E-03   .1843E-02
      .2941E-01   .1067E-03   .2044E-02
      .2939E-01   .1065E-03   .2244E-02
      .2928E-01   .1053E-03   .2444E-02
      .2868E-01   .9894E-04   .2644E-02
      .2794E-01   .9149E-04   .2845E-02
      .2766E-01   .8879E-04   .3045E-02
      .2711E-01   .8357E-04   .3245E-02
    D .2654E-01   .7839E-04   .3446E-02
      .2619E-01   .7536E-04   .3646E-02
      .2573E-01   .7142E-04   .3846E-02
      .2522E-01   .6730E-04   .4047E-02
      .2474E-01   .6348E-04   .4247E-02
      .2417E-01   .5924E-04   .4447E-02
      .2396E-01   .5766E-04   .4648E-02
```

```
      .2374E-01   .5614E-04   .5048E-02
      .2301E-01   .5112E-04   .5449E-02
      .2037E-01   .3546E-04   .5850E-02

ORUN NUMBER135
N=.436,K=.733,J=1.11,BETA=74
     RADIUS(IN)  VOLUME(IN3)  TIME(SEC)
      .0000E 00   .0000E 00   .8013E-04
      .1329E-01   .9848E-05   .1202E-03
      .2127E-01   .4036E-04   .3205E-03
      .2723E-01   .8472E-04   .5209E-03
      .3235E-01   .1420E-03   .7212E-03
      .3533E-01   .1850E-03   .9219E-03
      .3855E-01   .2404E-03   .1122E-02
      .4152E-01   .3002E-03   .1322E-02
      .4351E-01   .3455E-03   .1523E-02
      .4557E-01   .3970E-03   .1723E-02
      .4778E-01   .4576E-03   .1923E-02
      .4945E-01   .5072E-03   .2124E-02
      .5116E-01   .5617E-03   .2324E-02
      .5184E-01   .5843E-03   .2524E-02
      .5400E-01   .6605E-03   .2724E-02
      .5600E-01   .7367E-03   .3125E-02
      .5794E-01   .8161E-03   .3526E-02
      .5905E-01   .8637E-03   .3926E-02
      .5903E-01   .8631E-03   .4327E-02
      .5877E-01   .8516E-03   .4728E-02
      .5820E-01   .8270E-03   .5529E-02
      .5718E-01   .7843E-03   .6330E-02
      .5597E-01   .7354E-03   .7132E-02
      .5535E-01   .7112E-03   .7933E-02
      .5459E-01   .6826E-03   .8734E-02
      .5424E-01   .6695E-03   .9535E-02
      .5206E-01   .5919E-03   .1034E-01
      .5050E-01   .5403E-03   .1114E-01
    D .4898E-01   .4930E-03   .1194E-01
      .4940E-01   .5056E-03   .1274E-01
      .4914E-01   .4979E-03   .1354E-01
      .4824E-01   .4710E-03   .1434E-01

ORUN NUMBER 136
N=.330,K=.297,J=.917
     RADIUS(IN)  VOLUME(IN3)  TIME(SEC)
      .0000E 00   .0000E 00   .1002E-03
      .1437E-01   .1245E-04   .1001E-03
      .2018E-01   .3448E-04   .3004E-03
      .2380E-01   .5654E-04   .5008E-03
      .2718E-01   .8426E-04   .7011E-03
      .2820E-01   .9408E-04   .9018E-03
      .3159E-01   .1323E-03   .1102E-02
      .3287E-01   .1490E-03   .1302E-02
      .3549E-01   .1875E-03   .1503E-02
      .3561E-01   .1894E-03   .1703E-02
      .3868E-01   .2428E-03   .1903E-02
      .3821E-01   .2341E-03   .2104E-02
      .4095E-01   .2880E-03   .2304E-02
      .4171E-01   .3044E-03   .2905E-02
      .4143E-01   .2982E-03   .3706E-02
      .4098E-01   .2886E-03   .4507E-02
```

```
      .4057E-01   .2801E-03   .4908E-02
      .4049E-01   .2785E-03   .5309E-02
      .3970E-01   .2624E-03   .6110E-02

ORUN NUMBER 138
N=.300,K=.228,J=.805,BETA=56
     RADIUS(IN)  VOLUME(IN3)  TIME(SEC)
      .0000E 00   .0000E 00   .2992E-03
      .1029E-01   .4573E-05   .3320E-04
      .2089E-01   .3823E-04   .3657E-03
      .2935E-01   .1060E-03   .1031E-02
      .3171E-01   .1338E-03   .1363E-02
      .3427E-01   .1689E-03   .1696E-02
      .3587E-01   .1937E-03   .2028E-02
      .3697E-01   .2119E-03   .2361E-02
      .3695E-01   .2116E-03   .2693E-02
      .3772E-01   .2251E-03   .3025E-02
      .3745E-01   .2203E-03   .3358E-02
      .3648E-01   .2037E-03   .4023E-02
      .3606E-01   .1967E-03   .4688E-02
      .3562E-01   .1896E-03   .5353E-02
      .3480E-01   .1768E-03   .6017E-02
      .3404E-01   .1654E-03   .6682E-02
    D .3353E-01   .1581E-03   .7347E-02
      .3324E-01   .1540E-03   .8012E-02
      .3207E-01   .1383E-03   .9342E-02
      .3023E-01   .1158E-03   .1067E-01
      .2665E-01   .7935E-04   .1200E-01
      .2522E-01   .6729E-04   .1333E-01
      .2479E-01   .6391E-04   .1466E-01
      .2041E-01   .3567E-04   .1599E-01

ORUN NUMBER 138
N=.367,K=.383,J=.906,BETA=60
     RADIUS(IN)  VOLUME(IN3)  TIME(SEC)
      .0000E 00   .0000E 00   .2992E-03
      .8753E-02   .2811E-05   .3320E-04
      .2068E-01   .3710E-04   .3657E-03
      .2656E-01   .7862E-04   .6981E-03
      .3070E-01   .1214E-03   .1031E-02
      .3393E-01   .1639E-03   .1363E-02
      .3714E-01   .2148E-03   .1696E-02
      .3934E-01   .2555E-03   .2028E-02
      .4161E-01   .3023E-03   .2361E-02
      .4169E-01   .3039E-03   .2693E-02
      .4239E-01   .3196E-03   .3025E-02
      .4267E-01   .3258E-03   .3358E-02
      .4249E-01   .3217E-03   .4023E-02
      .4207E-01   .3123E-03   .4688E-02
      .4198E-01   .3104E-03   .5353E-02
      .4186E-01   .3078E-03   .6017E-02
      .4174E-01   .3050E-03   .6682E-02
      .4085E-01   .2859E-03   .7347E-02
      .3919E-01   .2524E-03   .8012E-02
      .3817E-01   .2334E-03   .8677E-02
    D .3708E-01   .2138E-03   .9342E-02
      .3511E-01   .1815E-03   .1067E-01
      .3227E-01   .1410E-03   .1200E-01
      .3286E-01   .1488E-03   .1333E-01
```

TABLE VI (CONT'D)

```
      .3154E-01    .1317E-03    .1466E-01
      .2704E-01    .8290E-04    .1599E-01
      .2741E-01    .8634E-04    .1732E-01

ORUN NUMBER 139
N=.410,K=.541,J=948
     RADIUS(IN)  VOLUME(IN3)  TIME(SEC)
      .0000E 00    .0000E 00    .1330E-03
      .1643E-01    .1862E-04    .1994E-03
      .2444E-01    .6125E-04    .5319E-03
      .3071E-01    .1215E-03    .8643E-03
      .3457E-01    .1733E-03    .1197E-02
      .3852E-01    .2398E-03    .1529E-02
      .4077E-01    .2844E-03    .1862E-02
      .4386E-01    .3540E-03    .2194E-02
      .4578E-01    .4025E-03    .2527E-02
      .4806E-01    .4656E-03    .2859E-02
      .5296E-01    .6231E-03    .3191E-02
      .4997E-01    .5234E-03    .3524E-02
      .5417E-01    .6667E-03    .3856E-02

ORUN NUMBER 139
N=.332,K=.288,J=.876,BETA=80
     RADIUS(IN)  VOLUME(IN3)  TIME(SEC)
      .0000E 00    .0000E 00    .1995E-03
      .1492E-01    .1394E-04    .1329E-03
      .2281E-01    .4976E-04    .4654E-03
      .2656E-01    .7856E-04    .7978E-03
      .3038E-01    .1177E-03    .1130E-02
      .3350E-01    .1576E-03    .1462E-02
      .3529E-01    .1843E-03    .1795E-02
      .3734E-01    .2184E-03    .2127E-02
      .3740E-01    .2194E-03    .2460E-02
      .3801E-01    .2304E-03    .2792E-02
      .3742E-01    .2198E-03    .3124E-02
      .3767E-01    .2243E-03    .3457E-02
      .3651E-01    .2041E-03    .4122E-02
      .3544E-01    .1867E-03    .4787E-02
      .3529E-01    .1843E-03    .5452E-02
      .3441E-01    .1709E-03    .6116E-02
      .3384E-01    .1626E-03    .6781E-02
    D .3315E-01    .1528E-03    .7446E-02
      .3212E-01    .1390E-03    .8111E-02
      .3137E-01    .1294E-03    .8776E-02
      .3079E-01    .1224E-03    .9441E-02
ORUN NUMBER 139
N=.335,K=.296,J=.915,BETA=78
     RADIUS(IN)  VOLUME(IN3)  TIME(SEC)
      .0000E 00    .0000E 00    .1662E-03
      .1611E-01    .1753E-04    .1662E-03
      .2310E-01    .5168E-04    .4987E-03
      .2745E-01    .8675E-04    .8311E-03
      .3121E-01    .1275E-03    .1164E-02
      .3573E-01    .1914E-03    .1829E-02
      .3798E-01    .2298E-03    .2494E-02
      .3868E-01    .2428E-03    .3158E-02
      .3865E-01    .2422E-03    .3491E-02
      .3812E-01    .2324E-03    .3823E-02
      .3775E-01    .2257E-03    .4156E-02
```

```
      .3727E-01    .2171E-03    .4488E-02
      .3599E-01    .1955E-03    .5153E-02
      .3648E-01    .2036E-03    .5818E-02
      .3624E-01    .1996E-03    .6483E-02
      .3802E-01    .2305E-03    .7148E-02
      .3748E-01    .2208E-03    .7813E-02
      .3588E-01    .1938E-03    .8478E-02
      .3433E-01    .1697E-03    .9143E-02
      .3318E-01    .1532E-03    .9807E-02
    D .3238E-01    .1425E-03    .1047E-01
      .3115E-01    .1268E-03    .1313E-01
      .2935E-01    .1060E-03    .1446E-01
      .2621E-01    .7556E-04    .1579E-01
      .2481E-01    .6408E-04    .1712E-01

ORUN NUMBER 140
N=.584,K=.914,J=.474,BETA=48
     RADIUS(IN)  VOLUME(IN3)  TIME(SEC)
      .0000E 00    .0000E 00    .8581E-04
      .3023E-02    .1157E-06    .5719E-04
      .6297E-02    .1047E-05    .2002E-03
      .8898E-02    .2954E-05    .3433E-03
      .1044E-01    .4772E-05    .4863E-03
      .1224E-01    .7695E-05    .6293E-03
      .1310E-01    .9437E-05    .7723E-03
      .1380E-01    .1101E-04    .9152E-03
      .1334E-01    .9950E-05    .1058E-02
      .1304E-01    .9307E-05    .1201E-02
      .1277E-01    .8734E-05    .1344E-02
    D .1231E-01    .7817E-05    .1487E-02
      .1158E-01    .6509E-05    .1773E-02
      .1059E-01    .4973E-05    .2059E-02
      .9013E-02    .3069E-05    .2345E-02
      .7158E-02    .1538E-05    .2631E-02

ORUN NUMBER 141
N=.300,K=.163,J=.751,BETA=42
     RADIUS(IN)  VOLUME(IN3)  TIME(SEC)
      .0000E 00    .0000E 00    .1142E-03
      .6990E-02    .1432E-05    .2850E-04
      .1208E-01    .7394E-05    .1712E-03
      .1503E-01    .1422E-04    .3139E-03
      .1631E-01    .1819E-04    .4566E-03
      .1773E-01    .2339E-04    .5993E-03
      .1805E-01    .2466E-04    .7420E-03
      .1839E-01    .2609E-04    .8847E-03
      .1856E-01    .2680E-04    .1028E-02
      .1836E-01    .2594E-04    .1170E-02
      .1843E-01    .2626E-04    .1313E-02
    D .1804E-01    .2463E-04    .1456E-02
      .1756E-01    .2271E-04    .1598E-02
      .1672E-01    .1960E-04    .1884E-02
      .1584E-01    .1666E-04    .2169E-02
      .1464E-01    .1315E-04    .2454E-02
      .1270E-01    .8588E-05    .2740E-02
      .9922E-02    .4095E-05    .3025E-02
      .6167E-02    .9831E-06    .3311E-02

ORUN NUMBER 141
```

```
N=.397,K=.407,J=.896,BETA=36
     RADIUS(IN)  VOLUME(IN3)  TIME(SEC)
      .0000E 00    .0000E 00    .9989E-04
      .7521E-02    .1784E-05    .4281E-04
      .1355E-01    .1043E-04    .1855E-03
      .1704E-01    .2075E-04    .3282E-03
      .1955E-01    .3132E-04    .4709E-03
      .2177E-01    .4329E-04    .6136E-03
      .2336E-01    .5345E-04    .7563E-03
      .2448E-01    .6152E-04    .8990E-03
      .2536E-01    .6841E-04    .1042E-02
      .2616E-01    .7509E-04    .1184E-02
      .2663E-01    .7922E-04    .1327E-02
      .2628E-01    .7616E-04    .1470E-02
      .2560E-01    .7036E-04    .1612E-02
      .2563E-01    .7064E-04    .1755E-02
      .2481E-01    .6402E-04    .1898E-02
    D .2407E-01    .5850E-04    .2040E-02
      .2381E-01    .5661E-04    .2183E-02
      .2238E-01    .4703E-04    .2468E-02
      .2171E-01    .4289E-04    .2754E-02
      .1961E-01    .3162E-04    .3039E-02
      .1752E-01    .2257E-04    .3325E-02
      .1240E-01    .7996E-05    .3610E-02
      .9450E-02    .3539E-05    .3895E-02

ORUN NUMBER 142
N=.439,K=.642,J=1.01,BETA=75
     RADIUS(IN)  VOLUME(IN3)  TIME(SEC)
      .0000E 00    .0000E 00    .1001E-03
      .7657E-02    .1882E-05    .4290E-04
      .1497E-01    .1406E-04    .1859E-03
      .1887E-01    .2819E-04    .3290E-03
      .2225E-01    .4617E-04    .4720E-03
      .2539E-01    .6866E-04    .6150E-03
      .2727E-01    .8502E-04    .7580E-03
      .2878E-01    .9994E-04    .9009E-03
      .3024E-01    .1160E-03    .1044E-02
      .3125E-01    .1280E-03    .1187E-02
      .3234E-01    .1419E-03    .1330E-02
      .3252E-01    .1442E-03    .1473E-02
      .3275E-01    .1473E-03    .1616E-02
      .3258E-01    .1450E-03    .1759E-02
      .3229E-01    .1413E-03    .1902E-02
      .3194E-01    .1367E-03    .2045E-02
    D .3087E-01    .1234E-03    .2331E-02
      .2919E-01    .1043E-03    .2617E-02

ORUN NUMBER 142
                   BETA=64
     RADIUS(IN)  VOLUME(IN3)  TIME(SEC)
      .0000E 00    .0000E 00    .1001E-03
      .4674E-02    .4281E-06    .4290E-04
      .6189E-02    .9937E-06    .1859E-03
      .7068E-02    .1480E-05    .3290E-03
      .7876E-02    .2048E-05    .4720E-03
      .7672E-02    .1893E-05    .6150E-03
      .7561E-02    .1813E-05    .7580E-03
      .7821E-02    .2006E-05    .9009E-03
```

TABLE VI (CONT'D)

```
          .7194E-02    .1561E-05    .1044E-02
        D .6476E-02    .1139E-05    .1187E-02
          .5555E-02    .7185E-06    .1330E-02
          .5115E-02    .5609E-06    .1473E-02
          .4312E-02    .3361E-06    .1759E-02

ORUN NUMBER 142
N=.268,K=.113,J=.670,BETA=44
        RADIUS(IN)  VOLUME(IN3)   TIME(SEC)
          .0000E 00    .0000E 00    .1287E-03
          .5706E-02    .7787E-06    .1430E-04
          .1070E-01    .5141E-05    .1573E-03
          .1318E-01    .9598E-05    .3004E-03
          .1388E-01    .1123E-04    .4434E-03
          .1558E-01    .1585E-04    .5864E-03
          .1637E-01    .1839E-04    .7294E-03
          .1640E-01    .1848E-04    .8723E-03
          .1604E-01    .1729E-04    .1015E-02
          .1574E-01    .1634E-04    .1158E-02
        D .1499E-01    .1413E-04    .1301E-02
          .1441E-01    .1254E-04    .1444E-02
          .1280E-01    .8790E-05    .1730E-02
          .1083E-01    .5323E-05    .2016E-02
          .9722E-02    .3853E-05    .2302E-02
          .6942E-02    .1403E-05    .2588E-02
          .4693E-02    .4332E-06    .2874E-02

ORUN NUMBER 143
N=.440,K=.471,J=.736,BETA=45
        RADIUS(IN)  VOLUME(IN3)   TIME(SEC)
          .0000E 00    .0000E 00    .1139E-03
          .4746E-02    .4482E-06    .2850E-04
          .1028E-01    .4551E-05    .1708E-03
          .1573E-01    .1633E-04    .4556E-03
          .1850E-01    .2653E-04    .5979E-03
          .1984E-01    .3273E-04    .7403E-03
          .2119E-01    .3992E-04    .8827E-03
          .2199E-01    .4462E-04    .1025E-02
          .2319E-01    .5233E-04    .1310E-02
          .2279E-01    .4964E-04    .1452E-02
        D .2284E-01    .4998E-04    .1594E-02
          .2264E-01    .4868E-04    .1879E-02
          .2198E-01    .4456E-04    .2164E-02
          .2173E-01    .4305E-04    .2449E-02
          .2137E-01    .4094E-04    .2733E-02
          .2092E-01    .3840E-04    .3018E-02
          .1923E-01    .2982E-04    .3303E-02
          .1756E-01    .2272E-04    .3588E-02
          .1735E-01    .2189E-04    .3872E-02
          .1480E-01    .1361E-04    .4157E-02
          .1436E-01    .1242E-04    .4442E-02

ORUN NUMBER 143
N=.378,K=.323,J=.817,BETA=31
        RADIUS(IN)  VOLUME(IN3)   TIME(SEC)
          .0000E 00    .0000E 00    .5695E-04
          .6903E-02    .1379E-05    .8545E-04
          .1378E-01    .1098E-04    .3701E-03
          .1866E-01    .2723E-04    .6548E-03
```

```
          .1978E-01    .3247E-04    .7972E-03
          .2193E-01    .4420E-04    .9396E-03
          .2323E-01    .5254E-04    .1224E-02
          .2384E-01    .5683E-04    .1367E-02
          .2309E-01    .5162E-04    .1509E-02
        D .2356E-01    .5487E-04    .1794E-02
          .2283E-01    .4994E-04    .2079E-02
          .2190E-01    .4404E-04    .2363E-02
          .2136E-01    .4086E-04    .2648E-02
          .2104E-01    .3907E-04    .2933E-02
          .2061E-01    .3671E-04    .3217E-02
          .1891E-01    .2836E-04    .3502E-02
          .1679E-01    .1983E-04    .3787E-02
          .1621E-01    .1786E-04    .4072E-02
          .1459E-01    .1303E-04    .4356E-02
          .1430E-01    .1227E-04    .4641E-02

ORUN NUMBER 143
N=.550,K=1.02,J=.685,BETA=37
        RADIUS(IN)  VOLUME(IN3)   TIME(SEC)
          .0000E 00    .0000E 00    .6821E-12
          .7696E-02    .1911E-05    .1424E-03
          .1115E-01    .5816E-05    .2847E-03
          .1406E-01    .1166E-04    .4271E-03
          .1694E-01    .2040E-04    .5695E-03
          .1832E-01    .2579E-04    .7118E-03
          .2112E-01    .3953E-04    .9966E-03
          .2213E-01    .4546E-04    .1139E-02
          .2243E-01    .4730E-04    .1281E-02
          .2300E-01    .5105E-04    .1566E-02
          .2281E-01    .4976E-04    .1708E-02
          .2273E-01    .4926E-04    .1851E-02
        D .2232E-01    .4666E-04    .1993E-02
          .2218E-01    .4576E-04    .2136E-02
          .2152E-01    .4181E-04    .2420E-02
          .2133E-01    .4072E-04    .2705E-02
          .2047E-01    .3598E-04    .2990E-02
          .1918E-01    .2958E-04    .3274E-02
          .1784E-01    .2381E-04    .3559E-02
          .1667E-01    .1944E-04    .3844E-02
          .1610E-01    .1749E-04    .4129E-02
          .1398E-01    .1147E-04    .4413E-02
          .1319E-01    .9618E-05    .4698E-02

ORUN NUMBER 143
N=.480,K=.620,J=.715
        RADIUS(IN)  VOLUME(IN3)   TIME(SEC)
          .0000E 00    .0000E 00    .8542E-04
          .8042E-02    .2181E-05    .5698E-04
          .1287E-01    .8930E-05    .1993E-03
          .1603E-01    .1727E-04    .3417E-03
          .1753E-01    .2258E-04    .4841E-03
          .1999E-01    .3351E-04    .6264E-03
          .2166E-01    .4261E-04    .7688E-03
          .2140E-01    .4109E-04    .9112E-03
          .2166E-01    .4259E-04    .1054E-02
          .2101E-01    .3891E-04    .1196E-02
          .1974E-01    .3227E-04    .1339E-02
          .1870E-01    .2742E-04    .1481E-02
```

```
        D .1698E-01    .2054E-04    .1766E-02
          .1519E-01    .1471E-04    .2051E-02
          .1395E-01    .1139E-04    .2335E-02
          .1203E-01    .7305E-05    .2620E-02
          .8498E-02    .2573E-05    .2905E-02
          .7058E-02    .1474E-05    .3189E-02

ORUN NUMBER 143
N=.559,K=.994,J=.642,BETA=39
        RADIUS(IN)  VOLUME(IN3)   TIME(SEC)
          .0000E 00    .0000E 00    .6821E-12
          .7044E-02    .1465E-05    .1424E-03
          .1030E-01    .4583E-05    .2847E-03
          .1276E-01    .8705E-05    .4271E-03
          .1801E-01    .2449E-04    .7118E-03
          .2034E-01    .3528E-04    .9966E-03
          .2095E-01    .3857E-04    .1139E-02
          .2159E-01    .4222E-04    .1281E-02
          .2259E-01    .4838E-04    .1566E-02
          .2259E-01    .4835E-04    .1708E-02
        D .2226E-01    .4625E-04    .1851E-02
          .2131E-01    .4058E-04    .2136E-02
          .2111E-01    .3945E-04    .2420E-02
          .2067E-01    .3702E-04    .2705E-02
          .2010E-01    .3403E-04    .2990E-02
          .1857E-01    .2684E-04    .3274E-02
          .1717E-01    .2123E-04    .3559E-02
          .1664E-01    .1932E-04    .3844E-02
          .1454E-01    .1288E-04    .4129E-02

ORUN NUMBER 143
N=.473,K=.676,J=.829
        RADIUS(IN)  VOLUME(IN3)   TIME(SEC)
          .0000E 00    .0000E 00    .1139E-03
          .4768E-02    .4543E-06    .2850E-04
          .1121E-01    .5909E-05    .1708E-03
          .1501E-01    .1417E-04    .3132E-03
          .1951E-01    .3114E-04    .5979E-03
          .2279E-01    .4967E-04    .7403E-03
          .2229E-01    .4647E-04    .8827E-03
          .2349E-01    .5438E-04    .1025E-02
          .2398E-01    .5787E-04    .1167E-02
          .2435E-01    .6059E-04    .1452E-02
          .2402E-01    .5814E-04    .1594E-02

ORUN NUMBER 143
N=.384,K=.336,J=.808,BETA=46
        RADIUS(IN)  VOLUME(IN3)   TIME(SEC)
          .0000E 00    .0000E 00    .1281E-03
          .4633E-02    .4169E-06    .1430E-04
          .1131E-01    .6060E-05    .1566E-03
          .1797E-01    .2432E-04    .4414E-03
          .1889E-01    .2826E-04    .5837E-03
          .2075E-01    .3749E-04    .7261E-03
          .2231E-01    .4655E-04    .1011E-02
          .2327E-01    .5286E-04    .1153E-02
          .2341E-01    .5384E-04    .1296E-02
          .2347E-01    .5422E-04    .1438E-02
          .2365E-01    .5546E-04    .1580E-02
```

TABLE VI (CONT'D)

```
D .2294E-01   .5066E-04   .1865E-02
  .2217E-01   .4570E-04   .2150E-02
  .2137E-01   .4093E-04   .2435E-02
  .2102E-01   .3897E-04   .2719E-02
  .2068E-01   .3710E-04   .3004E-02
  .1881E-01   .2792E-04   .3289E-02
  .1785E-01   .2383E-04   .3574E-02
  .1571E-01   .1625E-04   .3858E-02

ORUN NUMBER 143
N=.376,K=.307,J=.759,BETA=39
    RADIUS(IN)  VOLUME(IN3)  TIME(SEC)
     .0000E 00   .0000E 00   .8542E-04
     .7679E-02   .1899E-05   .5698E-04
     .1248E-01   .8151E-05   .1993E-03
     .1534E-01   .1513E-04   .3417E-03
     .1741E-01   .2213E-04   .4841E-03
     .1920E-01   .2966E-04   .6264E-03
     .2174E-01   .4309E-04   .9112E-03
     .2311E-01   .5176E-04   .1054E-02
     .2352E-01   .5456E-04   .1196E-02
     .2356E-01   .5485E-04   .1481E-02
     .2369E-01   .5577E-04   .1623E-02
    D.2329E-01   .5300E-04   .1766E-02
     .2293E-01   .5058E-04   .2051E-02
     .2190E-01   .4406E-04   .2335E-02
     .2187E-01   .4387E-04   .2620E-02
     .2120E-01   .3999E-04   .2905E-02
     .2012E-01   .3415E-04   .3189E-02
     .1822E-01   .2539E-04   .3474E-02
     .1650E-01   .1884E-04   .3759E-02
     .1497E-01   .1408E-04   .4044E-02
     .1537E-01   .1523E-04   .4328E-02

ORUN NUMBER 144
N=.536,K=.530,J=.403,BETA=69
    RADIUS(IN)  VOLUME(IN3)  TIME(SEC)
     .0000E 00   .0000E 00  -.1430E-04
     .4860E-02   .4811E-06   .1573E-03
     .6841E-02   .1342E-05   .3003E-03
     .8446E-02   .2526E-05   .4434E-03
     .9876E-02   .4039E-05   .5864E-03
     .1101E-01   .5601E-05   .7294E-03
     .1148E-01   .6337E-05   .8724E-03
     .1210E-01   .7423E-05   .1015E-02
     .1189E-01   .7040E-05   .1158E-02
     .1206E-01   .7359E-05   .1301E-02
     .1208E-01   .7389E-05   .1444E-02
     .1090E-01   .5430E-05   .1587E-02
   D .9523E-02   .3621E-05   .1730E-02
     .8973E-02   .3030E-05   .1873E-02
     .7718E-02   .1928E-05   .2159E-02
     .6850E-02   .1348E-05   .2445E-02
     .6017E-02   .9131E-06   .2731E-02

ORUN NUMBER 145
                   BETA=47
    RADIUS(IN)  VOLUME(IN3)  TIME(SEC)
     .0000E 00   .0000E 00   .1281E-03
```

```
     .5832E-02   .8317E-06   .1430E-04
     .7557E-02   .1809E-05   .1566E-03
     .8254E-02   .2358E-05   .2990E-03
     .8484E-02   .2560E-05   .4414E-03
     .8407E-02   .2491E-05   .5837E-03
     .8677E-02   .2739E-05   .7261E-03
     .8541E-02   .2613E-05   .8685E-03
     .8233E-02   .2340E-05   .1011E-02
   D .8007E-02   .2152E-05   .1153E-02
     .7590E-02   .1833E-05   .1296E-02
     .7496E-02   .1766E-05   .1438E-02
     .7379E-02   .1684E-05   .1580E-02
     .6050E-02   .9282E-06   .1865E-02

ORUN NUMBER 145
                   BETA=51
    RADIUS(IN)  VOLUME(IN3)  TIME(SEC)
     .0000E 00   .0000E 00   .5695E-04
     .7761E-02   .1960E-05   .8545E-04
     .9561E-02   .3665E-05   .2277E-03
     .1112E-01   .5770E-05   .3701E-03
     .1177E-01   .6840E-05   .5125E-03
     .1231E-01   .7827E-05   .6548E-03
     .1205E-01   .7346E-05   .7972E-03
     .1178E-01   .6855E-05   .9396E-03
     .1154E-01   .6441E-05   .1082E-02
     .1110E-01   .5732E-05   .1224E-02
     .1043E-01   .4757E-05   .1367E-02
     .9811E-02   .3960E-05   .1509E-02
     .9086E-02   .3145E-05   .1794E-02
     .7196E-02   .1563E-05   .2079E-02
     .4941E-02   .5056E-06   .2363E-02

ORUN NUMBER 149
N=.377,K=.392,J=.997,BETA=76
    RADIUS(IN)  VOLUME(IN3)  TIME(SEC)
     .0000E 00   .0000E 00   .4006E-04
     .1466E-01   .1320E-04   .1602E-03
     .1950E-01   .3108E-04   .3605E-03
     .2344E-01   .5400E-04   .5609E-03
     .2631E-01   .7639E-04   .7612E-03
     .2792E-01   .9132E-04   .9619E-03
     .2912E-01   .1035E-03   .1162E-02
     .3088E-01   .1235E-03   .1362E-02
     .3126E-01   .1281E-03   .1563E-02
     .3182E-01   .1351E-03   .1763E-02
     .3156E-01   .1319E-03   .1963E-02
     .3176E-01   .1343E-03   .2164E-02
     .3117E-01   .1271E-03   .2364E-02
     .3105E-01   .1255E-03   .2564E-02
     .3077E-01   .1221E-03   .2764E-02
   D .3046E-01   .1185E-03   .2965E-02
     .3035E-01   .1172E-03   .3165E-02

ORUN NUMBER 149
N=.477,K=.563,J=.824,BETA=84
    RADIUS(IN)  VOLUME(IN3)  TIME(SEC)
     .0000E 00   .0000E 00  -.4006E-04
     .1356E-01   .1046E-04   .2404E-03
```

```
     .1764E-01   .2303E-04   .4407E-03
     .2121E-01   .4000E-04   .6411E-03
     .2348E-01   .5432E-04   .8414E-03
     .2618E-01   .7530E-04   .1042E-02
     .2769E-01   .8908E-04   .1242E-02
     .2924E-01   .1049E-03   .1442E-02
     .3017E-01   .1152E-03   .1643E-02
     .3056E-01   .1197E-03   .1843E-02
     .3111E-01   .1263E-03   .2043E-02
     .3127E-01   .1283E-03   .2244E-02
     .3143E-01   .1302E-03   .2444E-02
     .3160E-01   .1323E-03   .2644E-02
     .3163E-01   .1327E-03   .2844E-02
     .3125E-01   .1280E-03   .3045E-02
   D .3119E-01   .1273E-03   .3245E-02
     .3064E-01   .1206E-03   .3646E-02
     .3159E-01   .1322E-03   .4046E-02
     .3227E-01   .1410E-03   .4447E-02
     .3275E-01   .1474E-03   .4848E-02
     .3335E-01   .1556E-03   .5248E-02
ORUN NUMBER 149
N=.389,K=.408,J=.906,BETA=80
    RADIUS(IN)  VOLUME(IN3)  TIME(SEC)
     .0000E 00   .0000E 00   .1803E-03
     .6156E-02   .9780E-06   .2000E-04
     .1497E-01   .1407E-04   .2203E-03
     .2007E-01   .3392E-04   .4207E-03
     .2336E-01   .5345E-04   .6210E-03
     .2592E-01   .7302E-04   .8217E-03
     .2779E-01   .8998E-04   .1022E-02
     .3043E-01   .1182E-03   .1222E-02
     .3170E-01   .1336E-03   .1423E-02
     .3335E-01   .1555E-03   .1623E-02
     .3457E-01   .1733E-03   .1823E-02
     .3575E-01   .1917E-03   .2024E-02
     .3643E-01   .2029E-03   .2224E-02
     .3679E-01   .2089E-03   .2424E-02
     .3689E-01   .2107E-03   .2624E-02
     .3748E-01   .2209E-03   .2825E-02
     .3725E-01   .2169E-03   .3025E-02
     .3770E-01   .2248E-03   .3225E-02
     .3742E-01   .2197E-03   .3426E-02
     .3761E-01   .2232E-03   .3626E-02
    D.3753E-01   .2217E-03   .3826E-02
     .3714E-01   .2149E-03   .4227E-02
     .3674E-01   .2079E-03   .4628E-02
     .3682E-01   .2094E-03   .5028E-02
     .3619E-01   .1989E-03   .5429E-02
     .3536E-01   .1854E-03   .5830E-02
     .3540E-01   .1861E-03   .6230E-02

ORUN NUMBER 150
N=.379,K=.388,J=.926,BETA=85
    RADIUS(IN)  VOLUME(IN3)  TIME(SEC)
     .0000E 00   .0000E 00   .6010E-04
     .1333E-01   .9933E-05   .1402E-03
     .1899E-01   .2874E-04   .3405E-03
     .2212E-01   .4539E-04   .5409E-03
     .2566E-01   .7084E-04   .7412E-03
```

TABLE VI (CONT'D)

```
          .2800E-01    .9209E-04    .9419E-03
          .2907E-01    .1030E-03    .1142E-02
          .3091E-01    .1239E-03    .1342E-02
          .3173E-01    .1340E-03    .1543E-02
          .3253E-01    .1443E-03    .1743E-02
          .3303E-01    .1512E-03    .1943E-02
          .3339E-01    .1562E-03    .2144E-02
          .3395E-01    .1641E-03    .2344E-02
          .3406E-01    .1658E-03    .2544E-02
          .3406E-01    .1657E-03    .2744E-02
          .3413E-01    .1667E-03    .2945E-02
        D .3437E-01    .1704E-03    .3145E-02

ORUN NUMBER 150
N=.406,K=.422,J=.834,BETA=78
       RADIUS(IN)  VOLUME(IN3)  TIME(SEC)
          .0000E 00    .0000E 00    .1803E-03
          .5177E-02    .5816E-06    .2000E-04
          .1381E-01    .1104E-04    .2203E-03
          .1813E-01    .2500E-04    .4207E-03
          .2101E-01    .3891E-04    .6210E-03
          .2338E-01    .5357E-04    .8217E-03
          .2549E-01    .6949E-04    .1022E-02
          .2696E-01    .8216E-04    .1222E-02
          .2806E-01    .9269E-04    .1423E-02
          .2894E-01    .1017E-03    .1623E-02
          .2983E-01    .1113E-03    .1823E-02
          .3022E-01    .1158E-03    .2024E-02
          .3092E-01    .1240E-03    .2224E-02
          .3128E-01    .1284E-03    .2424E-02
          .3176E-01    .1344E-03    .2624E-02
          .3106E-01    .1257E-03    .2825E-02
        D .2746E-01    .8684E-04    .3025E-02

ORUN NUMBER 150
N=.323,K=.233,J=.841,BETA=74
       RADIUS(IN)  VOLUME(IN3)  TIME(SEC)
          .0000E 00    .0000E 00    .1002E-03
          .1188E-01    .7028E-05    .1001E-03
          .1712E-01    .2105E-04    .3004E-03
          .1976E-01    .3238E-04    .5008E-03
          .2252E-01    .4791E-04    .7011E-03
          .2427E-01    .5995E-04    .9018E-03
          .2564E-01    .7073E-04    .1102E-02
          .2697E-01    .8224E-04    .1302E-02
          .2781E-01    .9022E-04    .1503E-02
          .2874E-01    .9953E-04    .1703E-02
          .2912E-01    .1035E-03    .1903E-02
          .2954E-01    .1081E-03    .2104E-02
          .2988E-01    .1119E-03    .2304E-02
          .2990E-01    .1122E-03    .2504E-02
          .2957E-01    .1084E-03    .2704E-02
          .2984E-01    .1114E-03    .2905E-02
        D .2945E-01    .1071E-03    .3105E-02
          .2900E-01    .1023E-03    .3506E-02
          .2867E-01    .9886E-04    .3906E-02
          .2841E-01    .9617E-04    .4307E-02
          .2829E-01    .9495E-04    .4708E-02
          .2854E-01    .9749E-04    .5108E-02
```

```
          .2760E-01    .8821E-04    .5509E-02
          .2616E-01    .7509E-04    .5910E-02
          .2653E-01    .7830E-04    .6310E-02
          .2541E-01    .6885E-04    .6711E-02
          .2366E-01    .5554E-04    .7112E-02

ORUN NUMBER 151
N=.456,K=.639,J=.869,BETA=73
       RADIUS(IN)  VOLUME(IN3)  TIME(SEC)
          .0000E 00    .0000E 00    .1809E-03
          .4497E-02    .3813E-06    .2010E-04
          .1449E-01    .1276E-04    .2210E-03
          .1878E-01    .2777E-04    .4220E-03
          .2256E-01    .4814E-04    .6230E-03
          .2474E-01    .6350E-04    .8241E-03
          .2741E-01    .8636E-04    .1025E-02
          .2902E-01    .1026E-03    .1226E-02
          .3082E-01    .1228E-03    .1427E-02
          .3129E-01    .1285E-03    .1628E-02
          .3332E-01    .1552E-03    .1829E-02
          .3345E-01    .1569E-03    .2030E-02
          .3391E-01    .1636E-03    .2231E-02
          .3372E-01    .1608E-03    .2432E-02
          .3471E-01    .1754E-03    .2633E-02
          .3438E-01    .1705E-03    .2833E-02
          .3400E-01    .1649E-03    .3034E-02
          .3397E-01    .1645E-03    .3235E-02
          .3408E-01    .1661E-03    .3436E-02
        D .3310E-01    .1521E-03    .3637E-02
          .3304E-01    .1513E-03    .4039E-02
          .3319E-01    .1534E-03    .4240E-02
          .3288E-01    .1491E-03    .4642E-02
          .3244E-01    .1432E-03    .5044E-02
          .3309E-01    .1520E-03    .5446E-02
          .3314E-01    .1527E-03    .5848E-02
          .3360E-01    .1591E-03    .6250E-02

ORUN NUMBER 152
N=.444,K=.532,J=.795,BETA=43
       RADIUS(IN)  VOLUME(IN3)  TIME(SEC)
          .0000E 00    .0000E 00    .5990E-04
          .1031E-01    .4598E-05    .1398E-03
          .1509E-01    .1441E-04    .3395E-03
          .1929E-01    .3008E-04    .5391E-03
          .2156E-01    .4204E-04    .7388E-03
          .2424E-01    .5975E-04    .9385E-03
          .2581E-01    .7212E-04    .1138E-02
          .2754E-01    .8757E-04    .1338E-02
          .2848E-01    .9690E-04    .1537E-02
          .2964E-01    .1092E-03    .1737E-02
          .3012E-01    .1146E-03    .1937E-02
          .3062E-01    .1204E-03    .2136E-02
          .3106E-01    .1257E-03    .2336E-02
          .3087E-01    .1234E-03    .2536E-02
          .3138E-01    .1297E-03    .2736E-02
          .3071E-01    .1215E-03    .2935E-02
          .3114E-01    .1267E-03    .3135E-02
          .3041E-01    .1180E-03    .3335E-02
        D .3083E-01    .1229E-03    .3534E-02
```

```
          .3062E-01    .1205E-03    .3934E-02
          .3089E-01    .1236E-03    .4333E-02
          .3157E-01    .1319E-03    .4732E-02
          .3209E-01    .1387E-03    .5132E-02
          .3097E-01    .1246E-03    .5531E-02
          .3039E-01    .1178E-03    .5930E-02
          .2874E-01    .9953E-04    .6729E-02
          .2787E-01    .9078E-04    .7528E-02
          .2672E-01    .7998E-04    .8327E-02
          .2529E-01    .6781E-04    .9125E-02

ORUN NUMBER 152
N=.421,K=.525,J=.922,BETA=44
       RADIUS(IN)  VOLUME(IN3   TIME(SEC)
          .0000E 00    .0000E 00    .1198E-03
          .9872E-02    .4035E-05    .7990E-04
          .1684E-01    .2004E-04    .2796E-03
          .2114E-01    .3961E-04    .4792E-03
          .2477E-01    .6375E-04    .6789E-03
          .2766E-01    .8877E-04    .8786E-03
          .2948E-01    .1075E-03    .1078E-02
          .3127E-01    .1282E-03    .1278E-02
          .3283E-01    .1484E-03    .1477E-02
          .3407E-01    .1659E-03    .1677E-02
          .3483E-01    .1773E-03    .1877E-02
          .3547E-01    .1871E-03    .2076E-02
          .3593E-01    .1946E-03    .2276E-02
          .3638E-01    .2019E-03    .2476E-02
          .3659E-01    .2055E-03    .2676E-02
          .3654E-01    .2047E-03    .2875E-02
          .3707E-01    .2137E-03    .3075E-02
        D .3737E-01    .2190E-03    .3275E-02
          .3738E-01    .2191E-03    .3474E-02
          .3725E-01    .2168E-03    .3874E-02
          .3727E-01    .2171E-03    .4273E-02
          .3815E-01    .2329E-03    .4672E-02
          .3767E-01    .2241E-03    .5072E-02
          .3782E-01    .2269E-03    .5471E-02
          .3818E-01    .2335E-03    .5870E-02

ORUN NUMBER 152
N=.524,K=.593,J=.498,BETA=44
       RADIUS(IN)  VOLUME(IN3)  TIME(SEC)
          .0000E 00    .0000E 00    .5990E-04
          .5636E-02    .7507E-06    .1398E-03
          .8994E-02    .3050E-05    .3395E-03
          .1177E-01    .6836E-05    .5391E-03
          .1353E-01    .1039E-04    .7388E-03
          .1542E-01    .1538E-04    .9385E-03
          .1676E-01    .1976E-04    .1138E-02
          .1771E-01    .2328E-04    .1338E-02
          .1843E-01    .2625E-04    .1537E-02
          .1914E-01    .2942E-04    .1737E-02
          .1931E-01    .3020E-04    .1937E-02
          .2001E-01    .3362E-04    .2136E-02
          .2158E-01    .4214E-04    .2336E-02
          .2035E-01    .3534E-04    .2536E-02
          .2058E-01    .3654E-04    .2736E-02
          .2082E-01    .3784E-04    .2935E-02
```

TABLE VI (CONT'D)

```
D .2078E-01    .3765E-04    .3135E-02
  .2024E-01    .3478E-04    .3335E-02
  .2082E-01    .3787E-04    .3734E-02
  .2082E-01    .3787E-04    .4133E-02
  .2112E-01    .3953E-04    .4533E-02
  .2027E-01    .3493E-04    .4932E-02
  .1991E-01    .3310E-04    .5331E-02
  .1932E-01    .3024E-04    .5731E-02
  .1939E-01    .3057E-04    .6130E-02
  .1905E-01    .2897E-04    .6929E-02
  .1838E-01    .2605E-04    .7728E-02
  .1694E-01    .2039E-04    .8526E-02
  .1707E-01    .2085E-04    .9325E-02
  .1560E-01    .1593E-04    .1012E-01

ORUN NUMBER 152
N=.352,K=.299,J=.875,BETA=45
     RADIUS(IN)   VOLUME(IN3)   TIME(SEC)
      .0000E 00    .0000E 00    .1002E-03
      .1172E-01    .6746E-05    .1001E-03
      .1713E-01    .2110E-04    .3004E-03
      .2069E-01    .3714E-04    .5008E-03
      .2307E-01    .5149E-04    .7011E-03
      .2546E-01    .6920E-04    .9018E-03
      .2723E-01    .8464E-04    .1102E-02
      .2880E-01    .1002E-03    .1302E-02
      .2941E-01    .1067E-03    .1503E-02
      .3044E-01    .1183E-03    .1703E-02
      .3093E-01    .1241E-03    .1903E-02
      .3165E-01    .1329E-03    .2104E-02
      .3185E-01    .1355E-03    .2304E-02
      .3241E-01    .1427E-03    .2504E-02
      .3227E-01    .1409E-03    .2704E-02
      .3285E-01    .1487E-03    .2905E-02
     D.3276E-01    .1475E-03    .3105E-02
      .3294E-01    .1499E-03    .3305E-02
      .3292E-01    .1497E-03    .3706E-02
      .3236E-01    .1421E-03    .4107E-02
      .3256E-01    .1448E-03    .4507E-02
      .3260E-01    .1453E-03    .4908E-02
      .3275E-01    .1474E-03    .5309E-02
      .3003E-01    .1136E-03    .6110E-02
      .3097E-01    .1245E-03    .6911E-02

ORUN NUMBER 153
N=.432,K=.593,J=.982,BETA=79
     RADIUS(IN)   VOLUME(IN3)   TIME(SEC)
      .0000E 00    .0000E 00    .4291E-04
      .1113E-01    .5774E-05    .1001E-03
      .1631E-01    .1821E-04    .2431E-03
      .1988E-01    .3294E-04    .3862E-03
      .2279E-01    .4968E-04    .5292E-03
      .2548E-01    .6936E-04    .6722E-03
      .2751E-01    .8729E-04    .8152E-03
      .2939E-01    .1065E-03    .9581E-03
      .3129E-01    .1285E-03    .1101E-02
      .3256E-01    .1448E-03    .1244E-02
      .3397E-01    .1644E-03    .1387E-02
      .3492E-01    .1786E-03    .1530E-02
```

```
      .3634E-01    .2013E-03    .1673E-02
      .3693E-01    .2112E-03    .1816E-02
      .3809E-01    .2318E-03    .1959E-02
      .3899E-01    .2486E-03    .2102E-02
      .3935E-01    .2556E-03    .2245E-02
      .3938E-01    .2562E-03    .2388E-02
      .3959E-01    .2602E-03    .2531E-02
      .3957E-01    .2598E-03    .2674E-02
      .3996E-01    .2677E-03    .2817E-02
      .3950E-01    .2585E-03    .2960E-02
      .3965E-01    .2615E-03    .3103E-02
      .3970E-01    .2625E-03    .3246E-02
      .3983E-01    .2651E-03    .3389E-02
      .3963E-01    .2611E-03    .3533E-02
      .3958E-01    .2601E-03    .3676E-02
     D.3943E-01    .2571E-03    .3819E-02
      .3900E-01    .2488E-03    .4105E-02
      .3870E-01    .2431E-03    .4391E-02
      .3896E-01    .2481E-03    .4677E-02
      .3902E-01    .2492E-03    .4963E-02
      .3935E-01    .2556E-03    .5249E-02
      .3973E-01    .2631E-03    .5535E-02
      .4025E-01    .2736E-03    .5821E-02
      .4101E-01    .2893E-03    .6107E-02
ORUN NUMBER 154
N=.342,K=.311,J=.950,BETA=45
     RADIUS(IN)   VOLUME(IN3)   TIME(SEC)
      .0000E 00    .0000E 00    .7135E-04
      .1188E-01    .7024E-05    .7135E-04
      .1749E-01    .2243E-04    .2140E-03
      .2006E-01    .3384E-04    .3567E-03
      .2302E-01    .5113E-04    .4994E-03
      .2504E-01    .6586E-04    .6421E-03
      .2715E-01    .8390E-04    .7848E-03
      .2835E-01    .9561E-04    .9275E-03
      .3032E-01    .1170E-03    .1071E-02
      .3119E-01    .1272E-03    .1213E-02
      .3242E-01    .1430E-03    .1356E-02
      .3338E-01    .1560E-03    .1499E-02
      .3424E-01    .1683E-03    .1641E-02
      .3476E-01    .1762E-03    .1784E-02
      .3520E-01    .1829E-03    .1927E-02
      .3595E-01    .1948E-03    .2069E-02
      .3606E-01    .1967E-03    .2212E-02
      .3631E-01    .2009E-03    .2355E-02
      .3683E-01    .2096E-03    .2497E-02
      .3654E-01    .2047E-03    .2640E-02
      .3670E-01    .2073E-03    .2783E-02
      .3668E-01    .2070E-03    .2926E-02
      .3688E-01    .2104E-03    .3068E-02
      .3663E-01    .2062E-03    .3211E-02
      .3666E-01    .2067E-03    .3354E-02
      .3618E-01    .1986E-03    .3496E-02
     D.3614E-01    .1980E-03    .3639E-02
      .3613E-01    .1978E-03    .3924E-02
      .3628E-01    .2003E-03    .4210E-02
      .3616E-01    .1983E-03    .4495E-02
      .3684E-01    .2098E-03    .4781E-02
      .3725E-01    .2169E-03    .5066E-02
```

```
      .3735E-01    .2186E-03    .5351E-02
      .3806E-01    .2313E-03    .5637E-02
      .3809E-01    .2317E-03    .5922E-02

ORUN NUMBER 154
N=.327,K=.272,J=.991,BETA=40
     RADIUS(IN)   VOLUME(IN3)   TIME(SEC)
      .0000E 00    .0000E 00    .9989E-04
      .1020E-01    .4455E-05    .4281E-04
      .1628E-01    .1808E-04    .1855E-03
      .1957E-01    .3144E-04    .3282E-03
      .2219E-01    .4581E-04    .4709E-03
      .2427E-01    .5995E-04    .6136E-03
      .2602E-01    .7390E-04    .7563E-03
      .2755E-01    .8772E-04    .8990E-03
      .2835E-01    .9556E-04    .1042E-02
      .2950E-01    .1077E-03    .1184E-02
      .2993E-01    .1125E-03    .1327E-02
      .3033E-01    .1171E-03    .1470E-02
      .3024E-01    .1160E-03    .1612E-02
      .3064E-01    .1206E-03    .1755E-02
      .3082E-01    .1228E-03    .1898E-02
      .3079E-01    .1224E-03    .2040E-02
      .3054E-01    .1195E-03    .2183E-02
      .3070E-01    .1214E-03    .2326E-02
      .3039E-01    .1177E-03    .2468E-02
      .3074E-01    .1218E-03    .2611E-02
    D .3069E-01    .1213E-03    .2754E-02
      .3081E-01    .1227E-03    .3039E-02
      .3057E-01    .1198E-03    .3325E-02
      .3033E-01    .1170E-03    .3610E-02
      .2989E-01    .1120E-03    .3895E-02
      .2980E-01    .1110E-03    .4181E-02
      .3002E-01    .1134E-03    .4466E-02
      .3011E-01    .1145E-03    .4752E-02
      .3046E-01    .1185E-03    .5322E-02
      .2993E-01    .1124E-03    .5893E-02
      .2961E-01    .1088E-03    .6464E-02

ORUN NUMBER 155
N=.540,K=1.25,J=.912
     RADIUS(IN)   VOLUME(IN3)   TIME(SEC)
      .0000E 00    .0000E 00    .1199E-03
      .4506E-02    .3835E-06    .3000E-04
      .1137E-01    .6166E-05    .1799E-03
      .1761E-01    .2289E-04    .3297E-03
      .2045E-01    .3585E-04    .4796E-03
      .2228E-01    .4642E-04    .6295E-03
      .2443E-01    .6113E-04    .7794E-03
      .2561E-01    .7048E-04    .9291E-03
      .2764E-01    .8856E-04    .1079E-02
      .2853E-01    .9738E-04    .1229E-02
      .3009E-01    .1142E-03    .1379E-02
      .3122E-01    .1276E-03    .1529E-02
      .3147E-01    .1308E-03    .1679E-02
      .3212E-01    .1390E-03    .1828E-02
      .3192E-01    .1364E-03    .2128E-02
      .3115E-01    .1268E-03    .2428E-02
      .3063E-01    .1205E-03    .2728E-02
```

TABLE VI (CONT'D)

```
         .2967E-01    .1096E-03    .3027E-02

ORUN NUMBER 155
N=.419,K=.458,J=.837,BETA=27
      RADIUS(IN)  VOLUME(IN3)  TIME(SEC)
         .0000E 00    .0000E 00    .1049E-03
         .6916E-02    .1387E-05    .4500E-04
         .1302E-01    .9258E-05    .1949E-03
         .1594E-01    .1698E-04    .3447E-03
         .1911E-01    .2925E-04    .4946E-03
         .2083E-01    .3792E-04    .6445E-03
         .2328E-01    .5294E-04    .7944E-03
         .2483E-01    .6418E-04    .9441E-03
         .2531E-01    .6800E-04    .1094E-02
         .2679E-01    .8069E-04    .1244E-02
         .2774E-01    .8954E-04    .1544E-02
         .2819E-01    .9400E-04    .1694E-02
         .2777E-01    .8980E-04    .1993E-02
         .2702E-01    .8275E-04    .2293E-02
         .2653E-01    .7829E-04    .2593E-02
         .2551E-01    .6963E-04    .2893E-02
        D.2452E-01    .6184E-04    .3192E-02
         .2210E-01    .4527E-04    .3792E-02
         .1975E-01    .3233E-04    .4391E-02
         .1443E-01    .1261E-04    .4991E-02
         .5910E-02    .8654E-06    .5590E-02

ORUN NUMBER 155
N=.452,K=.605,J=.871,BETA=35
      RADIUS(IN)  VOLUME(IN3)  TIME(SEC)
         .0000E 00    .0000E 00    .1349E-03
         .3883E-02    .2454E-06    .1500E-04
         .1285E-01    .8891E-05    .1649E-03
         .1575E-01    .1639E-04    .3147E-03
         .1869E-01    .2739E-04    .4646E-03
         .2048E-01    .3603E-04    .6145E-03
         .2217E-01    .4570E-04    .7644E-03
         .2366E-01    .5553E-04    .9141E-03
         .2441E-01    .6102E-04    .1064E-02
         .2561E-01    .7049E-04    .1214E-02
         .2621E-01    .7551E-04    .1364E-02
         .2635E-01    .7678E-04    .1514E-02
         .2617E-01    .7517E-04    .1813E-02
         .2551E-01    .6960E-04    .2113E-02
         .2482E-01    .6415E-04    .2413E-02
         .2397E-01    .5774E-04    .2713E-02
       D .2425E-01    .5979E-04    .3012E-02
         .2147E-01    .4151E-04    .3312E-02
         .1889E-01    .2829E-04    .3912E-02
         .1432E-01    .1231E-04    .4511E-02
         .1183E-01    .6951E-05    .5111E-02
         .6442E-02    .1121E-05    .5710E-02

ORUN NUMBER 156
N=.466,K=.816,J=1.05,BETA=81
      RADIUS(IN)  VOLUME(IN3)  TIME(SEC)
         .0000E 00    .0000E 00    .9014E-04
         .8812E-02    .2869E-05    .6006E-04
         .1559E-01    .1589E-04    .2104E-03
         .2066E-01    .3698E-04    .3606E-03
         .2399E-01    .5792E-04    .5109E-03
         .2702E-01    .8269E-04    .6611E-03
         .2921E-01    .1045E-03    .8113E-03
         .3107E-01    .1258E-03    .9619E-03
         .3261E-01    .1454E-03    .1112E-02
         .3402E-01    .1651E-03    .1262E-02
         .3491E-01    .1785E-03    .1412E-02
         .3634E-01    .2012E-03    .1563E-02
         .3700E-01    .2125E-03    .1713E-02
         .3791E-01    .2286E-03    .2013E-02
         .3823E-01    .2343E-03    .2314E-02
       D .3788E-01    .2280E-03    .2614E-02
         .3708E-01    .2138E-03    .2915E-02
         .3563E-01    .1897E-03    .3215E-02
         .3426E-01    .1687E-03    .3516E-02
         .3296E-01    .1503E-03    .3816E-02
         .3132E-01    .1289E-03    .4117E-02
         .2997E-01    .1129E-03    .4718E-02
         .2670E-01    .7980E-04    .5319E-02

ORUN NUMBER 156
N=.421,K=.485,J=.891,BETA=81
      RADIUS(IN)  VOLUME(IN3)  TIME(SEC)
         .0000E 00    .0000E 00    .4507E-04
         .1028E-01    .4558E-05    .1051E-03
         .1496E-01    .1403E-04    .2554E-03
         .1813E-01    .2499E-04    .4056E-03
         .2089E-01    .3822E-04    .5559E-03
         .2279E-01    .4963E-04    .7061E-03
         .2441E-01    .6098E-04    .8563E-03
         .2575E-01    .7161E-04    .1007E-02
         .2732E-01    .8553E-04    .1307E-02
         .2769E-01    .8907E-04    .1457E-02
         .2786E-01    .9072E-04    .1608E-02
         .2690E-01    .8165E-04    .1908E-02
         .2590E-01    .7290E-04    .2209E-02
         .2477E-01    .6374E-04    .2509E-02
         .2360E-01    .5510E-04    .2810E-02
       D .2275E-01    .4936E-04    .3110E-02
         .2148E-01    .4158E-04    .3411E-02
         .1998E-01    .3345E-04    .3711E-02
         .1499E-01    .1411E-04    .4312E-02
         .9458E-02    .3547E-05    .4913E-02
         .6688E-02    .1254E-05    .5514E-02

ORUN NUMBER 157
N=.372,K=.485,J=1.04
      RADIUS(IN)  VOLUME(IN3)  TIME(SEC)
         .0000E 00    .0000E 00    .4454E-04
         .1313E-01    .9495E-05    .1040E-03
         .1825E-01    .2549E-04    .2524E-03
         .2174E-01    .4308E-04    .4009E-03
         .2444E-01    .6120E-04    .5493E-03
         .2668E-01    .7962E-04    .6978E-03
         .2856E-01    .9771E-04    .8462E-03
         .2978E-01    .1107E-03    .9945E-03
         .3132E-01    .1288E-03    .1143E-02
         .3215E-01    .1394E-03    .1291E-02
         .3310E-01    .1522E-03    .1440E-02
         .3346E-01    .1571E-03    .1588E-02
         .3400E-01    .1648E-03    .1736E-02
       D .3441E-01    .1708E-03    .1885E-02

ORUN NUMBER 157
                       BETA=85
      RADIUS(IN)  VOLUME(IN3)  TIME(SEC)
         .0000E 00    .0000E 00    .1188E-03
         .5777E-02    .8082E-06    .2970E-04
         .9747E-02    .3883E-05    .1781E-03
         .1178E-01    .6848E-05    .3266E-03
         .1303E-01    .9277E-05    .4750E-03
         .1355E-01    .1042E-04    .6235E-03
         .1322E-01    .9697E-05    .7719E-03
         .1226E-01    .7731E-05    .9202E-03
         .1126E-01    .5988E-05    .1069E-02
         .1028E-01    .4558E-05    .1217E-02
       D .9519E-02    .3617E-05    .1366E-02
         .8235E-02    .2342E-05    .1514E-02
         .7392E-02    .1694E-05    .1662E-02
         .5622E-02    .7450E-06    .1811E-02

ORUN NUMBER 157
N=.393,K=.298,J=.700,BETA=66
      RADIUS(IN)  VOLUME(IN3)  TIME(SEC)
         .0000E 00    .0000E 00    .8907E-04
         .6530E-02    .1167E-05    .5943E-04
         .1046E-01    .4793E-05    .2078E-03
         .1316E-01    .9565E-05    .3563E-03
         .1515E-01    .1459E-04    .5047E-03
         .1633E-01    .1827E-04    .6532E-03
         .1668E-01    .1946E-04    .8016E-03
         .1637E-01    .1841E-04    .9499E-03
         .1625E-01    .1800E-04    .1099E-02
         .1564E-01    .1604E-04    .1247E-02
         .1497E-01    .1407E-04    .1396E-02
        D.1346E-01    .1022E-04    .1692E-02
         .1213E-01    .7476E-05    .1989E-02
         .1047E-01    .4808E-05    .2286E-02
         .8064E-02    .2198E-05    .2583E-02
         .6526E-02    .1165E-05    .2880E-02

ORUN NUMBER 158
N=.471,K=.756,J=.944
      RADIUS(IN)  VOLUME(IN3)  TIME(SEC)
         .0000E 00    .0000E 00    .7328E-04
         .5671E-02    .7646E-06    .3142E-04
         .1136E-01    .6143E-05    .1361E-03
         .1533E-01    .1511E-04    .2408E-03
         .1787E-01    .2394E-04    .3455E-03
         .2207E-01    .4510E-04    .5548E-03
         .2349E-01    .5433E-04    .6595E-03
         .2491E-01    .6480E-04    .7642E-03
         .2651E-01    .7816E-04    .8689E-03
         .2768E-01    .8895E-04    .9737E-03
         .2861E-01    .9824E-04    .1079E-02
         .3023E-01    .1159E-03    .1288E-02
```

TABLE VI (CONT'D)

```
ORUN NUMBER 158
N=.556,K=1.36,J=.876,BETA=78
      RADIUS(IN)  VOLUME(IN3)  TIME(SEC)
       .0000E 00   .0000E 00   .5235E-04
       .5689E-02   .7720E-06   .5235E-04
       .1001E-01   .4209E-05   .1570E-03
       .1477E-01   .1350E-04   .2617E-03
       .1709E-01   .2092E-04   .3664E-03
       .1878E-01   .2780E-04   .4711E-03
       .2124E-01   .4017E-04   .5757E-03
       .2246E-01   .4749E-04   .6804E-03
       .2356E-01   .5488E-04   .7851E-03
       .2501E-01   .6559E-04   .8898E-03
       .2611E-01   .7463E-04   .9946E-03
       .2723E-01   .8473E-04   .1100E-02
       .2738E-01   .8608E-04   .1204E-02
       .2837E-01   .9578E-04   .1309E-02
       .2878E-01   .9997E-04   .1518E-02
       .2909E-01   .1033E-03   .1728E-02
       .2915E-01   .1039E-03   .1937E-02
       .2888E-01   .1010E-03   .2146E-02
       .2817E-01   .9371E-04   .2356E-02
       .2748E-01   .8702E-04   .2565E-02
       .2651E-01   .7811E-04   .2775E-02
       .2580E-01   .7201E-04   .2984E-02
      D.2499E-01   .6548E-04   .3193E-02
       .2356E-01   .5484E-04   .3612E-02
       .2149E-01   .4163E-04   .4031E-02
       .1992E-01   .3313E-04   .4450E-02
       .1659E-01   .1914E-04   .4868E-02
       .1321E-01   .9661E-05   .5287E-02
       .9279E-02   .3349E-05   .5706E-02
       .7811E-02   .1998E-05   .6125E-02

ORUN NUMBER 159
N=.393,K=.280,J=.670,BETA=68
      RADIUS(IN)  VOLUME(IN3)  TIME(SEC)
       .0000E 00   .0000E 00   .8446E-04
       .4083E-02   .2852E-06   .2114E-04
       .8284E-02   .2384E-05   .1266E-03
       .1033E-01   .4620E-05   .2322E-03
       .1242E-01   .8028E-05   .3378E-03
       .1333E-01   .9930E-05   .4434E-03
       .1407E-01   .1169E-04   .5489E-03
       .1505E-01   .1430E-04   .6545E-03
       .1596E-01   .1706E-04   .7601E-03
       .1575E-01   .1639E-04   .8657E-03
       .1542E-01   .1536E-04   .9715E-03
       .1494E-01   .1398E-04   .1077E-02
       .1478E-01   .1353E-04   .1183E-02
       .1364E-01   .1065E-04   .1394E-02
      D.1247E-01   .8127E-05   .1605E-02
       .1142E-01   .6251E-05   .1816E-02
       .9789E-02   .3933E-05   .2027E-02
       .8598E-02   .2665E-05   .2239E-02
       .6815E-02   .1327E-05   .2450E-02

ORUN NUMBER 159
N=.570,K=1.46,J=.842
```

```
      RADIUS(IN)  VOLUME(IN3)  TIME(SEC)
       .0000E 00   .0000E 00   .6334E-04
       .4664E-02   .4254E-06   .4226E-04
       .9596E-02   .3705E-05   .1478E-03
       .1348E-01   .1027E-04   .2534E-03
       .1618E-01   .1776E-04   .3590E-03
       .1846E-01   .2639E-04   .4646E-03
       .2011E-01   .3409E-04   .5701E-03
       .2145E-01   .4139E-04   .6757E-03
       .2288E-01   .5026E-04   .7813E-03
       .2400E-01   .5798E-04   .8869E-03
       .2469E-01   .6309E-04   .9927E-03
       .2562E-01   .7050E-04   .1098E-02
       .2680E-01   .8074E-04   .1309E-02

ORUN NUMBER 162
N=.446,K=.432,J=.670,BETA=40
      RADIUS(IN)  VOLUME(IN3)  TIME(SEC)
       .0000E 00   .0000E 00   .4013E-04
       .5690E-02   .7723E-06   .6017E-04
       .8713E-02   .2774E-05   .1605E-03
       .1101E-01   .5593E-05   .2609E-03
       .1264E-01   .8459E-05   .3612E-03
       .1403E-01   .1158E-04   .4615E-03
       .1410E-01   .1174E-04   .5618E-03
       .1455E-01   .1291E-04   .6621E-03
     D .1487E-01   .1380E-04   .7625E-03
       .1402E-01   .1157E-04   .9629E-03
       .1253E-01   .8258E-05   .1164E-02
       .1101E-01   .5600E-05   .1364E-02
       .8217E-02   .2326E-05   .1565E-02

ORUN NUMBER 162
N=.355,K=.244,J=.769,BETA=40
      RADIUS(IN)  VOLUME(IN3)  TIME(SEC)
       .0000E 00   .0000E 00   .4013E-04
       .7696E-02   .1911E-05   .6017E-04
       .1084E-01   .5344E-05   .1605E-03
       .1349E-01   .1029E-04   .2609E-03
       .1453E-01   .1287E-04   .3612E-03
       .1625E-01   .1800E-04   .4615E-03
       .1663E-01   .1929E-04   .5618E-03
       .1770E-01   .2326E-04   .6621E-03
       .1813E-01   .2501E-04   .7625E-03
       .1855E-01   .2677E-04   .8628E-03
      D.1747E-01   .2234E-04   .9629E-03
       .1658E-01   .1913E-04   .1164E-02
       .1547E-01   .1552E-04   .1364E-02
       .1531E-01   .1505E-04   .1565E-02
       .1500E-01   .1414E-04   .1766E-02
       .1285E-01   .8906E-05   .1966E-02

ORUN NUMBER 162
N=.570,K=1.29,J=.738,BETA=27
      RADIUS(IN)  VOLUME(IN3)  TIME(SEC)
       .0000E 00   .0000E 00   .4547E-12
       .6837E-02   .1340E-05   .1003E-03
       .9631E-02   .3746E-05   .2006E-03
       .1335E-01   .9969E-05   .3010E-03
```

```
       .1519E-01   .1470E-04   .4013E-03
       .1650E-01   .1883E-04   .5016E-03
       .1789E-01   .2401E-04   .6019E-03
       .1847E-01   .2643E-04   .8026E-03
       .1835E-01   .2590E-04   .9029E-03
     D .1792E-01   .2415E-04   .1003E-02
       .1791E-01   .2408E-04   .1104E-02
       .1673E-01   .1962E-04   .1204E-02
       .1643E-01   .1861E-04   .1404E-02
       .1583E-01   .1663E-04   .1605E-02
       .1578E-01   .1648E-04   .1806E-02
       .1385E-01   .1115E-04   .2006E-02
       .9377E-02   .3457E-05   .2207E-02
       .6507E-02   .1155E-05   .2408E-02
       .6496E-02   .1149E-05   .2608E-02

ORUN NUMBER 164
N=.346,K=.289,J=1.18,BETA=74
      RADIUS(IN)  VOLUME(IN3)  TIME(SEC)
       .0000E 00   .0000E 00   .6000E-04
       .1045E-01   .4787E-05   .4000E-04
       .1602E-01   .1724E-04   .1400E-03
       .1964E-01   .3176E-04   .2400E-03
       .2206E-01   .4503E-04   .3400E-03
       .2385E-01   .5689E-04   .4400E-03
       .2556E-01   .7007E-04   .5400E-03
       .2698E-01   .8233E-04   .6400E-03
       .2805E-01   .9257E-04   .7400E-03
       .2881E-01   .1003E-03   .8400E-03
       .2943E-01   .1070E-03   .9400E-03
       .2938E-01   .1064E-03   .1040E-02
       .2918E-01   .1042E-03   .1140E-02
       .2895E-01   .1018E-03   .1240E-02
      D.2884E-01   .1006E-03   .1340E-02
       .2839E-01   .9599E-04   .1440E-02

ORUN NUMBER 164
N=.470,K=.782,J=.994,BETA=62
      RADIUS(IN)  VOLUME(IN3)  TIME(SEC)
       .0000E 00   .0000E 00   .5000E-04
       .7442E-02   .1728E-05   .5000E-04
       .1223E-01   .7665E-05   .1500E-03
       .1596E-01   .1705E-04   .2500E-03
       .1864E-01   .2715E-04   .3500E-03
       .2071E-01   .3725E-04   .4500E-03
       .2239E-01   .4705E-04   .5500E-03
       .2382E-01   .5670E-04   .6500E-03
       .2500E-01   .6553E-04   .7500E-03
       .2556E-01   .7000E-04   .8500E-03
       .2598E-01   .7358E-04   .9500E-03
       .2590E-01   .7283E-04   .1050E-02
       .2590E-01   .7285E-04   .1150E-02
      D.2549E-01   .6946E-04   .1250E-02
       .2576E-01   .7173E-04   .1350E-02
       .2510E-01   .6632E-04   .1450E-02

ORUN NUMBER 166
N=.357,K=.275,J=.915,BETA=50
      RADIUS(IN)  VOLUME(IN3)  TIME(SEC)
```

TABLE VI (CONT'D)

```
        .0000E 00     .0000E 00     .4002E-04
        .6465E-02     .1133E-05     .2668E-04
        .1022E-01     .4476E-05     .9338E-04
        .1144E-01     .6284E-05     .1601E-03
        .1445E-01     .1265E-04     .2268E-03
        .1487E-01     .1380E-04     .2935E-03
        .1650E-01     .1883E-04     .3602E-03
        .1760E-01     .2285E-04     .4269E-03
        .1819E-01     .2525E-04     .4936E-03
        .1952E-01     .3118E-04     .5603E-03
        .1955E-01     .3132E-04     .6270E-03
        .1999E-01     .3352E-04     .6937E-03
        .2029E-01     .3501E-04     .8271E-03
        .2033E-01     .3525E-04     .9610E-03
      D .1964E-01     .3178E-04     .1094E-02
        .1894E-01     .2851E-04     .1227E-02
        .1860E-01     .2700E-04     .1361E-02
        .1886E-01     .2812E-04     .1494E-02
        .1894E-01     .2850E-04     .1628E-02

ORUN NUMBER 169
N=.270,K=.175,J=1.14,BETA=76
       RADIUS(IN)   VOLUME(IN3)   TIME(SEC)
        .0000E 00     .0000E 00     .4664E-04
        .9378E-02     .3458E-05     .1999E-04
        .1408E-01     .1171E-04     .8666E-04
        .1759E-01     .2283E-04     .2199E-03
        .1928E-01     .3005E-04     .2866E-03
        .2058E-01     .3654E-04     .3532E-03
        .2144E-01     .4134E-04     .4198E-03
        .2201E-01     .4473E-04     .4864E-03
        .2251E-01     .4784E-04     .5531E-03
        .2336E-01     .5343E-04     .6197E-03
        .2404E-01     .5824E-04     .6863E-03
        .2504E-01     .6588E-04     .8196E-03
        .2461E-01     .6252E-04     .9529E-03
        .2343E-01     .5395E-04     .1086E-02
      D .2289E-01     .5033E-04     .1219E-02
        .2151E-01     .4177E-04     .1352E-02
        .2156E-01     .4206E-04     .1486E-02
        .2066E-01     .3701E-04     .1619E-02
        .2037E-01     .3545E-04     .1752E-02
        .1973E-01     .3222E-04     .1885E-02
        .1926E-01     .2998E-04     .2019E-02

ORUN NUMBER 170
N=.389,K=.509,J=1.30,BETA=66
       RADIUS(IN)   VOLUME(IN3)   TIME(SEC)
        .0000E 00     .0000E 00     .4669E-04
        .7528E-02     .1788E-05     .2001E-04
        .1335E-01     .9980E-05     .8671E-04
        .1684E-01     .2004E-04     .1534E-03
        .1962E-01     .3166E-04     .2201E-03
        .2119E-01     .3993E-04     .2868E-03
        .2310E-01     .5172E-04     .3535E-03
        .2434E-01     .6047E-04     .4202E-03
        .2566E-01     .7086E-04     .4869E-03
        .2655E-01     .7846E-04     .5536E-03
        .2719E-01     .8433E-04     .6203E-03
```

```
        .2763E-01     .8848E-04     .6870E-03
        .2761E-01     .8823E-04     .8204E-03
        .2718E-01     .8418E-04     .9543E-03
      D .2616E-01     .7510E-04     .1087E-02

ORUN NUMBER 171
N=.487,K=.782,J=.924,BETA=39
       RADIUS(IN)   VOLUME(IN3)   TIME(SEC)
        .0000E 00     .0000E 00     .1331E-04
        .7955E-02     .2111E-05     .5325E-04
        .1076E-01     .5218E-05     .1198E-03
        .1245E-01     .8087E-05     .1864E-03
        .1482E-01     .1365E-04     .2529E-03
        .1598E-01     .1713E-04     .3195E-03
        .1786E-01     .2390E-04     .3861E-03
        .1780E-01     .2364E-04     .4526E-03
        .1996E-01     .3337E-04     .5192E-03
        .2071E-01     .3727E-04     .5857E-03
        .2137E-01     .4093E-04     .6523E-03
        .2173E-01     .4305E-04     .7189E-03
        .2240E-01     .4716E-04     .7854E-03
        .2239E-01     .4707E-04     .9185E-03
        .2195E-01     .4435E-04     .1052E-02
        .2155E-01     .4195E-04     .1185E-02
      D .2047E-01     .3596E-04     .1345E-02

ORUN NUMBER 172
N=.304,K=.171,J=.856,BETA=42
       RADIUS(IN)   VOLUME(IN3)   TIME(SEC)
        .0000E 00     .0000E 00     .4002E-04
        .6997E-02     .1436E-05     .2668E-04
        .1003E-01     .4230E-05     .9338E-04
        .1213E-01     .7476E-05     .1601E-03
        .1308E-01     .9378E-05     .2268E-03
        .1434E-01     .1236E-04     .2935E-03
        .1554E-01     .1573E-04     .3602E-03
        .1620E-01     .1784E-04     .4269E-03
        .1657E-01     .1909E-04     .4936E-03
        .1767E-01     .2315E-04     .5603E-03
        .1736E-01     .2194E-04     .6270E-03
        .1799E-01     .2443E-04     .6937E-03
        .1742E-01     .2219E-04     .7604E-03
      D .1777E-01     .2352E-04     .8938E-03
        .1740E-01     .2207E-04     .1027E-02
        .1678E-01     .1980E-04     .1161E-02
        .1637E-01     .1841E-04     .1294E-02
        .1603E-01     .1727E-04     .1427E-02
        .1574E-01     .1635E-04     .1694E-02
        .1192E-01     .7097E-05     .1961E-02
        .7920E-02     .2083E-05     .2228E-02

ORUN NUMBER 172
N=.525,K=1.07,J=.894,BETA=29
       RADIUS(IN)   VOLUME(IN3)   TIME(SEC)
        .0000E 00     .0C00E 00     .6670E-05
        .7175E-02     .1549E-05     .6003E-04
        .1021E-01     .4465E-05     .1267E-03
        .1232E-01     .7832E-05     .1934E-03
        .1422E-01     .1206E-04     .2601E-03
```

```
        .1623E-01     .1794E-04     .3268E-03
        .1874E-01     .2761E-04     .3935E-03
        .2196E-01     .4443E-04     .4602E-03
        .2200E-01     .4467E-04     .5269E-03
        .2344E-01     .5399E-04     .5936E-03
        .2472E-01     .6338E-04     .6603E-03
        .2602E-01     .7391E-04     .7270E-03
        .2643E-01     .7741E-04     .8604E-03
        .2643E-01     .7744E-04     .9943E-03
        .2649E-01     .7795E-04     .1127E-02
        .2710E-01     .8350E-04     .1260E-02
      D .2663E-01     .7923E-04     .1394E-02
        .2469E-01     .6316E-04     .1527E-02

ORUN NUMBER 172
N=.448,K=.678,J=1.04,BETA=48
       RADIUS(IN)   VOLUME(IN3)   TIME(SEC)
        .0000E 00     .0000E 00     .1334E-04
        .8205E-02     .2316E-05     .5336E-04
        .1223E-01     .7663E-05     .1201E-03
        .1409E-01     .1173E-04     .1868E-03
        .1634E-01     .1830E-04     .2535E-03
        .1895E-01     .2852E-04     .3202E-03
        .1999E-01     .3349E-04     .3869E-03
        .2148E-01     .4156E-04     .4536E-03
        .2268E-01     .4890E-04     .5203E-03
        .2438E-01     .6074E-04     .5870E-03
        .2477E-01     .6375E-04     .6537E-03
        .2564E-01     .7070E-04     .7204E-03
        .2605E-01     .7414E-04     .7871E-03
        .2644E-01     .7753E-04     .8538E-03
        .2718E-01     .8424E-04     .9877E-03
        .2672E-01     .8003E-04     .1121E-02
      D .2636E-01     .7683E-04     .1254E-02
        .2553E-01     .6980E-04     .1388E-02
        .2557E-01     .7013E-04     .1521E-02
        .2434E-01     .6046E-04     .1788E-02
        .2316E-01     .5214E-04     .2055E-02
        .2059E-01     .3658E-04     .2322E-02
        .1494E-01     .1397E-04     .2588E-02
        .1339E-01     .1006E-04     .2855E-02
        .1164E-01     .6614E-05     .3122E-02
        .9526E-02     .3625E-05     .3389E-02
        .7649E-02     .1876E-05     .3656E-02

ORUN NUMBER 173
N=.778,K=10.05,J=1.04,BETA=70
       RADIUS(IN)   VOLUME(IN3)   TIME(SEC)
        .0000E 00     .0000E 00     .3321E-04
        .7987E-02     .2136E-05     .3321E-04
        .1161E-01     .6566E-05     .9959E-04
        .1544E-01     .1544E-04     .1661E-03
        .1870E-01     .2744E-04     .2325E-03
        .2178E-01     .4330E-04     .2989E-03
        .2265E-01     .4871E-04     .3653E-03
        .2411E-01     .5875E-04     .4317E-03
        .2500E-01     .6554E-04     .4981E-03
        .2693E-01     .8191E-04     .5646E-03
        .2735E-01     .8576E-04     .6310E-03
```

TABLE VI (CONT'D)

```
       .2875E-01    .9969E-04    .6974E-03
       .2893E-01    .1016E-03    .7638E-03
       .2917E-01    .1041E-03    .8967E-03
       .2906E-01    .1029E-03    .1030E-02
       .2866E-01    .9875E-04    .1163E-02
      D.2720E-01    .8442E-04    .1295E-02

ORUN NUMBER 174
N=.557,K=1.10,J=.681,BETA=45
      RADIUS(IN)  VOLUME(IN3)   TIME(SEC)
       .0000E 00    .0000E 00    .6663E-05
       .4926E-02    .5011E-06    .5997E-04
       .7037E-02    .1461E-05    .1266E-03
       .1018E-01    .4425E-05    .1932E-03
       .1098E-01    .5557E-05    .2598E-03
       .1229E-01    .7780E-05    .3265E-03
       .1279E-01    .8776E-05    .3931E-03
       .1326E-01    .9773E-05    .4597E-03
       .1334E-01    .9959E-05    .5263E-03
       .1297E-01    .9158E-05    .5930E-03
       .1330E-01    .9861E-05    .6596E-03
      D.1296E-01    .9118E-05    .7262E-03

ORUN NUMBER 174
N=.688,K=5.35,J=1.13,BETA=56
      RADIUS(IN)  VOLUME(IN3)   TIME(SEC)
       .0000E 00    .0000E 00    .1333E-04
       .6120E-02    .9610E-06    .5330E-04
       .1066E-01    .5079E-05    .1200E-03
       .1456E-01    .1294E-04    .1866E-03
       .1835E-01    .2593E-04    .2532E-03
       .2091E-01    .3833E-04    .3199E-03
       .2370E-01    .5586E-04    .3865E-03
       .2529E-01    .6781E-04    .4531E-03
       .2744E-01    .8670E-04    .5197E-03
       .2843E-01    .9636E-04    .5864E-03
       .2960E-01    .1088E-03    .6530E-03
       .3084E-01    .1230E-03    .7196E-03
       .3240E-01    .1426E-03    .8529E-03
       .3364E-01    .1597E-03    .9862E-03
       .3377E-01    .1615E-03    .1120E-02
       .3513E-01    .1818E-03    .1253E-02
     D .3377E-01    .1616E-03    .1386E-02
       .3345E-01    .1569E-03    .1520E-02
       .3240E-01    .1427E-03    .1786E-02
       .3236E-01    .1422E-03    .2053E-02
       .3257E-01    .1450E-03    .2319E-02
       .3226E-01    .1408E-03    .2586E-02
       .2750E-01    .8726E-04    .2852E-02
       .2568E-01    .7105E-04    .3119E-02
       .2603E-01    .7397E-04    .3385E-02
       .2354E-01    .5472E-04    .3652E-02
       .2199E-01    .4457E-04    .3918E-02

ORUN NUMBER 174
N=.431,K=.524,J=.930,BETA=79
      RADIUS(IN)  VOLUME(IN3)   TIME(SEC)
       .0000E 00    .0000E 00    .3332E-04
       .6169E-02    .9842E-06    .3331E-04
```

```
       .9739E-02    .3873E-05    .9998E-04
       .1249E-01    .8178E-05    .1666E-03
       .1406E-01    .1165E-04    .2332E-03
       .1566E-01    .1611E-04    .2999E-03
       .1752E-01    .2254E-04    .3665E-03
       .1849E-01    .2652E-04    .4331E-03
       .1942E-01    .3070E-04    .4997E-03
       .2083E-01    .3789E-04    .5664E-03
       .2114E-01    .3965E-04    .6330E-03
       .2150E-01    .4170E-04    .6996E-03
       .2187E-01    .4384E-04    .7663E-03
       .2181E-01    .4349E-04    .8995E-03
       .2211E-01    .4532E-04    .1033E-02
       .2113E-01    .3957E-04    .1166E-02
     D .2046E-01    .3590E-04    .1300E-02
       .1880E-01    .2786E-04    .1433E-02
       .1746E-01    .2233E-04    .1699E-02
       .1511E-01    .1448E-04    .1966E-02
       .1295E-01    .9101E-05    .2232E-02
       .9514E-02    .3611E-05    .2499E-02
```

TABLE VII

BUBBLE FREQUENCY AND DEPARTURE DATA

```
RUN NUMBER = 107
RADIUS  FREQUENCY  RADIUS X
INCHES  1/SECONDS  FREQUENCY
.02800         81       2.28
.05209         26       1.34
.02619         33        .87

RUN NUMBER = 108
RADIUS  FREQUENCY  RADIUS X
INCHES  1/SECONDS  FREQUENCY
.05353         22       1.18

RUN NUMBER = 109
RADIUS  FREQUENCY  RADIUS X
INCHES  1/SECONDS  FREQUENCY
.05823         46       2.69
.05914         46       2.74
.03657         46       1.69
.04479         36       1.62
.06458         24       1.55

RUN NUMBER = 110
RADIUS  FREQUENCY  RADIUS X
INCHES  1/SECONDS  FREQUENCY
.06626         24       1.57
.03168         77       2.44

RUN NUMBER = 111
RADIUS  FREQUENCY  RADIUS X
INCHES  1/SECONDS  FREQUENCY
.01168        430       5.02
.01834        273       5.02
.02799         91       2.55
.01438        231       3.33
.02444        177       4.33
.02688         70       1.88
.01986        273       5.43
.02515         70       1.76
.01719        334       5.75

RUN NUMBER = 112
RADIUS  FREQUENCY  RADIUS X
INCHES  1/SECONDS  FREQUENCY
.03669        104       3.81
.04150         97       4.03
.03615         97       3.51
.06578         31       2.04
.03800        177       6.72
.02339         91       2.13
.02457         67       1.64

RUN NUMBER = 114
RADIUS  FREQUENCY  RADIUS X
INCHES  1/SECONDS  FREQUENCY
.02289        122       2.79
.03380         79       2.68

RUN NUMBER = 115
RADIUS  FREQUENCY  RADIUS X
INCHES  1/SECONDS  FREQUENCY
.02252        217       4.89
.02242         94       2.11
.04266        111       4.73
.02991        116       3.47
.01767        172       3.04
.02863        151       4.33

RUN NUMBER = 116
RADIUS  FREQUENCY  RADIUS X
INCHES  1/SECONDS  FREQUENCY
.04396         60       2.64
.05472         48       2.65
.02483        122       3.02
.02397        116       2.78
.02972        102       3.03
.03097        172       5.33
.04717         91       4.28
.02896        185       5.35

RUN NUMBER = 117
RADIUS  FREQUENCY  RADIUS X
INCHES  1/SECONDS  FREQUENCY
.01440        333       4.79
.02350        263       6.17
.02309        172       3.97
.01561        263       4.10
.02311        200       4.62
.04358        200       8.70
.02966        116       3.44

RUN NUMBER = 118
RADIUS  FREQUENCY  RADIUS X
INCHES  1/SECONDS  FREQUENCY
.04810         37       1.78
.03352        151       5.07
.03050        172       5.25
.03892         82       3.19
.02722        116       3.16
.02563        128       3.28

RUN NUMBER = 119
RADIUS  FREQUENCY  RADIUS X
INCHES  1/SECONDS  FREQUENCY
.02001         70       1.41
.02315        185       4.28
.01175         75        .88
.01829        116       2.12
.00928         98        .91

RUN NUMBER = 120
RADIUS  FREQUENCY  RADIUS X
INCHES  1/SECONDS  FREQUENCY
.04176         38       1.60
.01133        173       1.96
.02365        103       2.43
.05340         88       4.71
.02785         77       2.15

RUN NUMBER = 121
RADIUS  FREQUENCY  RADIUS X
INCHES  1/SECONDS  FREQUENCY
.01545        108       1.67
.01249        171       2.14
.01884        213       4.01
.02164        128       2.76

RUN NUMBER = 122
RADIUS  FREQUENCY  RADIUS X
INCHES  1/SECONDS  FREQUENCY
.03730         81       3.01
.01340        260       3.49
.00756        108        .82
.01067        213       2.27
.02826        115       3.25
.01665        213       3.54
.02154        115       2.48

RUN NUMBER = 125
RADIUS  FREQUENCY  RADIUS X
INCHES  1/SECONDS  FREQUENCY
.01652        334       5.52
.02421        120       2.91
.04787         91       4.36
.02527        143       3.62
.03522        104       3.65
.04271         91       3.89

RUN NUMBER = 126
RADIUS  FREQUENCY  RADIUS X
INCHES  1/SECONDS  FREQUENCY
.03373        120       4.06
.04332        111       4.83
.05618         61       3.45
.03079        158       4.88
.05352         73       3.93
.04620         64       2.96

RUN NUMBER = 128
RADIUS  FREQUENCY  RADIUS X
INCHES  1/SECONDS  FREQUENCY
.04170         75       3.11
.02217        147       3.26

RUN NUMBER = 130
RADIUS  FREQUENCY  RADIUS X
INCHES  1/SECONDS  FREQUENCY
.01368        217       2.97
.00681        238       1.62
.01651        200       3.30
.01095        263       2.88
.01401        151       2.12
.01339        333       4.45
.01369        217       2.97

RUN NUMBER = 132
RADIUS  FREQUENCY  RADIUS X
INCHES  1/SECONDS  FREQUENCY
.01278        200       2.55
.01074        263       2.82
.01693        333       5.63
.01610        294       4.73
.01274         98       1.25
.02123        106       2.26
.01892        238       4.50
.02843        135       3.84
.01982        263       5.21

RUN NUMBER = 133
RADIUS  FREQUENCY  RADIUS X
INCHES  1/SECONDS  FREQUENCY
.02507        217       5.44
.03168         49       1.57
.00767        454       3.48
.00839        384       3.22
.01015        135       1.37
.01479        217       3.21
.01034        294       3.04
.01267        454       5.75
.01605        294       4.71

RUN NUMBER = 134
RADIUS  FREQUENCY  RADIUS X
INCHES  1/SECONDS  FREQUENCY
.01368        151       2.07
.01868        128       2.39
.01353        185       2.50
.01892        217       4.11
.02568        143       3.66
.01251        294       3.67
.02010         70       1.41
.01385        238       3.29

RUN NUMBER = 137
RADIUS  FREQUENCY  RADIUS X
INCHES  1/SECONDS  FREQUENCY
.03361         81       2.73
.04167         55       2.28

RUN NUMBER = 138
RADIUS  FREQUENCY  RADIUS X
INCHES  1/SECONDS  FREQUENCY
.02768         57       1.57
.03688         46       1.71

RUN NUMBER = 139
RADIUS  FREQUENCY  RADIUS X
INCHES  1/SECONDS  FREQUENCY
.03234         46       1.50
.03889         55       2.13

RUN NUMBER = 140
RADIUS  FREQUENCY  RADIUS X
INCHES  1/SECONDS  FREQUENCY
.01289        636       8.19
.01190        104       1.24
.01016        636       6.46
```

TABLE VII (CONT'D)

```
.01236          466          5.76
.01042          226          2.35
.01227          538          6.60

RUN NUMBER = 141
RADIUS  FREQUENCY  RADIUS X
INCHES  1/SECONDS  FREQUENCY
.01867          539         10.06

RUN NUMBER = 142
RADIUS  FREQUENCY  RADIUS X
INCHES  1/SECONDS  FREQUENCY
.01604          777         12.46
.03134          171          5.34
.01916          636         12.18
.03462          333         11.53

RUN NUMBER = 143
RADIUS  FREQUENCY  RADIUS X
INCHES  1/SECONDS  FREQUENCY
.02264          305          6.91
.02335          305          7.13
.02320          260          6.03
.02373          305          7.25
.02317          281          6.51
.02354          305          7.19

RUN NUMBER = 144
RADIUS  FREQUENCY  RADIUS X
INCHES  1/SECONDS  FREQUENCY
.00885          226          2.00
.01030          538          5.54
.00813          466          3.79
.02076          538         11.17
.01112          538          5.98
.02374          137          3.25

RUN NUMBER = 145
RADIUS  FREQUENCY  RADIUS X
INCHES  1/SECONDS  FREQUENCY
.00844          639          5.39
.01063          468          4.98
.01929          281          5.42
.01185          639          7.57
.01724          213          3.67
.01870          201          3.75

RUN NUMBER = 146
RADIUS  FREQUENCY  RADIUS X
INCHES  1/SECONDS  FREQUENCY
.01056          411          4.34
.00856          636          5.44
.00757          538          4.07
.00530          636          3.37
.00884          636          5.62
.00797          636          5.07
.01260          636          8.01
.01605          411          6.60
.00668          411          2.75
```

```
.01085          411          4.46

RUN NUMBER = 147
RADIUS  FREQUENCY  RADIUS X
INCHES  1/SECONDS  FREQUENCY
.01971          668         13.16
.01887         1113         21.00
.02609          668         17.42
.01540          668         10.28
.04017          244          9.81
.01245          527          6.56
.01058          770          8.15
.01051          668          7.02
.01159          527          6.11
.00910          911          8.28
.01204         1113         13.40

RUN NUMBER = 148
RADIUS  FREQUENCY  RADIUS X
INCHES  1/SECONDS  FREQUENCY
.01394          436          6.08
.01445          436          6.30
.01307          372          4.86
.01080         1115         12.04
.01724          436          7.52
.02040          528         10.77

RUN NUMBER = 149
RADIUS  FREQUENCY  RADIUS X
INCHES  1/SECONDS  FREQUENCY
.02819          263          7.41
.03782          122          4.60
.01778          333          5.92
.00989          238          2.35
.03042           85          2.57
.00989          333          3.29

RUN NUMBER = 150
RADIUS  FREQUENCY  RADIUS X
INCHES  1/SECONDS  FREQUENCY
.03115           57          1.79
.01474          454          6.69
.03427          111          3.80

RUN NUMBER = 151
RADIUS  FREQUENCY  RADIUS X
INCHES  1/SECONDS  FREQUENCY
.03089           90          2.80
.03315           84          2.80

RUN NUMBER = 152
RADIUS  FREQUENCY  RADIUS X
INCHES  1/SECONDS  FREQUENCY
.03084          102          3.15
.02064          238          4.92
.03314          143          4.74
.03758          107          4.00

RUN NUMBER = 154
```

```
RUN NUMBER 154
RADIUS  FREQUENCY  RADIUS X
INCHES  1/SECONDS  FREQUENCY
.03624           87          3.14
.01671          369          6.16
.02741          111          3.05
.01407          369          5.19

RUN NUMBER = 155
RADIUS  FREQUENCY  RADIUS X
INCHES  1/SECONDS  FREQUENCY
.02391          136          3.26
.01319          267          3.52
.02206          171          3.77
.02885          131          3.77

RUN NUMBER = 156
RADIUS  FREQUENCY  RADIUS X
INCHES  1/SECONDS  FREQUENCY
.01744          350          6.11
.01506          317          4.77
.01570          102          1.61
.01509          162          2.45
.02395          230          5.50
.03322          126          4.17

RUN NUMBER = 157
RADIUS  FREQUENCY  RADIUS X
INCHES  1/SECONDS  FREQUENCY
.00927          156          1.45
.01055          181          1.91
.00866          172          1.49
.02455          114          2.79

RUN NUMBER = 158
RADIUS  FREQUENCY  RADIUS X
INCHES  1/SECONDS  FREQUENCY
.02537          101          2.55
.01693           74          1.25

RUN NUMBER = 159
RADIUS  FREQUENCY  RADIUS X
INCHES  1/SECONDS  FREQUENCY
.01350          351          4.74
.01246          126          1.57
.02717          137          3.73

RUN NUMBER = 165
RADIUS  FREQUENCY  RADIUS X
INCHES  1/SECONDS  FREQUENCY
.01588          713         11.32
.01528          666         10.17
.01534          713         10.94
.01387          713          9.89
.01353          768         10.39
.01421          768         10.91
.01542          768         11.84
.01753          713         12.50
.01874          624         11.69
.01405          768         10.79
```

```
.01476          666          9.82
.01067          832          8.88
.01030          832          8.57
.00998          908          9.06

RUN NUMBER = 160
RADIUS  FREQUENCY  RADIUS X
INCHES  1/SECONDS  FREQUENCY
.02461          911         22.41
.02650          182          4.83
.01554         1113         17.29

RUN NUMBER = 161
RADIUS  FREQUENCY  RADIUS X
INCHES  1/SECONDS  FREQUENCY
.00584         1429          8.34
.00588         1429          8.40
.00608         1429          8.68
.00560         1429          8.00
.00553         1429          7.90
.00864         1111          9.60
.00917         1111         10.19
.00866         1111          9.62
.00700         1429         10.01
.01001         1111         11.12
.01287          909         11.70
.01059         1429         15.12
.01395          909         12.68
.01188          909         10.80
.00548         1429          7.83
.01236         1111         13.74
.00857         1429         12.24
.00736          667          4.91
.00806         1429         11.51
.00686         1111          7.62
.00830         1429         11.86

RUN NUMBER = 162
RADIUS  FREQUENCY  RADIUS X
INCHES  1/SECONDS  FREQUENCY
.01030         1108         11.41
.01858          203          3.78
.01297         1108         14.36
.01466          203          2.98
.01269          906         11.50

RUN NUMBER = 163
RADIUS  FREQUENCY  RADIUS X
INCHES  1/SECONDS  FREQUENCY
.02481          149          3.70
.02239          123          2.76

RUN NUMBER = 164
RADIUS  FREQUENCY  RADIUS X
INCHES  1/SECONDS  FREQUENCY
.01244         1111         13.83
.02598          169          4.40
.01660          909         15.09
.02859          159          4.54
```

TABLE VII (CONT'D)

.01535	1111	17.06

RUN NUMBER = 166

RADIUS INCHES	FREQUENCY 1/SECONDS	RADIUS X FREQUENCY
.01608	999	16.07
.01945	789	15.35

RUN NUMBER = 167

RADIUS INCHES	FREQUENCY 1/SECONDS	RADIUS X FREQUENCY
.01055	1152	12.15
.01126	384	4.33
.00917	998	9.15
.00815	384	3.13
.00960	1152	11.06
.00801	384	3.08
.00963	1361	13.11
.00964	319	3.07

RUN NUMBER = 169

RADIUS INCHES	FREQUENCY 1/SECONDS	RADIUS X FREQUENCY
.02040	790	16.12
.00932	1001	9.32
.02271	283	6.43
.01408	429	6.04
.01537	1364	20.97
.01638	455	7.45
.02348	143	3.36
.02202	334	7.34

RUN NUMBER = 170

RADIUS INCHES	FREQUENCY 1/SECONDS	RADIUS X FREQUENCY
.01481	789	11.68
.01533	1153	17.68
.01084	1363	14.78
.00934	999	9.33
.01299	882	11.46
.02266	254	5.76
.01571	999	15.70
.02654	263	6.98

RUN NUMBER = 171

RADIUS INCHES	FREQUENCY 1/SECONDS	RADIUS X FREQUENCY
.02180	320	6.97
.01087	1669	18.15
.03158	366	11.57
.02208	653	14.42
.01489	715	10.65
.01749	366	6.41
.01630	791	12.89

RUN NUMBER = 172

RADIUS INCHES	FREQUENCY 1/SECONDS	RADIUS X FREQUENCY
.02556	205	5.25
.01790	254	4.55
.02748	246	6.75

RUN NUMBER = 173

RADIUS INCHES	FREQUENCY 1/SECONDS	RADIUS X FREQUENCY
.01412	1369	19.33
.02862	152	4.35
.01168	1369	15.99
.03219	181	5.84

RUN NUMBER = 174

RADIUS INCHES	FREQUENCY 1/SECONDS	RADIUS X FREQUENCY
.00567	1364	7.73
.03371	211	7.12
.00999	283	2.83
.01276	385	4.91

APPENDIX C

TYPICAL COMPUTER PLOTS

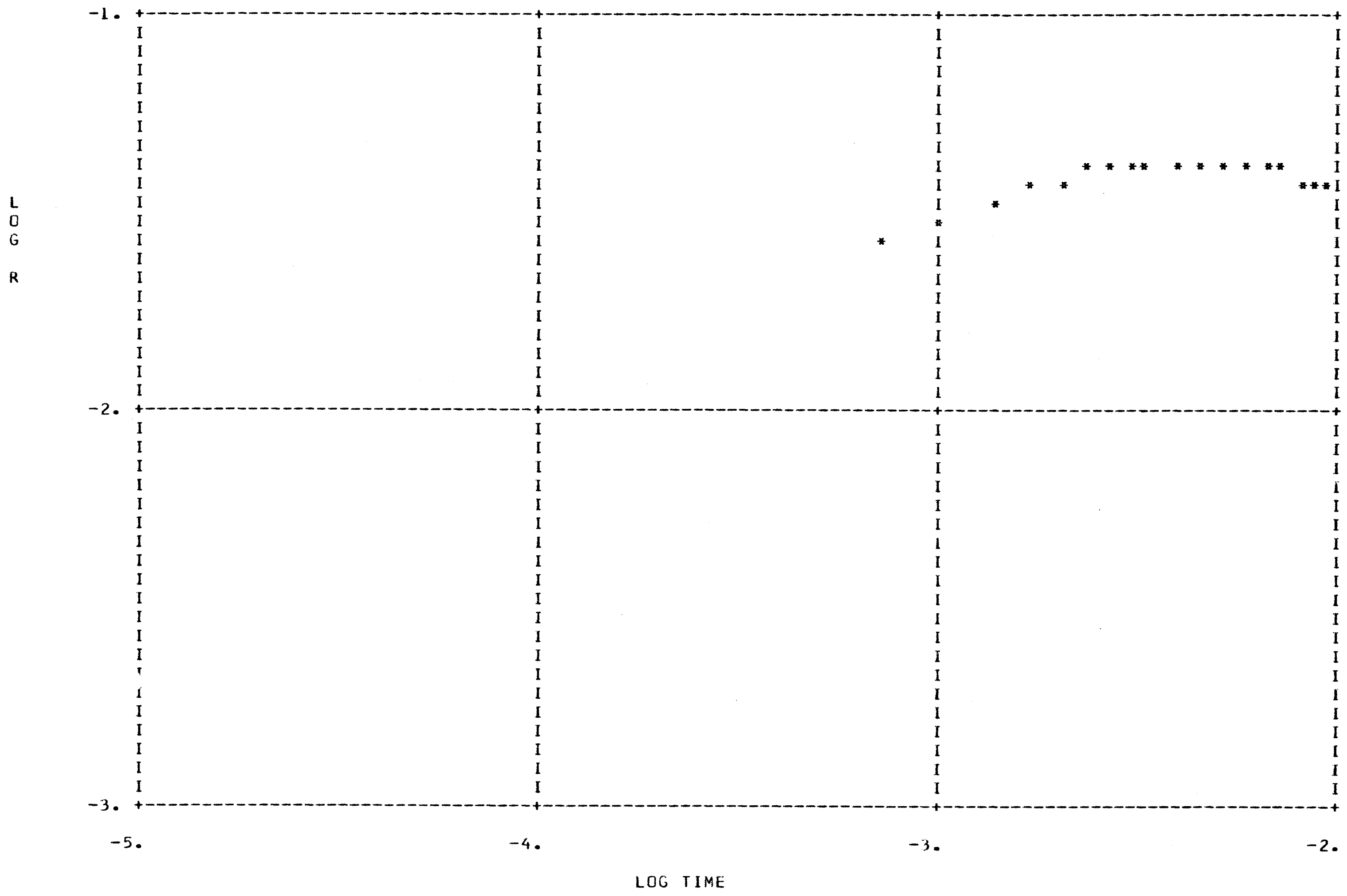

```
RUNNO =          138,        GEES =      1.000000,        HFLUX =  3.885417E 04
```

Figure 52. Typical Logarithmic Computer Plot.

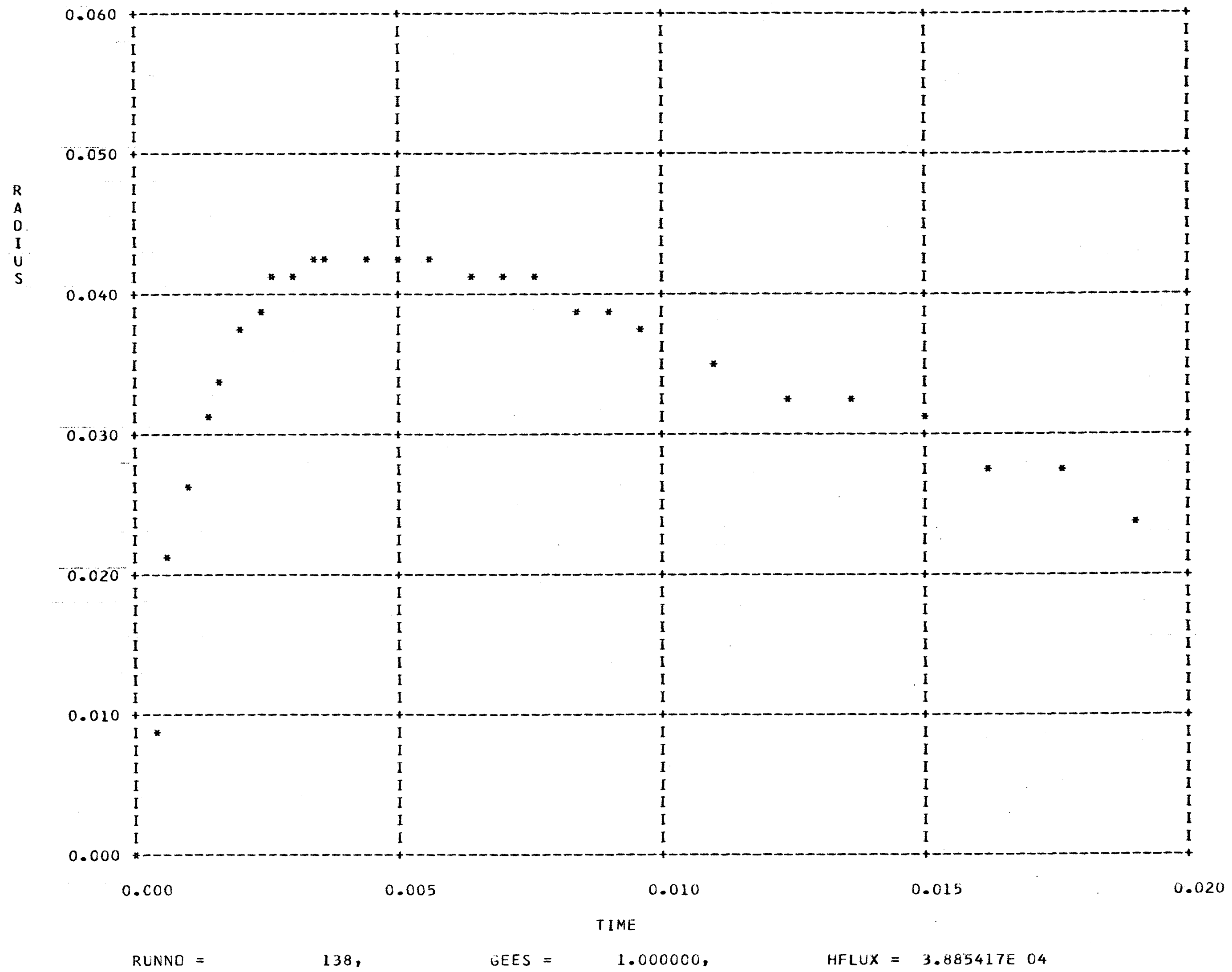

Figure 53. Typical Cartesian Computer Plot.

BIBLIOGRAPHY

1. Merte, H., and Clark, J. A. "Pool Boiling in an Accelerating System," Trans. ASME Journal of Heat Transfer, Series C, 83 (1961) 233.

2. Merte, H., A Study of Pool Boiling in an Accelerating System, Ann Arbor, The University of Michigan, Industry Program of the College of Engineering, IP-408, 1959.

3. Plesset, M. S. "The Dynamics of Cavitation Bubbles," Journal of Applied Mechanics, 16, 1949.

4. Fritz, W. "Calculation of the Maximum Volumes of Vapor Bubbles," Physik Zeitschrift, 36, (1935) 379.

5. Jakob, M. Heat Transfer, New York, John Wiley & Sons, Inc. (1949) Vol. 1.

6. Usiskin, C. M., and Siegel, P. "An Experimental Study in Reduced and Zero Gravity Fields," Trans. ASME Journal of Heat Transfer, Series C, 63 (1961) 243.

7. Staniszewski, B. E. Nucleate Boiling Bubble Growth and Departure, MIT, Technical Report No. 16, Cambridge, Massachusetts, August, 1959.

8. Han, Chi-Yeh, and Griffith, P. The Mechanism of Heat Transfer in Nucleate Pool Boiling, MIT, Report No. 7673-19, Cambridge, Mass. March, 1962.

9. Plesset, M. S., and Zwick, S. A. "The Growth of Vapor Bubbles in a Superheated Liquid," Journal of Applied Physics, 25 (1954) 493.

10. Forster, H. K., and Zuber, N. "Growth of a Vapor Bubble in a Superheated Liquid," Journal of Applied Physics, 25, (1954) 474.

11. Griffith, P. "Bubble Growth Rates in Boiling," Trans. ASME, 80, (1958) 721.

12. Bankoff, S. G., and Mikesell, R. D. "Bubble Growth Rates in Highly Subcooled Nucleate Boiling," Chemical Engineering Progress Symposium Series, 55, 1959.

13. Dergarabedian, P. "Observations on Bubble Growths in Various Superheated Liquids," U.S. Naval Ordinance Test Station, NAVORD Report 5009, China Lake, California, January, 1956.

14. Dergarabedian, P. "The Rate of Growth of Vapor Bubbles in Superheated Water," *Trans. ASME Journal of Applied Mechanics*, *75*, (1953) 537.

15. Dergarabedian, P. "Observation of Bubble Growths in Various Superheated Liquids," *Journal of Fluid Mechanics*, *9*, 1960.

16. Forster, H. K., and Zuber, N. "Bubble Dynamics and Boiling Heat Transfer," *Trans. ASME Journal of Heat Transfer*, *81* (1959) 37.

17. Forster, H. K., and Grief, R. "Heat Transfer to a Boiling Liquid-Mechanism and Correlations," *Trans. ASME Journal of Heat Transfer*, *81*, (1959) 37.

18. Forster, H. K. "On Conduction of Heat Into a Growing Vapor Bubble," *Journal of Applied Physics*, *25*, 1954.

19. Forster, H. K. "Diffusion in a Moving Medium With Time-Dependent Boundaries," *AIChE Journal*, *3-4*, 1957-58.

20. Forster, H. K., and Adelberg, M. "Discussion of Paper No. 60-HT-10," *Trans. ASME Journal of Heat Transfer, Series C*, 84 (1961) 251.

21. Rohsenow, W. "A Method of Correlating Heat Transfer Data for Surface Boiling of Liquids," Trans. ASME, 74 (1952) 959.

22. Kutateladze, S. S. *Heat Transfer During Condensation and Boiling*, Mashziz, Leningrad, 1949 and 1952, AEC Translation 3770, Tech. Inf. Serv., Oak Ridge, Tenn.

23. Michenko, N. "On the Problem of Heat Transfer in Nucleate Boiling," *Energemashinostroenie*, *17*, (1960).

24. Labountzov, D.A. "Generalized Correlation for Nucleate Boiling," *Teploenergetika*, *7*, No. 5 (1960) 76.

25. Levy, S. "Generalized Correlation of Boiling Heat Transfer," *Trans. ASME Journal of Heat Transfer*, *81*, (1959) 37.

26. Mumm, J. F. *Heat Transfer to Boiling Water Forced Through a Uniformly Heated Tube*, Argonne National Laboratory Report No. ANL5276.

27. Chang, Y. P. *An Experimental Modification of Nucleation Theory and Its Application to Boiling Heat Transfer*, Argonne National Laboratory Report No. ANL6304, February, 1961.

28. Chang, Y. P., and Snyder, N. W. "Heat Transfer in Saturated Boiling," *Chemical Engineering Progress Symposium Series*, *56*, No. 30, 1960.

29. Zuber, N., Tribus, M., and Westwater, J. W. "The Hydrodynamic Crisis in Pool Boiling of Saturated and Subcooled Liquids," *International Developments in Heat Transfer*, Part 2, No. 27, (1961) 230.

30. Costello, C. P., and Adams, J. M. "Burnout Heat Fluxes in Pool Boiling at High Accelerations," *International Developments in Heat Transfer*, Part 2, No. 30, (1961) 255.

31. Ivey, H. J. *Preliminary Results on the Effect of Acceleration on Critical Heat Flux in Pool Boiling*, United Kingdom Atomic Energy Authority, Reactor Development Division, Report No. AEEW-R99, September, 1961.

32. Hsu, Y. Y. "On the Size Range of Active Nucleation Cavities on a Heating Surface," *Trans. ASME Journal of Heat Transfer, Series C*, *84* (1962) 207-213.

33. Costello, C. P., and Tuthill, W. E. "Effects of Acceleration on Nucleate Boiling," *Chemical Engineering Progress Symposium Series*, *57*, No.32 (1961) 189.

34. Hirano, F., and Nishikawa, K. "The Phenomena of Boiling - Part 3," *Machinery Research*, Japan, *8*, No. 5 (1956) 521.

35. Benjamin, J. E., and Westwater, J. W. "Bubble Growth in Nucleate Boiling of Binary Mixtures," *International Developments in Heat Transfer*, Part 2, No. 24 (1961) 212.

36. Bankoff, S. G., and Mason, J. P. "Heat Transfer from the Surface of a Steam Bubble in Turbulent Subcooled Liquid Stream," *AIChE Journal*, *8*, No. 1 (March, 1962) 30.

37. Clark, H. B., Strenge, P. S., and Westwater, J. W. "Active Sites for Nucleate Boiling," *Chemical Engineering Progress Symposium Series*, *55*, No. 29, 1959.

38. Hsu, Y. Y., and Graham, R. *An Analytical and Experimental Study of the Thermal Boundary and Ebullition Cycle in Nucleate Boiling*, NASA, Technical Note TND-594, May, 1961.

39. Moore, F. D., and Mesler, R. B. "The Measurement of Rapid Surface Temperature Fluctuation During Nucleate Boiling of Water," *AIChE Journal*, *7*, No. 4, (December, 1961) 621.

40. Strenge, P. H., Orell, A., and Westwater, J. W. "Microscopic Study of Bubble Growth During Nucleate Boiling," *AIChE Journal*, *7* No. 4 (December, 1961) 578.

41. Summary of Conference on Bubble Dynamics and Boiling Heat Transfer Held at the Jet Propulsion Laboratory, June 14 and 15, 1956, JPL, Memo 20-137, Pasadena, California, December, 1956.

42. Westwater, J. W. Things We Don't Know About Boiling Heat Transfer, Department of Chemistry and Chemical Engineering, University of Illinois, 1960.

43. Clark, J. A., et al. Low Heat-Flux Boiling, Department of Mechanical Engineering, The University of Michigan, Ann Arbor, Michigan, First Quarterly Progress Report, January, 1962.

44. Balzhiser, R. E., et al. Liquid Metal Boiling Literature Survey, The University of Michigan, ORA Project 04526, September, 1961.

45. Lamb, H. Hydradynamics, New York, Dover Publications, Sixth Ed. (1945) 122.

46. Harrach, W. G. "A Study of Low Heat Flux Subcooled Nucleate Pool Boiling," Ph.D. Thesis, Lehigh University, 1960.

47. Reference Tables for Thermocouples, United States Department of Commerce, National Bureau of Standards, NBS No. 561, 1955.

48. Slember, R. J. "An Investigation of Pool Boiling Under Increased Fluid Body Force Conditions," Ph.D. Thesis, University of Pittsburgh, 1961.

49. Adams, J. M. "A Study of the Critical Heat Flux in an Accelerating Pool Boiling System," Ph.D. Thesis, University of Washington, 1962.

50. Graham, R. W., and Hendricks, R. C. A Study of Multi-G Accelerations on Nucleate-Boiling Ebullition, NASA Technical Note D-1196, May, 1963.

51. Fritz, W., and Ende, W. "Verdampfungsvorgang Nach Kinematographischen Augnahmen and Dampfblassen," Phys. Zeit. bd. 37, 1936.

52. Ellion, M. E. "A Study of the Mechanism of Boiling Heat Transfer," Jet Propulsion Laboratory Memorandum No. 20-88, Pasadena, California, March, 1954.

53. Griffith, P. "Bubble Growth Rates in Boiling," MIT, Report No. 8, Cambridge, Mass. June, 1956.

54. Rohsenhow, W. M., and Clark, J. A. "A Study of the Mechanism of Boiling Heat Transfer," Trans. ASME, 73, No. 5, (July, 1951) 609.

55. Zuber, N. "Hydrodynamic Aspects of Boiling Heat Transfer," Ph.D. Thesis, University of California, June, 1959.

56. Siegel, R., and Usiskin, C. M. "A Photographic Study of Boiling in the Absence of Gravity," Trans. ASME Journal of Heat Transfer, Series C, 81, (1959) 230-236.

57. Kline, S. J., and McClintock, F. A. "Describing Uncertainties in Single-Sample Experiments," Mechanical Engineering 75, 1953.

58. Zuber, N. "Nucleate Boiling. The Region of Isolated Bubbles," International Journal of Mass and Heat Transfer, 6, No. 6, Jan. 1963.

59. Siegel, R., and Kenshock, E. G. "Effects of Reduced Gravity on Nucleate Boiling Bubble Dynamics in Saturated Boiling," Paper presented at AIChE Meeting, San Juan, Puerto Rico, Sept. 1963. To be published in AIChE Journal.

60. Clark, J. A., and Merte, H. "Nucleate, Transition, and Film Boiling Heat Transfer at Zero Gravity," Paper presented at the Second Symposium on Physical and Biological Phenomena Under Zero-G Conditions, Los Angeles, Jan. 1963.

61. Gaertner, R. F. "Photographic Study of Nucleate Pool Boiling on a Horizontal Surface," ASME-63-WA-76.